EUROPEAN COMMISSION

Community Research

SEVENTH FRAMEWORK PROGRAMME

CARBOWASTE

Treatment and Disposal of Irradiated Graphite and Other Carbonaceous Waste

Grant Agreement Number: FP7-211333

Deliverable D-4.0.0

Summary Report on Work Package 4

Author(s): **Corrado Rizzato[1], Dirk Vulpius[1], Abbie Jones[2], Gabriel Piña[3], Mary Lou Dunzik-Gougar[4]**

[1]Forschungszentrum Jülich (Germany); [2]University of Manchester (UK); [3]CIEMAT (Spain); [4]PBMR (South Africa) / Idaho State University (USA)

Reporting period: e.g. 01/04/2008-31/03/2013

Date of issue of this report : 30/04/2013

Project co-funded by the European Commission under the Seventh Framework Programme (2007 to 2011) of the European Atomic Energy Community (EURATOM) for nuclear research and training activities		
Dissemination Level		
PU	Public	
RE	Restricted to the partners of the CARBOWASTE project	
CO	Confidential, only for specific distribution list defined on this document	**X**

Start date of project : **01/04/2008** Duration : **60 Months**

Distribution list

Person and organisation name and/or group	Comments
WP4 Members	
Executive Board	
Co-ordinator	

CARBOWASTE		
Work package: 4 **Task: :** 4.0	**CARBOWASTE document no:** CARBOWASTE-1304-D-4.0.0	**Document type:** Deliverable
Issued by: Forschungszentrum Jülich GmbH (DE) **Internal no.:** CW1304-Deliverable-4-0-0-c		**Document status:** Final

Document title

Summary Report on Work Package 4

Executive summary

Thermal, chemical and microbiological treatments have been considered in the light of decontamination of i-graphite.
Thermal treatments have been accounted in order to remove volatile radionuclides, as Tritium ,Radiocarbon and Chlorine-36. Inert gases, oxygen and steam have been used as adduct gases at different temperatures. The removal mechanism of Tritium has been identified in literature: results obtained in FZJ and IPNL are in line with the proposed model. An inert gas thermal treatment is a promising option for Tritium selective removal. The addition of water showed to strongly enhance H-3 removal by isotopic exchange reactions, but a dilution of the radionuclide is taking place.
A first approach model for Radiocarbon removal has been identified, together with the main possible removal routes: removal by slight oxidation of the enriched surfaces, migration of interstitials and stable radiocarbon in the graphene layers. Inert gas thermal treatments showed a saturation of the removal after short time due to the exhaustion of adsorbed/embedded reactants. Oxygen thermal treatment revealed to have high reaction rates and low radionuclide selectivity. Water steam thermal treatment showed to be effective for C-14 removal, despite the significant mass losses compared to the inert case.
The MINOS (Multi INert Oxidising Step) process has been established: it is aimed to optimising the removal of Tritium by inert gas treatment and Radiocarbon by separating reactant loading and chemical reactions. Chlorine-36 was not directly detectable due to its low specific activity; several investigations on virgin graphite and implanted Cl-37 revealed the existence of at least two chemical forms, one of which is thermally stable. However, more investigations on i-graphite are needed.
Chemical treatments have been considered with acidic, natural, alkaline and organic agents: only the first ones showed relevant removal efficiencies depending on the radionuclide of interest and on the molar concentrations/mixtures implied. Intercalation processes are promising from the point of view of radionuclide selective separation from the graphite matrix; however, the usage of acids would dilute the tritium in a secondary waste: a preliminary separation is advised.
Treatments with microorganisms focused on the removal of radiocarbon. Any process that will mobilise/remove the easily accessible fraction will ultimately reduce the risks associated with graphite disposal. From that point of view fungi, generating organic acids to promote attachment and access to nutrients, would be ideal for the treatment of graphite, in preference to bacteria; microbes could have a number of adverse effects on the safety of a nuclear waste repository, including causing corrosion of metal waste containers that will promote adverse secondary effects. The fate and mobility of C-14 in the biomass are of fundamental importance for the graphite disposal strategy to be adopted.

Revisions

Rev.	Date	Short description	Author	Internal Review	Task Leader	WP Leader
00	30/04/2013	First issue	Vulpius FZJ	von Lensa FZJ	Vulpius FZJ	Vulpius FZJ
01	30/05/2013	2nd Issue	Rizzato FZJ	Von Lensa FZJ	Vulpius FZJ	Vulpius FZJ

Table of Content

1. Objectives of Work Package 4 5
2. Mechanistic Background of Impurity Removal 5
2.1 Structure of Nuclear Graphite, Impurities and Nuclear Activation 5
3. Graphite Decontamination by Thermal Treatment 20
3.1 Release of Tritium 20
3.1.1 Background 20
3.1.2 Release of Tritium during inert gas thermal treatments 22
3.1.3 Release of Tritium during thermal treatments with Oxygen/Nitrogen 33
3.1.4 Release of Tritium during thermal treatments with water steam 35
3.1.5 Comparison of Tritium removal in different regimes 41
3.2 Release of Radiocarbon 46
3.2.1 Background 46
3.2.2 Release of Radiocarbon during inert gas thermal treatments 47
3.2.3 Release of Radiocarbon during thermal treatments with Oxygen/Nitrogen 55
3.2.4 Release of Radiocarbon during thermal treatments with water steam 57
3.2.5 Comparison of Radiocarbon Removal in Different Regimes/Gases 61
3.3 Release of other Radionuclides 69
3.4 Detection and removal of Surface Contamination 70
3.5 Waste Management Strategies 72
3.6 Thermal Treatments: Summary 74
4. Graphite Decontamination with Liquid Agents 79
4.1 Experimental 79
4.1.1 Test Samples 79
4.1.2 Test Methods 81
4.2 Results and Discussion 87
4.2.1 Long Term Leaching (UoM) 87
4.2.2 Soxhlet Extraction (FzJ) 94
4.2.3 INR Inorganic Agents Leaching Test 101
4.2.4 CIEMAT Inorganic Agents Leaching Tests 103
4.2.5 ENEA Organic Agents Leaching Test 108
4.3 Decontamination with Liquid Agents: Main Achievements 111
5. Graphite Decontamination by Microbiological Treatment 114
5.1 Bacterial growth with NaCl replaced by the carbon-containing sodium salts 117
5.2 Bacterial growth with glucose carbon replaced by carbon-containing sodium salts . 120
5.3 Bacterial growth with glucose and NaCl replacement by carbon-containing sodium salts 121
5.4 Experiments with 14C-labelled sodium salts 123
5.5 Decontamination by Microbiological Treatment: Summary 126
6. Future Developments/needs 127
6.1 Identification of open issues 127
6.2 Multi-Scale Modelling of Graphite 129
7. Conclusions 132
8. References 136
List of Figures 138
List of Tables 143

1. Objectives of Work Package 4

The aim of Work Package 4 is the development of methods for the decontamination of neutron-irradiated graphite. To do this, it is necessary to know the location and the chemical form of the contaminating radionuclides (see Work Package 3). With this knowledge, general strategies for the removal of these radionuclides can be elaborated (Task 4.1). Then, these general strategies can be transformed in real methods of physical (Task 4.2), chemical (Task 4.3) and microbiological treatment (Task 4.4).

2. Mechanistic Background of Impurity Removal

2.1 Structure of Nuclear Graphite, Impurities and Nuclear Activation

Nuclear graphite is an artificially produced product manufactured from filler and binder materials [1]. For the graphite moderator mainly petroleum or pitch coke is used for the filler and, as a binder, mainly coal-tar-pitch. However, in the case of the fuel compact or pebble matrix a mixture of crushed artefacts and natural graphite bound in formaldehyde resin is used. These components retain their principal structures in the fabricated graphite despite been subject to high temperature baking and graphitising processes. The microstructure of carbon brick, which can be considered as an interim stage product of the nuclear graphite, underlines these observations. In Fig. 2.1, a large filler particle surrounded by not well-graphitised binder material can be seen.

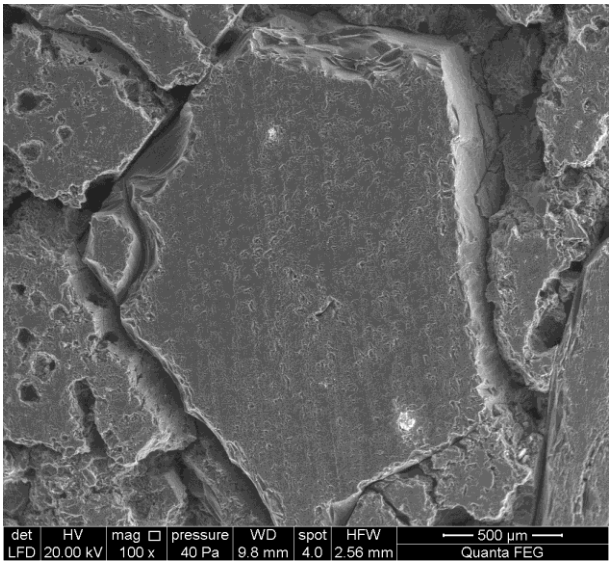

Figure 2.1-a: Scanning electron micrograph of carbon brick, Large Field Detector

This binder material is where most of the impurities are located, as can be seen in Fig. 2.1-b. The white dots are impurities which can be detected by back-scattering electrons. These impurities mainly consist of oxides of aluminium, silicon and iron, but the easily neutron-activated elements such as cobalt and nickel are always affiliated to these main impurities.

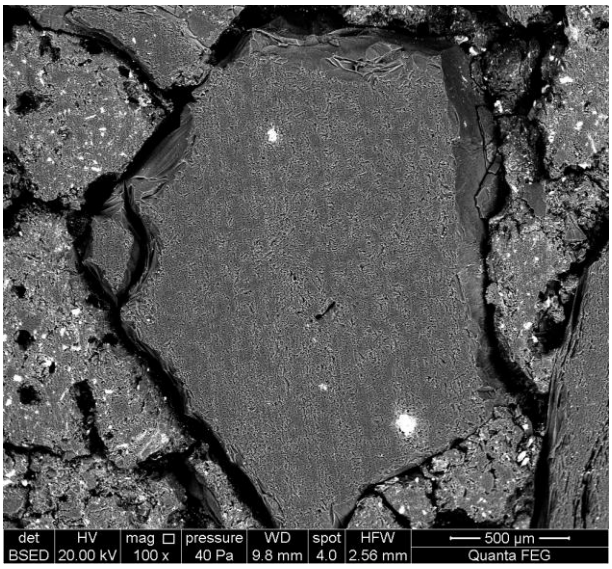

Figure 2.1-b: Scanning electron micrograph of carbon brick in back-scattering electron mode

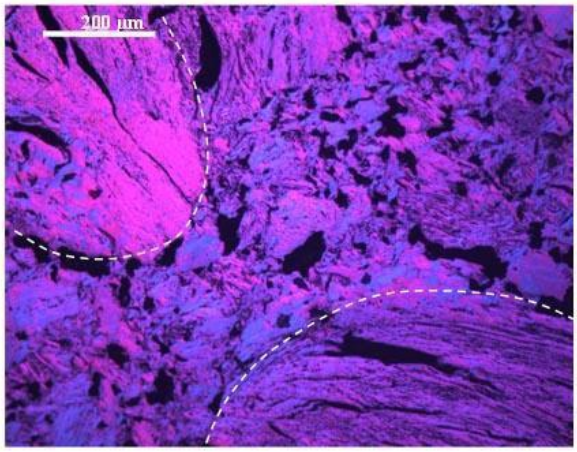

Figure 2.2: Optical microscope in polarised light showing the different components making up nuclear graphite [see CW-T-3.2.3]

Figure 2.2 shows an example of nuclear graphite observed at the optical microscope in polarised light: the grains or flakes of petroleum coke, characterised by large, optically anisotropic domains can be clearly distinguished (two are encircled by a dotted line in the image on the right), separated by the coal-tar pitch binder. The binder is characterised by small isochromatic domains and, more particularly, a considerable porosity, a characteristic initially attributed to volatile molecules during the nuclear graphite manufacturing process (highest temperature of treatment between 2500°C and 3000°C). [see CW-T-3.2.3]

For what concerns the impurities, it needs to be checked whether a similar distribution as in Figs. (2.1-a,b) takes place also in nuclear graphite, even after graphitization and purification processes. The difficulties on the impurities detection are underlined by the relatively low concentrations together with the detection limits of the used equipment.

Another important element for neutron activation in nuclear graphite is nitrogen. The isotope ^{14}N leads to forming ^{14}C with a cross section of 1.93 barn (for thermal neutrons). Graphite has a high affinity to adsorb nitrogen on its surfaces. These surfaces are not only the outer surfaces, but also the inner surfaces of the pore system. The adsorption profile of nitrogen can be measured by secondary ion mass spectroscopy (SIMS). Fig. 2.3 shows the depth profiles of ^{14}N (detected as CN−) in irradiated and virgin reflector graphite from the Jülich experimental high-temperature pebble-bed reactor (AVR). These profiles were recorded after conditioning of the samples in vacuum for 3 days to avoid erroneous signals due to atmospheric nitrogen. Despite of these conditions, the profiles show an increased amount of nitrogen towards the surface of the graphite samples. Quantum mechanical calculations allowed demonstrating that nitrogen should be adsorbed on graphite surfaces not by physisorption but by chemisorption to form covalent bonds [2, 3].

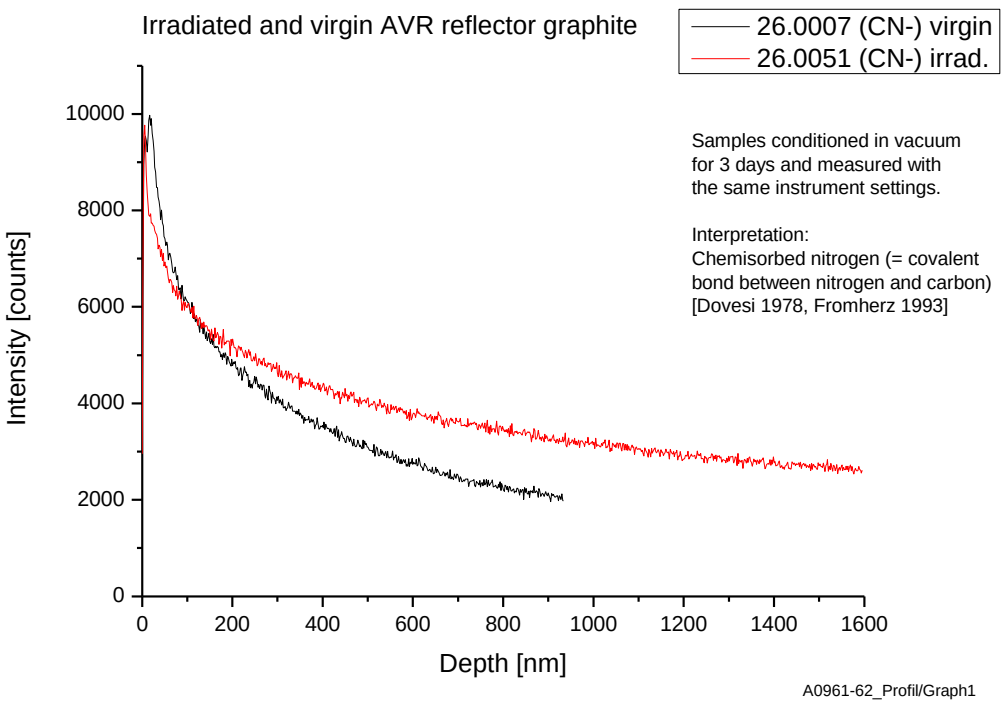

Figure 2.3: Depth profiles of 14N (detected as CN−) in irradiated and virgin AVR reflector graphite

The covalent bonds created from atmospheric nitrogen are at the basis of the relatively high amounts measured in nuclear graphite (approx. 300 ppm). Under neutron irradiation, the nitrogen will be activated to form radiocarbon. However, the presence of small amounts of nitrogen in the raw materials, even after graphitization, cannot be excluded: it is believed that such a contribution to the total amount of nitrogen in graphite represents the major one.

An important question is: which is the location and the chemical bond of radiocarbon in neutron-irradiated nuclear graphite? The recoil energy of the ^{14}C atoms resulting from the (n,p) nuclear reaction is 41.4 keV. This energy is high enough to break any chemical bond. However, once a nitrogen atom is activated and the subsequent ^{14}C atom recoils, it is very probable that, after lowering its energy due to successive collisions, it will form another bond. Accordingly, the following question is: where are free binding sites for ^{14}C in graphite? Free binding sites are in vacancy structures on the surface of the graphite crystallites and micro-

crystallites (see Fig. 2.4), between the graphite lattice planes (see Fig. 2.5) and, finally, on any carbon atom with free binding valences in disordered graphite structures or in amorphous carbon parts. Therefore, it can be postulated that ^{14}C is concentrated in neutron-irradiated nuclear graphite on surfaces, in near-surface structures and in disordered or amorphous parts of incompletely graphitised binder or filler materials, as well as in neutron-damaged structures presenting dangling bonds (see Fig. 2.6).

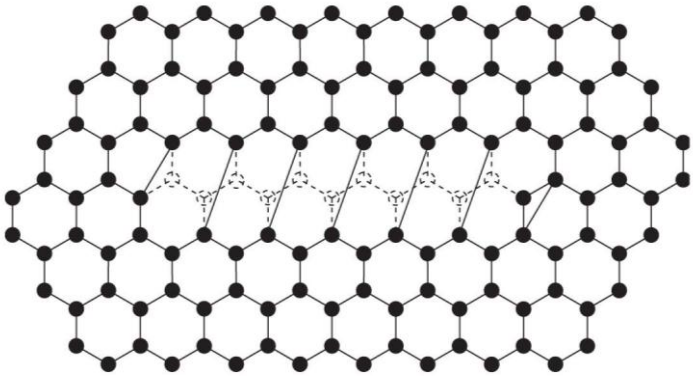

Figure 2.4: Possible vacancy structures on graphite surfaces [4]

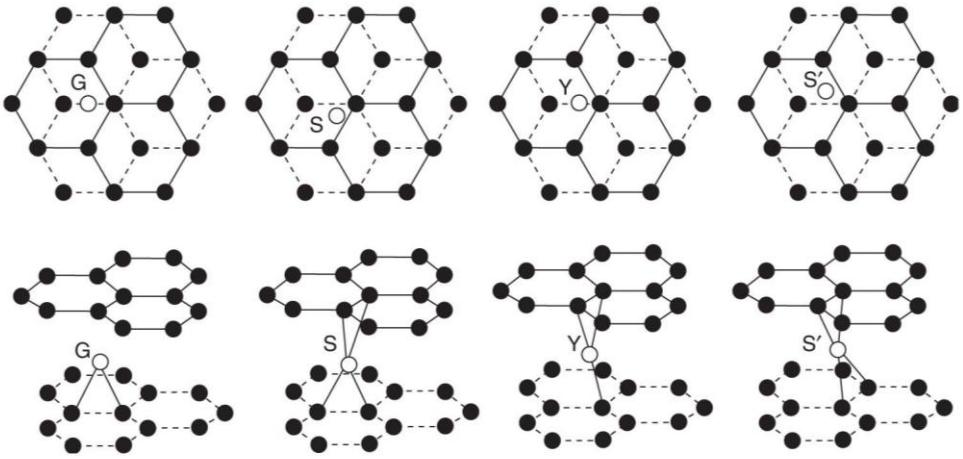

Figure 2.5: Possible places of carbon atoms between the graphite lattice planes [4]

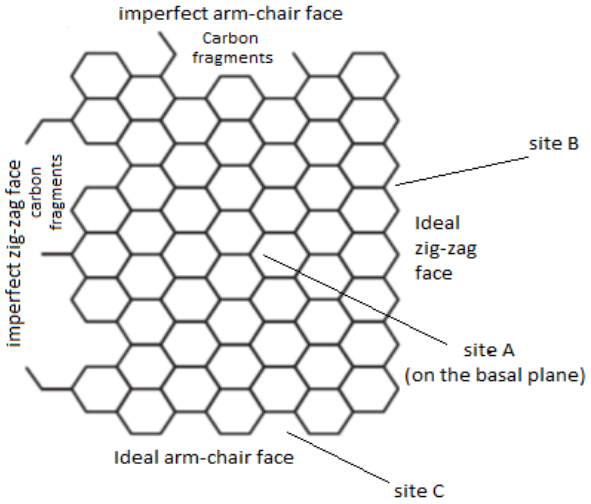

Figure 2.6: Schematic view of a grapheme layer with perfect and imperfect zig-zag and arm-chair faces

An important experimental observation is that the distribution of radionuclides in neutron-irradiated nuclear graphite is inhomogeneous. Initially, this hypothesis derived from the observation of different activities and radionuclide inventory of the graphite samples, even of the ones coming from the same position of the same reactor.
The inhomogeneous distribution of radionuclides in neutron-irradiated nuclear graphite has been proven also by secondary ion mass spectrometry (SIMS): a graphite sample from the reflector of the AVR high-temperature reactor was measured, with an averaged ^{14}C inventory of 3.3E+05 Bq/g; it was found a ^{14}C signal at 14.0039 u (see Fig. 2.7). A second measurement point was taken from the very same sample and no radiocarbon was detected (see Fig. 2.8). To validate the measurements, a ^{14}C reference material was measured (chemical form: graphite) with an activity of 3.7E+08 Bq/g and a considerable signal at 14.0036 u was measured (exact mass number of 14C = 14.00324 u). With the reference signal, the related ^{14}C inventory of the AVR sample was calculated in 2.0E+07 Bq/g which is 60 times higher than the averaged ^{14}C inventory! From this result it can be concluded that ^{14}C is present in irradiated graphite (at least partly) as "hotspots".
Another assumption may be drawn from the SIMS measurements. SIMS was the only method by which ^{14}C was "chemically" detected, due to the low detection limit of the apparatus. In the mass spectra ^{14}C appeared only as single carbon ion. Other ^{14}C fragments were not found. A direct conclusion from the SIMS measurements to the speciation of ^{14}C is not possible because SIMS shows only molecular fragments; however, by analogy it could be postulated that ^{14}C could be bound in irradiated graphite in the same way like the ^{12}C-^{13}C atoms in any graphite because the main ^{12}C-^{13}C fragments of any graphite obtained using SIMS are the single ^{12}C-^{13}C ion.

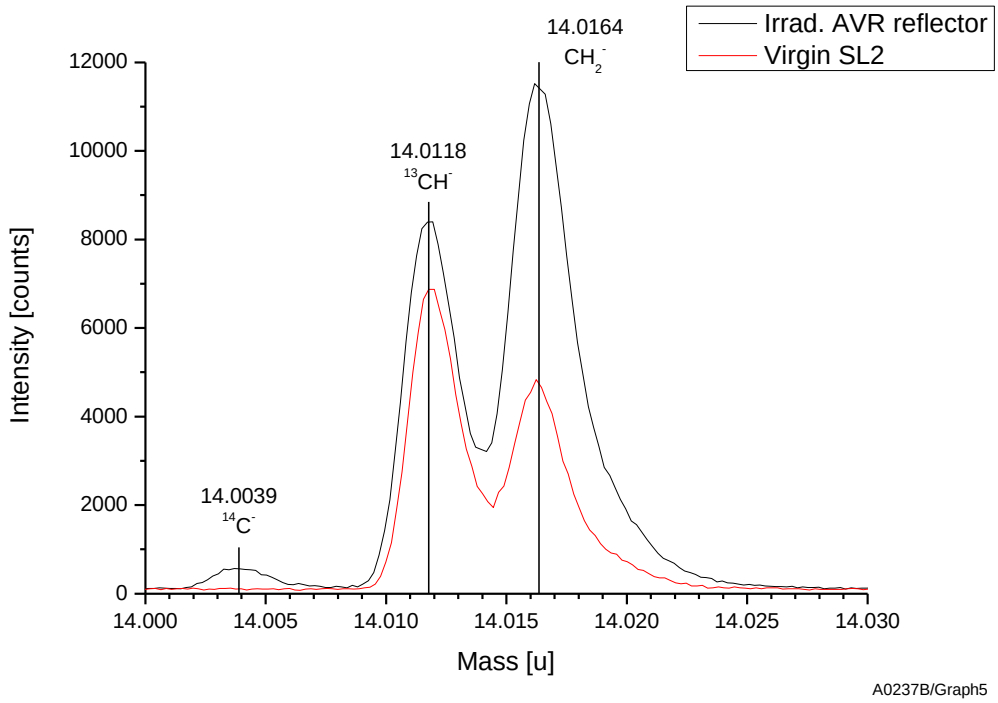

Figure 2.7: Secondary ion mass spectra of irradiated AVR reflector graphite in comparison to virgin Saint-Laurent A2 graphite in the region of 14C

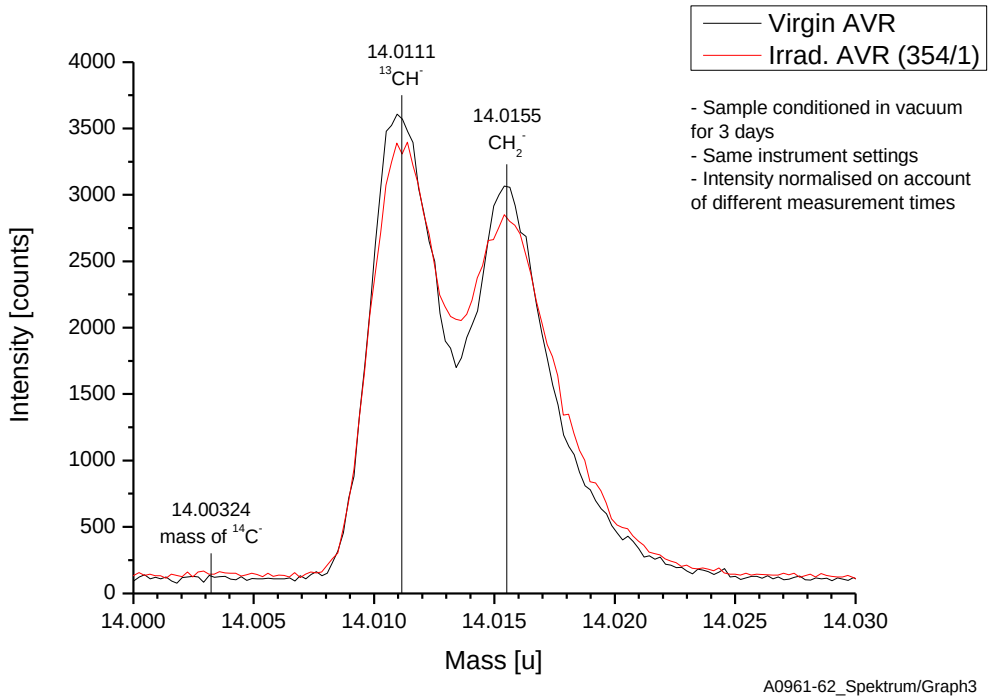

Figure 2.8: Repeat secondary ion mass spectra of irradiated AVR reflector graphite (same sample as in Fig. 2.7) in comparison to virgin AVR reflector graphite in the region of ^{14}C

The mass spectrometric detection of other radionuclides than ^{14}C is difficult because their concentrations are much lower than the one of ^{14}C. The analysis of the spectra, partially reported in Fig. 2.7, revealed a weak peak at the exact mass number of ^{3}H: 3.01605 u (see Fig. 2.9); other ^{3}H peaks were not found. An assignment of this peak to defined structured elements is difficult because such a peak may come from several combinations such as adsorbed HTO or C─T and C─OT groups. Nevertheless, the following assumption may be made: if ^{3}H is detectable, then it must come from a hotspot similarly as ^{14}C. An important indication of this fact is the inhomogeneous distribution of inactive hydrogen fragments in the mass spectrum of all types of graphite (virgin and irradiated) as shown in Fig. 2.10. Also ^{6}Li, one of the precursors of ^{3}H, is heterogeneously distributed. Therefore, it can be assumed that at least one part of ^{3}H in neutron-irradiated graphite is located in the vicinity of ^{6}Li. It is probable that this ^{3}H has formed compounds with the surrounding carbon atoms so that it is present at the end as C─T compound.

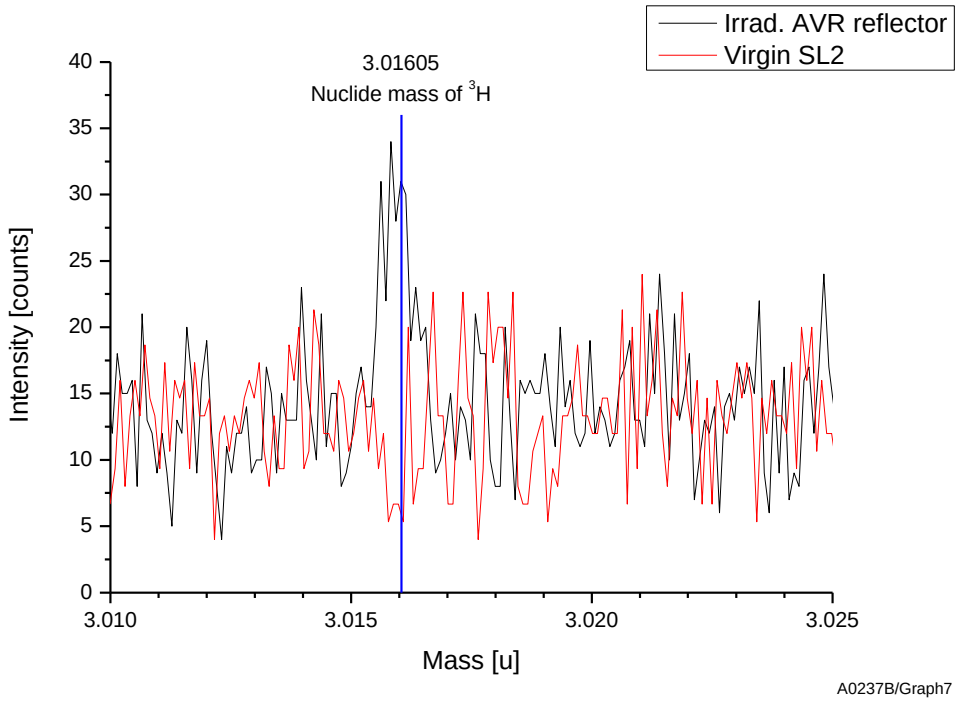

Figure 2.9: Secondary ion mass spectra of irradiated AVR reflector graphite in comparison to virgin Saint-Laurent A2 graphite in the region of 3H (same spectra as in Fig. 2.7)

As already indicated, SIMS offers the possibility to determine the spatial distribution of ions. Interesting ions in the negatively charged ion spectrum are H−, CH−, O−, OH−, CN− and Cl−. All these ions are distributed in a very heterogeneous way and in partially as hotspots, as it can be observed in Fig. 2.10.

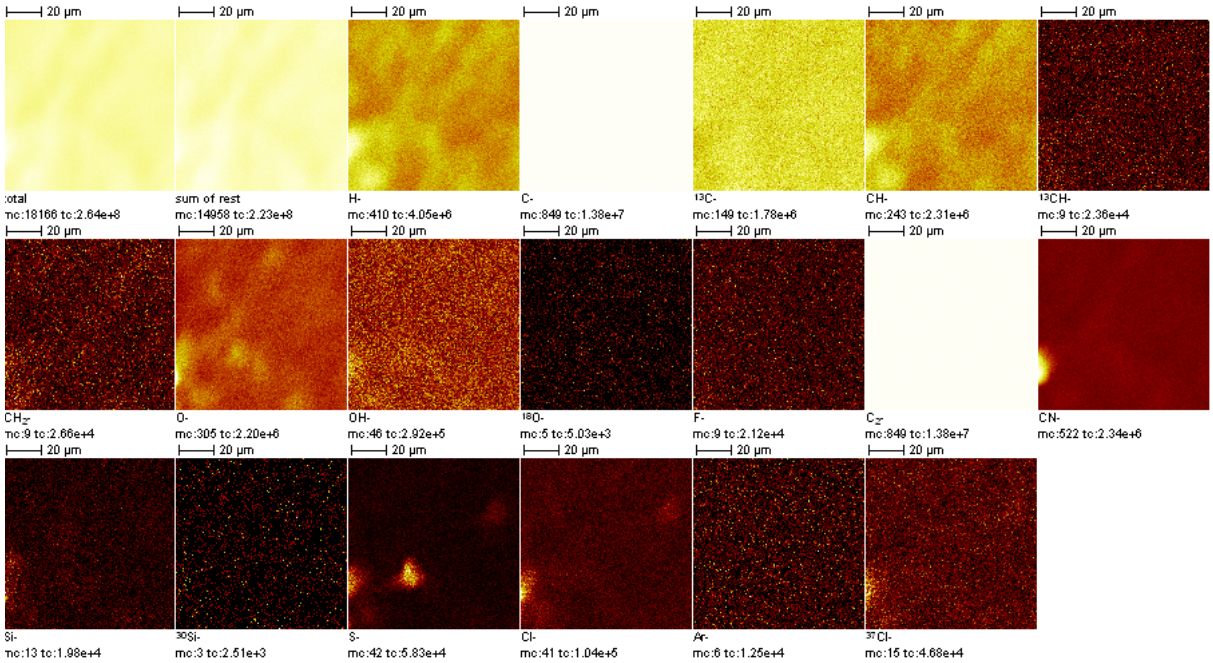

Figure 2.10: Spatial distribution of negatively charged ions
(sample: irradiated Saint-Laurent A2 graphite from the position 5120)

This finding is mainly important for the CN− fragment because ^{14}N (natural amount: 99.64%) is activated to ^{14}C by neutron irradiation in a nuclear reactor. In spite of the relatively high recoil energy of 41.4 keV, ^{14}C will remain in the vicinity of its precursor. The recoil of a ^{14}C atom has been simulated by molecular dynamic (MD) Monte Carlo calculations, in particular focusing on the transport behaviour of ^{14}C in irradiated nuclear graphite [5]. As can be seen in Fig. 2.11, the ^{14}C atom loses its kinetic energy in a perfect graphite lattice structure after a displacement distance of nearly 600 Å (60 nm). Therefore, ^{14}C will be concentrated in this region. After the detection of ^{14}N on graphite surfaces (see Fig. 2.3) and the corresponding conclusion for the presence of ^{14}C, the detection of ^{14}N as hotspot is the "second mode" of existence of ^{14}C in neutron-irradiated graphite.

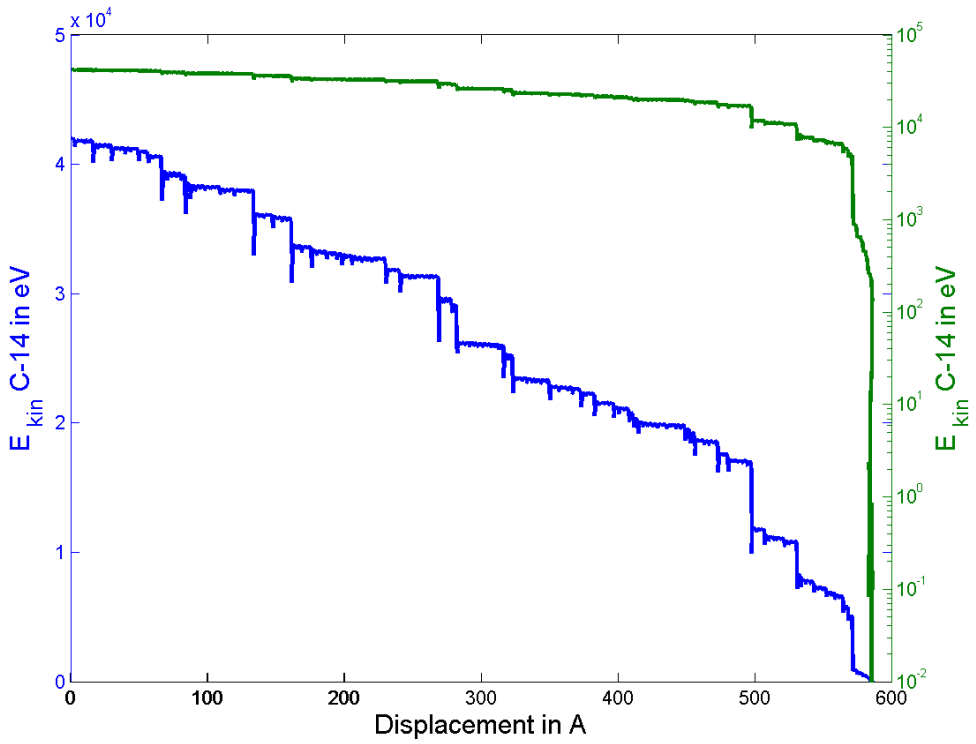

Figure 2.11: Displacement and energy loss of a 14C atom in a perfect graphite lattice structure [5]

Metal ions like Na+, Mg+, K+, Ca+, Fe+ etc. appear clearly in the positively charged ion spectrum as hotspots, as can be seen in Fig. 2.12. Similarly, the easily neutron-activated isotopes $^{6}Li+$, $^{10}B+$ and $^{59}Co+$ appear also in regions of higher concentration, although very weak due to their low total concentrations. It can be concluded that radionuclides formed from these isotopes (e.g. ^{3}H, ^{41}Ca, ^{55}Fe, ^{60}Co) will also remain in their local environment. This means that these radionuclides appear as hotspots or regions of higher concentration. A proof of this is given by digital autoradiography. In Fig. 2.13 an autoradiographic image of the same sample, used already for the SIMS measurements, is shown. The black dots which are caused by accumulation of beta-emitters are clearly visible. A surface contamination can be excluded because the measured surface was artificially generated by sawing the specimen from a larger sample.

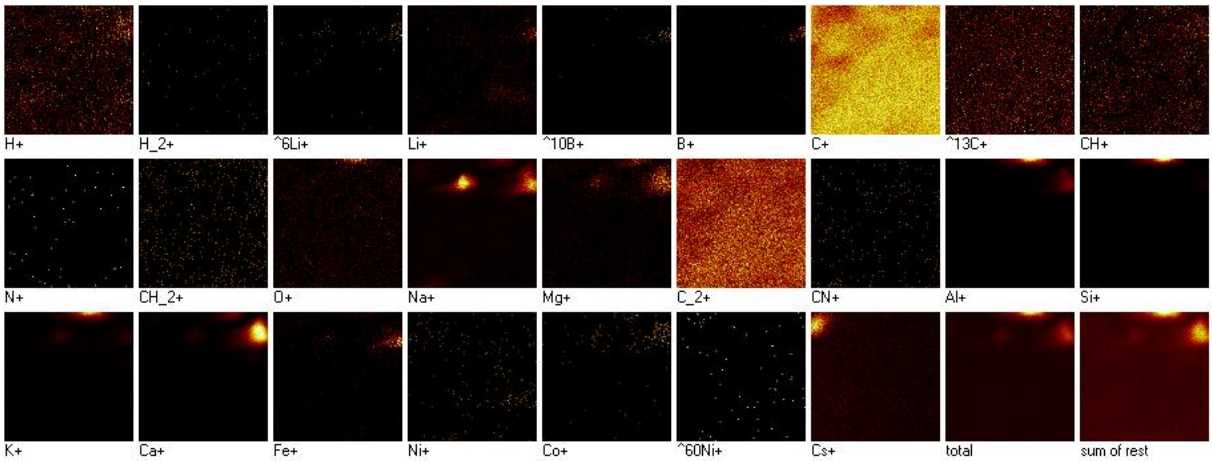

Figure 2.12: Spatial distribution of positively charged ions
(sample: irradiated Saint-Laurent A2 graphite from the position 5120)

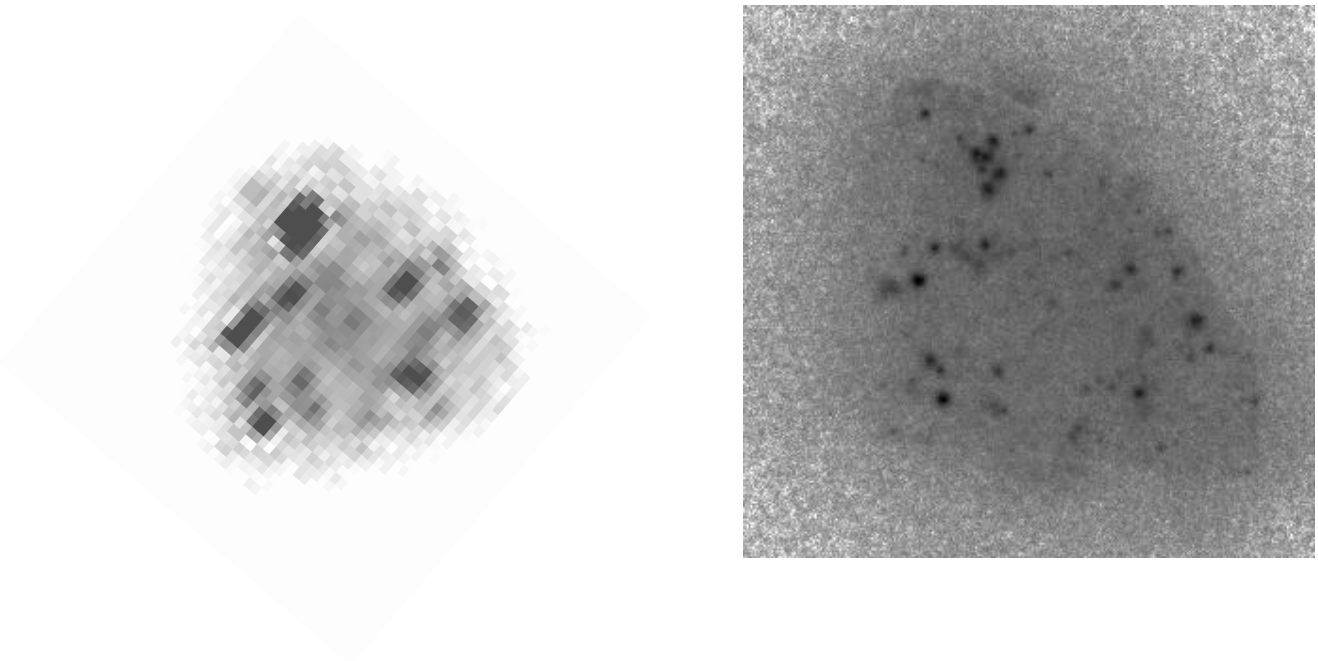

Figure 2.13: Spatial distribution of beta-emitters determined by digital autoradiography (sample: irradiated Saint-Laurent A2 graphite from the position 5120; specimen diameter: 12 mm, thickness: 3 mm, mass: 0.2196 g)
Left: Istant Imager (proportional Counter tube – FH Jülich); Right: Phosphor Imager (FZJ); Upper side of the sample.

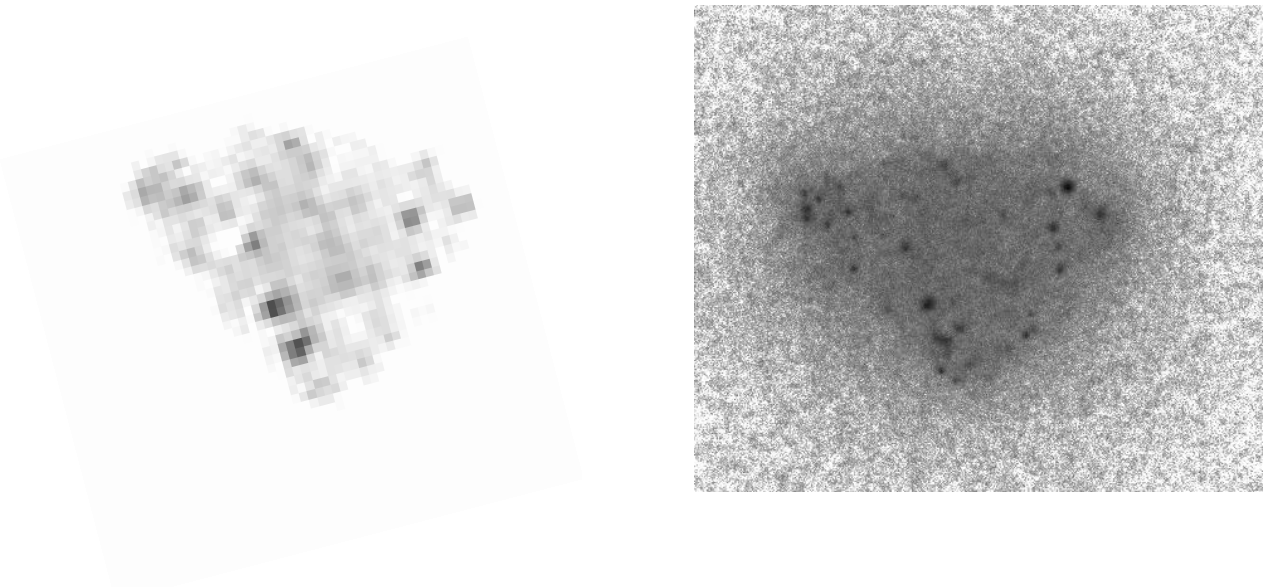

Figure 2.14: Spatial distribution of beta-emitters determined by digital autoradiography (sample: irradiated Saint-Laurent A2 graphite from the position 5120; specimen diameter: 12 mm, thickness: 3 mm, mass: 0.2196 g)
Left: Istant Imager (proportional Counter tube – FH Jülich); Right: Phosphor Imager (FZJ); Lower side of the sample.

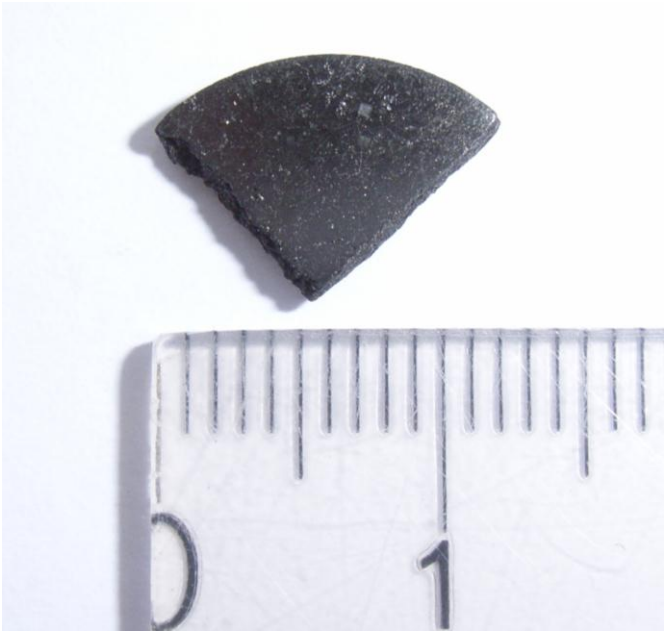

Figure 2.15: Optical image of the investigated sample

The radionuclide content of irradiated graphite can arise via two routes: neutron activation of the original elements in the graphite and contamination of the graphite from activated material from other components in the reactor circuit. It has been proposed that the origin of a particular radionuclide will be linked to its final bonding and location within the microstructure, and is thought that surface bound, contamination material, may be more easily removed during the application of various treatment options. Therefore an understanding of the origin of the radionuclides, and whether they are internal or external in origin, can lead to a deeper understanding of the removal behaviour during treatment.

It would have been difficult, if not impossible, to quantify the levels of contamination during operation, therefore work concentrated on identifying the original impurity content of UK graphite grades and comparing activation calculations based on this data with experimental characterisation of irradiated samples from a variety of reactors.

The first step in this study was to undertake a literature review to identify sources of impurity inventory data for UK nuclear graphite grades. Nuclear grade graphite is a relatively pure material, and a number of purification steps are undertaken in order to reduce the concentrations of impurities, however it is inevitable that some impurity elements will remain, and may even be introduced during purification. Sources of data for the impurity content of UK graphite grades is extremely limited, and in most cases incomplete or referring to material of poor providence. Neutron activation calculations were performed within WP3 by a number of partners using this type of impurity data. The results from these calculations, and the experimental isotopic characterisation work, as summarised in WP3: T-3.4.3 Modelling of Isotope Release Mechanism. These calculations give an indication of the final activity of the radionuclides, however no account is taken of the bonding and location within the microstructure.

The location of radionuclides was investigated at UoM using both Autoradiography and X-ray Tomography (XCT). Autoradiography provides a visual representation of the distribution of activity within a sample, giving an indication of location of the radionuclides. This technique was used at UoM to study several samples from the Oldbury reactor, which highlighted the inhomogeneity of the spread of activity within a sample, and between samples.

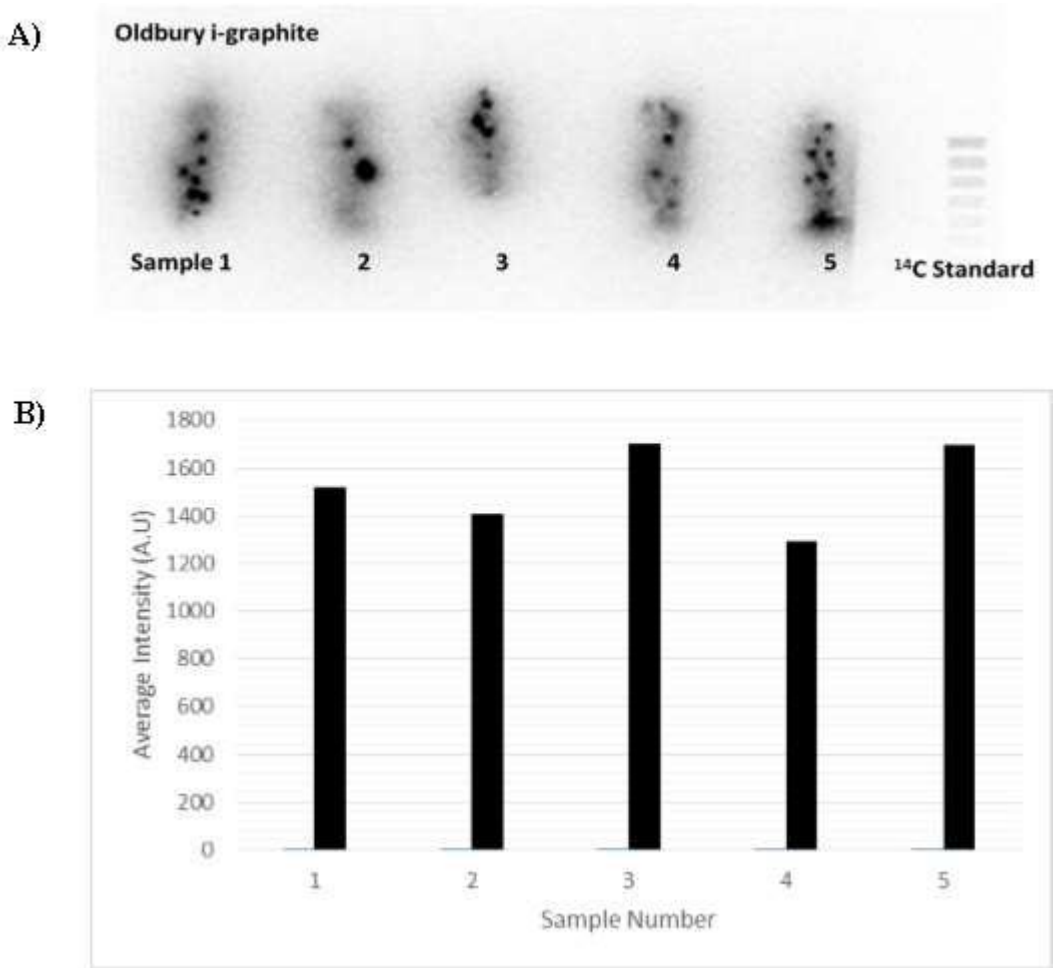

Figure 2.16: Autoradiograph showing increasing greyscale intensities with exposed Oldbury samples, B) graph showing the average intensity for Oldbury samples.

Similar results have been obtained in FZJ (see Figs. 2.13-14-17). The origin of heterogeneous radionuclide distribution is up to now unknown. Several SEM (scanning Electron Microscope) investigations tried to correlate the presence of hot spots with some impurities: it was not possible to detect any impurity associated to the positions showing higher activities.

XCT at UoM has been used to analyse a number of samples from the materials test reactor BEPO (British Experimental Pile Zero). This technique can be used to construct a 3D representation of the microstructure of the graphite. From these scans the open and closed porosity were highlighted and areas of high attenuation, representing metallic impurity and activation products, identified.

Irradiated graphite analysis was performed with the samples contained within a 'harwell can', this ensured that no radioactive graphite dust would contaminate the tomography equipment. No filter was applied during the analysis as the can is made from aluminium which acts as a filter. A calibration of the can's thickness versus attenuation using highly orientated pyrolytic graphite (HOPG) as a reference standard inside the can is shown in Figure X where intensity shown to exhibit a linear relationship with thickness. The reconstruction of the 2D images was completed using Amira© software and are shown in Figure 2.18.

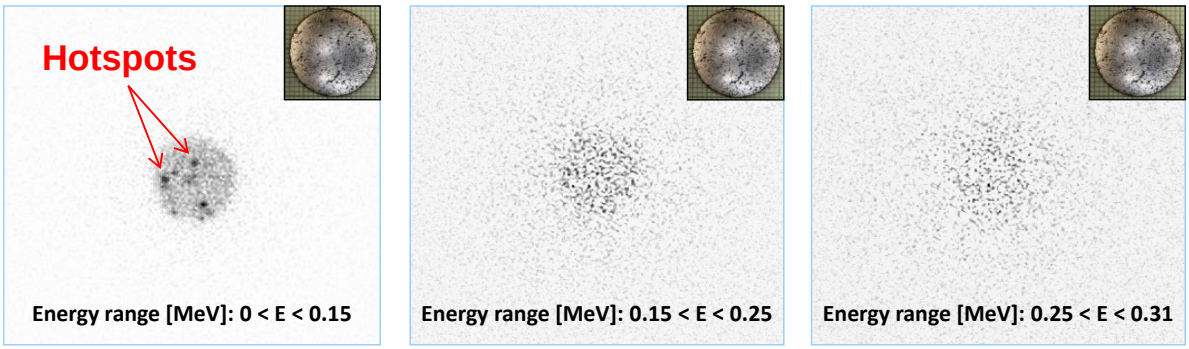

Figure 2.17 a-c: Autoradiography of Saint-Laurent A2 graphite at different energy ranges

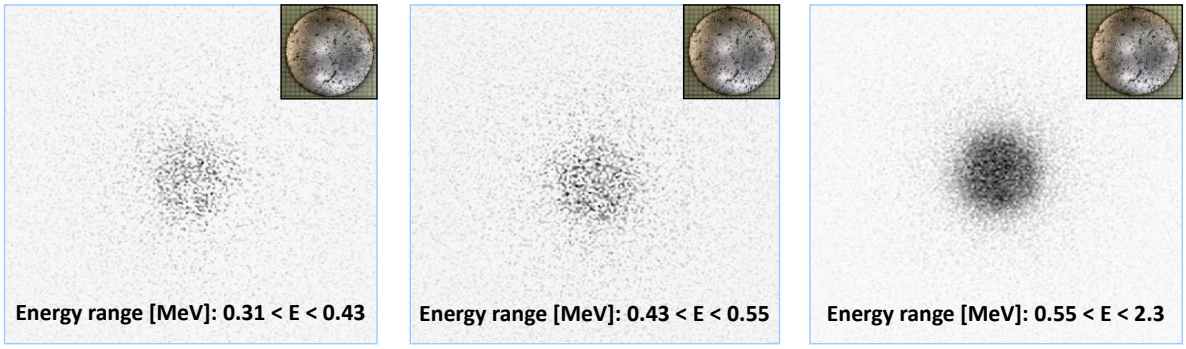

Figure 2.17 d-f: Autoradiography of Saint-Laurent A2 graphite at different energy ranges

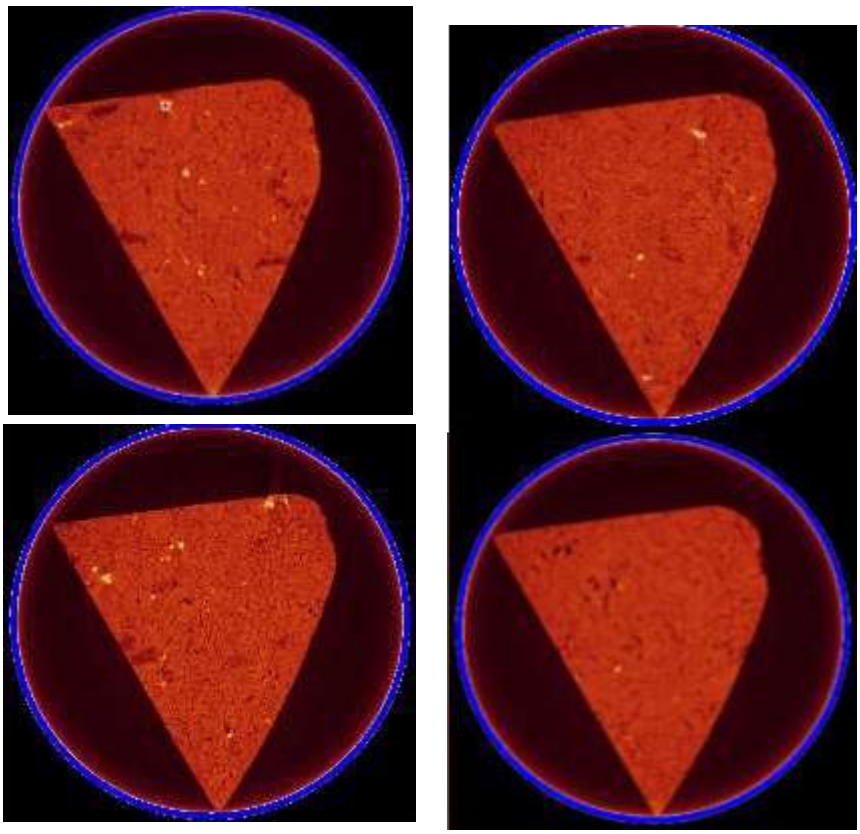

Figure 2.18: 2D tomography Radiographs of BEPO sample 16 graphite contained within a “Harwell can”.

3D volume reconstructions of BEPO sample 16 have been processed using Amira© software and are shown in Figure 2.19. The porosity distribution was calculated and is equivalent to 17.2% porosity. The blue regions display the internal porosity and the red is the high attenuation spots. It can be noted that high attenuations spots are contained within the porosity and are non-uniformly distributed.

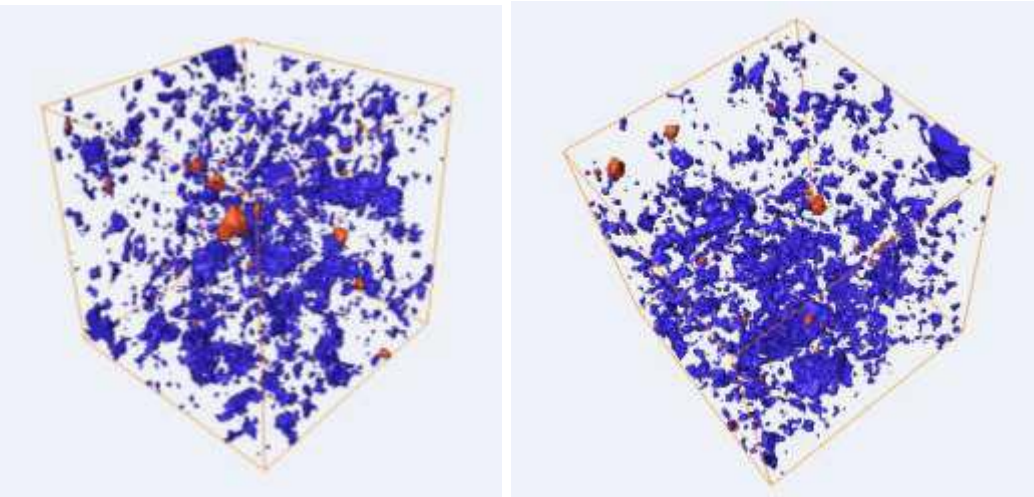

Figure 2.19: 3D volume reconstructions of BEPO Graphite using Amira© software

It was recognised that a model to describe the mechanistic behaviour of radionuclides during treatment would require understanding of the activation process, atomistic behaviour during activation as well as incorporation of experimental characterisation results and large scale neutron activation models. Although significant research in these areas was undertaken within Carbowaste and other projects there was limited interaction to bring these studies together in a unified description of the behaviour of the radionuclides. To attempt to develop a way forward a meeting was hosted at the University of Manchester on 28th November 2012. The aim of the meeting was to bring together experts in the fields of atomistic modelling, experimental characterisation and neutron activation modelling with the purpose of identifying areas for future research. The meeting concentrated on the origin, production, location and final activity of Carbon-14, with a number of presentations dealing with each area:

- Location of activation products
- Chemical speciation of activation products
- Temperature induced migration of activation products
- Agglomeration of activation products at pore surfaces/grain boundaries
- Impact of radiolytic corrosion on release of activation products
- Structural change of irradiated graphite by irradiation

More details can be found in D-4.1.3. It was recognised that the modelling is an important area for future work and an understanding of these issues would aid in the development of future successful treatment options as well as in the development of new graphite grades.

3. Graphite Decontamination by Thermal Treatment

Treatment of neutron-irradiated nuclear graphite is not only a possibility for industrial waste management but also a possibility to study the binding relations and the release mechanisms of radionuclides in neutron-irradiated nuclear graphite. With this information, industrial processes for nuclear waste management can be developed.
A suitable method to study the binding relations and the release mechanisms of radionuclides in neutron-irradiated nuclear graphite is a thermal treatment in inert gases. The use of inert gases inhibits the oxidation of the graphite matrix: only pyrolysis processes or reactions of adsorbed gases can occur. Therefore, the release kinetics of radionuclides from neutron-irradiated nuclear graphite can be investigated.

3.1 Release of Tritium

3.1.1 Background

A theoretical model of Katayama [18] showed that tritium trapped on the graphite surface of a small particle (with diameter in the order of μm) can be removed rapidly even at room temperature, through isotopic exchange reaction with water steam. In the model, even a water partial pressure of 10 Pa could be sufficient to obtain the same removal factors as in the case of a thermal treatment at 900 °C with 100 Pa hydrogen stream. However, tritium trapped the graphite showed to be released only at temperatures higher than 1000 K.
The high mobility of trapped tritium, occurring only at high temperatures, has been discussed previously in another theoretical model from Fromherz at al. [3]
Atsumi et al.[15] developed and validated a model to describe the behaviour of hydrogen in graphite, before and after neutron irradiation, represented in a schematic way in Fig. 3.1.1.

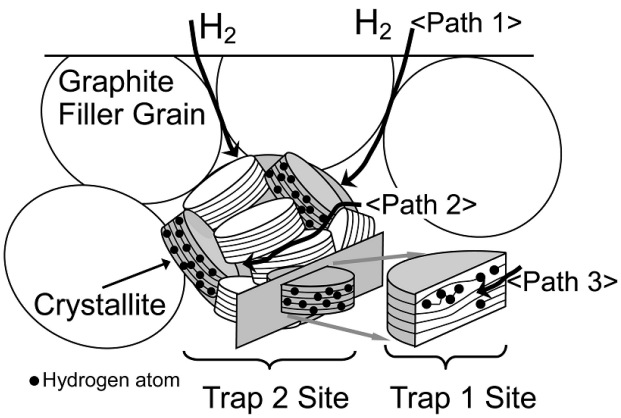

Figure 3.1.1: Model of Atsumi for Hydrogen trapping sites and transport in graphite [31,32]

The model identifies two trapping sites for hydrogen in graphite: interstitial cluster loop edge sites (trap 1) with an enthalpy of 4.6 eV and carbon dangling bonds at edge surfaces of crystallites (trap 2) with an adsorption enthalpy of 2.6 eV. The trap 2 is predominant in unirradiated graphite and it represents normally 80% of the total. In addition, neutron

irradiation showed to increase hydrogen retention up to 100 times more than that in unirradiated graphite, with a prominence of trap 1 sites. [31]
Concerning the hydrogen absorption mechanism, similar but reversed than the desorption one, at the initial stage hydrogen can reach a graphite filler grain through open pores (path 1 in Fig. 3.1.1); then the molecules dissociate into atoms and migrate into a filler grain along graphite crystallites in a sequence of trapping and detrapping (path 2 in Fig. 3.1.1); this stage can be reproduced as a diffusion-controlled process. The last stage of hydrogen migration should be an intercalate diffusion between graphite lamella (path 3): this stage is controlled by the detrapping reactions at trap 2. Trap 1 sites revealed experimentally to be more stable than trap 2, during high temperatures thermal treatments (1550 °C). On the other hand, the desorption process should be controlled by detrapping from Traps 1 and 2, due to a higher energy of trapping (2.6 and 4.6 eV respectively) than the activation energy of diffusion (about 1.3 eV) [34]. More in detail, some Thermal Desorption Spectra of hydrogen from graphite showed two peaks, respectively at 735 K and 1220 K: such results could be interpreted with a diffusion-controlled process. However, the fundamental process of desorption for both peaks would be recombination but, due to the long path to the surface, hydrogen will be successively trapped and detrapped, resulting in an apparent diffusion as the dominant process of desorption. [33]
Even though TDS spectra showed two peaks, it is believed they are actually three: the desorption of hydrogen with an activation energy of 1.3 eV is assumed to be a recombination-controlled process. [33]
In conclusion, three kinds of desorption processes are representative of hydrogen desorption in graphite.
Many experiments on different graphite grades [26, 30] showed that tritium release is, in general, increasing with the temperature. In particular, Fachinger et al. [30] observed a fast initial release of tritium under thermal treatment in argon atmosphere, connected with the desorption from the active superficial sites: tritium desorption was not limited by diffusion in pores; however it was supposed that higher temperatures would have resulted in higher fractional releases. Tritium release from graphite started from 800 °C, increasing with temperature.
From the previous theoretical and experimental findings, it seems that tritium can be released by implying high temperatures.

3.1.2 Release of Tritium during inert gas thermal treatments

Treatment of neutron-irradiated nuclear graphite is not only a possibility for industrial waste management but also a possibility to study the binding relations and the release mechanisms of radionuclides in neutron-irradiated nuclear graphite. With this information, industrial processes for nuclear waste management can be developed.
A suitable method to study the binding relations and the release mechanisms of radionuclides in neutron-irradiated nuclear graphite is a thermal treatment in inert gases. The use of inert gases inhibits the oxidation of the graphite matrix: only pyrolysis processes or reactions of adsorbed gases can occur. Therefore, the release kinetics of radionuclides from neutron-irradiated nuclear graphite can be investigated.

3.1.2.1 Merlin Graphite

In Figure 3.1.2(a-b) the release of tritium from Merlin graphite in inert gases at different temperatures is shown. Several massive graphite samples from the thermal column of the Jülich Material Test Reactor "Merlin" were used (trepanned plug specimens; diameter: 8 mm, length: 37…50 mm, mass: 3-4 g). One can see that the release of tritium depends on the treatment temperature. At 1300 °C, 93.6% of the tritium inventory of the graphite sample was removed within about 10 hours, whereas the mass loss of the graphite matrix was negligible (< 1%).

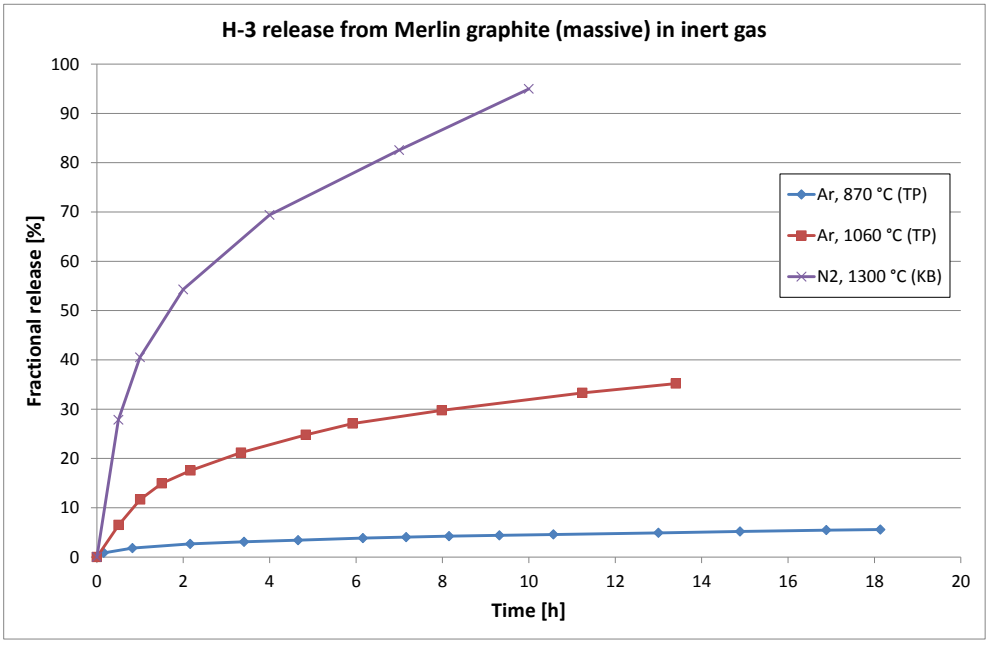

Figure 3.1.2(a): Release of tritium in inert gases at different temperatures

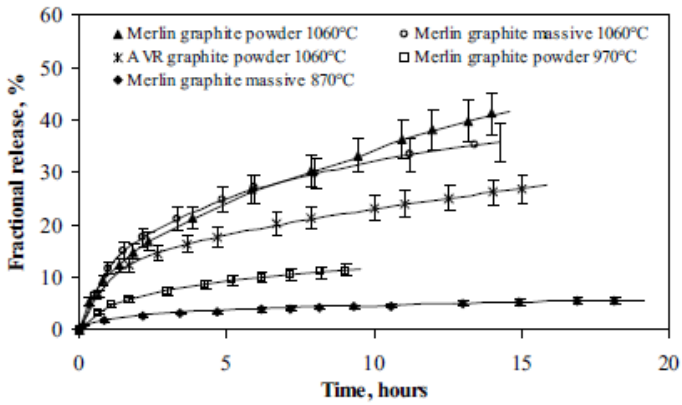

Figure 3.1.2(b): Release of tritium in inert gases at different temperatures

In particular, Fig. 3.1.2(b) is underlining an important aspect: the sample form is of fundamental importance form the point of view of RN release; in particular, comparing the results of the same graphite (Merlin), in powder form and massive form, no difference can be noticed in the removal efficiencies, at the same temperature. It can be concluded, then, that the dimensions/form of the sample is not significant from the point of view of Tritium release. However, it has to be underlined that the pulverization process is likely to free consistent amounts of radionuclides, including Tritium, so a massive sample is advised to be implied.
The release of tritiated water (HTO) from Merlin graphite in nitrogen at 1100 °C plotted as diffusion reaction is shown in Figure 3.1.3. The fit of the data points is a straight line with a correlation factor of 0.9933. This is an indication of a predominant apparent diffusion reaction; it can be explained with a molecular migration process, as stated by Atsumi, in which hydrogen migrates along graphite crystallites in a sequence of trapping and detrapping process: this stage can be reproduced as a diffusion-controlled process [15].

The Tritium release kinetics best corresponds to a diffusion reaction, in accordance with the modelled release mechanism previously described. A first order or a second order reaction is not applicable. However, the graph for a diffusion reaction (fractional release vs. square root time) is not perfectly linear, as can be seen in Figures 3.1.3 and 3.1.4. However, uncertainties must be considered. Moreover, it is reasonable to assume that diffusion is not the only reaction which is taking place and leading to a release of tritium. As tritium must be bound within the graphite matrix in a certain way, additional energy is necessary to remove it from its binding places. Such additional reactions could be: desorption of tritiated water (HTO) and pyrolysis of tritiated hydrocarbons (C─T or C─OT). In addition, the presence of small amounts of oxygen/water in the adduct gases could favour the oxidation of HT to HTO and/or the isotopic exchange respectively. An indication that there are different reactions is given by the observed inversion of the release ratios of HT and HTO: at 866 °C the release of HTO is predominant whereas at 1063 °C the release of HT is predominant. This behaviour is comprehensible by considering that at lower temperatures more HTO is released because desorption requires less energy and that at higher temperatures more HT is released because pyrolysis requires more energy. However, the dependence of HTO/HT ratio with temperature needs more investigations to be confirmed, depending also on the graphite grade and on the controllability of the boundary experimental conditions.

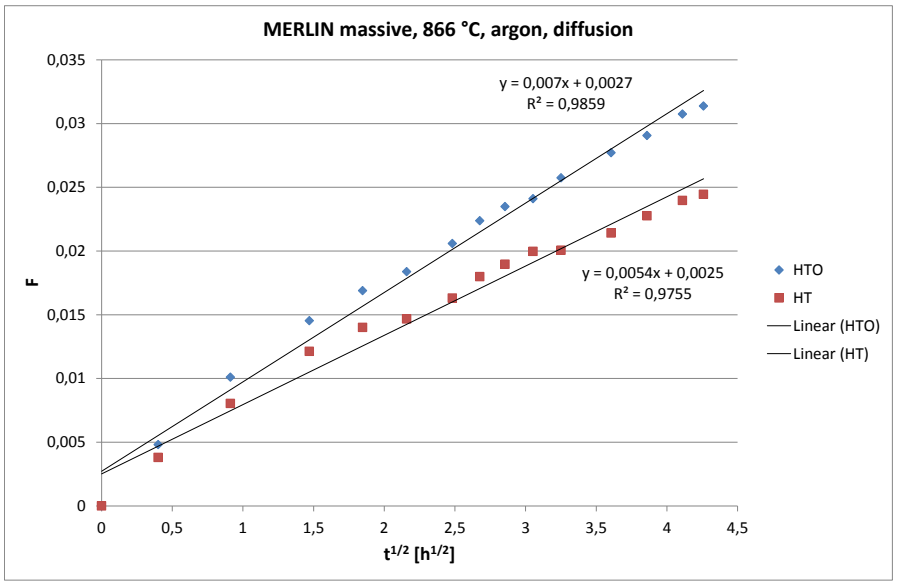

Figure 3.1.3: Release of tritium in argon at 866 °C plotted as diffusion reaction.

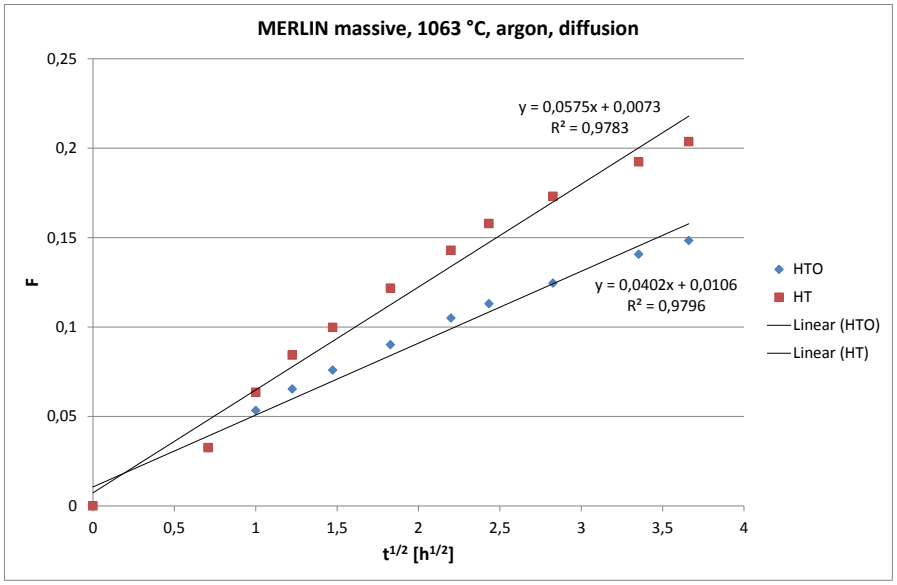

Figure 3.1.4: Release of tritium in argon at 1063 °C plotted as diffusion reaction.

The data from Figures 3.1.3 and 3.1.4 can be used to estimate the activation energy for the apparent diffusion reaction (diffusion plus desorption or pyrolysis). Diffusion is described by the following equation:

$$\frac{\partial c}{\partial t} = D\Delta c \tag{3.1}$$

where D is the diffusion coefficient. The solution of the differential equation presuming spherical pore geometry results in

$$F = \sqrt{\frac{36D't}{\pi}} \tag{3.2}$$

where F is the fractional release of the diffusing material and D' the reduced diffusion coefficient ($D' = D/R^2$, R = diffusion radius). The reduced diffusion coefficient is controlled by temperature according to

$$D' = D'_0 \cdot e^{-\frac{E_D}{k_B T}} \tag{3.3}$$

where E_D is the activation energy for diffusion and k_B the Boltzmann constant. Determining the reduced diffusion coefficient for two temperatures, the activation energy can be calculated by

$$E_D = k_B \cdot \frac{T_1 \cdot T_2}{T_2 - T_1} \cdot \ln\left(\frac{D'_2}{D'_1}\right) \tag{3.4}$$

The tritium releases plotted in Figures 3.1.3 and 3.1.4 are divided into the chemical forms HT and HTO. Therefore, activation energies can be calculated for the release of HT and HTO. The apparent activation energy for the release of tritium as HT amounts to 3.15 eV and as HTO to 2.33 eV. The average amounts to 2.74 eV. This value is in good agreement with Fischer et al. [21] which found 2.78 eV. On the other hand, Atsumi [15] found 2.6 eV. In addition, Atsumi [20] stated that the cristallite-boundary diffusion activation energy of 1.3 eV can be considered only when the trapping effect can be negligible, i.e. when the hydrogen is not significantly trapped e.g. at the edge surfaces of cristallites. The difference between HT and HTO could be explained by different desorption/formation energies of these diffusing species: HTO is possibly only adsorbed on the surface of the graphite particles whereas HT must be formed by pyrolysis. In general, desorption energies are lower than pyrolysis energies. However, more investigations are necessary to better understand whether Tritium is released initially as HT and then partially oxidized to HTO or HT and HTO are formed directly at the sample side, without further significant secondary reactions.

3.1.2.2 AVR graphite

In the AVR, the operational temperatures were rather high (outlet temperature of 950°C[22]) and some of the defects caused by neutron irradiation could be annealed. It is reported in a number of publications that the mobility of hydrogen molecules in undamaged graphite is rather slow [21, 23, 24]. The other reason may be related to the fact that under the high temperature conditions of AVR tritium diffuses inside graphite grains [25, 21], so the fraction that is still present in the graphite is more difficult to be removed due to its more stable nature. Another factor that could influence the more difficult removal of H-3 is the neutron fluence: the higher it is the more are the interstitials/inter-layer H-3 atoms, more stable than the ones laying on the grains boundary (see model of Atsumi [15] for more details). A first calculation of the diffusion coefficient of H-3 for some cases is reported in Table 3.1.1: it can be observed how D is much lower in the AVR case than in the Merlin graphite. A visual on-line comparison of the different results obtained with AVR and Merlin graphite can be observed in Fig.

3.1.2(b). Indicatively, after 10 hours of treatment in argon, a massive sample of AVR graphite can release about 20% of H-3, against about 30% in the case of Merlin.

Type of graphite	Temperature, °C	Diffusion coefficient D, cm^2/s^{-1}
Merlin	870	5.70E-14
Merlin	970	7.40E-13
Merlin	1060	6.19E-12
AVR	1060	1.70E-12

Table 3.1.1: Diffusion coefficients of H-3 at different temperatures for Merlin and AVR graphite [26]

3.1.2.3 Saint Laurent A2 and Oldbury2 graphite

The identification of the driving release mechanisms from the SLA2 and Oldbury2 graphite is much more complex than in the previous cases: the number of variables affecting the graphite behaviour under thermal treatment is considerable, so it is difficult to separate the different effects and histories (temperature, neutron fluence, radiolytic corrosion, etc.). It has to be underlined that the CO_2-cooled graphite has already experienced significant mass losses (up to 40%) during the reactor operation, leading to the removal of the most mobile fractions of both H-3 and C-14. For this reason, it is believed, following the results of the experiments performed in FZJ, that the most stable H-3 (as interstitials for example) and the most stable C-14 (coming probably from the activation of C-13) are embedded in the graphite matrix in a quite stable way, much more than in the other cases reported here.

The release of HTO and HT from Magnox Oldbury 2 graphite in nitrogen at 1100 °C plotted as diffusion reaction is shown in Figures 3.1.5 and 3.1.6, respectively. In both cases, the fit of the data points is a straight line with a correlation factor of 0.9978 and 0.9954, respectively. These reactions are clearly diffusion-like reactions. The removal of Tritium from SLA2 graphite showed similar behaviour (here not reported).

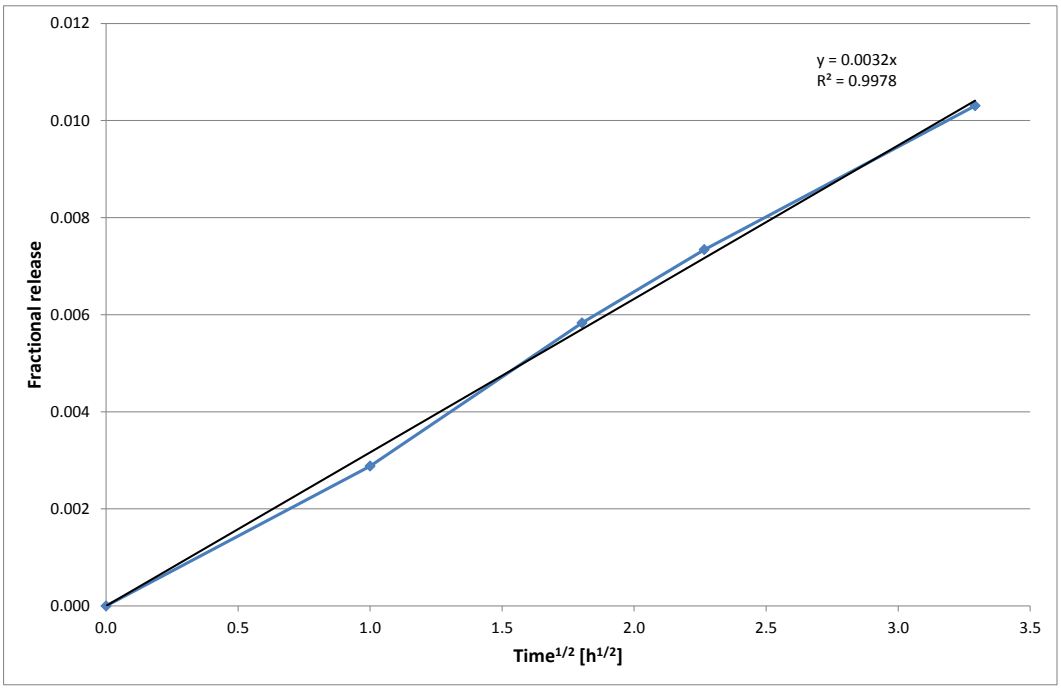

Figure 3.1.5: Release of HTO from Magnox Oldbury 2 graphite in nitrogen at 1100 °C plotted as diffusion reaction.

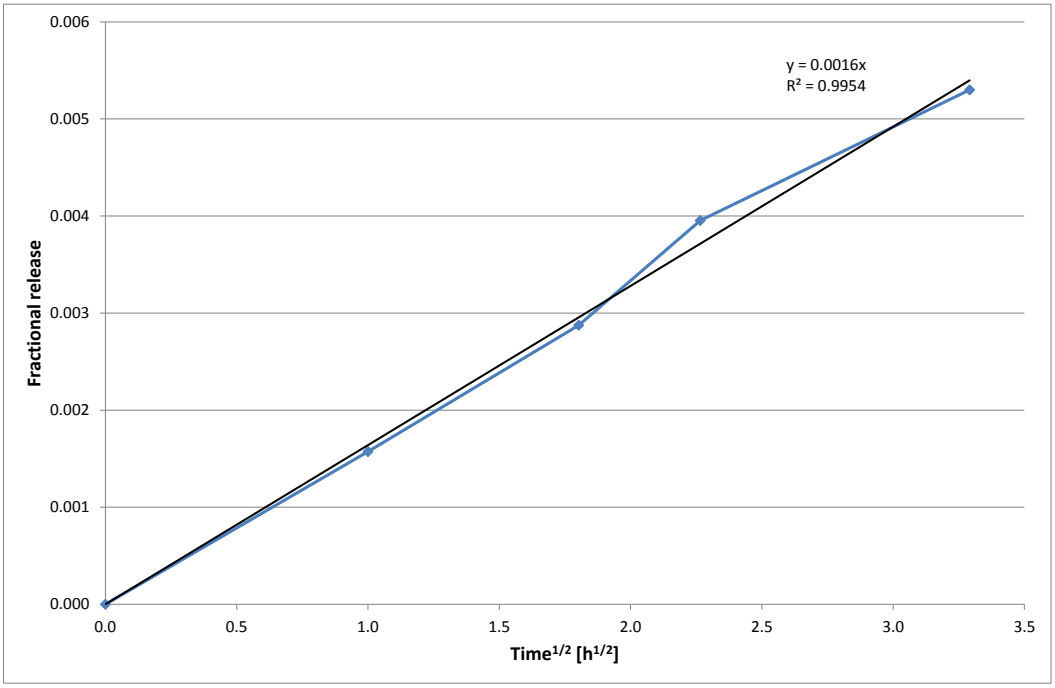

Figure 3.1.6: Release of HT from Magnox Oldbury 2 graphite in nitrogen at 1100 °C plotted as diffusion reaction

3.1.2.4 Decontamination Factors for Tritium in inert gas thermal treatments: a comparison

The decontamination factor is a well-defined parameter in the engineering science, defined by the ratio of initial specific radioactivity to final specific radioactivity resulting from a separation process [27]. The assessment of decontamination factors follows the rule: 1000 and above is excellent; 10 and below is poor [28].
In other words, the decontamination factor is a value higher than 1. "1" means that no decontamination has occurred. The reciprocal of the decontamination factor is the residual relative specific activity.
In the following, Figs. 3.1.7-10 show an overview of the obtained decontamination factors for Tritium in relation to the applied temperature under inert atmosphere.
The uncertainties on the decontamination factors have been estimated, starting from the calibration of the LSC equipment with H-3 and C-14 standards, by performing repeated measures.

Several experiments revealed traces of oxygen in the treatment gases, obtaining de facto a not-ideal inert atmosphere. In a practical situation, an inert atmosphere is really difficult to establish. On the other hand, the presence of small amounts of oxygen could or could not affect significantly the results: the higher the oxygen concentration, the higher the mass loss. In a certain way, "high" or "low" amounts of oxygen are relative so, in general, a threshold cannot be pre-fixed. Experimental results provided in D-4.3.6 revealed that a concentration of 1% O_2 in the adduct gases resulted in high mass losses (>10%), depending on treatment time, temperature and graphite grade. A high mass loss is not preferable for several reasons:

- High mass losses reveal high removal of C-12, which is diluting the removed fraction of C-14; since the most used method for C-14 capture is a precipitation as a carbonate, a high dilution of radiocarbon is producing a higher volume of total "not-concentrated" waste at the end of the process; similar considerations are feasible for isotopic separation. In fact, the intention of a thermal treatment is to remove "selectively" the volatile radionuclides, as much as possible, limiting the corrosion of the graphite matrix.
- Considering, for example, a direct disposal of the graphite, purified from the mobile radionuclides through a thermal treatment, a high mass loss would result in the impairment of the structural characteristics of the interested specimen, leading to easier structural failures and consequently escape of radionuclides.

Following the above-mentioned considerations, a mass loss threshold for an industrial thermal purification process could be fixed to 5%, but it is strongly depending on every single case, so it cannot be assumed as a general constrain. Nevertheless, the mass loss is an important factor that is revealing up to which extent an inert experiment can be considered such.
Another important consideration about the presence of oxygen (or other oxidising agents as water) stands on its effect on the efficiency of radionuclide removal: it is strongly bound with the driving mechanism of H-3 and C-14 removal.
The analysis of the release of H-3 with the temperature can be performed through the Fig. 3.1.7-10. Not considering in detail, for the moment, the oxygen effect, the Tritium removal shows a raising trend with the treatment temperature. Linking this observation to the identified

driving mechanism for Tritium removal, modelled by Atsumi et al [15], high removal efficiencies (and then Decontamination Factors) are expected for temperatures higher than 1200 °C: from this point, the higher the temperature, the shorted is the time necessary to obtain the same results. This finding is in accordance with the Deuterium implantation and thermal treatment investigations performed by N. Toulhoat, N. Moncoffre and Y. Pipon (IPNL-University of Lyon, D-4.2.3). Hypothetically, it seems to be possible to remove practically 100% of H-3 in a selective and efficient way from Merlin graphite (a DF of 30 corresponds to a fractional release of about 97%). One has to be careful before generalising this statement for all the different graphite grades and histories.

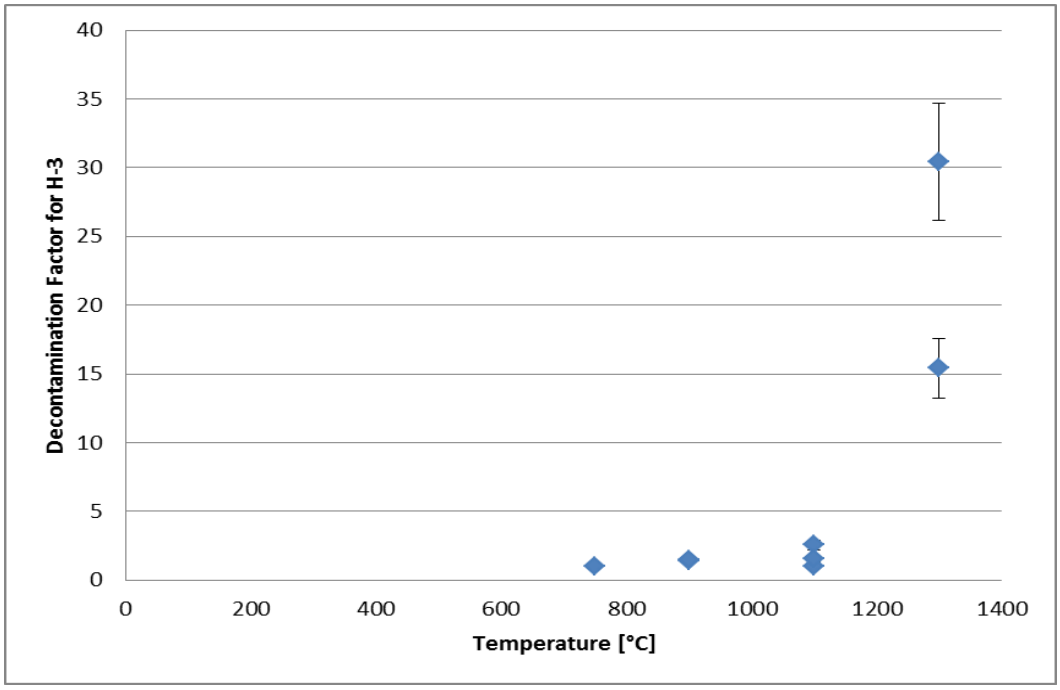

Figure 3.1.7: Decontamination factors of H-3 for Merlin graphite in function of the isothermal treatment temperature

Few Saint Laurent A2 samples were analysed due to several unforeseen problems with the laboratory equipment. In any case, not only for the case of Saint Laurent Graphite, a statistical evaluation is most of the times difficult to establish due to:

- Limited availability of samples
- Consistent amount of variables affecting the results
- Time-consuming procedures and analyses

Despite that, the analysis of Figure 3.1.9 reveals an atypical behaviour under inert gas experiments, compared to the one experienced with Merlin graphite. In particular, despite the presence of oxygen in the adduct gases which resulted in mass losses up to 2.43%, the fractional removal (and consequently DF) of H-3 showed to be really low, for the same temperature applied. As observed for Merlin graphite, the trend of H-3-release is a raising function with the temperature, but the efficiency in this case is very small (fractional removals up to 65% at 1300 °C after 10.5 h treatment, against 97% for Merlin samples).

In order to explain this fact, the historical background of the samples has to be taken into account. It is considered a sample from height 1680 mm, irradiation temperature of 443 °C,

SLA2 sleeve, irradiation atmosphere CO_2. Even though the neutron fluence experienced by the specimen was not the highest, since it was positioned in the lower part of the reactor core, a radiolytic corrosion took place anyway: a direct measurement of that can be performed through the density analyses of the different samples. Even though the values reported in Fig. 3.1.8 are not representative of all the graphite from the same position due to the fact that the measurements were performed with few and small samples, a significant mass loss during operation can be noticed: ~11%. Up to now, the effects of radiolytic corrosion with regards to Tritium (or Radiocarbon) removal have not been investigated. Up to some extent, this phenomenon can be correlated with the effect of oxygen in the adduct gases during a thermal treatment: there is an effect on H-3 removal (better explained in Chapter 3.1.3-5), but it is much weaker than the temperature effect. In the case of radiolytic corrosion, instead, the effect could be relevant even at relatively low temperatures (not sufficient otherwise to remove Tritium), due to the fact that all the open - even micro - pores are filled with CO_2: under neutron irradiation, the corrosion process may occur even in the bulk of the graphite in a "chemical-neutron irradiation regime", removing a significant part of the mobile Tritium. It is believed, then, linking to the model of Atsumi [15], that the H-3 fraction still present in the graphite at the end of the UNGG reactor´s life is the most immobile one, with the highest activation energy for its removal due to its interlayer/interstitial position (about 4.6 eV, according to Atsumi [15]). Consequently, a thermal treatment in inert gas with higher temperatures is necessary to decontaminate the graphite from Tritium in this special case. No data is available for temperatures higher than 1300°C, due to the fact that the available equipment was not designed to work at higher temperatures.

Density of Virgin SLA2 sample	Density of SLA2 h.1680mm sample	Density of SLA2 h.5120mm sample
~1.69 g/cc	~1.61 g/cc	~1.51 g/cc

Table 3.1.2: Comparison among sample densities before and after irradiation in the reactor core. Indicative values.

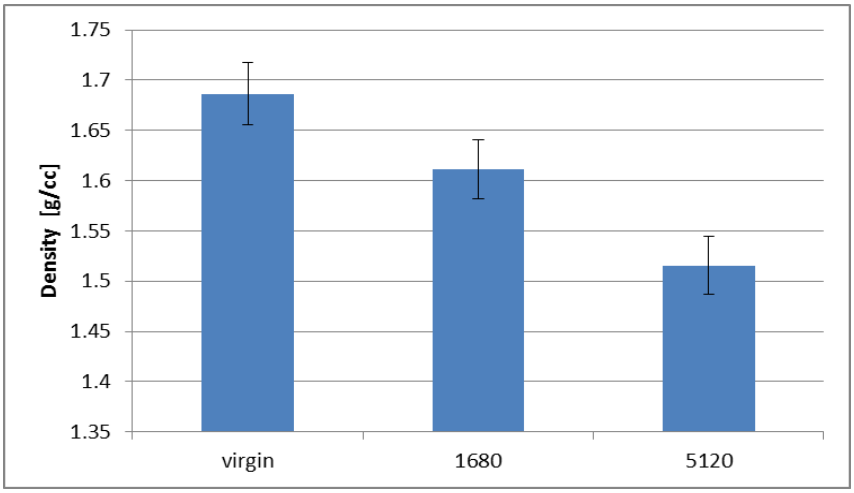

Figure 3.1.8: Comparison among sample densities before and after irradiation in the reactor core at vertical position 1680 mm and 5120 mm, SLA2 sleeve graphite. Indicative values.

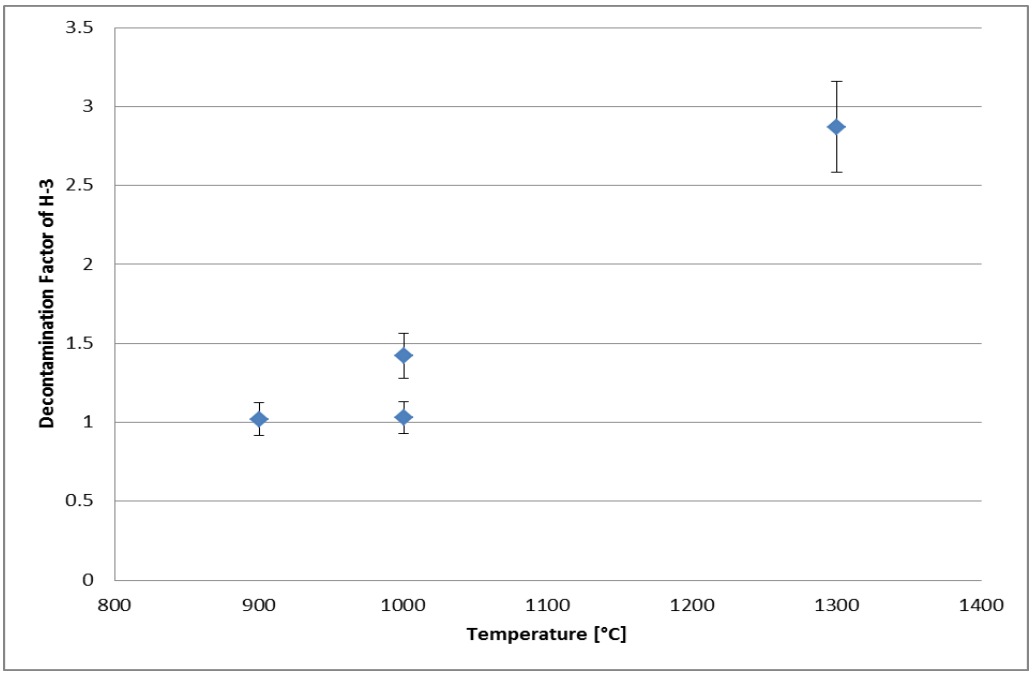

Figure 3.1.9: Decontamination factors of H-3 for SLA2 graphite in function of the isothermal treatment temperature

A similar behaviour to the SLA2 graphite has been experienced with the Oldbury 2 graphite. The Tritium release is quite limited (see Fig. 3.1.10): a possible explanation of such behaviour is similar to the considerations performed for SLA2 graphite. Some preliminary calculations of the mass loss during operation revealed up to 40% mass loss; in other words, a strong corrosion took place during operation and it is reasonable to expect a significant removal in-situ of C-14 and possibly H-3. No detailed studies are available in order to better understand the effect of radiolytic corrosion with regards to H-3 and C-14 removal.

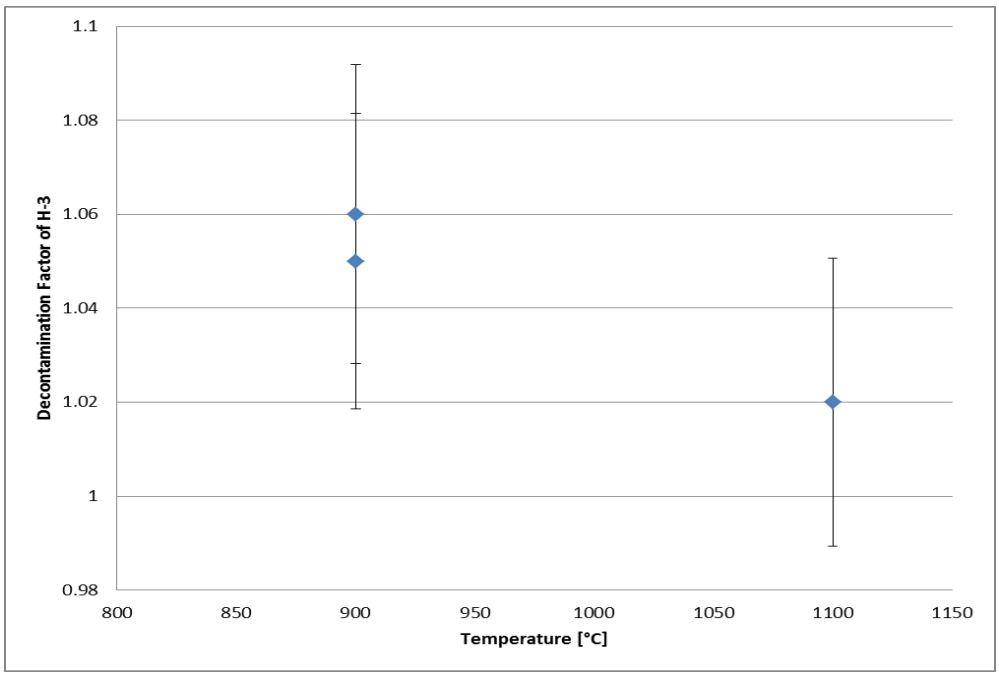

Figure 3.1.10: Decontamination factors of H-3 for Oldbury 2 graphite in function of the isothermal treatment temperature

In the case of AVR graphite, a particular behaviour in a middle way between Merlin and UNGG/Magnox graphite is observed. For example, tritium is removed up to 27% (DF=1.4) after 15 hours of treatment at 1060°C: this difference can be explained by the different operational conditions. The average gas-outlet temperature of the AVR was about 950°C [29], in Merlin reactor the operational temperature of thermal columns was the ambient one and in the UNGG/Magnox reactor the temperature was in the middle, depending on the sample´s position in the core, up to 446°C. Nevertheless, in Fig. 3.1.11 it is possible to observe that a raising trend of Tritium release with the temperature is still present, even though the removed fraction is much lower than the one in the case of Merlin graphite. Also in the present case, the traceability of the samples represented a problem, so the temperature and neutron dose is not known precisely.

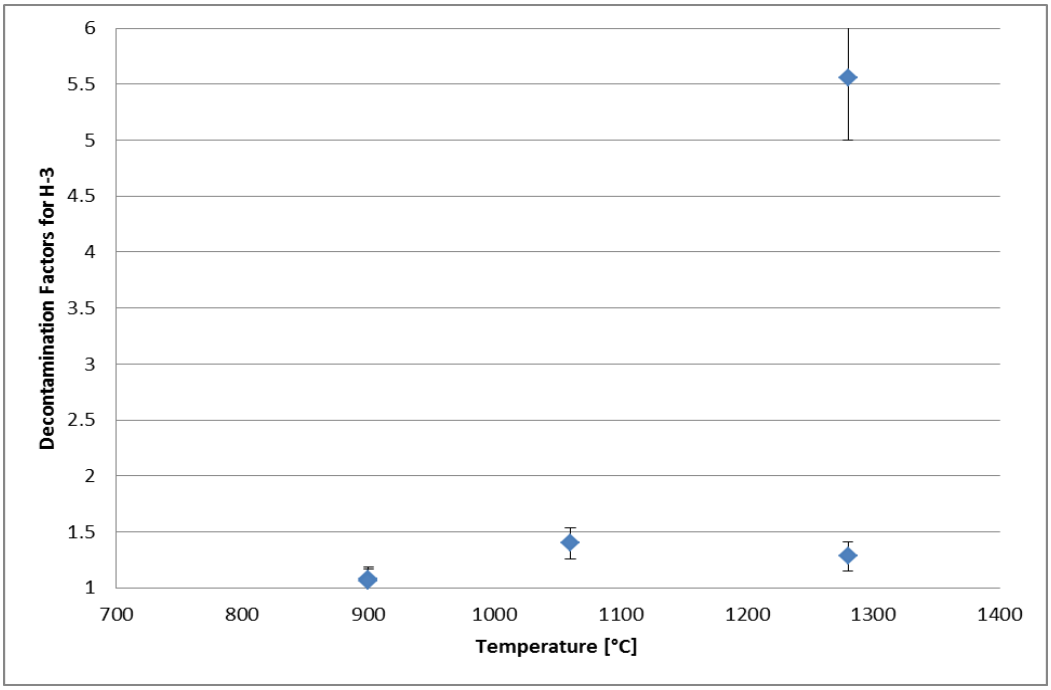

Figure 3.1.11: Decontamination factors of H-3 for AVR graphite in function of the isothermal treatment temperature

3.1.3 Release of Tritium during thermal treatments with Oxygen/Nitrogen

Thermal treatment experiments of i-graphite under gaseous conditions ranging from 0.1 to 1% oxygen could an option for conditioning i-graphite for final disposal. Results showed that radionuclides can be separated from the graphite body via this technique.

As reported in the previous sections, obtaining absolute inert conditions is quite difficult. The release mechanism for H-3 seems to fit well with the model of Atsumi [15], i.e. a similar diffusion driven mechanism. Considering then the additional presence of oxygen, it is interesting to understand the related effects, considering small quantities in the adduct gases. A "standard" experiment is repeated with graphite coming from similar positions of the Merlin reactor´s thermal column: in the first one a relatively low amount of oxygen was introduced (around 1400 ppm), while in the second one a higher amount was adopted (estimated around 3700 ppm). It is reasonable to expect, with equal treatment´s boundary conditions (e.g. temperature, heating rate, gas flow, etc.), higher mass loss with higher oxygen concentrations: it was measured, in fact, a mass loss of 0.9% against 2.43% for the same treatment time. A direct consequence of an enhanced corrosion of the graphite bulk, due to the presence of oxygen, is a lower selectivity on the removal of e.g. Tritium. Nevertheless, not considering the mass loss, taking into account the uncertainty of the measurements, there are small differences between the two curves: this fact can lead to thinking that H-3 removal is slightly influenced by the presence of oxygen (see Fig. 3.1.14 for comparison).
Another experiment, performed in previous times in inert gas, showed a sudden ingress of oxygen (of unknown amount) resulting in visible changes in the release curves (see Fig. 3.1.12): the increase in the on-line tritium release curve showed to be small compared to the similar, but pronounced, effect on radiocarbon removal (see Fig. 3.1.13).

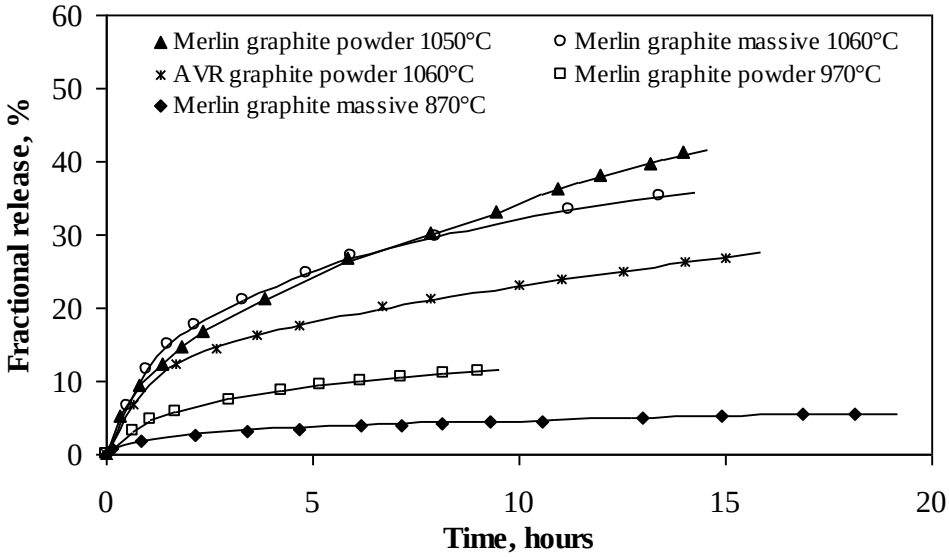

Figure 3.1.12: Tritium release in argon atmosphere: a small ingress of oxygen occurred after 8-9 hours during the experiment "Merlin graphite powder 1050°C" [26]

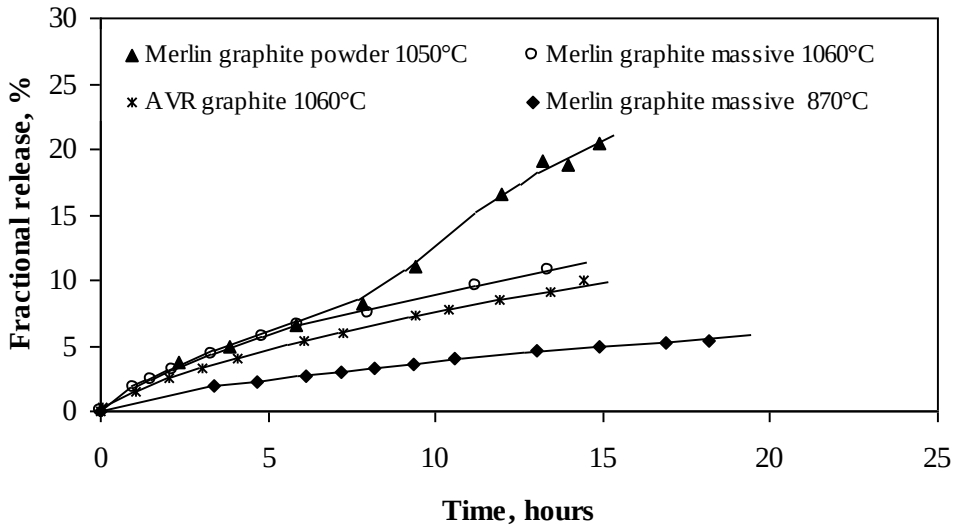

Figure 3.1.13: ^{14}C release from AVR and Merlin graphite in argon: a small ingress of oxygen occurred after 8-9 hours during the experiment "Merlin graphite powder 1050°C" [26]

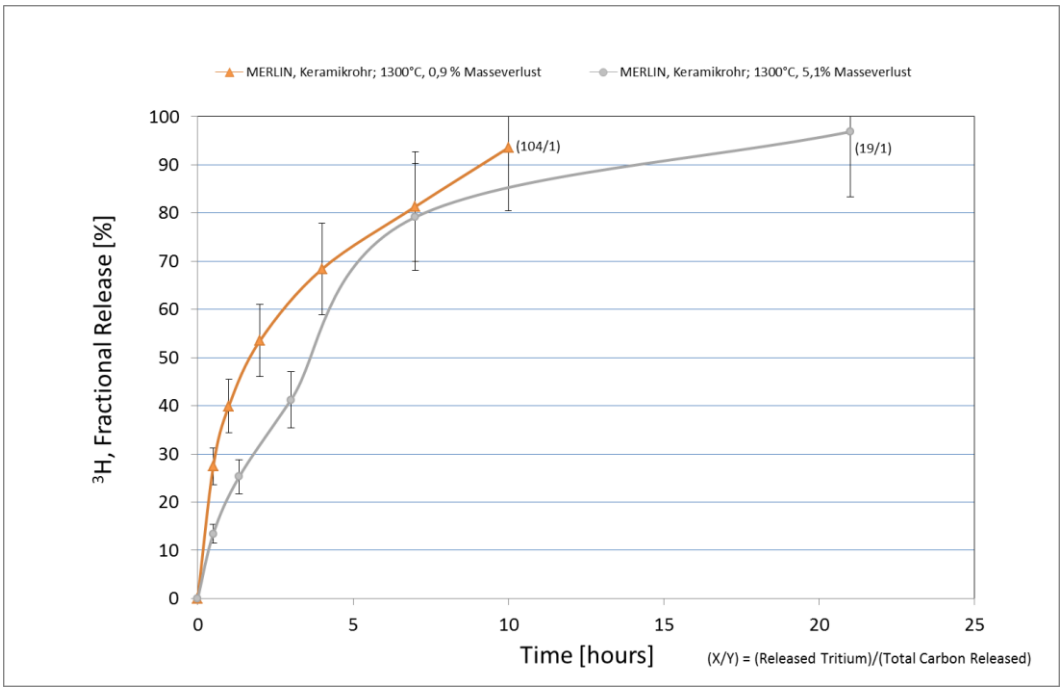

Figure 3.1.14: Comparison among two tritium release curves from similar experiments, with different oxygen amounts in the adduct gases

In conclusion, it can be stated that small amounts of oxygen in the adduct gases are not effective from the point of view of H-3 removal, considering a continuous thermal treatment with steady conditions; on the contrary, the increased corrosion of the graphite bulk results in lower enrichment of the removed H-3 and, consequently, in a lower efficiency of the selective extraction process. The driving removal mechanism seems to be in agreement with a diffusion-like one, as modelled by Atsumi [15].

3.1.4 Release of Tritium during thermal treatments with water steam

An option for graphite thermal treatment involves the usage of water steam as reactive gas. The regimes taking place in the porous graphite are the same as the ones for the oxygen, but the temperature thresholds are shifted towards higher values (roughly 300 °C higher).
The steam reforming treatment consists in reacting water steam on i-graphite in order to oxidising carbon through, e.g., the following reactions:

$$C + H_2O \leftrightarrow CO + H_2 \quad \text{(primary reaction)} \quad (3.5)$$
$$CO + H_2O \leftrightarrow CO_2 + H_2 \quad \text{(secondary reaction)} \quad (3.6)$$
$$C + 2\,H_2 \leftrightarrow CH_4 \quad \text{(secondary reaction)} \quad (3.7)$$
$$2\,CO \leftrightarrow C + CO_2 \quad \text{(secondary reaction)} \quad (3.8)$$

The process has to be controlled in order to limit the oxidation rate, otherwise a complete gasification of the sample will take place without any selectivity on the removal of radionuclides. The parameters of the treatment process are several: pressure, temperature, gas flow, humidity, treatment time. The available equipment in FZJ allowed preliminary optimization of some parameters, as e.g. humidity and temperature, by performing several experiments on virgin materials. The unavailability of samples of all the graphite grades constituted a problem from the statistical point of view; because of that, further optimizations should be performed with the target materials, starting from the virgin ones and, at the end, using irradiated graphite.

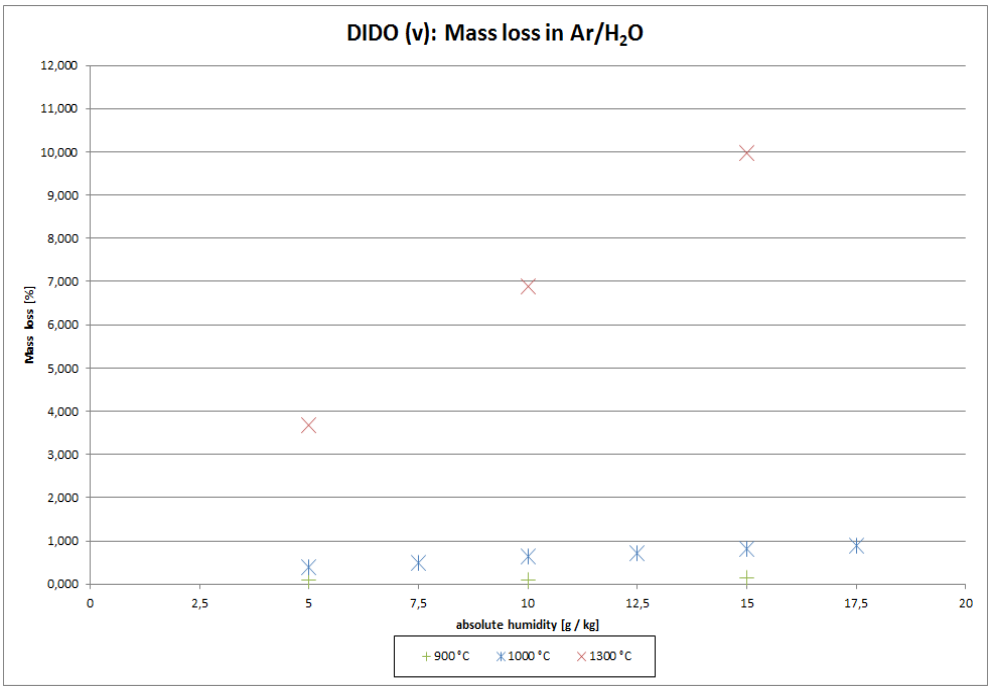

Figure 3.1.15: Mass loss of DIDO virgin graphite at different temperatures and humidity, 2 h isothermal

Following the preliminary experiments, the temperature of 1000°C was chosen for the treatment, with an absolute humidity of 10 g/kg (in argon), in order to have limited mass losses during the treatment.

From the point of view of Tritium removal it was expected from the very beginning to have an increased release due to the addition of water steam, favouring in such a way isotopic exchange reaction(s) on the one hand and diluting the radionuclide on the other hand.

3.1.4.1 Merlin Graphite

The applied procedure for the thermal treatment process consisted on reaching the maximum temperature in inert atmosphere (Argon) and then injecting the steam in the gas flow. In such a way a direct on-line confirmation of the effect of steam on the Tritium release can be highlighted by Figs. 3.1.16-17.

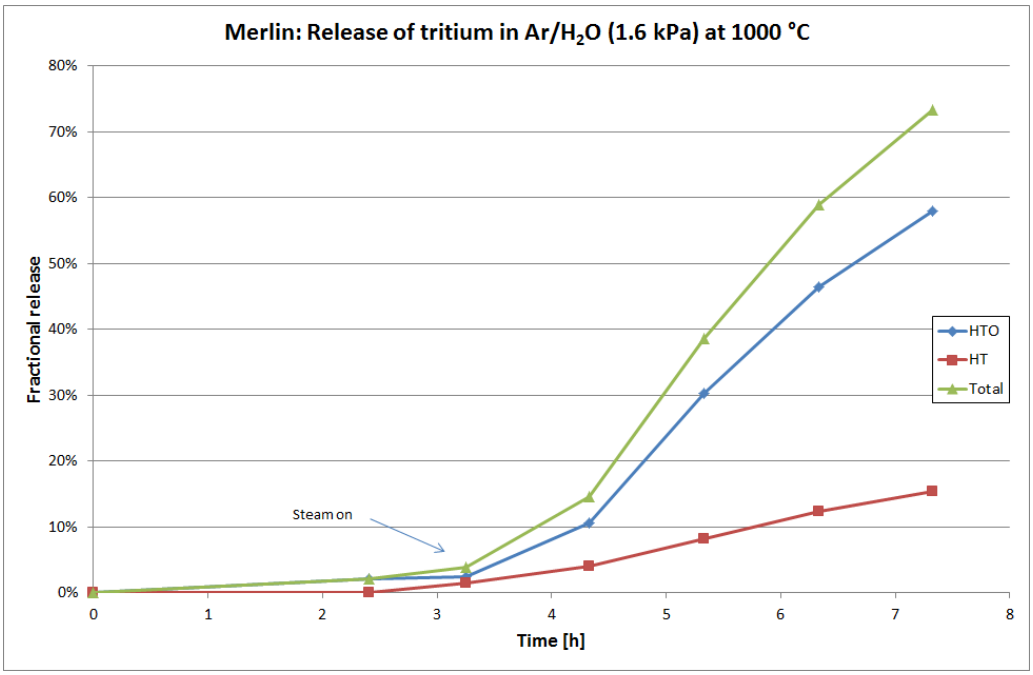

Figure 3.1.16: Release of Tritium from Merlin-1 sample (mass loss after 4 h of isothermal steam reforming: 1.45%)

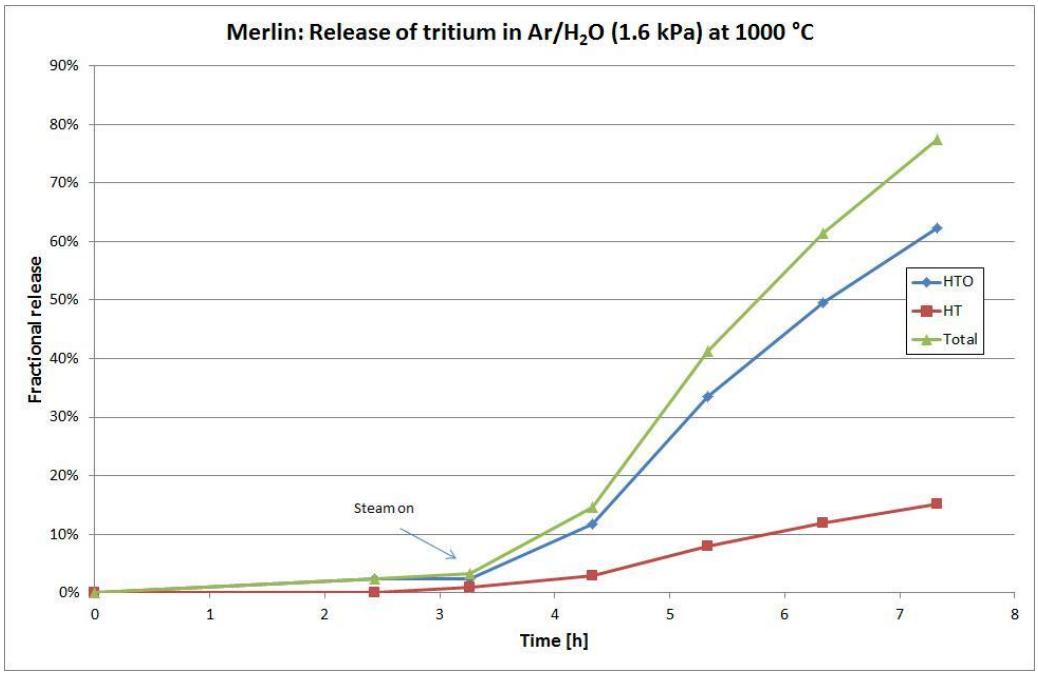

Figure 3.1.17: Release of Tritium from Merlin-2 sample

A general comparison among the release curves of Tritium reveals no significant differences. It can be stated that most of the release is based on the isotope exchange reaction(s) (see Eq. 3.5-8). Some isotope exchange reactions involving graphite surfaces are:

$$HTO_{(g)}+(-CH)_{(surface)} \Leftrightarrow H_2O_{(g)}+(-CT)_{(surface)} \quad (3.9)$$

$$HTO_{(g)}+(-C\text{-}OH)_{(surface)} \Leftrightarrow H_2O_{(g)}+(-COT)_{(surface)} \quad (3.10)$$

$$HT_{(g)}+(-CH)_{(surface)} \Leftrightarrow H_{2(g)}+(-CT)_{(surface)} \quad (3.11)$$

$$HT_{(g)}+(-C\text{-}OH)_{(surface)} \Leftrightarrow H_{2(g)}+(-COT)_{(surface)} \quad (3.12)$$

Moreover, further reactions in the gas phase cannot be excluded. The hypothesized reaction mechanism is the Langmuir-Hinshelwood one, where a first adsorption of reactants take place, followed by the chemical reaction with the carbon atoms and by the desorption of the products. However, the Eley-Rideal mechanism cannot be excluded, depending on the availability of surface area and relative active sites. Further investigations could clarify the reaction mechanism.

An open issue is the original chemical form of Tritium: how is it present in the graphite? In what chemical form it is released? The collected data (See e.g. Fig. 3.1.17) revealed a marked predominance of HTO and a minor presence of HT. However, it cannot be excluded that secondary reactions occurred, so it is possible that a major fraction in form of HT was originally released. Further investigations should clarify this point, since a recycling of the radionuclide could be possible.

Katayama and Nishikawa [18] performed a study on the release behavior of tritium from graphite particles by isotopic exchange; one of the main findings was the predominance of reactions (Eq. 3.9-10) compared to reactions (Eq. 3.11-12): a partial pressure of 10 Pa partial pressure of water at room temperature was removing the same tritium as 100 Pa partial pressure of hydrogen at 900°C. However, the effect focused mainly on the superficial tritium, since its migration at low temperatures is negligible. Nevertheless, the predominant effect of water compared to hydrogen points in the direction of its implication in small quantities as an

effective removal agent. The minimum amount of water vapour to be used in the gas stream during thermal treatment still needs to be optimized in order to limit as much as possible the dilution of the radionuclides.

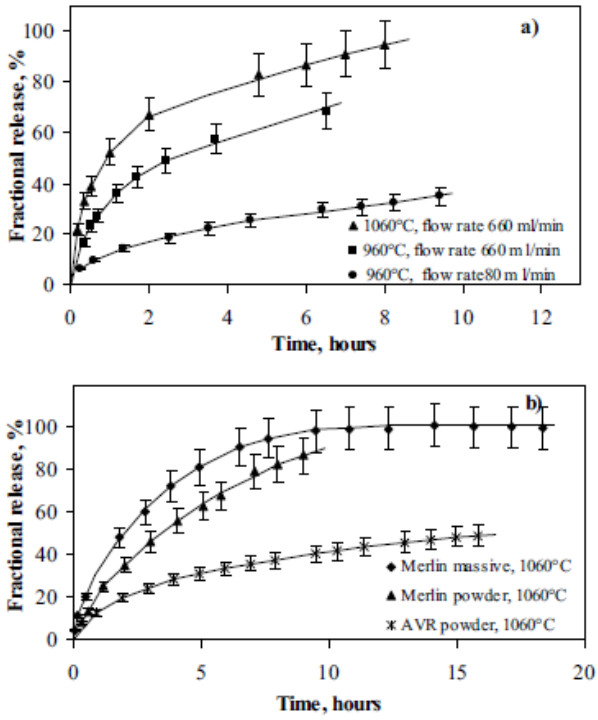

Figure 3.1.18-19: Release of Tritium from Merlin and AVR graphite:
18 – Tritium release from Merlin graphite powder during oxidation at saturated water vapour pressure 7.4 kPa;
19 – Tritium release from Merlin and AVR graphite at 1060°C and saturated water vapour pressure 2.3 kPa.[26]

Tritium release from Merlin graphite powder at temperatures of 960°C and 1060°C during oxidation with water steam at a vapour pressure 7.4 kPa is shown in Figure 3.1.18 (a). At 960°C experiments were performed at two different flow rates of carrier gas. The influence of flow rate on ^{3}H release was observed: the increase of argon/steam flux from 80 mL/min to 660 mL/min gives a more than twofold increase of tritium release from 30 % to 65 %. The sample mass loss in these experiments was 3.2 and 4 %, respectively, which is higher in comparison with graphite treatment in argon atmosphere. At 1060°C, about 90 % of the total tritium inventory was removed from Merlin graphite after 8 hours accompanied by a sample mass loss of 32 %.

The results of graphite treatment at lower water vapour pressure (2.3 kPa) are shown in Figure 3.1.18 (b). One can see that the same amount of tritium was released from Merlin graphite at the temperature of 1060°C after 8 hours as in the experiment with water vapour pressure 7.4 kPa (Figure 3.1.18 (b)). The corresponding sample mass loss was 22%. This fact is an indication that the isotopic exchange reaction(s) is not limited by the amount of water vapour present in the pore system during the treatment or, on the other hand, is presenting the same exchange rate after a certain threshold: a small amount of vapour is sufficient to remove tritium with the same efficiency. This value still needs to be minimised, in order to remove the tritium in a fast and efficient way, without oxidising significantly the graphite.

3.1.4.2 AVR graphite

In the case of AVR graphite the fraction of released tritium is lower than the one in the experiments under inert atmosphere, as well as the one from Merlin graphite (see Figs. 3.1.18-b and 3.1.12). As an indicative comparison, 10 hours at 1060°C with 2.3 kPa steam partial pressure resulted in about 40% of H-3 removal for AVR, against 90-100% for Merlin graphite in the same conditions. This fact can be directly linked with the model of Atsumi [15] and the irradiation conditions: high temperatures, inert atmosphere and possibly high neutron damage; in such conditions the most mobile tritium is diffusing, while the most stable one (with an estimated activation energy of 4.6 eV) is supposed to be more stable inside the graphite. This observation is resulting, from a thermal treatment point of view, in higher temperatures necessary to mobilise it with reasonable diffusion coefficients and, then, reasonable treatment times.

3.1.4.3 Saint Laurent A2 graphite

In the case of SLA2 graphite some experiments were performed in FZJ with the following parameters: maximum temperature 1000°C, flow 60 mL/min, 10 hours isothermal. The on-line H-3 release is shown in Figs. 3.1.20-21. Samples were taken from two different positions in the reactor, in the graphite moderator. This case is the only one on which samples were properly traced. Sample R1 came from the bottom side of the reactor, irradiated at 443°C, while sample R4 came from the middle of the reactor, irradiated at 391°C. Accordingly, the most active sample was R4, with a dose rate more than double than sample R1. Experiments with SLA2 graphite were performed from the beginning with water steam; the regime temperature was reached at 3h15´.

Figure 3.1.20: Release of tritium in Ar/$H_2$0 1.6 kPa at 1000°C, SLA2 R1 sample

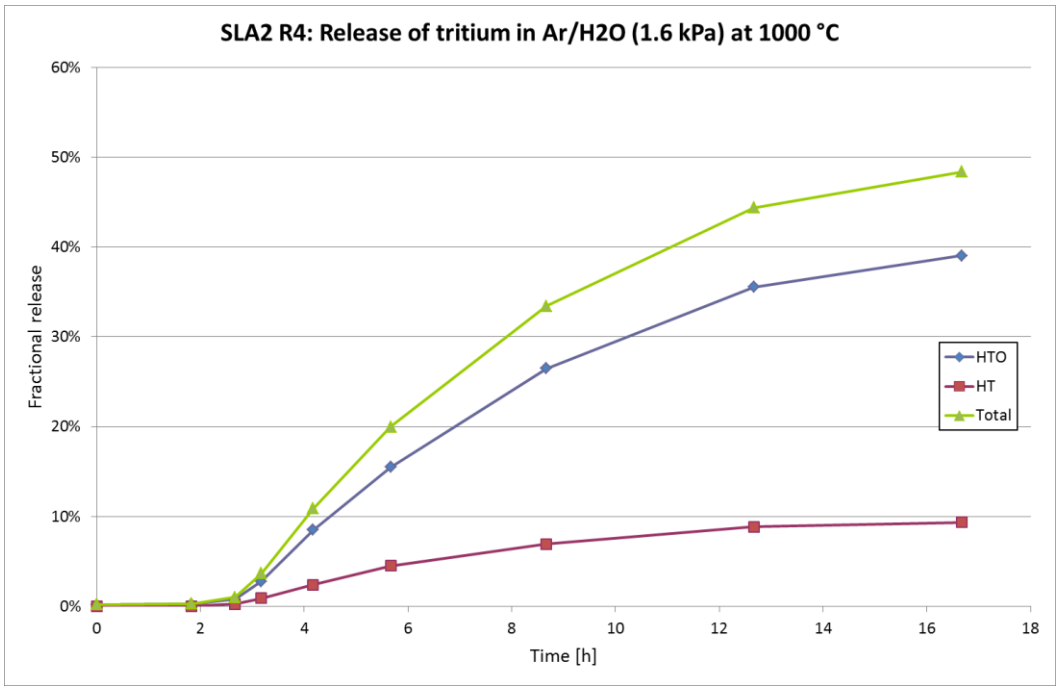

Figure 3.1.21: Release of tritium in Ar/H_20 1.6 kPa at 1000°C, SLA2 R4 sample

A comparison among the releases from Figs. 3.1.20-21 allows identifying higher fractional releases in the case of the most irradiated sample (48%±5% against 37%±5%). This fact could be directly linked to the neutron fluence, but the amount of the investigated samples is not sufficient to perform this correlation from a statistical point of view. In addition, the radiolytic corrosion must not be neglected. The mass loss after 10 hours of treatment revealed to be nearly the same in both cases: about 2.2%±0.1%.

In line of principle, a higher reactivity would be expected from the most irradiated sample due to the higher specific surface area caused by radiation damage. Accordingly, it is very probable that the most significant influence on the reaction rates and removal behavior of ^{14}C and ^{3}H from SLA2 graphite is the neutron fluence, coupled with the radiolytic corrosion: such corrosion is higher in SLA2 R4 than in SLA2 R1 and correlates directly to the neutron fluence. In fact, on the one hand a higher surface area is produced due to neutron irradiation, while on the other hand a corrosion process is taking place, leading to releasing of radionuclides in-situ. An indication on the importance of the two effects, coming from the results obtained in FZJ, seems to point in the direction of neutron fluence predominance; however, more experiments are necessary in order to confirm such a statement and to have statistically valuable results.

3.1.5 Comparison of Tritium removal in different regimes

The application of a continuous process with constant parameters revealed several facts, here reported. For a comparison of different treatments, only Merlin Graphite is here considered. In the case of inert gas thermal treatments the removal of Tritium showed to be higher, for the same amount of time, for higher temperatures. The enrichment, as can be seen in Fig. 3.1.22, is quite high (green curve, 1300 °C) when the adduct gases are relatively clean: this can be verified by the obtained mass loss. In the present case, an example of unclean gases is the blue line in Fig. 3.1.22: the mass loss after 10 hours is about 1.4%, much higher than the 0.2-0.4% obtained in all other cases. In addition, massive samples revealed higher selectivity for what concerns Tritium removal.

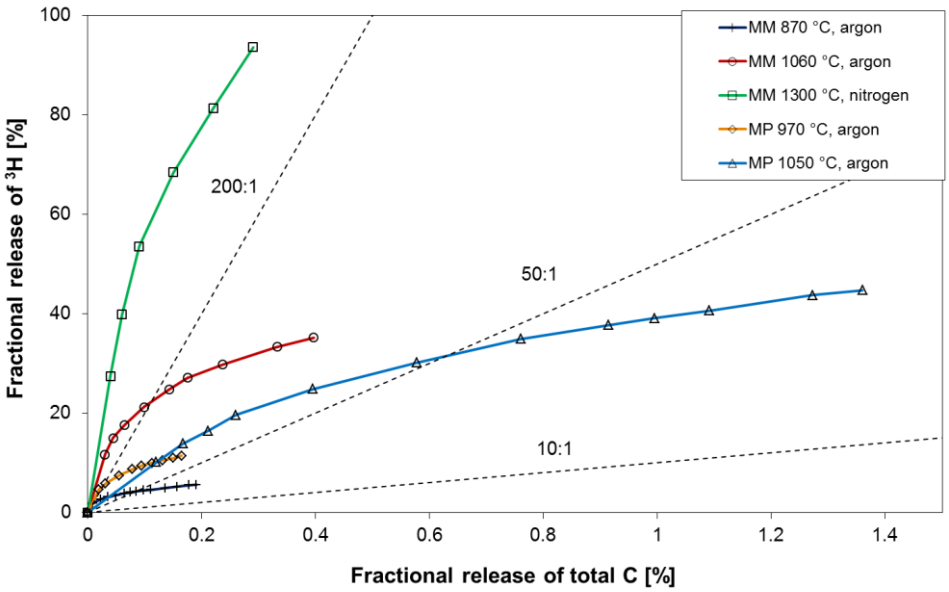

Figure 3.1.22: Overview of Tritium removal against mass loss for different samples and temperatures in inert gases

A comparison with a similar treatment in water steam, with same treatment time and temperature, reveals the fact that the usage of steam (10 g/kg or 1.6 kPa of partial pressure) is accelerating the release: 70-80% of Tritium was released within 4 hours at 1000°C in steam against a fractional removal of 20-25% in pure argon at the same temperature.
On the other hand, the same fractional release can be obtained at lower temperatures in the case on which steam is used. This can be observed in Fig. 3.1.23: high releases can be obtained even at temperatures lower than 1000°C. The release of Tritium is faster in the case of water steam, due to the acceleration of the migration process in the presence of isotope exchange reactions. The optimization of the treatment parameters still has to be done, but some indications can be obtained from the collected data: lower temperatures are favouring Tritium release in a selective way, since the steam concentration profile in the sample is approaching the idealistic "regime I"; unfortunately, water-graphite reactions are not significant for temperatures lower than 800°C, without catalysts. Lower temperatures are allowing lower reaction rates on the one hand, lower migration of interstitials on the other hand, but the "superficial" Tritum on the surfaces accessible to steam can be isotopically exchanged, resulting in the end with higher enrichment of H-3 in the off-gases (see Fig. 3.1.23, blue and purple line). However, the

removed fraction is expected to be lower than the cases at higher temperatures, for the above-mentioned reasons: the selection of the optimal parameters depends on the graphite history. Another important indication coming from the collected results is related to the sample shape: massive samples are releasing H-3 in a more selective way, probably due to the higher surface area of powder samples, resulting in higher corrosion rates. Higher temperatures and flows are favouring H-3 release, but the mass loss becomes significant.

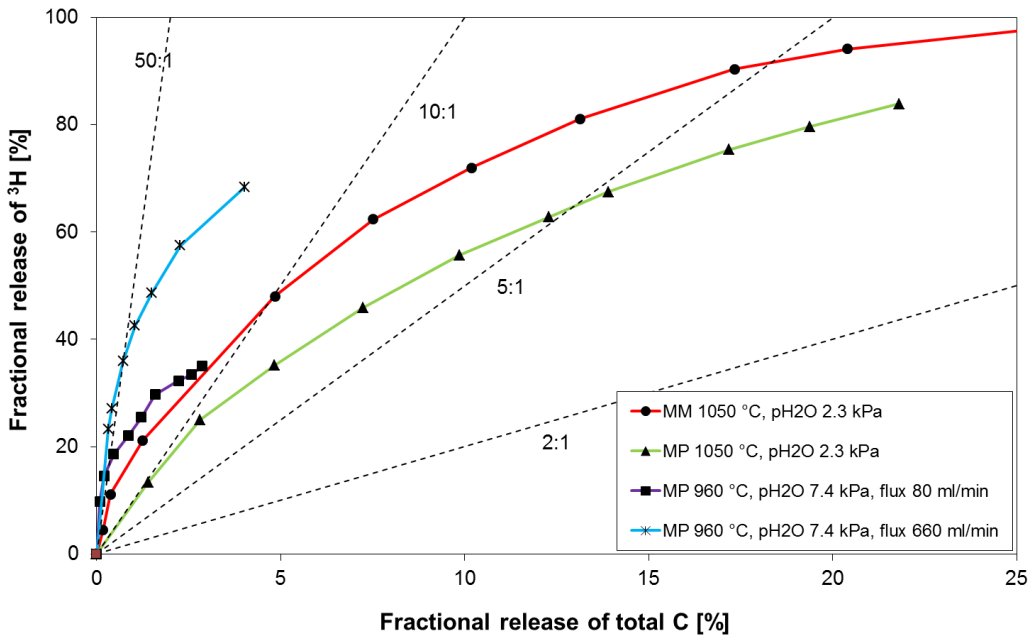

Fig. 3.1.23: Overview of Tritium removal against mass loss for different samples and temperatures

The application of steam is favouring tritium removal only in the last step of the removal process (see scheme in Fig. 3.1.25 [15]), i.e. molecular diffusion: when tritium has already migrated to the grain surface, the presence of water is going to influence its removal, resulting in a faster release, depending on the applied temperature and steam partial pressure. In particular, three different factors can be identified:

- *Temperature Effect*: As observed in the inert gas thermal treatments, the diffusion-like process is governed by temperature. All steps of tritium removal are involved, starting from the interlayer migration of interstitials, detrapping at the crystallites and diffusing toward the grains and finally to the gas phase.
- *Corrosion*: Depending on the applied temperature and steam partial pressure, a regime will establish in the graphite, with a consequent steam concentration profile (see Fig. 3.1.24). Assuming regime II, i.e. in-pore diffusion controlled regime, occurring between 800°C and 1250°C, the inner part of the sample will be interested by reactions in a lower extent than the outer part, depending on the sample size and temperature. The macro/microscopic corrosion is leading to remove tritium together with carbon; in Fig. 3.1.25 one can observe how the presence of a corrosion process is partially favouring the tritium removal, even though in a less enriched way, in particular in the first two steps and partially in the third, starting from the left side.

- *Steam*: The presence of steam, with a more or less pronounced concentration profile, is favouring isotopic exchange reactions. The contact among water and Tritium is favoured in the first two steps in Fig. 3.1.25, and partially in the third one.

For what concerns the water steam treatment, in conclusion, the process is driven by three interconnected mechanisms of different importance, i.e. temperature with presence of steam as first and corrosion as second.

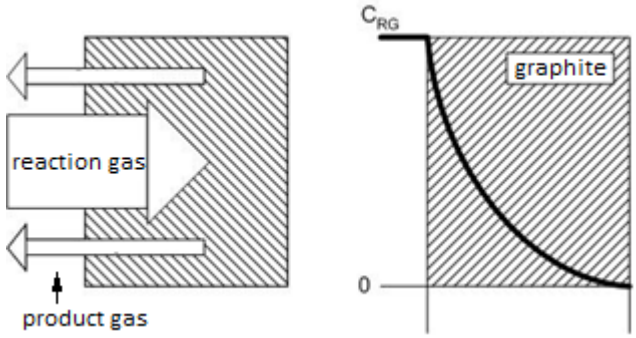

Fig. 3.1.24: Schematic representation of regime II, in-pore diffusion controlled regime

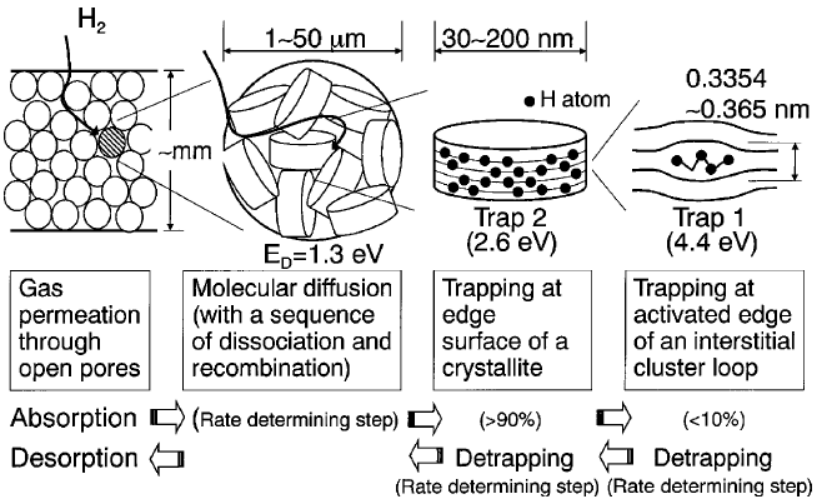

Fig. 3.1.25: Schematic illustration of the model proposed by Atsumi on hydrogen trapping and transport in a graphite material [15]. The reported values are not the most recent ones (e.g. 4.4 eV instead of 4.6) and the percentages (90%,10%) are referred to unirradiated graphite.

A comparison of the identified effects with other treatments is revealing that:

- Oxygen treatment, especially in regime II and III, is not a good option for Tritium removal since the main effect is a simple corrosion of the graphite, followed by a less important Tritium diffusion due to the applied temperature.
- Inert gas treatments are difficult to obtain with “chirurgical” boundary conditions. However, the presence of small amounts of impurities is of minor effect for what concerns Tritium removal. The main driving mechanism in this case is the temperature effect, resulting in higher and faster removal at higher temperatures, with results depending on the relative abundance of different trapping sites with different activation energies.
- Steam treatments are removing higher amounts of Tritium at lower temperatures due to the triple effect of temperature-corrosion-isotopic exchange. However, a diluted radionuclide is obtained at the end, with mass losses that could be limited. The

optimization of process parameters will lead to removing H-3 in an optimised way with low mass losses and limited dilution, in reasonable times from the industrial point of view.

In conclusion, one of the promising treatments for tritium removal is implying high temperatures and argon (or nitrogen) atmosphere, to obtain at the same time high fractional releases of tritium and low graphite burn-off. The usage of Nitrogen as purge gas must be cautiously considered for temperatures higher than 1200-1300°C.

The removal efficiency is expected to be high for not-corroded graphite that experienced low irradiation temperature and relatively low neutron fluence. As the neutron fluence rises – directly correlable to some activation products as Co-60 – the presence of interstitial atoms increases, leading to higher activation energies for Tritium removal. The temperature during operation is of fundamental importance under many aspects:

- Wigner energy can be prevented/released at medium temperatures, possibly with "roasting" cycles if the operational temperature is too low (e.g. ambient temperature);
- Low operational temperatures do not allow the migration of interstitials, so it can be assumed that most of the tritium will stay in the graphite (Merlin); Medium/high operational temperature will allow annealing of defects and migration of some radionuclides (AVR). High-temperature-irradiated not-corroded graphite (as in AVR) showed lower decontamination factors due to the fact that high temperatures favoured the migration of Tritium during reactor operation; it is hypothesised that the remained Tritium is more stable (e.g. present as interstitial), fact confirmed by several experiments: higher temperatures are necessary for its removal. Moreover, it cannot be excluded that part of the Tritium diffused towards the carbon-brick insulation barrier of the reactor.
- The presence of radiolytic corrosion heavily influences the graphite behaviour under thermal treatment and consequently under disposal conditions. It is reasonable to expect that the most labile fractions of C-14 and H-3 have been already removed in an enhanced way during reactor operation (UNGG/Magnox), so further decontamination from volatile radionuclides is possible but more difficult and less efficient compared to the other cases, since the residual fraction is the most stable one.

In general, higher temperatures provide higher decontamination factors in inert gas treatments, with different removal efficiencies depending on the graphite coming from different reactors, as described above. As a general statement, temperatures higher than 1100 °C are recommended for a tritium-removal process in inert gases: treatment times are decreasing significantly by raising the temperature. These findings are in accordance to the Deuterium implantation and thermal treatment investigations performed by N. Toulhoat, N. Moncoffre and Y. Pipon (IPNL-University of Lyon), reported in D-4.2.3. It seems to be possible to remove completely the Tritium from i-graphite but further investigations, especially with massive samples, are necessary to confirm the findings here reported.

The model of Atsumi [15] fits well with the findings of FZJ and IPNL. However, the multitude of influencing parameters during the graphite lifetime and the treatment must be taken into account, singularly identified and their influence must be better understood.

In FZJ, the maximum applied temperature was 1300 °C, provided by the available equipment; higher temperatures could be achieved e.g. with an induction furnace, resulting in a more straightforward Tritium removal. It could be possible that a threshold temperature, beyond

which the gained removal is insignificant compared to the effort necessary for reaching such a temperature, but it still needs to be investigated.

3.2 Release of Radiocarbon

3.2.1 Background

In the past no models have been established for radiocarbon removal: only some experimental data is available. A common approach adopted in the past, underlined by the findings within the CARBOWASTE project, was to neglect the history/nature of the considered graphite: such a material, already quite complex, experienced a series of conditions affecting its behaviour under disposal, over than its radionuclide distribution. Starting from the manufacture, going through the storage history, the operational history inside the reactor and the storage conditions after irradiation, graphite is experiencing a consistent number of parameters affecting its structure, radionuclide distribution and, at the end, behaviour under thermal treatment and final disposal. For this reason, any nuclear graphite is a unique case. In some cases, similar behaviours are detected under thermal treatment, but this can be linked to similar histories and/or main sources of contamination.
The origin and location of C-14 is out of the scope of the present work package: it has analysed in WP3.
Takahashi et al. [19] measured, through SIMS analyses, nitrogen (CN-) concentrated mostly near the graphite surface, in the first tens of nm (about 30 nm). Moreover, after a thermal treatment at 400°C, no differences were observed: it was stated that nitrogen is sorbed on the graphite surface in a stable way. The variation of nitrogen concentration in the depth direction suggested that nitrogen molecules cannot penetrate interior of nuclear-grade graphite, protected by scale-like graphite planes, so the nitrogen stays mainly on the surface. C-14 release was estimated to occur from the first superficial nanometer of the graphite surface. It has to be underlined, however, that the investigated samples had very low radioactivity and the experiments were performed at relatively low temperatures. It is expected that highly radioactive graphite, as the AVR one, will show considerable amounts of mobile carbon due both to the old-grade manufacture and radiation damage.
Some experiments have shown that most of the C-14 is located on the outer and inner surfaces of the porous graphite, in the case of AVR and MERLIN graphite [30].
Thermal treatments of T. Podruzina [26] showed results related to the temperature, the used sample and the utilized gases. The most promising results, concerning AVR reflector graphite, were obtained at 1060 °C in inert atmosphere (argon), with a fractional release $\%^{14}C/\%^{12}C=20$ and mass loss in the order of 1%.

The theoretical implications related to the experimental results will be presented in the following chapters.

3.2.2 Release of Radiocarbon during inert gas thermal treatments

Similarly to what has been done in the case of Tritium, Radiocarbon has been investigated through application of inert gas thermal treatments at different temperatures, with the scope of improving the knowledge of the temperature effect on its removal and, indirectly, investigating its bonding/chemical stability/location. The maximum temperature applied was 1300 °C. The used gases were mainly Argon and Nitrogen. The on-line measurements allowed studying the release kinetic of Radiocarbon during a thermal treatment in relation to the applied temperature.

3.2.2.1 Merlin Graphite

The release of radiocarbon in inert gas (without ingress of air) seems to be a temperature-dependent diffusion process in which gases like ^{14}CO and $^{14}CO_2$ are released, formed by oxidation of radiocarbon in the pore system. This process is often overlain by a radiocarbon release caused by simple corrosion of the outer layers of the graphite matrix. In particular, this effect occurs when the inert gas contains traces of oxidising gases (e.g. oxygen, water) due to small leakages of the used furnace (e.g. thermal permeability of the oven tube).

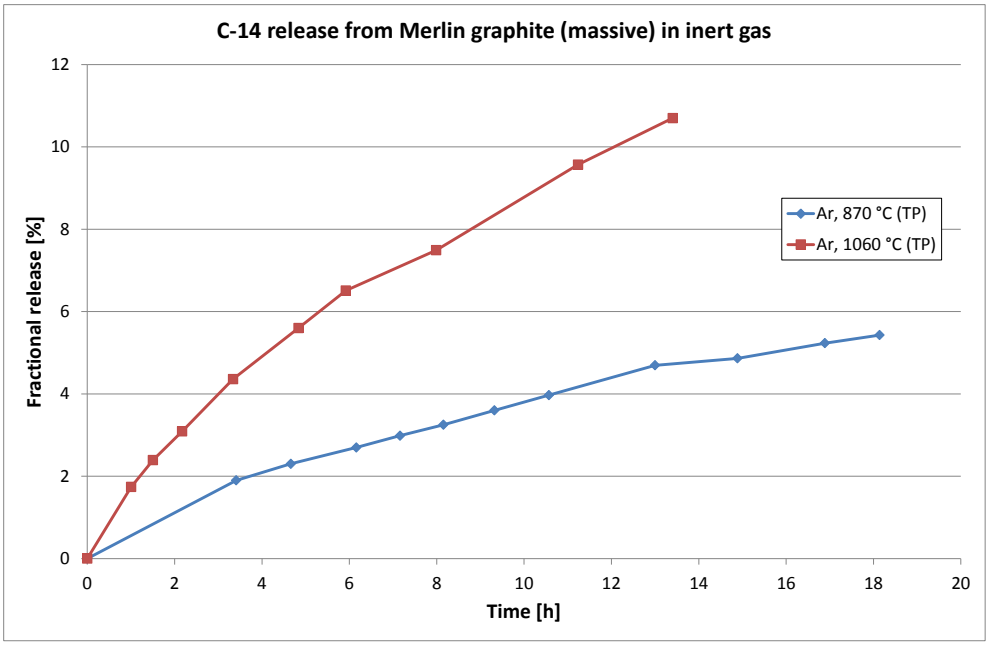

Figure 3.2.1: Release of radiocarbon in inert gas at different temperatures

The release of radiocarbon in inert gas is also dependent on the amount of adsorbed oxidising gases. Several experiments revealed that a simple addition of oxidising gases increases the release of radiocarbon but increases also the corrosion of the graphite matrix, leading to a less effective radiocarbon removal. This fact can be observed in Fig. 3.2.2: after about 8 hours from the beginning of the experiment a small ingress of air resulted in a sudden increase of the C-14

removal rate. This fact suggests that the removal of C-14 is bound to the presence of oxidants. The sample mass loss was in all cases lower than 1.4%.

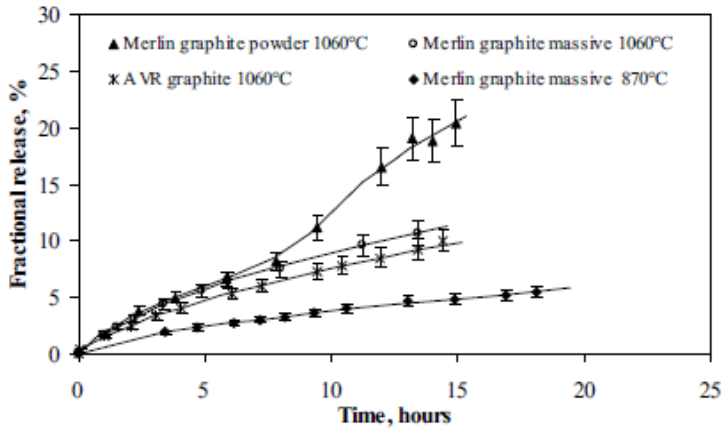

Figure 3.2.2: Release of radiocarbon in inert gas at different temperatures [26]

The kinetic description of the thermal release of radiocarbon from graphite is derived from two kinds of experiments:

- Nearly-inert gas experiments (as shown in Figure 3.2.1) and
- Experiments in which the treatment gas contained a defined (small) amount of oxygen.

Real inert gas experiments give the chance to study the diffusion of radiocarbon through the graphite matrix. The graphical test for a diffusion reaction is made by plotting the fractional release of radiocarbon vs. the square root of time (see Figure 3.2.3). Application of Eq. 3.9–11 results in an apparent activation energy of 1.17 eV.

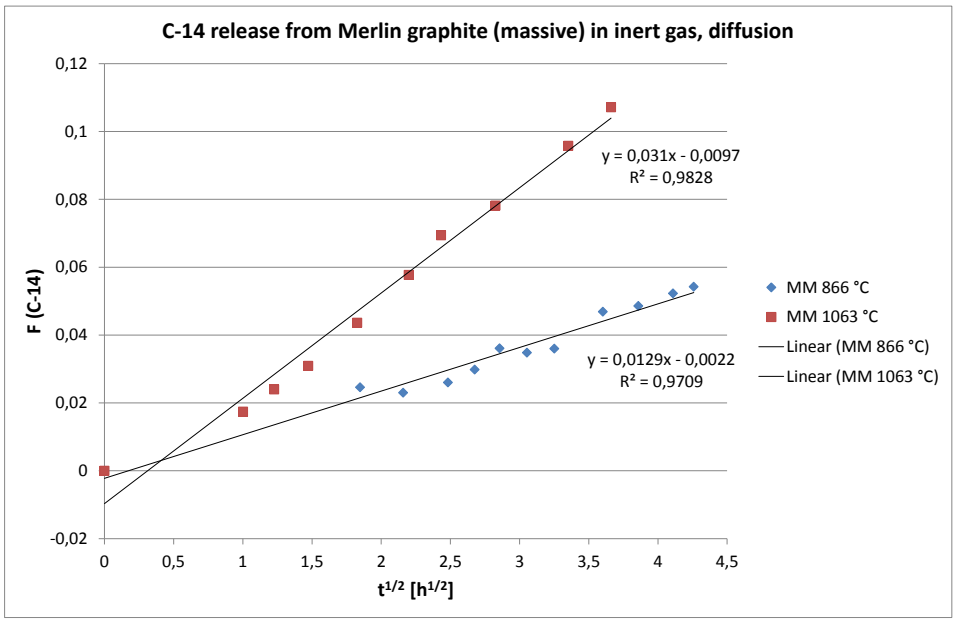

Figure 3.2.3: Release of radiocarbon in inert gas at different temperatures as diffusion reaction

The apparent diffusion activation energy is the sum of the real diffusion activation energy and the formation energy of the diffusing species. To determine the formation energy of the diffusing species it is necessary to study the oxidation process of the graphite matrix, since the release of radiocarbon is related with it. Therefore, experiments were performed with a treatment gas containing a defined amount of oxygen. The results of these experiments are given in Figure 3.2.4. MERLIN graphite was treated with nitrogen + 1% oxygen. Two different temperatures were applied: 700 °C and 900 °C.

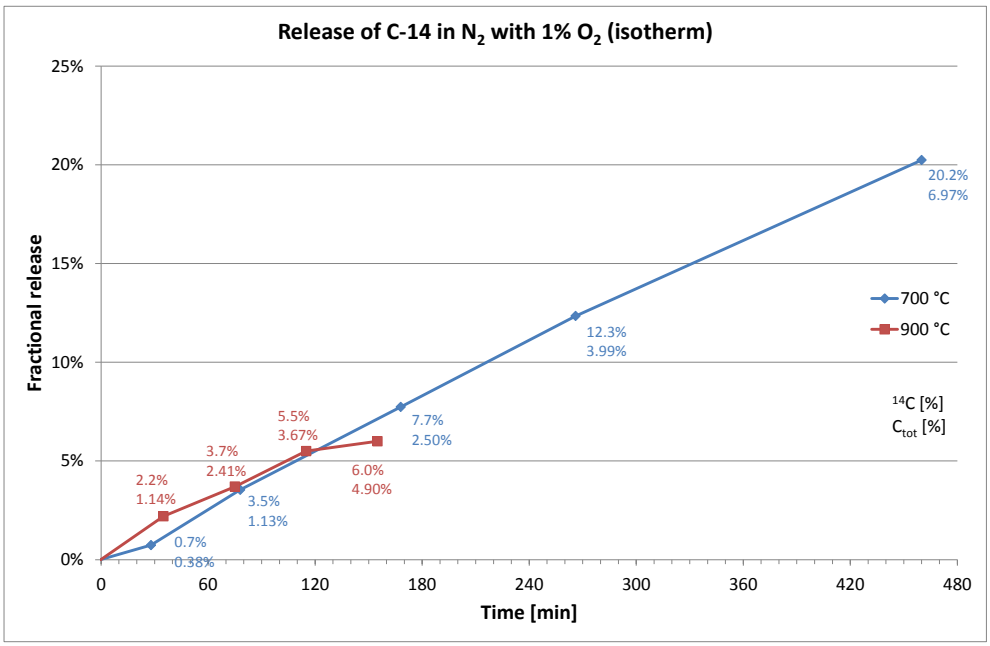

Figure 3.2.4: Release of radiocarbon in nitrogen with 1% oxygen at different temperatures (the upper number gives the % ^{14}C released and the lower number the % carbon consumed)

One can see that the release isotherms are quite linear with time up to a certain point at which the "removable part" of radiocarbon is consumed and they lie upon each other. In kinetic terms this means that the reaction between radiocarbon and oxygen is of zero order (independent on the concentration of radiocarbon and oxygen) and that the reaction rate is independent on the temperature.

The thermal release of radiocarbon is always coupled with an oxidation of the graphite matrix. To obtain more information about the release mechanism and the release kinetics of radiocarbon, it is necessary to study the oxidation behaviour of the graphite matrix. In Figure 3.2.5 the release of total carbon (all carbon isotopes of graphite) for the above-mentioned experiments with MERLIN graphite is shown. One can see that the reaction mechanism is of zero order again, but there is also – as expected – a temperature dependence of the reaction rate: the higher the temperature the higher the reaction rate.

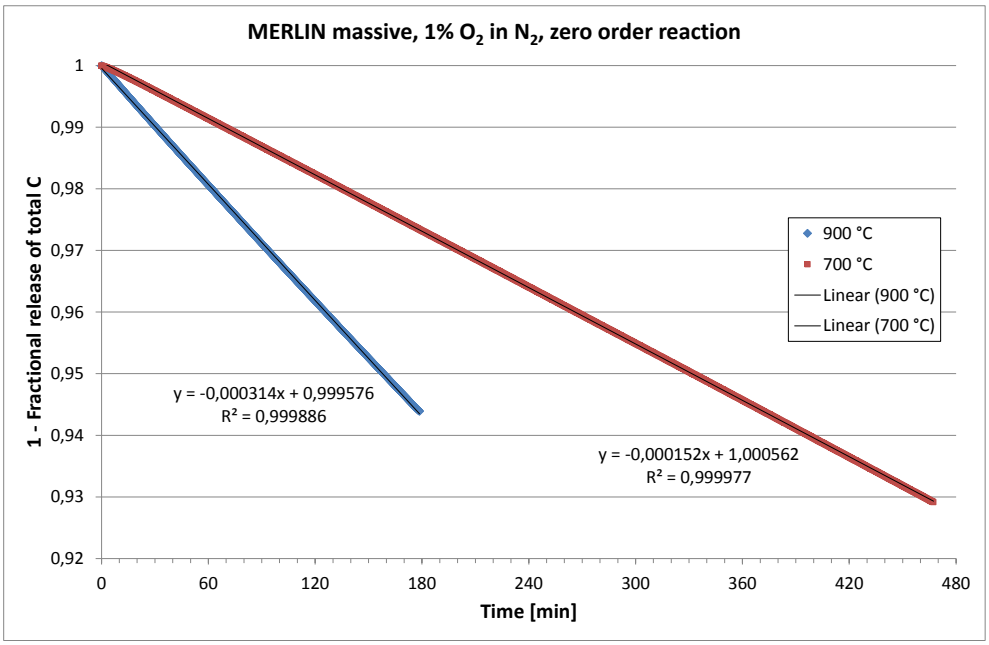

Figure 3.2.5: Release of total carbon in nitrogen with 1% oxygen at different temperatures

With the temperature dependence, the activation energy for the oxidation of the graphite matrix can be calculated. The reaction rate of a zero order reaction is defined by

$$c(\mathrm{A}) = -k \cdot t + c_0(\mathrm{A}) \tag{3.13}$$

A plot of the concentration of the starting material (= 1 − fractional release of total carbon) vs. time should give a straight line with a slope of $-k$ (= reaction rate constant). From the known dependence of the reaction rate constant on the temperature (Arrhenius equation), the activation energy E_A can be calculated:

$$E_\mathrm{A} = R \cdot \frac{T_1 \cdot T_2}{T_2 - T_1} \cdot \ln\left(\frac{k_2}{k_1}\right) \tag{3.14}$$

With Eq. (3.14), it can be calculated an activation energy of 34.4 kJ/mol (= 0.36 eV). With this result the true activation energy for the diffusion of radiocarbon through the graphite matrix can be obtained: a simple subtraction of the activation energy for the oxidation of the graphite matrix from the apparent diffusion activation energy results in Eq. (3.15).

$$1.17\ \mathrm{eV} - 0.36\ \mathrm{eV} = 0.81\ \mathrm{eV} \tag{3.15}$$

A comparison of different experimental curves, obtained in not-ideal inert atmosphere in at different regime temperatures and for different sample shapes, is reported in Fig. 3.2.6. All the other experiments revealed traces of oxygen in the adduct gases with a maximum of 20-30 ppm (indicatively).[1] Some indications on the parametric influence on C-14 removal can be obtained by Fig. 3.2.6. In particular, as cited already previously, high temperatures seem not to be very effective in a continuous treatment: the established regime would permit a superficial oxidation of the sample, without affecting the inner part. Except the oxidation process, due to either adsorbed gases or oxidants in the adduct gases, a migration of interstitials could take place at high temperatures (starting from 1200-1300°C). However, a separation of those effects is not simple: more systematic investigations are necessary.
Another important observation can be done with regard to the sample shape: the case "MM 1050°C argon", where the mass loss resulted in 1,4% at the end of the process, reveals higher mass losses together with higher releases of C-14. In other words, the selectivity on the release is much lower than in the other cases (3-7 times lower), probably due to the higher specific surface of the powdered sample exposed to reactions (further explanations are reported in Section 3.2.5).

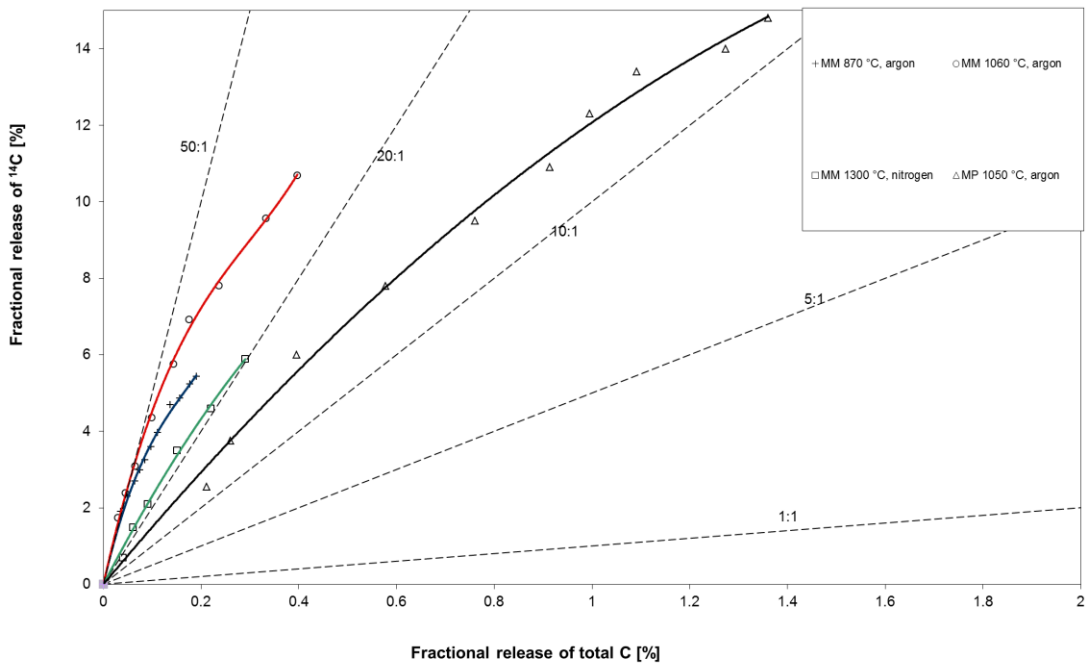

Figure 3.2.6: Release of total carbon in argon/nitrogen for Merlin graphite (MM=massive; MP=powder) at different temperatures

[1] Measurement made ex post. The value is only an estimation. However, the obtained results are helpful for the identification of the driving mechanisms of C-14 removal, taking the boundary conditions into consideration.

3.2.2.2 Saint Laurent A2 and Oldbury 2 Graphite

The release of $^{14}CO_2$ and ^{14}CO from Magnox Oldbury 2 graphite in nitrogen at 1100 °C shows also a diffusion character, as can be seen in Figures 3.2.7 and 3.2.8. This implies that both species must be already formed in the graphite bulk: it is possible that the chemical bonds are already formed. This can be imagined as ^{14}C─O surface complexes like shown in Figure 3.2.9. The formation of volatile compounds such as $^{14}CO_2$ and ^{14}CO is then possible by supplying thermal energy and breaking the ^{12}C─^{14}C bonds; secondary reactions involving ^{14}CO are not excluded. Another option is the presence of small amounts of oxidizing species in the adduct gases: due to the difficulty on the control of boundary conditions, it is not possible to separate the two effects in an ideal way. However, it is reasonable to expect that, after some time at high temperature, the pyrolysing process terminates due to the exhaustion of the pyrolysable functional groups for that certain temperature; it follows, then, an oxidation of the graphite due to the traces of oxidisers present in the adduct gases. Looking at Figs. 3.2.8-9 it can be noticed that the fractional releases of Radiocarbon in the case of Oldbury2 graphite are up to 4 times lower than the C-14 releases from Merlin graphite, under the same conditions: it has to be considered, in fact, the history of the graphite. In particular, the radiolytic corrosion occurred during reactor operation is likely to have removed already a significant part of the C-14, since the experienced mass losses at the end of the reactor´s life were up to 40%, much more than the one measured in the treatment experiments.

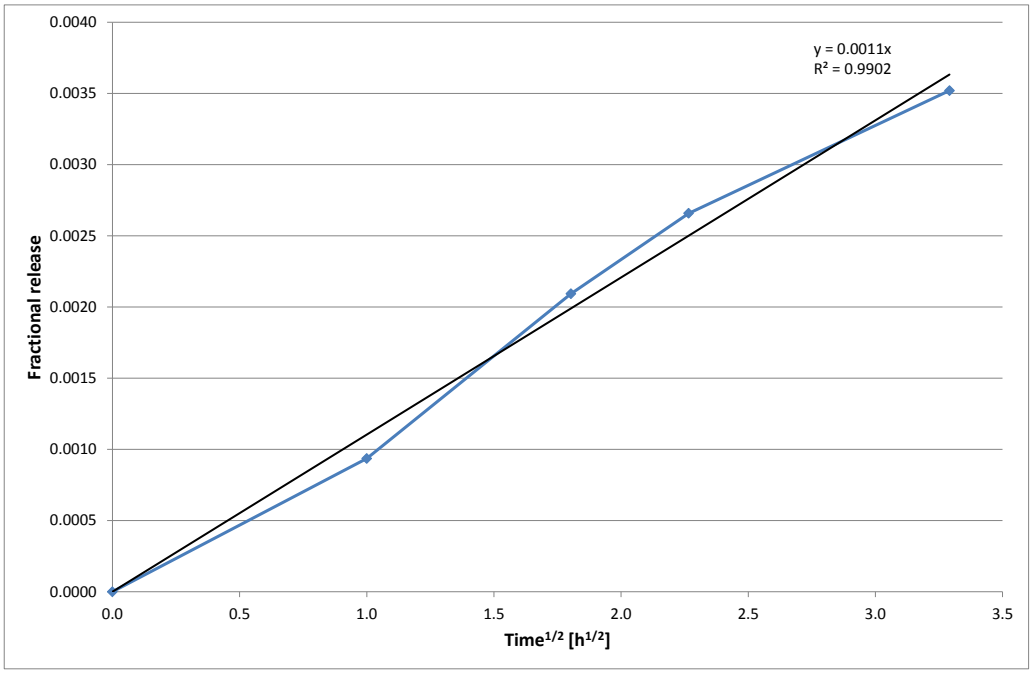

Figure 3.2.7: Release of $^{14}CO_2$ from Magnox Oldbury 2 graphite in nitrogen at 1100 °C plotted as diffusion reaction

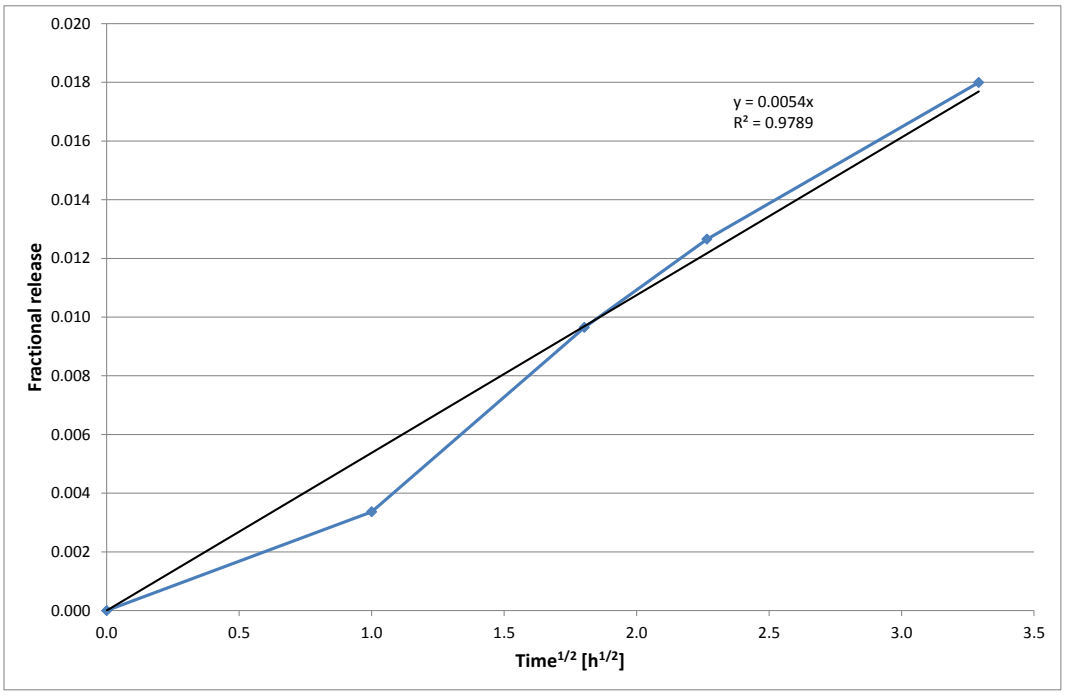

Figure 3.2.8: Release of ^{14}CO from Magnox Oldbury 2 graphite in nitrogen at 1100 °C plotted as diffusion reaction

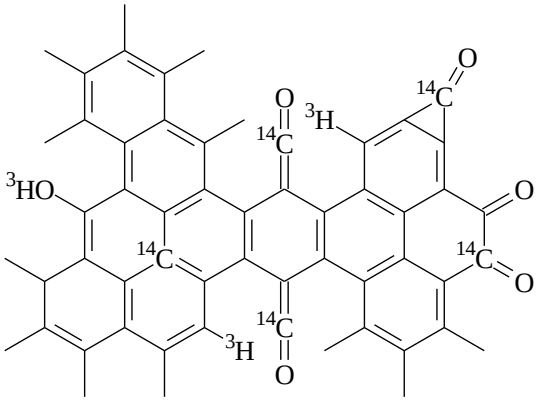

Figure 3.2.9: Model of a graphite surface with ^{3}H and ^{14}C as functional groups (surface complexes)

For what concerns the release of $^{14}CO_2$ and ^{14}CO from Saint Laurent A2 graphite the on-line values are reported in Figs. 3.2.10-11.

The hypothesis of a diffusion-dominating phenomenon seems to be validated for $^{14}CO_2$ also in this case (see Fig. 3.2.10). In the case of ^{14}CO the curve fitting is much worse than the previous case (see Fig. 3.2.8): it is reasonable to expect an overlapping of different phenomena, not excluding e.g. secondary reactions (Bouduard reaction, thermal gradient effects on the gas phase species, etc.). However, the measured values here presented for the Saint Laurent A2 case are affected by significant errors (about 11%) since the removed activity was very low. Future investigations should be performed to check the validity of the present results.

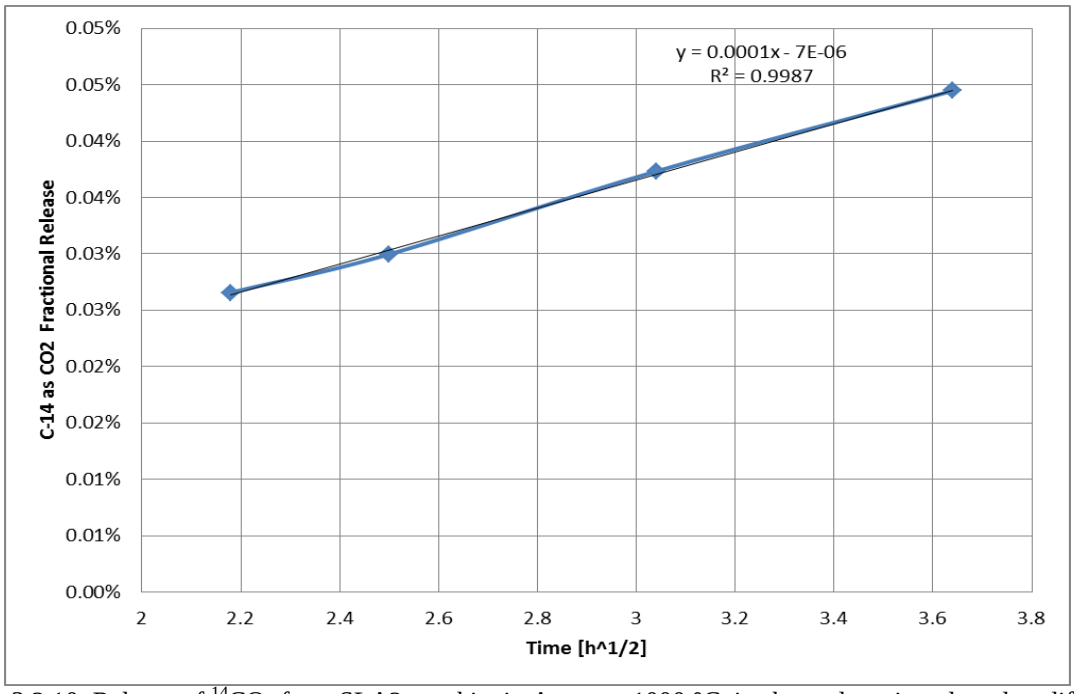

Figure 3.2.10: Release of $^{14}CO_2$ from SLA2 graphite in Argon at 1000 °C, isothermal section plotted as diffusion reaction

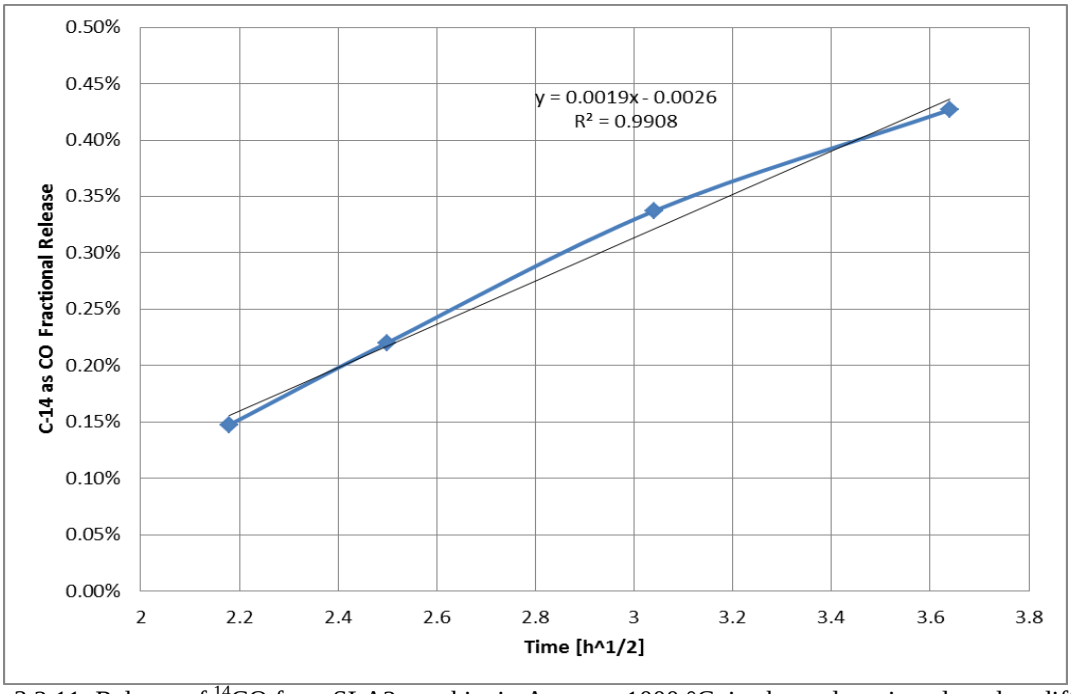

Figure 3.2.11: Release of ^{14}CO from SLA2 graphite in Argon at 1000 °C, isothermal section plotted as diffusion reaction

Excluding the presence of oxidants in the adduct gas, after a first step on which a pyrolysation process together with the reaction of adsorbed gases takes place, no further radiocarbon can be released. The next step, in line of thought, consists on adding oxydants (as oxygen or water) in a continuous way in small concentrations. In general, the decontamination factors of Radiocarbon in inert gases are quite limited.

3.2.3 Release of Radiocarbon during thermal treatments with Oxygen/Nitrogen

The oxidation of nuclear graphite is not a simple process where oxygen reacts with homogeneous carbon. Due to the porous structure of nuclear graphite, there are three oxidation regimes with oxygen [8] (the same regimes take place with steam at about 300°C higher):

- Uniform oxidation inside the porous material (chemical regime, < 500 °C).
- Location-dependent oxidation inside the porous material (in-pore diffusion controlled regime, 500…900 °C).
- Surface oxidation (boundary layer controlled regime, > 900 °C).

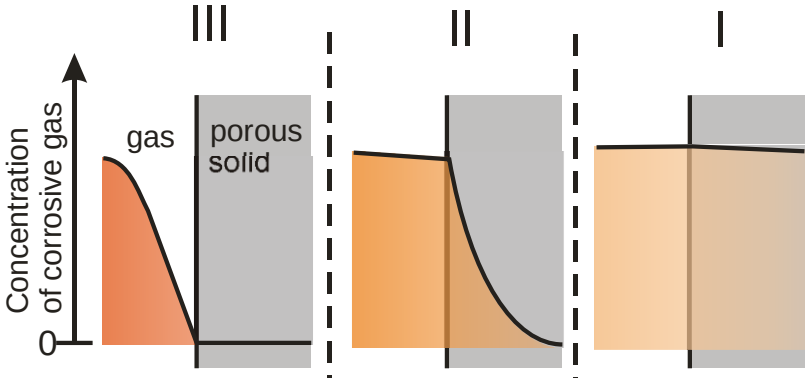

Figure 3.2.12: Profile of Oxygen (water) in the three regimes taking place in graphite depending on the applied temperature.

At low temperatures, the oxidation occurs on the surfaces of the whole pore system (inner surfaces, right image of Fig. 3.2.12), but it is very slow. At high temperatures, the oxidation occurs on the outer surfaces of the graphite sample, and it is very fast (left image of Fig. 3.2.12). Between both temperature ranges, there is a transitional range: 500-900 °C for oxygen, 800-1200 °C for water steam (central image of Fig. 3.2.12). The selective thermal release of radiocarbon from nuclear graphite (without complete incineration of the graphite matrix) occurs in this transitional range. This means that the release of radiocarbon occurs in a significant fraction from the surfaces of the pore system. If there is an enrichment of radiocarbon in the off-gas, it can be assumed that radiocarbon is enriched on the surfaces of the pore system. Therefore, the selective thermal release of radiocarbon from nuclear graphite is a local effect and not a kinetic effect. This is the reason why a temperature increase does not increase the amount of released radiocarbon without increasing the bulk oxidation of the graphite matrix.
To visualise this process, it is advantageous to plot the fractional release of radiocarbon vs. the fractional release of total carbon for each temperature. This is shown for Merlin graphite in Fig. 3.2.13. It can be seen that the enrichment factor of radiocarbon in the off-gas is higher at 700 °C than the one at 900 °C: in the latter, the ratio of released $^{14}C/^{12}C$ is nearly 1, which indicates that the release of radiocarbon occurs by simple incineration of the graphite matrix.

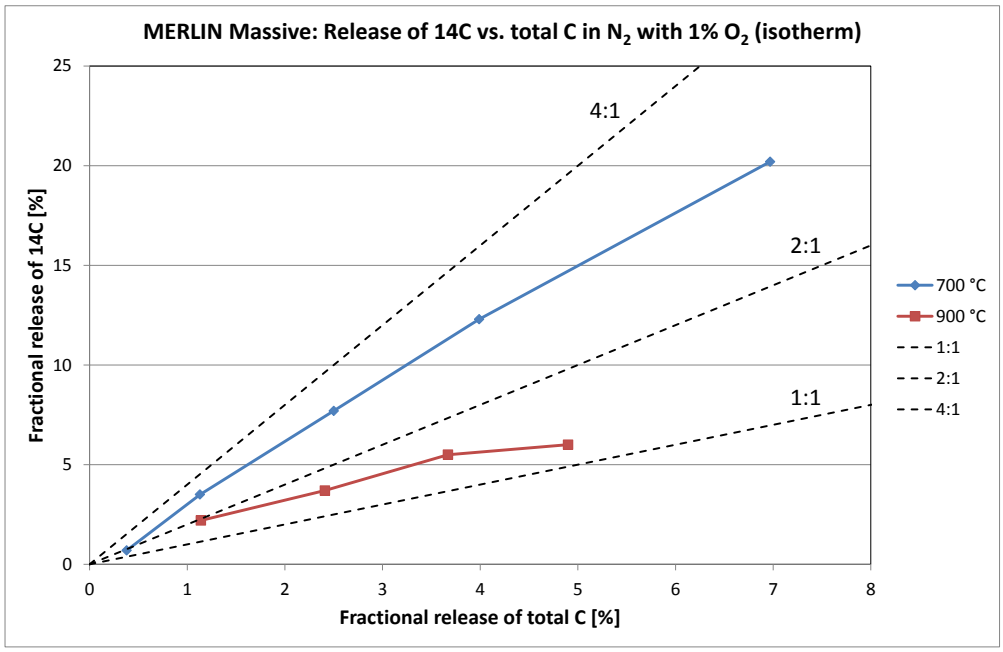

Figure 3.2.13: Fractional release of radiocarbon vs. fractional release of total carbon in nitrogen with 1% oxygen at different temperatures

3.2.4 Release of Radiocarbon during thermal treatments with water steam

The oxidation of graphite with steam starts releasing C-14 at 800°C: the quantity of evolved C-14 was very small due to negligible reaction rate of graphite and water steam at this temperature. C-14 releases became significant above 800°C.
In the case on which ^{14}C is deposited only on the outer surfaces of a graphite sample, or it is incorporated in near-surface layers, it can be removed by simple oxidation with oxygen. Unfortunately, oxygen showed to be too aggressive in order to reach ^{14}C deposits in the pore system of graphite: at temperatures at which oxygen reacts with graphite, it oxidises the graphite sample only on the outer surfaces. The result is a high mass loss at low ^{14}C release.
This problem can be solved by application of mild oxidising agents like steam. Steam reacts with graphite to form carbon monoxide and hydrogen at temperatures higher than 800 °C (see Eq. (3.5)). Carbon monoxide reacts with steam to form carbon dioxide and hydrogen (see Eq. (3.6), here reported).

$$CO + H_2O \leftrightarrow CO_2 + H_2 \tag{3.6}$$

3.2.4.1 Merlin and AVR Graphite

On-line releases from Merlin graphite are shown in Fig. 3.2.14(a) for different flow rates and temperatures with a steam partial pressure of 7.4 kPa. It is clear how the flow is influencing the release of radiocarbon: since it is an oxidation process, providing higher flow allows producing more reactants, depending on the temperature and the regime, releasing then more C-14. This fact can be confirmed also by Fig. 3.2.14(b). At a temperature of 960°C an experiment was performed with two different flow rates. As in the case of tritium, with increasing flow rate the amount of C-14 released also increased from 11 % to 24 % after 7 hours. The mass loss of graphite sample amounted to 2.5 % and to 4 %, respectively. This gives the ratio of released isotope fractions as 4.4 and 6, correspondingly. Comparing these results with treatment at a higher temperature (1060°C) after 7 hours, where the mass loss was unacceptably high, leading to a non-enriched removal of radiocarbon, it can be concluded that the graphite oxidation at a lower temperature is more effective in order to eliminate C-14 without significant burn-off of the total graphite mass.

A first comparison of Merlin thermal column and AVR reflector graphite is shown in Fig. 3.2.15(a)-(b). With the same conditions, despite the high mass loss, the Merlin graphite showed to be more reactive and released higher relative fractions of C-14. However, more systematic analyses should be performed in the future to better understand the influence of the many influencing parameters, taking into account also the history of the graphite.

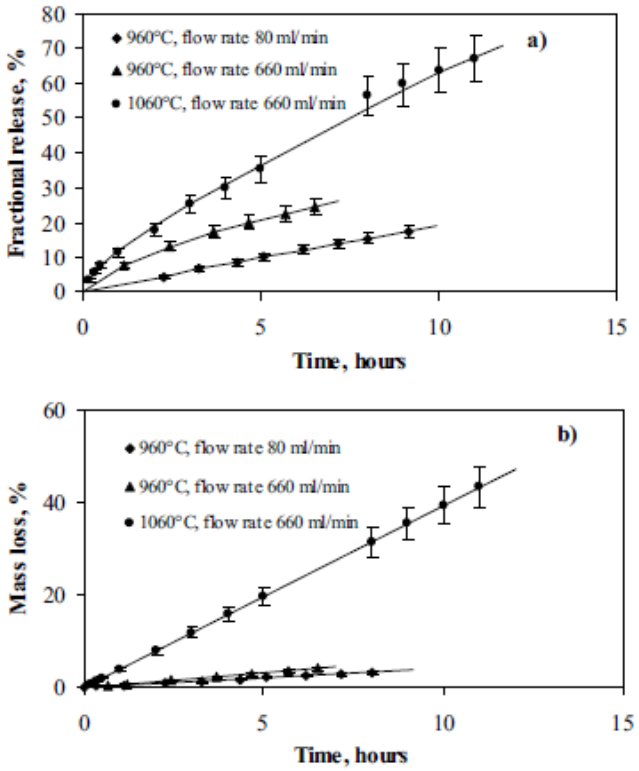

Figure 3.2.14-a,b: Fractional release of C-14 (a) and mass loss (b) during Merlin graphite oxidation with water steam (7.4 kPa) [26]

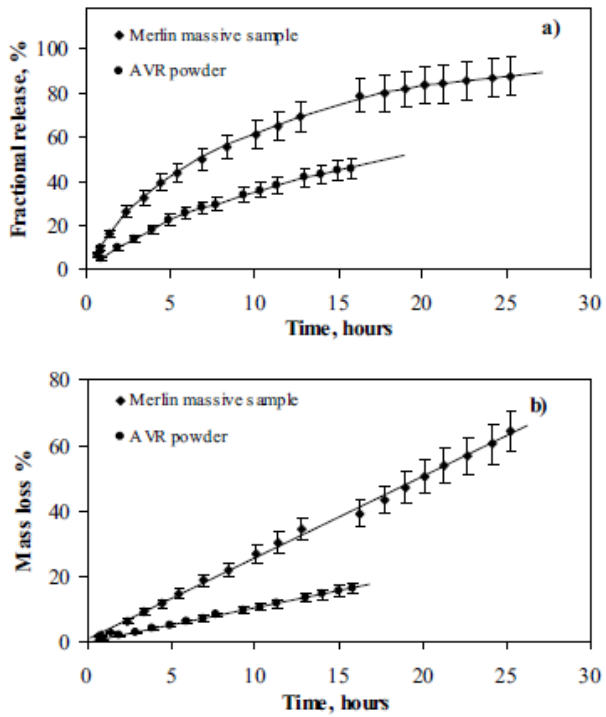

Figure 3.2.14-c,d: Fractional release of C-14 (a) and mass loss (b) during Merlin and AVR graphite oxidation with water steam (2.3 kPa) at 1060°C. [26]

The effect of steam injection during thermal treatment on the C-14 removal can be observed in Figs. 3.2.15-16: at 1000°C in argon a steam partial pressure of 1.6 kPa was injected. Immediately, the release trend changed significantly.

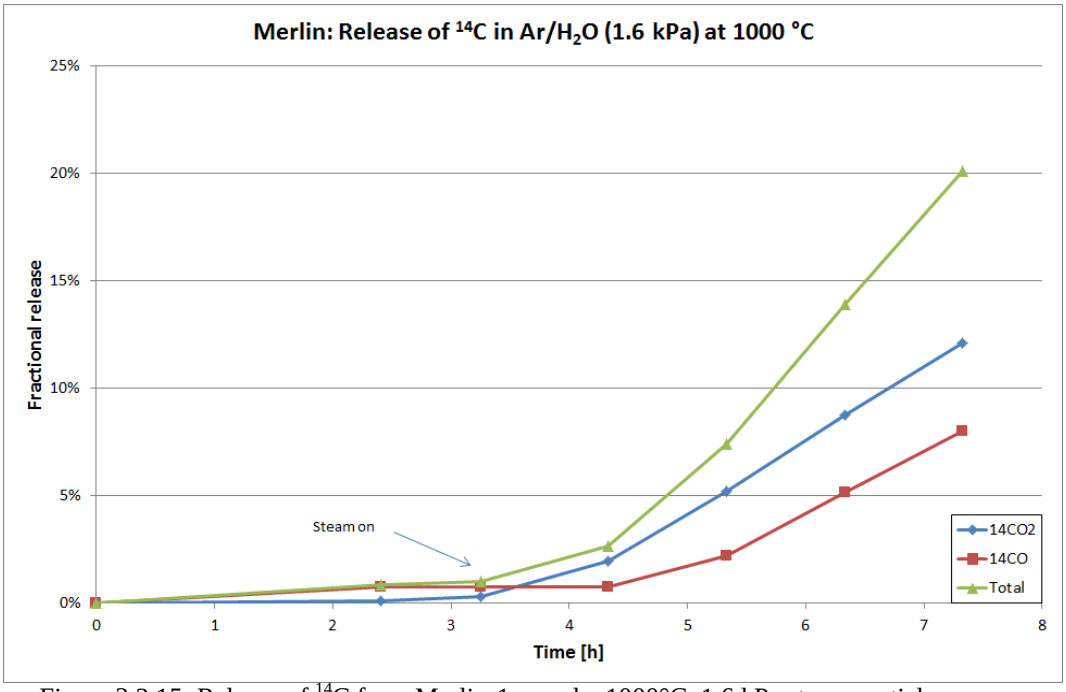

Figure 3.2.15: Release of ^{14}C from Merlin-1 sample, 1000°C, 1.6 kPa steam partial pressure.

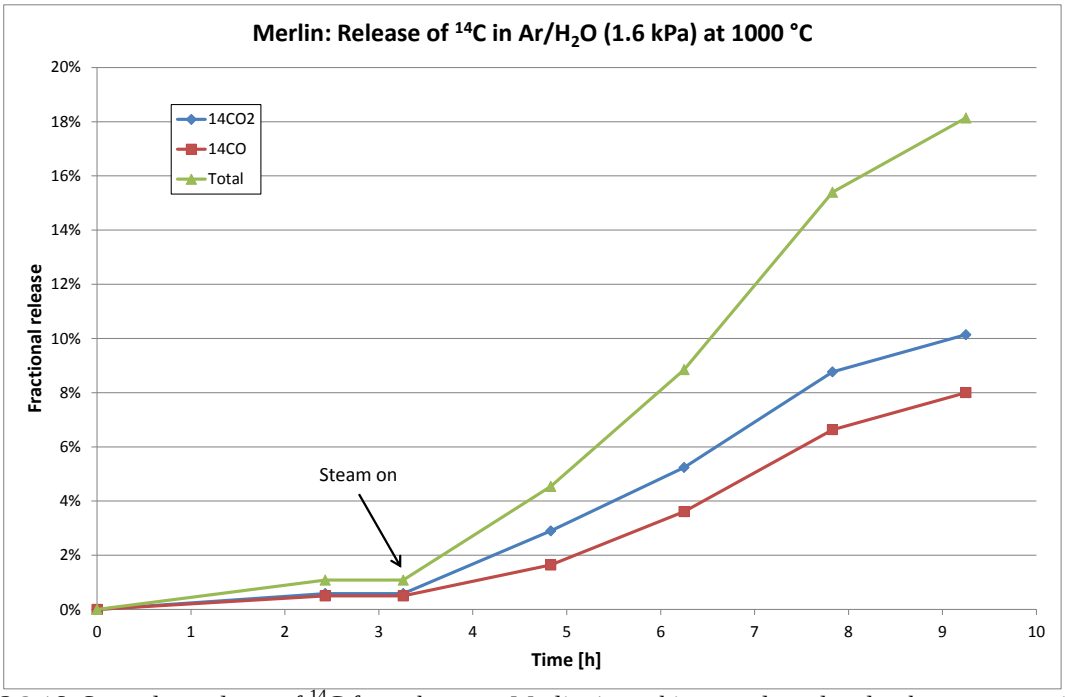

Figure 3.2.16: Secondary release of ^{14}C from the same Merlin-1 graphite sample and under the same experimental conditions as indicated in Fig. 3.2.15 (mass loss after 6 h of isothermal steam reforming: 2.19%)

The total release of ^{14}C from Melin-1 sample after two treatments amounted to 29.0% with a total mass loss of 3.64% and an isothermal treatment time of 10 h in all. This corresponds to an enrichment factor of [^{14}C]/[total carbon in the gas phase] of 8.0. This means that the concentration of ^{14}C in the gas phase, considered over the entire process, is 8.0 times higher than the average concentration in the graphite sample. Accordingly, a real selective ^{14}C release can be performed by steam thermal treatment.

3.2.4.2 Saint Laurent A2 Graphite

The case of Saint Laurent A2 moderator graphite is showing a similar relative behaviour than the case of inert gas experiments: the fractional removal is generally lower than the one in the other cases, probably due to the radiolytic effect that already removed a significant part of C-14. As an indicative comparison, a 4 hours treatment with the same conditions resulted in about 11-20% C-14 removal for Merlin graphite against 6-8% in the case of SLA2. The mass loss at the end of the process was about 2.2% in both cases.

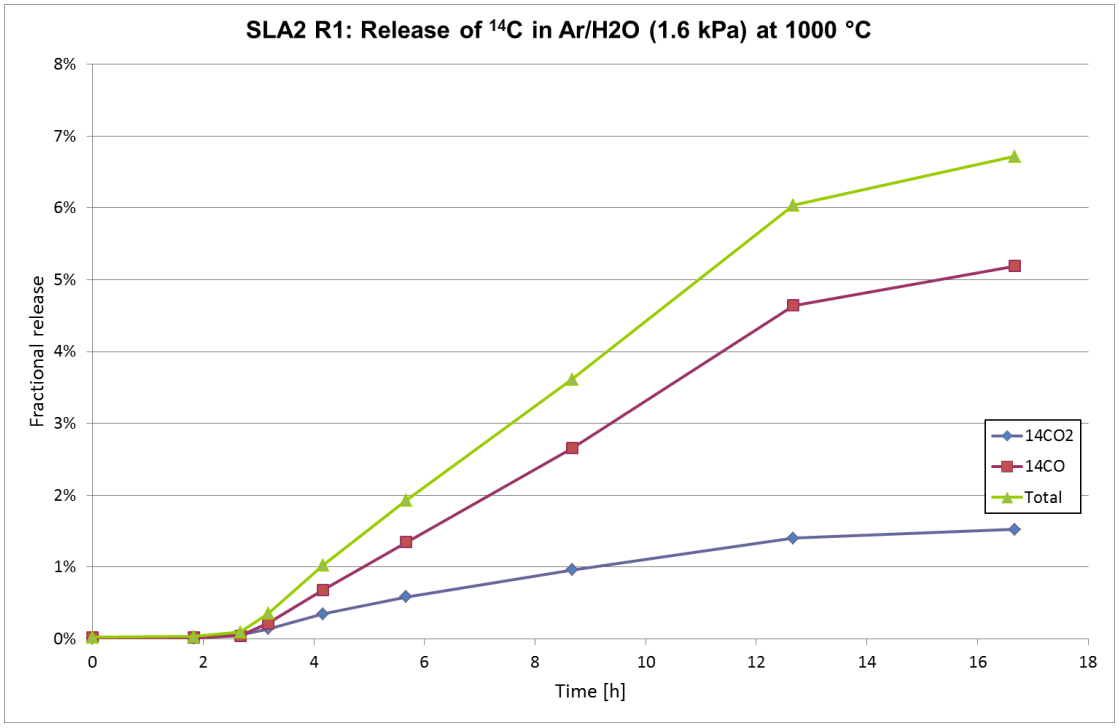

Figure 3.2.17: Release of ^{14}C from SLA2 R1 sample, 1000°C, 1.6 kPa steam partial pressure

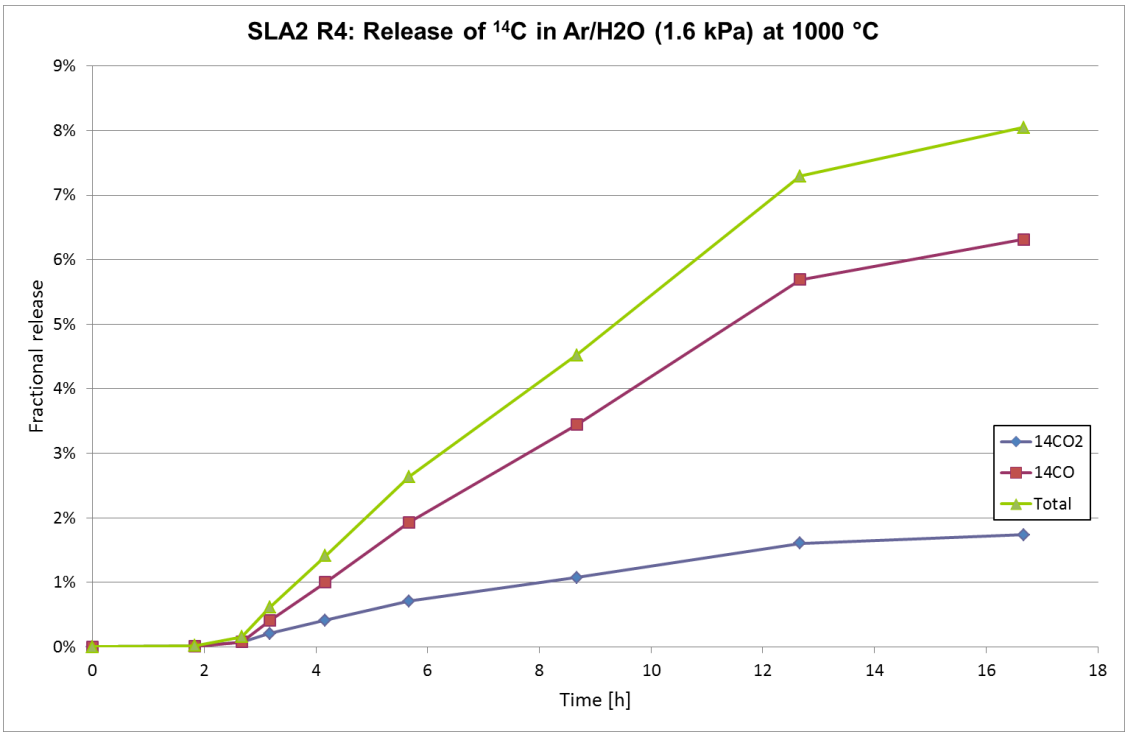

Figure 3.2.18: Release of ^{14}C from SLA2 R4 sample, 1000°C, 1.6 kPa steam partial pressure.

3.2.5 Comparison of Radiocarbon Removal in Different Regimes/Gases

As reported in the previous sections, the removal of radiocarbon is related with the presence of oxidants, both adsorbed or in the adduct gases. This can be firstly revealed by Fig. 3.2.19-a,b, assuming small impurities in the adduct gases. Despite the presence of low amounts of oxidants, the mass loss is limited: 1.4% after 10 hours in the case of Merlin powder and 0.4% maximum in the case of Merlin massive samples. The maximum enrichment of C-14 lays in the zone 20:1-50:1. It is important underlining that considering the absolute release of a radionuclide is meaningless without taking into account the mass loss, so release entities must be always coupled in order to get a realistic evaluation of the effectiveness/efficiency of the treatment.

Another interesting observation from Fig. 3.2.19-a stands on the evolution of the releases´ slope: it starts with high enrichment and then it flattens more and more, approaching slowly the 1:1 slope (simple burning without selective removal). A possible explanation of this fact could stand on the adsorbed/embedded reactants that, after having reacted, are not being replaced during the thermal treatment, due to the regime that is taking place and/or the lacking of oxidising species in the adduct gas. So, de facto, the “reacting volume” is higher at the beginning and it becomes smaller due to the established regime. In the case of an ideal inert environment during thermal treatment, a fast release of radiocarbon is taking place, followed by a saturation of the curve (see e.g. Fig. 3.2.23).

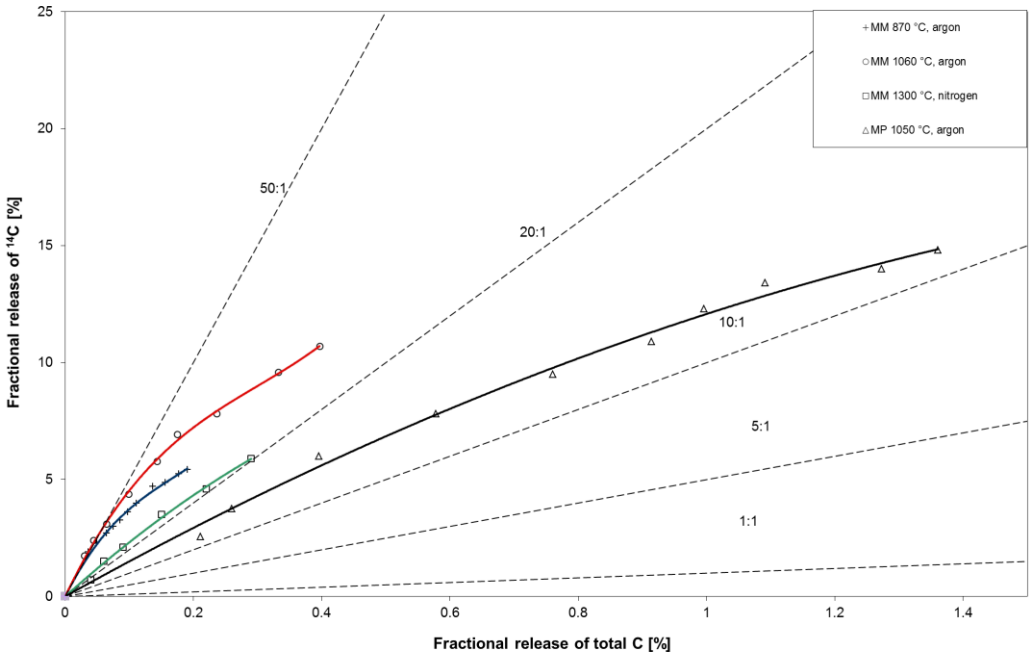

Figure 3.2.19-a: Comparison among different treatments in inert gases at different temperatures (MM=merlin massive, MP=merlin powder)

In general, a direct comparison among inert gases and water steam thermal treatments reveals that the release of Radiocarbon in inert gases is rather limited: it has been proven that its removal is related with the corrosion of the graphite. Accordingly, a treatment under inert atmosphere is not effective since, after relatively short time, the reactants (adsorbed or present as impurities in the treatment chamber) are exhausted, with no further release taking place.
The next step, in line of thought, consists on applying oxidising gases, as oxygen or steam, in order to enhance the graphite corrosion and, then, the release of radiocarbon.
The application of relatively small quantities of oxygen (up to 1%) resulted in unacceptably high mass losses (12-54%), with releases below 30% for 700°C, 800°C and 1300°C experiments. This data supports the theory of a non-leachable/non-removable fraction of C-14 within the graphite structure (probably coming from C-13 or embedded in a stable way in the graphitic structure).

The application of steam in different quantities (7.4 kPa, 2.3 kPa and 1.6 kPa) allowed enhancing the total removal of C-14, in concomitance with a higher mass loss than the inert gas case and a lower mass loss than the oxygen case. Relatively lower temperatures revealed to be more effective since the mass losses were more limited while the radiocarbon removal remained significant. Other parameters, as the steam partial pressure, still need to be optimized.

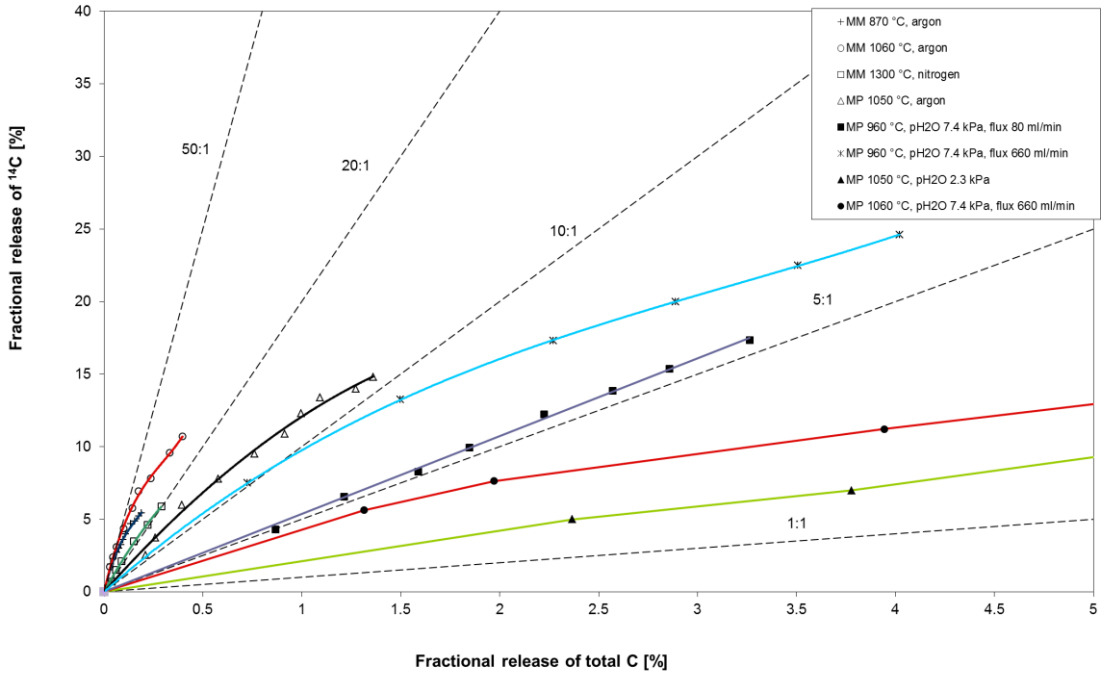

Figure 3.2.19-b: Comparison among different treatments with steam and argon, at different temperatures.

In conclusion, two phenomena have been identified: diffusion-driven removal of radiocarbon under inert gases and zeroth order reaction of the total carbon under slightly oxidizing atmosphere. The removal of radiocarbon, moreover, showed to be correlated with the oxidation of graphite: it is strongly bound with the presence of oxidizing agents; on the other hand, the presence of e.g. small amounts of oxygen are increasing at the same time the C-14 release and the mass loss, resulting in a less selective removal.

Following these findings the possible routes for radiocarbon removal are:

- Diffusion of C-14 atoms from interstitials or defects to the outer surface of the graphite matrix;
- Selective removal of C-14 from the enriched layers near to the surfaces by slight oxidation;

The dilemma that has to be faced is dual: considering the diffusion of C-14 under inert gases, the removal is frozen after some time due to the exhaustion of the oxidants (chemisorbed and/or present in the treatment chamber at the starting of the treatment). Following the line of thought, the next option would be accelerating the process by providing slight amounts of oxidising gases, in a continuous process at high temperature: the temperature, however, affects in a opposite way the reaction rate (higher with T.) and the established regime (mass-transfer controlled regime at high T.), resulting in a surface decontamination at high temperatures without affecting significantly the bulk material. On the other side, low temperature result in a chemical regime with very low reaction rates and low diffusion coefficients.

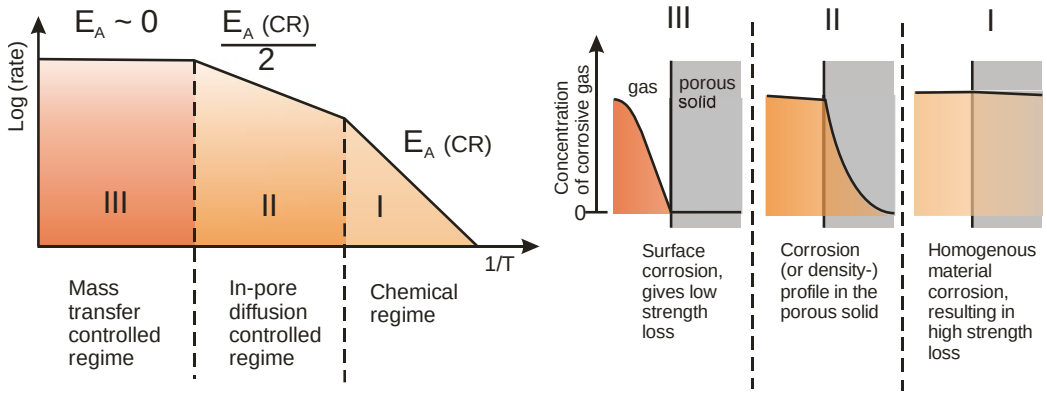

Figure 3.2.20: Schematic view of the controversial effect of temperature on reaction rates and regime in porous media.

Separation of these steps showed to be effective for what concerns radiocarbon removal, in some preliminary experiments (see Fig. 3.2.22-23): a multi-step process MINOS (Multi Inert Oxidising Step) performed by reloading the graphite sample surface with atmospheric oxygen and by repeating the same thermal treatment in inert gases, as it can be seen in Figure 3.2.22 [7]. The process takes advantage of the ability of graphite to adsorb gases at its active sites (see Fig. 3.2.22).

After a first inert gas roasting at high temperature, in order to remove Tritium and to desorb the captured gases, a reloading is predicted with e.g. oxygen at low temperature, favouring in such a way the adsorption of reactants. The next step consists on a second roasting under inert gases, in order to allow the local reactions of the adsorbed gases and hinder the massive corrosion of graphite. These two steps can be iterated until the decontamination is satisfactory. At the end, a conditioning improvement by different methods or other treatments (e.g. chemical, microbiological, etc.) can be applied.

A first approach to the MINOS process, with intermediate exposure of the sample at ambient air between the roastings, is reported in Fig. 3.2.23. Such experiment shows the influence of adsorbed oxygen on the release of radiocarbon and seems to be the most promising way to remove C-14 from graphite in a selective way.

A scheme of the proposed MINOS process is reported in Fig. 3.2.21.

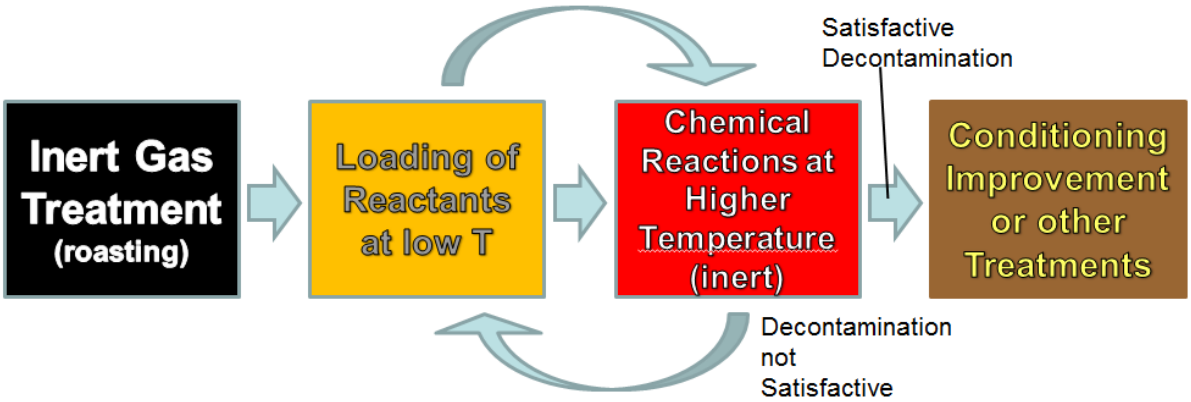

Figure 3.2.21: Scheme of the MINOS process

A schematic view of the active sites in a graphene layer is shown in Fig. 3.2.22.

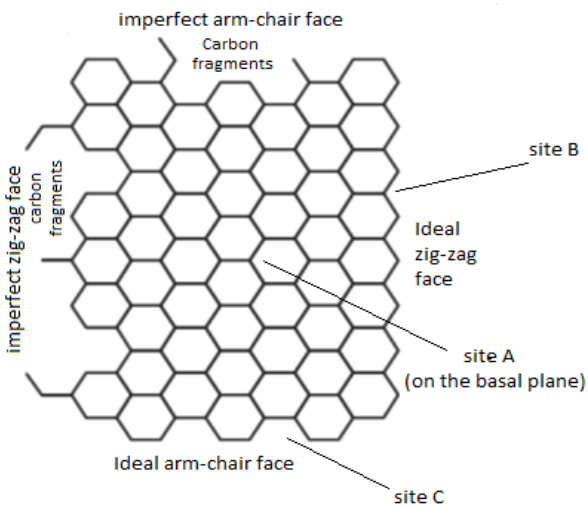

Figure 3.2.22: Schematic view of a graphene layer with active sites, with ideal and imperfect edge structures.

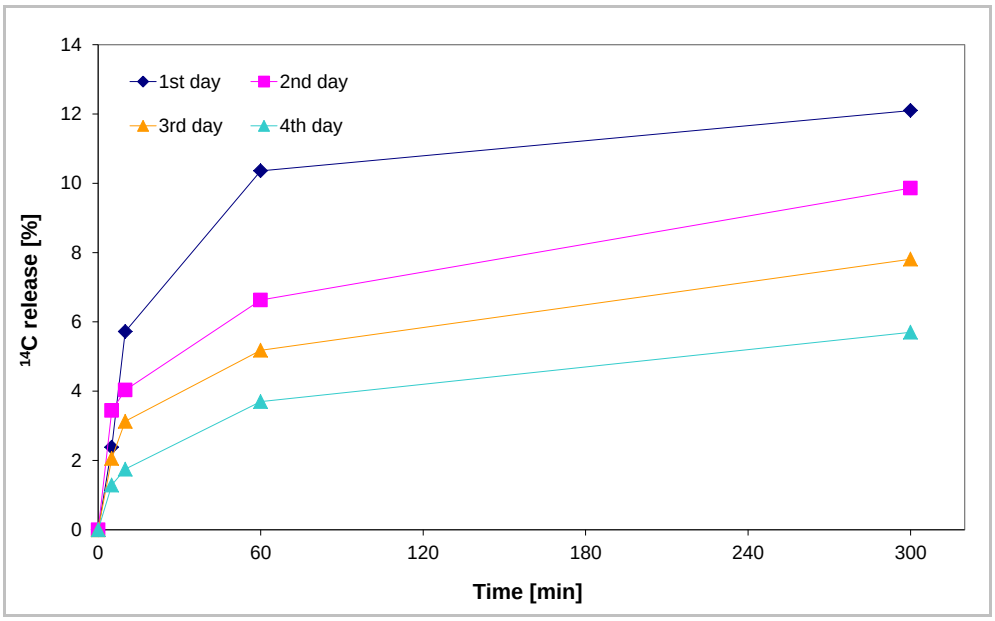

Figure 3.2.23: Repeated thermal treatment of AVR reflector graphite at 900 °C under nitrogen atmosphere after intermediate exposure of the sample to air at room temperature for 20 hours (cumulated ^{14}C release: 35.5%, cumulated release of total carbon: 2.7%, ^{14}C enrichment in the gas phase: 13-20:1) [7]

In a simplified way, the MINOS process is involving the advantages of the different treatments applied (inert, oxidising with steam/oxygen) without their relative disadvantages: exhaustion of reactants in the case of inert thermal treatment, high mass losses and lower selectivities in the case of steam or oxygen treatments. A direct comparison of the first results obtained is reported in Fig. 3.2.24a-b (green line with enrichment between 20:1 and 50:1).

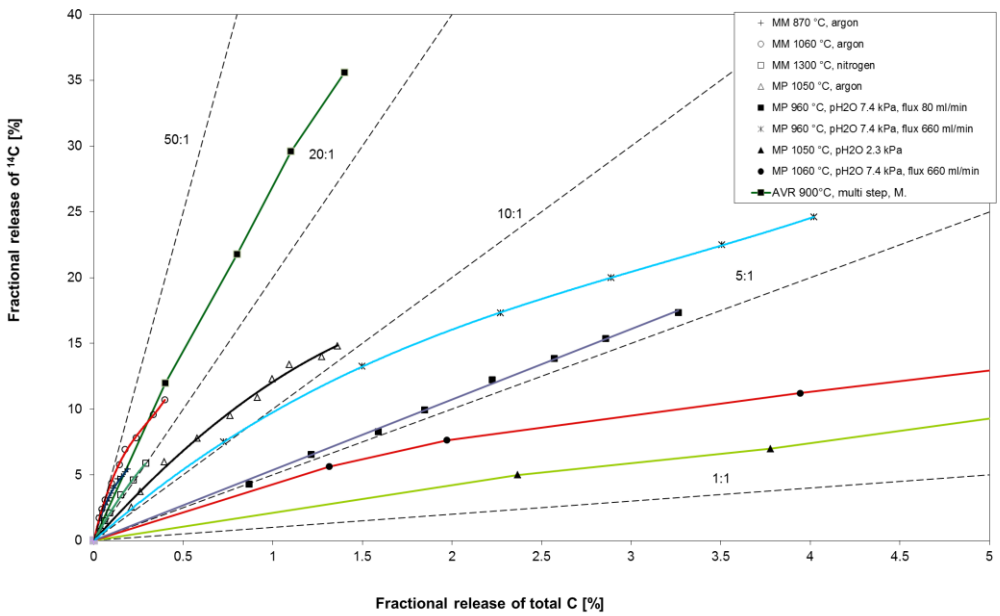

Figure 3.2.24(a): Comparison among different treatments with different gases and temperatures together with the first results of MINOS process, zoomed.

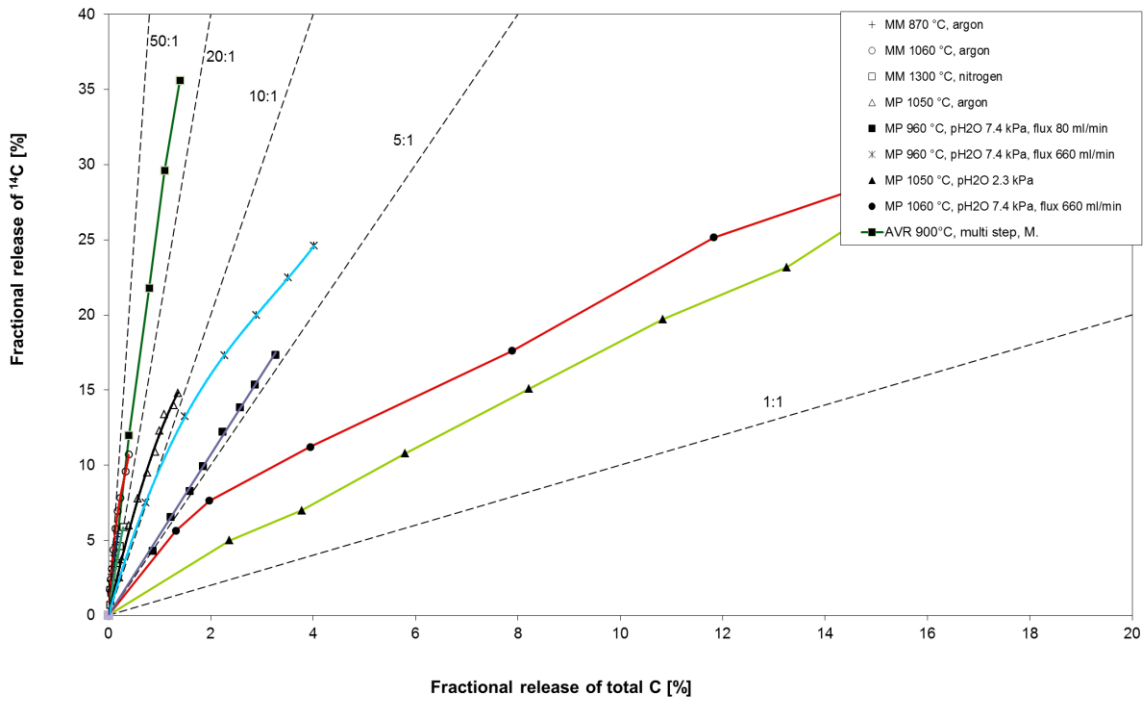

Figure 3.2.24(b): Comparison among different treatments with different gases and temperatures together with the first results of MINOS process.

The application of different regimes allowed developing the MINOS process, based on the following first-approach model for Radiocarbon removal from graphite.

It is considered a simplified first-approach model of graphite with:

- Neutron damage defects
- C-14 enriched surfaces (measured indirectly by [26],[30],[38])
- Different locations (a: basal plane; b,c:edge structures; d: recoiled atoms; e: graphene-embedded C-14)

The model is in accordance with the identified removal routes, based on the experimental observations:

- Diffusion of C-14 atoms from interstitials or defects to the outer surface of the graphite matrix;
- Selective removal of C-14 from the enriched layers near to the surfaces by slight oxidation (or interaction with leachants);

An overview of the model is reported in Fig. 3.2.25-26, before and after thermal treatment (e.g. MINOS). It can be observed (Fig. 3.2.26) how the application of a thermal treatment could be able of removing only part of the C-14, due to its different locations and related behaviour under treatment/leaching. In particular, the superficial C-14 is the first to be removed (sites a,b,c), while the most stable structures are (d) and (e). The application of sufficiently high temperatures is annealing the defects and it is favouring the formation of a more stable structure (approaching the ideal graphite): accordingly, the migration of interstitial C-14 atoms cannot be excluded. Future Molecular Dynamic (MD) calculations should clarify this point. For what concerns the radiocarbon in (e), there is no possibility to remove it in a selective way without oxidising the entire structure. Even a chemical approach would not be effective, due to the identical chemical behaviour of the carbon isotopes (C-12 and C-14). The presence of an "immobilised" fraction of radiocarbon is in accordance with all the performed experiments.

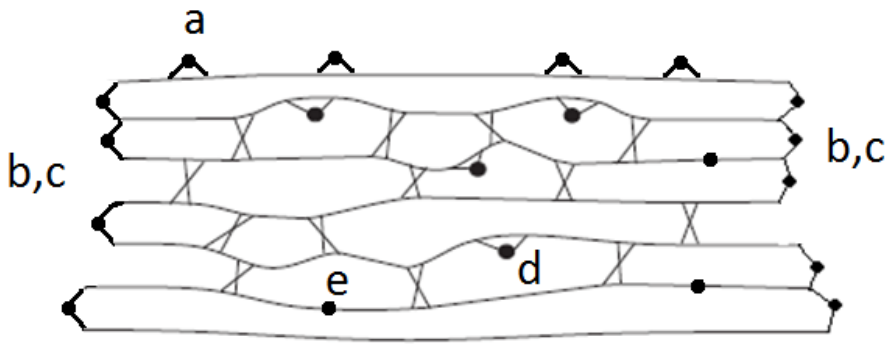

Figure 3.2.25: First Approach model (FZJ) of C-14 location/removal, before thermal treatment (based on neutron damaged structure of [35])

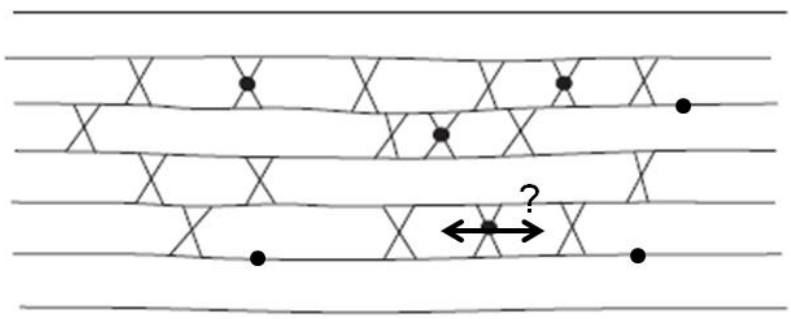

Figure 3.2.26: First Approach model (FZJ) of C-14 location/removal, after thermal treatment (based on neutron damaged structure of [35])

In the next future, the clarification of some points has to be done, as the possible diffusion of interstitial C-14, the systematic correlation of graphite behaviour with sample position in the reactor and the origin of radionuclide distribution, together with an improvement of the model related not only to a thermal treatment but also to the leaching behaviour.

3.3 Release of other Radionuclides

The present work focused mainly on H-3 and C-14 but it has not to be neglected that other radionuclides, as Cl-36, are very mobile in the environment, so a selective removal would be preferred. The problem related to Cl-36 is its very low specific activity (10-100 Bq/g in general): experiments performed with samples in the order of 1 g result in very low activities and Cl-36 beta spectra showed to be comparable with the background, with the equipment used at FZJ. However, several SIMS analyses (some of them are reported in D-3.3.2) performed on virgin massive samples revealed the effectiveness of a thermal treatment in inert atmosphere, with a Cl-37 and Cl-35 removal up to 70% and 90% respectively in the particular case of Saint Laurent A2 graphite. Similar results were obtained with virgin AVR graphite. The link between virgin and irradiated graphite goes through many influencing factors: final remarks cannot be done at the present state, but the above-described results give a hint about Chlorine behaviour under thermal treatment. However, the temperature-dependent removed fraction still needs to be deeper investigated. Other authors reported removal up to 30% for implanted Cl-37 on graphite, with a peak around 350°C followed by a shoulder at 450 °C [36]; it was reported, through XPS analyses, that the removed part was mainly the inorganic Chlorine (as HCl) [37].
However, the implantation experiments and the SIMS analyses interested a limited thickness of the sample: the findings should be confirmed in the next future also for the bulk sample.
In conclusion, it is hypothesised that, depending on the temperature, neutron fluence and operational conditions, part of the most labile Cl-36 is probably removed during operation.

Other non-volatile radionuclides, like Co-60, Eu-154/155, Ba-133, Cs-134/137 showed to be retained in an excellent way in SLA2 graphite during thermal treatment. In general, considering also other nuclear graphite, the only isotope that showed a partial removal at temperatures higher than 1000°C was Cs-(137), with a fractional removal up to 20-35%, depending on the case.

3.4 Detection and removal of Surface Contamination

A special case is when the radionuclide contamination is on the surface of the graphite sample. In Fig. 3.4.1 the release of ^{14}C from graphite, taken from a test assembly (TA), treated in N_2 with 0.1% O_2 at 900 °C is shown. The release isotherms for ^{14}CO and $^{14}CO_2$ are quite linear. This means that the release process is not mainly a diffusion process but a simple oxidation of ^{14}C with the added amount of O_2 in the treatment gas. The released amount of ^{14}C compared to the mass loss of the graphite sample is also significant: 57.7% of ^{14}C could be released with a mass loss of only 0.70%. This high amount of released ^{14}C was never reached in all the other experiments.
Therefore, the surface of the thermally treated graphite sample was analysed by autoradiography and significant shadows were found, typical for surface contaminations (see Figs. 3.4.2(a,b)). This is in accordance with the information from the graphite supplier: the surface of the used graphite sample is a real surface which was in contact with coolant gas in a test assembly facility. The coolant gas was CO_2. It is possible that the coolant gas contained ^{14}C compounds or ^{14}C-containing particles and deposited them on the surfaces of the reactor internals. In that way, a thin film with a high concentration of ^{14}C was formed on the surface of the graphite sample: such a surface contamination can be easily removed by slight oxidation. However, the origin of the contamination is not completely clarified: also in this case, the traceability of the sample represented a problem.

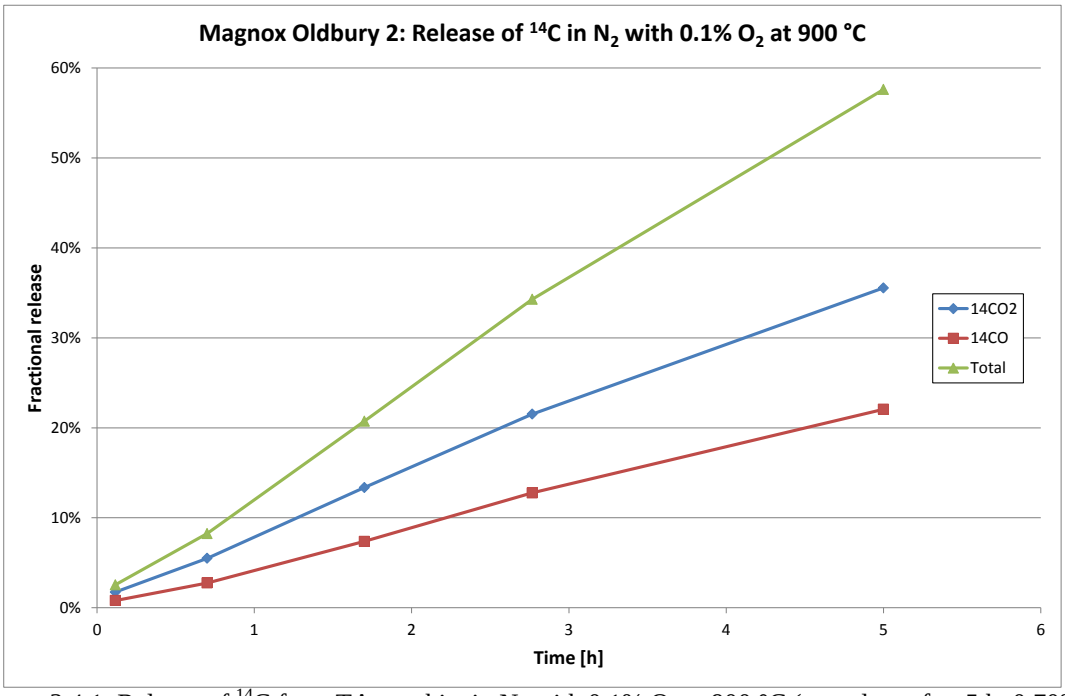

Figure 3.4.1: Release of ^{14}C from TA graphite in N_2 with 0.1% O_2 at 900 °C (mass loss after 5 h: 0.70%)

Figure 3.4.2(a,b): Spatial distribution of beta-emitters on the surface of the TA (Test Assembly) graphite sample from Fig. 3.34 after thermal treatment determined by digital autoradiography (specimen diameter: 15 mm, thickness: 5 mm, mass: 0.7684 g)

The spherical fuel elements of a high-temperature pebble-bed reactor are another example for surface contamination. It is well-known that the surface of the pebbles is enriched with ^{14}C, like it is shown in Fig. 3.5.3 [16]. Also this contamination can be removed by the described oxidation method.

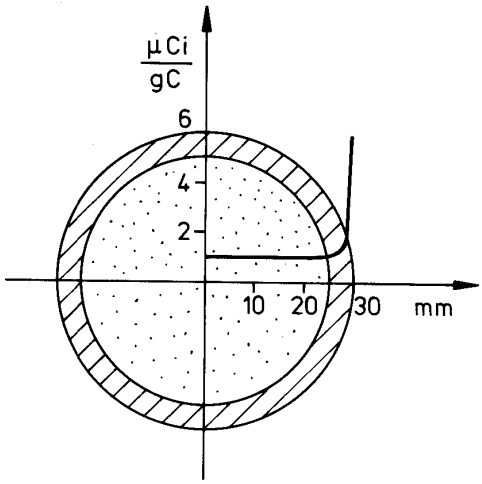

Figure 3.4.3: ^{14}C profile of an HTR fuel pebble [16]

3.5 Waste Management Strategies

Considering neutron-irradiated nuclear graphite as waste, the specific radioactivity of graphite is important to decide what is the best waste management strategy. The specific radioactivity of Merlin graphite is relatively low, whereas the specific radioactivity of Magnox Oldbury 2 graphite is one to two orders of magnitude higher (see Table 3.5.1). Therefore, a treatment process for Magnox graphite is more favourable than for Merlin graphite. However, the removability of tritium and ^{14}C from Magnox graphite is low, excluding the case of surface contamination. In general, the residual tritium and ^{14}C are strongly bound in Magnox graphite, probably as a consequence of radiolytic corrosion. For this reason, it can be concluded that Magnox graphite is a good "retainer" for tritium and ^{14}C. This facilitates the waste management strategy for Magnox graphite because the risk tritium and ^{14}C leaching in an uncontrolled way is relatively low, since this material has been already "pre-treated" in situ.

Nuclide	Specific Activity [Bq/g]	
	Merlin	Magnox Oldbury 2
^{3}H	1.00E+03	4.49E+04
^{14}C	3.24E+02	4.41E+04

Table 3.5.1: Isotopic inventory of Merlin and Magnox Oldbury 2 graphite (date: 15th June 2012).

The same conclusion can be stated in principle also for UNGG Saint-Laurent A2 graphite. The investigated UNGG samples showed only low ^{14}C releases during thermal treatment in inert gas. However, the removability of tritium, especially in form of HTO, showed to be significantly higher. Therefore, it may be advantageous removing tritium by thermal treatment since it could be released in an uncontrolled way, for example by exchanging with humidity.
Thermal treatment of irradiated graphite may be a good method for preparation of final disposal even if the removability of ^{14}C is only moderate or low. It is well-known from the manufacturing process that graphite structure is formed by high-temperature treatment. It is also well-known that thermal treatment of irradiated graphite leads to an annealing process of structural defects. Therefore, it can be concluded that loosely bound ^{14}C on the surfaces of the graphite crystallites or between the graphite lattice planes will be incorporated more stably in the graphite lattice by thermal treatment, at least partially. This can be imagined when considering Fig. 3.5.1: Carbon atoms in different structural units form step by step the well-known C_6 rings of the graphite lattice planes which then form the stable graphite crystals. In this way the ^{14}C atoms are totally equal to the other $^{12,13}C$ atoms which normally form natural graphite. A fraction of ^{14}C is thus immobilised and cannot be released without destruction of the graphite matrix.

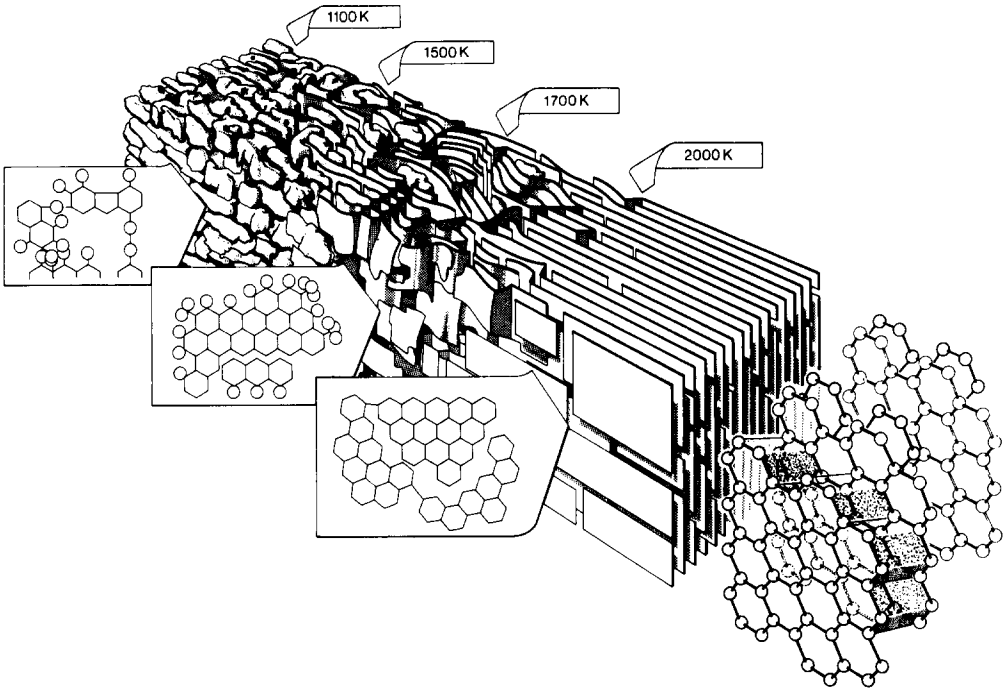

Figure 3.5.1: A model of changes from mesophase to graphite during heat treatment [17]

Another approach deals with the possibility of a partial reduction of the radionuclide inventory of irradiated graphite by appropriate methods, such as inert gas/steam/MINOS thermal treatment. Such a treatment can be adopted if thereby, for example, the final disposal of irradiated graphite is simplified. To answer this question, a cost-benefit analysis is necessary: various options, partially presented in this report, have to be analysed for their economic and social profit.

3.6 Thermal Treatments: Summary

Thermal treatments have been accounted as a possible way of decontamination of i-graphite. In particular, the present work dealt with thermal treatments under inert gases (Argon or Nitrogen), oxygen and steam.
Several experiments, performed on virgin graphite as on irradiated one at FZJ, underlined the presence of oxidising species in the graphite matrix, together with other impurities. Such species are e.g. adsorbed gases, adsorbed water, on the surfaces, or embedded in the graphite matrix as a result of the manufacture process and the history of the sample. The application of an inert atmosphere is favouring the desorption/pyrolysis/reaction of the above-mentioned species, resulting in a slight oxidation of the graphite, with typical mass losses lower than 0.5-1%. The intention of thermal treatments was then to operate under argon atmosphere, in order to measure the off-gases and to connect their release with the embedded species and with temperature. A general quantitative evaluation of such adsorbed/embedded species cannot be provided since the relative amounts are strongly correlated with the graphite history; in addition, the sample preparation could affect the results, especially when small samples are used; moreover, most of the times, the complete history and conditions of a graphite sample are unknown. However, what has to be underlined is the fact that an inert gas thermal treatment is involving also chemical reactions, which are leading to a partial removal of volatile radionuclides in the form of e.g. water, H_2, CO, CO_2, CH_4.
Thermal treatments in inert gases, without any leakage, revealed the exhaustion of chemical reactions after a certain time, with saturation of the radionuclide emissions. Following the line of thought, the next step consists on applying oxidants, as oxygen or steam, in order to improve the removal of certain radionuclides by (radio-)chemical reactions.

Thermal treatments implying oxygen as reacting gas, in concentrations up to 1%, revealed to be inefficient from the point of view of radionuclide selectivity: graphite is a relatively stable material and it starts oxidising at relatively high temperatures. The application of oxygen revealed high reaction rates, but focused on the surface (regime II and II), resulting in a non-selective removal of radionuclide and a simple corrosion of the sample

Thermal treatments with water steam revealed to be promising from the point of view of both Tritium and Radiocarbon. Water vapour is a “mild” oxidising agent, which starts reacting at 800°C. The advantage of steam is the fact that all regimes establishing in the porous material are shifted upwards in temperature of about 300°C, compared to the case of oxygen. Accordingly, lower oxidation rates are possible in concomitance with a deeper penetration of the reactants in the sample.

Carbon Dioxide could be used as reactive gas in a thermal treatment: it is another mild oxidant that should be investigated more in detail. However, a dilution of C-14 is expected in the secondary waste produced.

For what concerns Tritium selective removal from i-graphite in inert gases, the model which best describes the mechanism is the one developed by Atsumi (see Chapter 7.1.1.1), on which hydrogen is present in different trap-sites with different removal activation energies. The

mechanism can be reproduced as a diffusion-controlled one. Experimental data from FZJ confirmed these findings on several i-graphite coming from different reactors and histories:

- Low-temperature-irradiated not-corroded graphite (as in MERLIN) showed the highest Decontamination Factors (DF), increasing with the treatment temperature, up to 30 for a treatment at 1300 °C 21 h isothermal.
- High-temperature-irradiated not-corroded graphite (as in AVR) showed lower decontamination factors due to the fact that high temperatures favoured the migration of Tritium during reactor operation; it is hypothesised that the remained Tritium is more stable (e.g. present as interstitial or clusters), fact confirmed by several experiments: higher temperatures are necessary for its removal. Moreover, it cannot be excluded that part of the Tritium diffused from the carbon-brick insulation barrier to the reactor. Decontamination factors obtained at FZJ resulted in about 5 maximum for a treatment at 1280 °C 7h isothermal.
- Medium-temperature-irradiated and corroded graphite (as in UNGG and MAGNOX) showed very low DF (up to 1.4) due probably to the fact that the graphite experienced high radiolytic corrosion during reactor operation (up to 40%): trap 1 sites are believed to be the major fraction remained.

Diffusion coefficients for Tritium have been calculated in the order of 10^{-12} cm^2/s at 1060 °C; activation energies are in accordance with the ones reported by Atsumi and Fischer: 1.3 eV (no significant trapping, verified also by IPNL), 2.6 eV (Trap 2) and 4.6 eV (Trap 1).
In general, higher temperatures provide higher decontamination factors, with different removal efficiencies depending on the graphite coming from different reactors, as described above. As a general statement, temperatures higher than 1100 °C are recommended for a tritium-removal process: treatment times are decreasing significantly by raising the temperature. The maximum temperature applied up to now has been 1300°C: in the next future, investigations at higher temperature could result in a more straightforward removal of Tritium from i-graphite.
These findings are in accordance with the Deuterium implantation and thermal treatment investigations performed by N. Toulhoat, N. Moncoffre and Y. Pipon (IPNL-University of Lyon), reported in D-4.2.3. It seems to be possible removing completely Tritium from i-graphite but further investigations, especially with massive samples (10^2-10^3 g), are necessary to confirm the findings here reported and to optimize the maximum dimension necessary for an efficient removal in an industrial scale. From the speciation point of view, further clarifications on the fraction of HT/HTO released are necessary, excluding secondary reactions.

The addition of limited amounts of oxygen revealed an apparent positive effect on Tritium removal; however, considering the fractional removal with the mass loss, it results that the enhanced decontamination is simply due to an oxidation process. In that way, a selective decontamination of graphite from Tritium by using oxygen is not advisable.

Steam thermal treatment showed a marked effect on Tritium removal, even at relatively low steam partial pressures (1.6 kPa). The phenomena taking place during such a treatment have been identified: temperature effect, as in the case of inert gas experiments; corrosion effect, as in the case of oxygen experiments, with the difference of a lower reaction rate and a more homogeneous reactant distribution inside the sample; isotopic exchange effect, due to the presence of water vapour inside the porous structure. The influence of these effects on H-3 removal is, in descendent order, isotopic exchange, temperature and corrosion.

A comparison with similar treatments in argon, with same treatment time and temperature, reveals the fact that the usage of steam (10 g/kg or 1.6 kPa of partial pressure) is accelerating the release: 70-80% of Tritium was released within 4 hours at 1000°C in steam against a fractional removal of 20-25% in pure argon at the same temperature, for the same graphite grade. On the other hand, the same fractional release can be obtained at lower temperatures in the case on which steam is used. High tritium release can be obtained even at temperatures lower than 1000°C: the acceleration of the migration process is favoured by the presence of isotope exchange reactions. A comparison of the different graphite grades is providing similar observations as in the case of inert thermal treatment. In particular, Merlin graphite provided again the highest fractional releases; on the other hand, graphite irradiated under CO_2 at moderated temperatures resulted in limited tritium removal, up to 20% after 4 hours at 1000°C against about 70% in the Merlin case.

For what concerns radiocarbon, in the past no models have been established: only some experimental data was available. Several molecular dynamics simulations performed at INBK-Aachen showed that the C-14 formation process is associated with the recoil of ^{14}C atoms with a kinetic energy in the range of some keV (2.56 keV for the ^{13}C activation and 42 keV for the activation of ^{14}N) leading to its removal from the lattice site. The transfer of ^{14}C is accompanied by various interactions and ionization processes that result in a disorder of the lattice structure as well as in the formation of further displacements (interstitial atoms and vacancies). The recoiled atom showed to be displaced by a mean distance of about 50-60 nm with a starting energy of 42 keV (due to the neutron activation of N-14), with an initial smooth energy loss of about 100 eV/Å and a sudden energy drop after getting energies lower than 5 keV, probably caused by electronic interaction and ionization (Bragg-curve-like behavior). ^{14}C from ^{13}C-activation is also displaced from its original position, but the range is limited to few lattice distances. However, the result depends on the type of the potentials governing the interaction between the individual atoms in the short range and the recoil direction in relation to the orientation of the crystal lattice. Resulting from the symmetrical character of the individual atoms at the c-layers, the mean range and the transport of the primary C-14 showed not to be significantly influenced by the temperature variation. This result, however, needs to be verified by detailed modeling of the boundary conditions. In addition, Molecular Dynamics (MD) simulations showed that a significant accumulation of C-14 in the vicinity of grain boundaries or surfaces (pores) caused only by the stopping processes (potentials) is not expected with the assumed model. Improvements of MD modeling could clarify this point.
Assuming as the main contributor to C-14 formation the N-14 adsorbed on the surfaces, considering the MD results and in particular the recoil range of C-14, it seems to be confirmed that the removal of radiocarbon could occur because of a slight oxidation of the graphite surfaces, assuming its superficial enrichment. Experimental results showed that the removal of radiocarbon is correlated with the oxidation of graphite; FZJ and ITU experienced selective removal of C-14 during Thermal Treatments in inert gases. However, the presence of e.g. small amounts of oxygen showed to increase at the same time the C-14 release and the mass loss, resulting in a less selective removal.
Following these findings the possible routes for radiocarbon removal are:

- Diffusion of C-14 atoms from interstitials or defects to the outer surface of the graphite matrix;
- Selective removal of C-14 from the enriched layers near the surfaces by slight oxidation;

Considering the possible identified removal mechanisms, the "temperature effect problem" must be considered: temperature is affecting in opposite ways the reaction rates and the established regime in the graphite sample. A separation of the steps, i.e. reactant loading and chemical reactions, could be an effective solution to remove C-14 more selectively without high corrosion of the graphite.
Concerning the C-14 DFs for graphite coming from different reactors, several experiments proven that, in general, low values can be achieved with a continuous process (up to 1.2) with a limited mass loss. A special case is the graphite from UNGG and Magnox, which experienced high mass losses during operation in the reactor: the surface-enriched assumption is less reasonably applicable, since it is believed that the main contribution to the remained C-14 is C-13, supposed to be homogeneously distributed and embedded in the graphite. Considering a possible diffusion of C-14 during thermal treatment, low DFs are expected anyway in comparison with not-corroded graphite, since a "quasi in-situ treatment" already occurred.
Concerning the removable fraction of C-14, a total decontamination seems not to be achievable, unless an isotopic separation process is established. A first-approach model has been established. The removable fraction depends strongly on the graphite history; a particular recommendation for thermal treatments in inert atmosphere is the application of separate treatment steps: the MINOS (Multi INert Oxidising Step) process has been established. It consists on separating the loading of reactants and occurring of chemical reactions, allowing in such a way a targeted removal of tritium as first and radiocarbon-enriched surfaces as second. Preliminary tests of the MINOS process have shown promising results.

In order to fix some thresholds, as e.g. mass loss and C-14 removal target, a dedicated study that takes into account graphite history, together with an individual management strategy, should be established.
Concerning the creation of a dedicated model for C-14 removal in nuclear graphite, several factors have to be considered: the situation at the open surface of the crystallites is not clear, the radiation damage changes the structure and, in addition, orthogonal/parallel migration pathways have to be accounted. At the present state of the art, a full-scale model is difficult to create.

Several SIMS analyses (as reported in D-3.3.2) performed in FZJ on virgin massive samples revealed the effectiveness of a thermal treatment in inert atmosphere, with a significant removal of Cl-37 and Cl-35. The link between virgin and irradiated graphite goes through many influencing factors: final remarks cannot be done at the present state, but the above-described results give a hint about Chlorine behaviour under thermal treatment. The temperature-dependent removed fraction still needs to be deeper investigated. Other authors reported removal up to 30% for implanted Cl-37 on Saint Laurent graphite, with a peak around 350 °C followed by a shoulder at 450 °C [37]; it was reported, through XPS analyses, that the removed part was mainly the inorganic Chlorine (as HCl) [38]. However, the implantation experiments and the SIMS analyses interested a limited thickness of the sample: the findings should be confirmed in the next future also for the bulk sample. In conclusion, it is hypothesised that, depending on the temperature, neutron flux and operational conditions, part of the most labile Cl-36 has been probably removed during reactor operation.

In conclusion, thermal treatments implying small amounts (>1%) of oxygen are advisable exclusively for surface decontamination, since the reaction rates are excessively high and the profile of reactants is approaching regime III even at relatively limited temperatures.
Steam thermal treatments are promising from the point of view of radiocarbon removal: the dilution of Tritium is generating secondary waste that has to be considered. However, it could be possible to optimize the steam partial pressure/flow in order to have a limited dilution of Tritium in the off-gases. Optimization of several treatment parameters has still to be performed in the next future.

In the case a thermal treatment is going to be exclusively applied as the only "conditioning process" prior to final disposal, the leaching behaviour of C-14 and other residual volatile radionuclides is expected to be significantly improved. On the other hand, in the case a thermal treatment is thought to be part of a multi-step decontamination process (e.g. exfoliation, chemical separation, etc.), it is recommended to use it as the first step since it is able to remove selectively several volatile radionuclides (as H-3, C-14, Cl-36), which otherwise would be diluted in the used chemicals (e.g. acids), while metals showed to be effectively retained (except for Caesium).

A general recommendation is to consider any nuclear graphite with its own history as a unique case, since the effectiveness of a thermal treatment is significantly affected by several variables, as irradiation temperature, neutron flux, irradiation atmosphere, storage conditions, manufacture process and parameters, presence of impurities, etc. In addition, a systematic correlation with the above-mentioned parameters still needs to be done in order to have a better understanding of volatile radionuclides´ removal mechanisms and to develop a variable-dependent model for every single i-graphite (UNGG, HTTR, Magnox, MTR, etc.).

An inert gas thermal test could be a promising method to understand the key features of any i-graphite from the point of view of the release related to the mass loss: it could be a good indicator of the i-graphite treatability. Consequently, once the characterization has been performed, the relative management strategy can be assessed.

4. Graphite Decontamination with Liquid Agents

Chemical decontamination is usually carried out by leaching with the selected reagents the material to be decontaminated by immersing them in a flask/tank containing the reagent, which is then agitated.

When selecting a suitable chemical decontamination process, in addition to the general considerations and in view of the variety of chemical decontamination processes available, several criteria must be considered in a detailed analysis based on site specific conditions. Most of the criteria are related to the specific features of nuclear graphite, such as:
Structural damage in the material in relation with history of operation (to determine contamination profile);

Nature of the contamination; distribution of contamination
Effectiveness of previously used chemical decontamination processes; Requirements (e.g. recycling versus disposal); quantity and type of secondary waste from decontamination and conditioning; time and costs
Chemical decontamination normally consists of consecutive treatments of contaminated materials with different chemicals that dissolve the contaminant in some cases other treatments could be combined with the chemical treatments.
Treatment of graphite with liquid decontamination agents is an alternative option to the gas phase reactions. Mineral acids, alkaline solutions, dissolved oxidising agents, organic washing detergents or such combinations may dissolve the contamination in the graphite. Leaching tests will be undertaken to determine decontamination factors

4.1 Experimental

Four types of process were testing within task 4.3. The Long term semi-dynamic leaching test performed by University of Manchester, Short term Leaching tests, Leaching test with organic agent added with ultrasonic devices and Solid-Liquid extraction (soxhlet decontamination process)

4.1.1 Test Samples

4.1.1.1 Long Term Leaching Samples (UoM)

Two types of irradiated graphite material were used in this project. Irradiated graphite samples were collected from the British Experimental Pile Zero (BEPO) Energy Reactor that shut down in 1968 resulting in 43 years of decay to date this allows an easy manage in Lab. Samples from channels 1 and 16 were treated in the study. The second irradiated graphite material was sourced from the Wylfa Magnox Reactor 1. Two samples were trepanned from the fuel channel wall, sample 1413/02 9U comes from an upper position in brick nine and sample 1319/12 8U comes from an upper position in brick eight. Initial inventory is provided and calculate for decontamination factors.

4.1.1.2 Soxhlet Extraction (FZJ)

The samples used in the Soxhlet Extraction tests were removed from the thermal columns of Merlin reactor during the reactor block's demolition. Ten individual graphite bricks were removed from the bottom right channel of thermal column II in the reactor block. A sample was removed from each one of these graphite bricks.
Each of these 10 samples was analyzed for radionuclides by LSC and γ spectrometry. The results of this analysis showed that the samples contain the following radionuclides: ^{3}H, ^{14}C, ^{60}Co, ^{133}Ba, ^{152}Eu, ^{154}Eu and ^{155}Eu. The reactor graphite's total inventory of contaminants was determined using ICP-MS measurements.
The samples for the second series of tests were taken from the core's graphite jacket of AVR reactor. The coordinates of the samples are not available so that it is not possible to correlate the results with the neutron flux or neutron history of the reactor. The samples available for selection comprised 11 samples from previous test series. These series of tests were performed in order to create a database about the AVR's HTR's activity inventory. The samples for the following tests were selected on the basis of their activity concentrations and dose output (by ALARA criterion). The results of this analysis showed that the samples contained the same radionuclides as shown by the previous measurement, and which are as follows: ^{60}Co, ^{133}Ba, $^{134/37}$Cs, ^{154}Eu and ^{155}Eu

4.1.1.3 INR Inorganic Agents Treatment Samples

Irradiated graphite samples used in experiments comes from TRIGA reactor at Pitesti. According to the analyses performed by gamma ray spectrometry, respectively gamma spectrometry and the analyses performed by proportional counter, the irradiated graphite from TRIGA reactor (referring at the samples used in experiments) contains/is characterized by the following nuclides and radioactive index: Co-60, Eu-152, Eu-154, Cs-137, C-14, H-3.

4.1.1.4 CIEMAT Inorganic Agents Treatment Samples

CIEMAT studied the influence of several factors on the decontamination of i-graphite powder from sleeves of an Uranium Natural Graphite Gas reactor (UNGG) by chemical treatment with liquid agents and then the decontamination of i-graphite block.

Initial activity was characterized in a homogenize sample of sleeves powder. The nuclides identify over detection limits and the ones used for decontamination factor calculation are: ^{3}H, ^{14}C, ^{60}Co, ^{94}Nb, ^{137}Cs , ^{154}Eu, $^{239/40}$Pu and ^{241}Am.

4.1.1.5 Organic Treatment at ENEA

ENEA received 15 cylindrical samples from Latina NPP. They are taken from the drilling of the core in two different radial positions (channel 7 and 8): from each sample were removed both the surface layer exposed to the fuel channel and the innermost layer; the approximate mean weight is 5 g.
The removal of the layer exposed to the channel ensures that the activity present in the sample is representative only of the contribution due to neutron activation.

Seven samples come from the Channel 8 (08F08), while the other eight from Channel 7 (07S07); For each of these 2 groups, the samples come from different level named: *S*, Superior, *C*, Central and *I*, Inferior.
All the samples used in the chemical treatment were firstly crushed by a miller with Titanium knives and then finely grinded by a miller with ceramic knives. From each of them a representative homogenous aliquot were taken and weighted.

4.1.2 Test Methods

4.1.2.1 Long Term Leaching (UoM)

The long term leaching experiments were performed at University of Manchester and constituted part of the PhD thesis of Lorraine McDermott and the summary of the experimental setup and results presented under this point have been collected from the corresponding Carbowaste Technical report.
The determination of release of radiocarbon and tritium carried out in this investigation is making by LSC selecting the cocktails between two options for best determination conditions in combination with aqueous phase 2.5 M in hydrogen peroxide through the results of the quenching (tSIE) in background measurements.
The leaching conditions used are often driven by repository environment or ground water systems. Sample history, size and availability also affect the number of experiments and repeats that can be performed. This gives rise to many different approaches to the experimental conditions and length of test. However often water conditions are used as a standardized method of comparison with amount leached at 100 days also used.

The leaching experiment focused on ^{3}H and ^{14}C removal with minimal damage and weight loss to i-graphite. This research aims to reducing the isotopic inventory of the i-graphite and provide data on the mobility of ^{3}H and ^{14}C within this material. In the test performed a SEMIDINAMYC TESTING (IAEA) with constant monitoring temperature between 20-25ºC over a well known inventory and history samples. Homogeneity of samples were tested by autoradiography beta and gamma determinations and methods for ^{3}H and ^{14}C determinations were validated in the RRT performed in the framework of CARBOWASTE.
Short term (< 90 days) and Long term (> 90 days) experiments were performed according to IAEA methodology as well as the applied frequency of sampling and leaching rate (cumulative and fractional leaching rates).
Both solid and powder samples were used and the surface for leaching calculation was determined by BET analyses. Acidic, Alkaline, Oxidizing, Water and pH buffers were used as leachants.
The leaching program involved two stages, Stage One focusing on proof of concept and Stage Two utilizing other treatment options in addition to leach testing Magnox Wylfa graphite. Testing frequency employed was once weekly until leach rate remained steady then once every two weeks, then monthly as deemed appropriate.
In Stage 1 for BEPO graphite was leached during 85 days with the following conditions: Water (solid and powder), $KBrO_3$ 0.1 M, 0.2M, 0.3M, 0.4M, (powder and solid with 3M) and H_2O_2 0.5M, 1.0M, 1.5M, 2.0M, 2.5M (powder and solid with 1.5M).

In Stage 2 BEPO and MAGNOX graphite were leached during 190 days with the following conditions: Water (MAGNOX: solid and BEPO: powder, Buffer pH 1 (MAGNOX: solid and BEPO: powder), Buffer pH 13 (MAGNOX: solid and BEPO: powder, H_2O_2 0.5 M (MAGNOX and BEPO: powder), H_2O_2 1.5 M (BEPO: powder), $KBrO_3$ 0.5 M (MAGNOX and BEPO: powder), H_2SO_4 0.1M (BEPO: powder), HCl 1M (BEPO: powder) and H_3PO_4 1M (MAGNOX and BEPO: powder).

4.1.2.2 Soxhlet Extraction (FZJ)

Soxhlet extraction is a distillation-based solid-liquid extraction method. It entails heating the liquid phase to boiling point inside a round-bottomed flask using a heating mantle. The resulting steam travels through the riser pipe into the condenser, where it condenses and drips into the extraction thimble to which the Soxhlet extractor is fitted. The extraction thimble contains the solid material. The extracting agent will continue to rise inside the Soxhlet extractor until it reaches the level of the drain and the solvent flows back into the flask. During the filling phase, the solvent can extract the soluble substances from the solid material. This process is continuously repeated.

Soxhlet extraction has the advantage of being able to achieve a high level of concentration of the substance being extracted using only a small amount of solvent. Its only disadvantage is its high energy consumption.
For Merlin and AVR samples the system was similar but not the same. The Soxhlet extraction was performed with both organic and inorganic agents:
INORGANIC; Neutral: H_2O demonized, Acidic (Different concentrations): HCl, HNO_3, H_2SO_4, Alkaline (Different concentrations): NaOH solution.
ORGANIC; Alcohols: C_2H_5OH, ethanol, Ketone (aprotic, dipolar): acetone, Carboxylic acids: acetic acid 6 M and 12 M, Aromatics: Toluene,Halogenated hydrocarbons: CCl_4, 1-Br-butane, Hydrocarbons: cyclohexane, n-hexane and n-pentane

Soxhlet extraction was used for Merlin reactor samples. The amount of solvent used was 60 mL respectively. The test period was approx. 5 hours. In the tests in which HNO_3, the resulting gasses were transferred into a water flask filled with 0.1 M NaOH by means of an argon stream (p = 1 bar). For comparison, some of the tests were performed without introducing argon. These tests showed that the period of time required to complete each leaching cycle was 2-3 times as long when using argon. This increase is due to the triple neck flask's large volume and the longer time needed to heat the flask for each leaching process. The leaching solutions were filled into appropriate flasks. An aliquot of the leaching solution was removed and analyzed by LSC and γ -spectrometry.

The extraction thimbles that were used for solvents with low-volatility at room temperature were rinsed with water and dried. After this, the solid material samples were removed from the extraction thimble. The samples were subsequently heated at 70°C until there was no longer any detectable difference in their weight.

After the tests, approx. 0.15 g were taken from each solid material sample respectively, transferred into a test tube and, just as with the liquid samples, measured by γ -spectrometry.

The experimental set-up used for the AVR graphite differed from the Merlin tests in the volume or the size of the condensers, the Soxhlet extractors and the extraction thimbles were adjusted to the sample volume and were 5-mL instead of 30-mL. The amount of solvent used was 50 mL respectively. The temperature control (3 steps) of the heating mantle was adjusted in accordance with the acids' boiling point.

In each of the tests, the gasses that developed during the tests were transferred into three washing bottles (by means of an argon stream p = 1 bar). The first washing bottle was filled with 0.1 M HNO_3 for capturing tritium and chloride, the second and third washing bottles contained 0.1 M NaOH each for capturing C-14 in the form of $^{14}CO_3^{2-}$.

The extraction thimble with the sample in liquid extraction with sulphuric acid was suspended in a vial in the round-bottomed flask. A hot plate with a magnetic stirrer was used to heat the sample. The sulphuric acid was thoroughly mixed with the magnetic stir bar. The flask temperature was kept at 80°C by means of a water bath. The water bath's temperature was kept constant with the aid of an adjustable hot plate. Following the completion of the AVR tests, the leaching solutions were filled into PE bottles. An aliquot of each of the leaching solutions was removed and analyzed by LSC and γ spectrometry. The solvent contained in the quartz wool from the extraction thimbles was removed and added to the leaching solutions. The extraction thimbles were subsequently rinsed with water and dried. The liquid used to rinse them was collected and its level of activity determined by LSC.

After the drying process, the solid material samples were removed from the extraction thimbles the samples rinsed with water to remove the solvent residues and then transferred into measuring test tubes. They were subsequently placed into a glass beaker and carefully heated at 70°C to remove the residual moisture until their weight remained constant.

4.1.2.3 INR Inorganic Agents Leaching Test

The experiments for removal of Co-60, Eu-152 & Eu-154 consisted in contacting the i-graphite (under the powder form) with different acids and mixtures of acids:
HNO_3 65% [1-g], HNO_3 65% (1:1) [2-g], HCl 37% [3-g], HCl 37%(1:1) [4-g], H_2SO_4 98% [5-g], H_2SO_4 98%(1:1) [6-g], H_3PO_4 85% [7-g], H_3PO_4 85% (1:1) [8-g], HNO_3 65% : H_3PO_4 85% (1:1) [9-g], (HNO_3 65% : H_3PO_4 85%): water (1:1) [10-g], (HCl 37%: HNO_3 65% (1:1)): water (1:1) [12-g], HCl 37%:H_2SO_4 98% (1:1) [13-g], (HCl 37%: H_2SO_4 98% (1:1)): water (1:1) [14-g], oxalic acid 10% [15-g], citric acid 10% [16-g], oxalic acid 10% : citric acid 10% [17-g].

For all experiments the contacting time was 6 days. The vials were periodically mechanically shaken. After the contacting period a known quantity of demineralised water was added and then they were centrifuged for 7 minutes and filtrated. The both, filtrates and graphite samples, were measured.

4.1.2.4 CIEMAT Inorganic Agents Leaching Test

It has been studied the decontamination of Cs, Co, Eu, Pu and Am with several leachants: nitric, hydrochloric, phosphoric, sulphuric with citric and oxalic acids of different concentrations and mixtures of them. The method followed is sketched on figure 4.1.1.

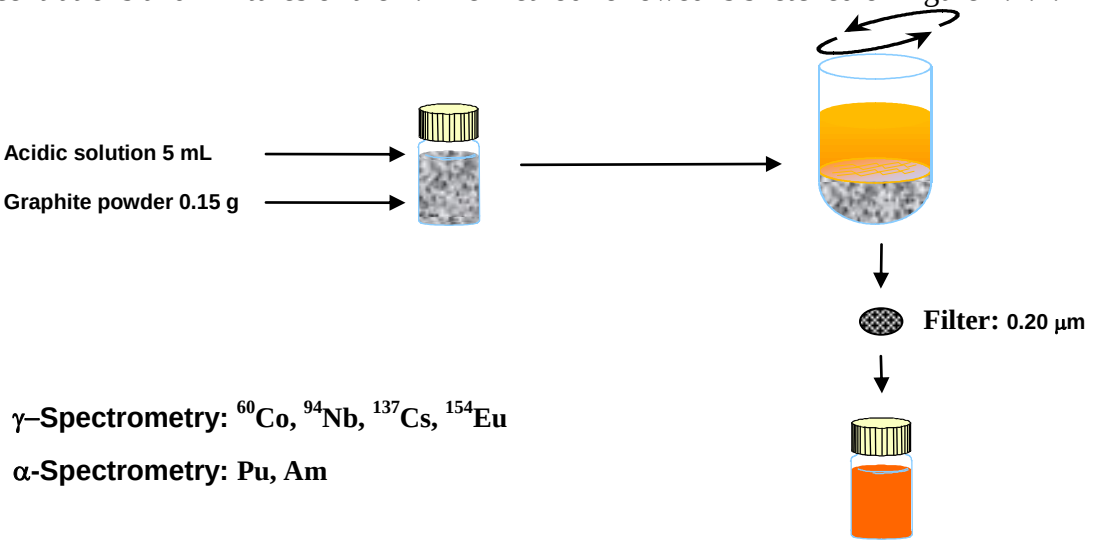

Figure 4.1.1: Method followed to study the decontamination of ^{60}Co, ^{241}Am, $^{239,40}Pu$, ^{137}Cs, ^{94}Nb and ^{154}Eu in i-graphite powder with several leachants.

In all the experiments a mixture of 0.15g of graphite powder and a solution volume of 5 mL was put into a vial and was shaken for 24 hours. Then, the mixture was centrifuged and the supernatant was removed and passed through a 0.20 µm filter. The filtrate was measured both by alpha and gamma spectrometry. The leaching procedure was carried at three different temperatures 20, 60 and 80 ºC and using different concentrations.

Leachants tested were: 6M HCl at 20ºC, 3M HCl at 20ºC, 60ºC and 80ºC; 9M H_2SO_4 at 20ºC, 3M H_2SO_4 at 20ºC, 60ºC and 80ºC; 7M HNO_3 at 20ºC, 3M HNO_3 at 20ºC, 60ºC and 80ºC and, 3M H_3PO_4 at 20ºC, 60ºC and 80ºC. Second set of experiments was performed with this mineral acids mixing with 0.5 M Citric or Oxalic acids (not both in the same experiment) as complexant agents, the experiments were performed at 20ºC: 0.5M Citric acid with 3M HCl, 3M H_2SO_4, 3M HNO_3, 3M H_3PO_4 and alone 0.5M citric acid, and 0.5M Oxalic acid with 3M HCl, 3M H_2SO_4, 3M HNO_3, 3M H_3PO_4 and alone 0.5M oxalic acid.

The study of the decontamination of ^{14}C and ^{3}H in irradiated graphite powder was carried out with several leachants: 0.1M sodium hydroxide, 0.1M sodium hydroxide with hydrogen peroxide, 3M nitric acid and mixtures of nitric, hydrochloric and sulphuric acids. In all the experiments a mixture of 0.15 g of graphite powder and a solution.

The experiments were performed with: 0.1M NaOH at 20ºC, 0.1M NaOH: H_2O_2 at 20ºC, 3M HNO_3 at 20ºC, H_2SO_4 98%:HNO_3 65% (4:1) at 20ºC, H_2SO_4 98%:HNO_3 65% (1:4) at 20ºC, H_2SO_4 98% at 20ºC, H_2SO_4 98% at 80ºC, HNO_3 65% -HCl 37% (1:3) at 80ºC and H_2SO_4 98%:HNO_3 65% (1:4) at 80ºC.

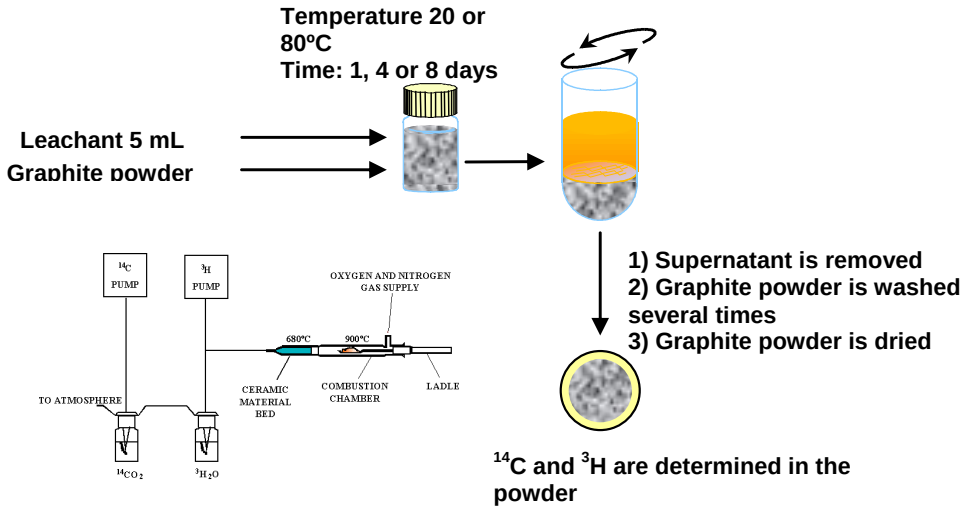

Figure 4.1.2: Experimental set-up for leaching experiment for tritium and radiocarbon including separation procedures for determination.

In all the experiments a mixture of 0.15 g of graphite powder and a solution volume of 5 mL was put into a vial and it was shaken for 24 hours. The leaching procedure was carried at two different temperatures, 20 and 80 ºC. The mixture was centrifuged and the supernatant was removed, the powder was washed several times with deionized water and, finally, it was dried and the dried powder was separate in catalytic furnace and measured by LSC for both determinations ^{14}C and ^{3}H.

4.1.2.5 ENEA Organic Agents Leaching Test

The i-graphite from Latina NPP, like as all the graphite coming from moderators exposed to a neutron flux (for Latina NPP is up to 5x1022 n/cm2), presents a wide range and amounts of activation products.

This distribution of activated elements concerns the bulk of the samples, mainly in the closed porosity or between the typical graphite layers. Anyway, there are not usually involved chemical bonds. So that, in order to achieve an exhaustive and valid extraction for activation products, it is important to increase the surface area of the sample. This should allow to the solvent to reach the inner layers/areas (i.e. closed pores, crystallites, etc.) and extract contaminants in solution.
In order to identify gamma radioactive isotopes and to determine the amount of radioactive material, the samples have been characterized by means of a gamma spectrometry system.

This distribution of activated elements concerns the bulk of the samples, mainly in the closed porosity or between the typical graphite layers. Anyway, there are not usually involved chemical bonds. So that, in order to achieve an exhaustive and valid extraction for activation products, it is important to increase the surface area of the sample. This should allow to the solvent to reach the inner layers/areas (i.e. closed pores, crystallites, etc.) and extract contaminants in solution.

The main idea is to apply an exfoliation-like process on the graphite by organic solvents (liquid-phase exfoliation) to produce un-functionalized and non-oxidized graphene layers in a stable homogeneous dispersion. This process, helped by mild sonication, consists in separating the individual layers in a more or less regular manner. Such a separation, being sufficient to remove all the inter-planar interactions, thanks to the dipole-induced/dipole interactions between graphenes and organic solvents, results in a dispersion of the graphite in a workable media. This facilitates processing, treatment and easy characterization for the contaminants recoveries (Figure 4.1.3).

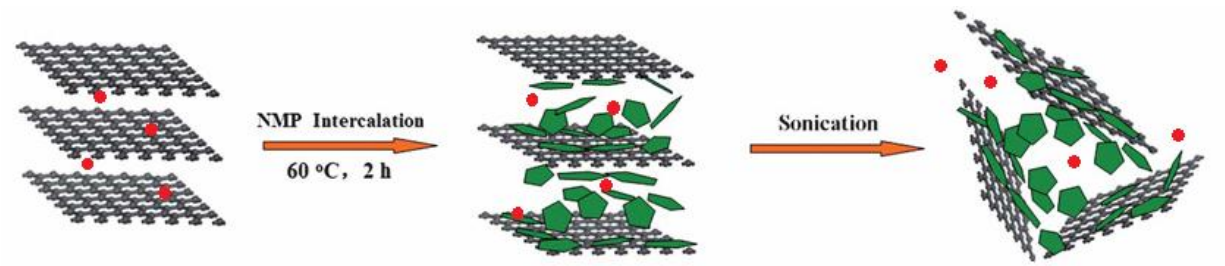

Figure 4.1.3: Representation of the main steps for the graphite exfoliation process promoted by organic solvents and ultrasound assisted

Moreover, no oxidation process is neither performed nor super-strong acid actions. This would lead to non-oxidized products so the graphite would be completely recovered as it is.
The main steps in this process are:

- Organic Solvents choice;
- Low-power Sonication time
- Centrifugation/Extraction
- Removal Efficiency (as % of the recovered activities after treatment with respect to the original values before the treatment)

In order to overcome the van der Waals-like forces between graphite layers to yield a good exfoliation and dispersing the resulted graphene sheets in a stably liquid media, highly polar **organic solvents** have to be used. As suggested from the scientific literatures, the following ones have been firstly tested:

- N,N-Dimethylacetamide (DMA)
- N,N-Dimethylformamide (DMF)
- N-Methyl-2-pyrrolidone (NMP)

All of them are dipolar solvents, miscible with water, aqueous acid solution and most other solvents; they show good solvency properties, able to dissolve a wide range of chemicals. As suggested from literature works on graphite exfoliation processes, the optimal ratio powder/solvent has to be equal or superior to 1:100. So 10ml of organic solvent for about 0.1g of each grounded i-graphite sample were chosen.

Sonication plays an important role in the experimental process as it facilitates the solubilisation and exfoliation of graphite. As it mentioned in literature, the sonication times ranged from 30 min to many hours. The common thing is the bath sonication power should be the lowest possible but there was no reference value. This wide range of sonication time and

lack in mention of power is a great problem in reproducibility. The sonication process is sensitive to many factors, as example: sonic energy input to the sample is sensitive to the water level; exact position of the sample in the bath; volume of the dispersion undergoing to sonication; vessel/vials shapes.
Due to this equipment-related variability the results could differ and be critically depending on the sonication time. 10 hours with a 35W Power Sonication Bath was applied.
Although the right **centrifugation** rate should be widely tested in order to remove all large aggregates to be reprocessed by following exfoliation step, a high centrifugation rate (12000rpm) followed by a filtration step was chosen. The supernatant liquid phases coming from the centrifugation are filtered on RC (Regenerated Cellulose) Filter Disk of 0.2µ and the solutions are clear or grayish.

Radiocarbon has been measured by Liquid Scintillation Counting after pre-treatment of an aliquot of each samples (about 0.12g/sample) by acid digestion with H_2SO_4-HNO_3-$HClO_4$ mixture at 200°C in closed equipment under inert gas-flow (N_2). The $^{1}4C$ (as CO_2) were trapped with washing bottles with NaOH 0.1M. The solutions obtained are completely clear and colorless. An aliquot of each solution is taken has been added with Scintillation Cocktail and measured by Liquid Scintillation Analyzer in dual-label mode with $^{3}H/^{14}C$ reference standards.

4.2 Results and Discussion

4.2.1 Long Term Leaching (UoM)

The Long term leaching test in the phase one was carried out using H_2O, H_2O_2 and $KBr0_3$ leachants. Solid samples from BEPO reactor channels 16 and 20 (0.5 g) were used throughout the 84 day test.

4.2.1.1 Tritium Releas at phase one

The cumulative fraction of ^{3}H released under **water conditions** for 84 days indicates that ^{3}H release began quickly the release of ^{3}H was extremely low as 3.1% of the total tritium inventory from the powdered sample and 1.8% from the solid sample. These release rates illustrate both the mobility of HTO species within the graphite is likely to be bound to the surface groupings which are susceptible to exchange with hydrogen ions in the water and that the differences observed between solid and powder material may be due to a function of exposed surface area.

The steady-state leach rate appears to have been achieved for ^{3}H after 60 days. The low reactive nature seen in this experiment leads to the conclusion that any activity removed under water conditions was surface contamination and easily removed regardless of the conditions employed. These samples had >97% of the ^{3}H and remaining at the end of this experiment.

$KBrO_3$ was used in concentrations ranging from 0.1M – 0.5M. The results obtained for ^{3}H release. All samples were powdered in order to maximize the surface area and leached under varied potassium bromate concentrations. As with water the ^{3}H results show a very slow release, this is only marginally increased with increasing concentrations. 4.2% of the total ^{3}H inventory was released under 0.1M $KBrO_3$ conditions, compared with 5.4% released under

0.4M $KBrO_3$ and 5.6% under 0.5M $KBrO_3$ conditions. Compared to leaching by water (3.4%) it could be concluded that the oxidizing environment provided by the potassium bromate and notably the BrO_3(-) ion, has little effect on leach rate and on ^3H interaction and promotes the HTO exchange theory which is examined with water.

H_2O_2 was used in concentrations ranging from 0.5M – 2.5M. The ^3H release under H_2O_2 began quickly and 9.7% of the total ^3H was released under 0.5M H_2O_2 conditions, compared with the maximum of 17.4% of the total ^3H inventory released under 2.5M H_2O_2. It is clear by the significant increase in the rate of ^3H released is observed under hydrogen peroxide conditions that radiolysis and isotopic exchange of the ^3H with the hydrogen peroxide is considered to be the mechanism behind this increased release rate. Hydrogen peroxide promotes radiolysis and the exchange of HTO from the graphite to the leachant in comparison to the water condition results where only the 3.1% of ^3H is released. In figure 4.2.1 tritium release under H_2O_2 leaching rates are plotted

$$H_2O_2 \rightarrow OH^{\bullet} + OH^{\bullet} \quad \text{Hydroxyl radicals}$$
$$H^{\bullet} + OH^{\bullet} \rightarrow H_2O \quad \text{Isotopic exchange – Radicals}$$
$$H^{+} + OH^{-} \rightarrow H_2O \quad \text{Isotopic exchange – Hydroxyl ion}$$

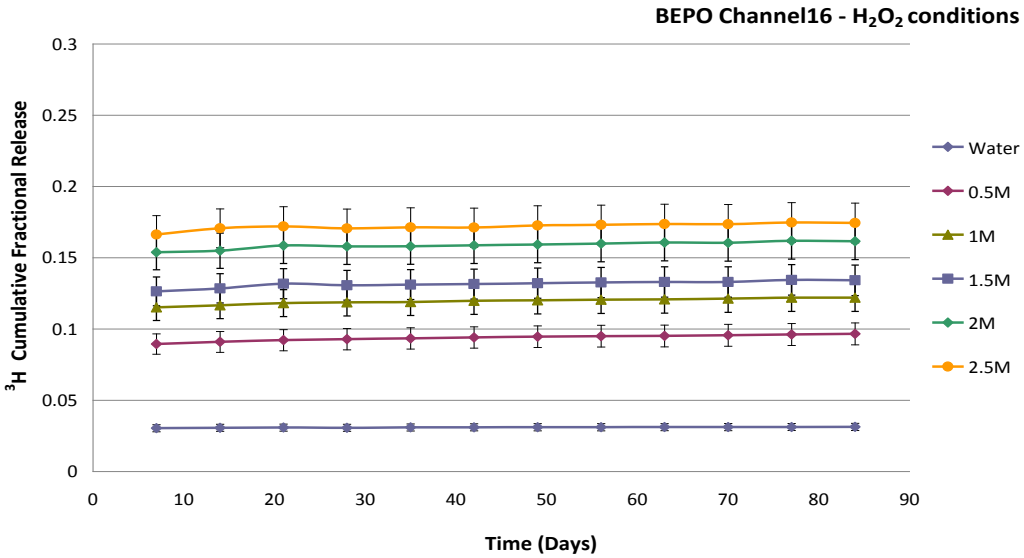

Figure 4.2.1: Powder BEPO ^3H release under H_2O_2 conditions

Comparing the release rates of ^3H for solid versus powder BEPO samples studies with $KBrO_3$ and H_2O_2 were performed. The ^3H release under 0.3M $KBrO_3$ conditions presents 2.1% for the solid sample and 5.2% of the the powdered sample. The release of ^3H under 1.5M H_2O_2 conditions presents 13.4% for the powdered sample and 4.7% for the solid sample.

Comparing powder to solid release rates of tritium, surface area has enabled a significant increase in isotopic release of ^3H. Under 0.3M potassium bromate conditions the solid release rate after the initial points is minimal showing a decrease in release towards 84 days. The powder however is increasing still at day 84, this result was one of the driving factors behind

extending the phase two leaching experiment to over 100 days to observe when all the mobile or reactive forms of ^{3}H are released.

4.2.1.2 Radiocarbon Release at phase one

^{14}C release of BEPO powder under **water** conditions presents a very slow release rate of ^{14}C with 0.87% of the total ^{14}C inventory released from the powdered sample and 0.34% of the total ^{14}C inventory from the solid sample. The speciation responsible for this release indicates dissolved $^{14}CO_2$ as there is approximately 0.04% by volume of CO_2 is present in the atmosphere and water typically contains less than 10 mg/L, however several hundred mg/L of CO_2 can be dissolved into water should the appropriate conditions be met the limited release of ^{14}C under water conditions is most probably derived from dissolved $^{14}CO_2$ species.

The results obtained for ^{14}C release from leaching BEPO samples under **$KBrO_3$** conditions indicates a maximum of 5.7% released from the total ^{14}C inventory under 0.5M $KBrO_3$ conditions. This can be compared to release under water conditions (approximately 1% of the total ^{14}C inventory). Bromine is well known as an intercalation element capable of separating the graphite layers, the bromate ion BrO_3^- present in potassium bromate has had little effect on the graphite structure which is observed through the limited release of ^{14}C. Lower release rates for ^{14}C than expected where achieved under potassium bromate conditions, which leads to the conclusion that mobile/weakly bound isotopes are being removed/release, however due to the large size of the bromate ion and the reduced concentration there is little further interaction occurring between the graphite and the potassium bromate solution after 60 days.

The ^{14}C released under **H_2O_2** conditions for powder BEPO Channel 16 samples presents 11.7% of the total ^{14}C inventory and a maximum of 15.4% under concentrations >2M H_2O_2. The mechanism behind the release of ^{14}C by H_2O_2 is thought to be chemical oxidation by intercalation of any surface bound ^{14}C .With 15 % of the inventory has been released the bulk of the activity has remained locked within the graphite micro-structure. In figure 4.2.2

Differences found between release rates of two BEPO samples can not be based on the inventory and reactor history reasons, the most probable reason is the distribution of ^{3}H and ^{14}C is not uniformed throughout the bulk of the material.

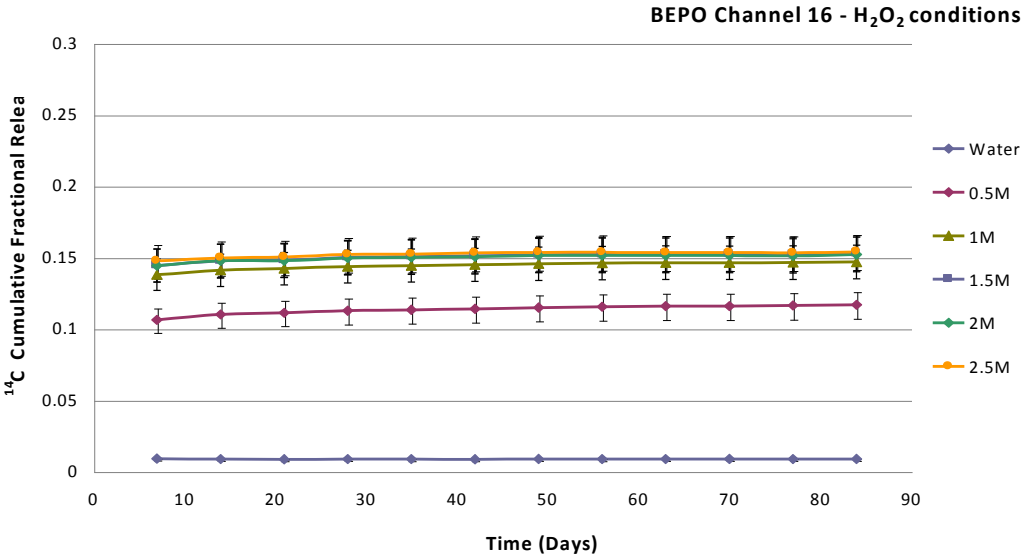

Figure 4.2.2: Powder BEPO ^{14}C release under H_2O_2 conditions

Comparing ^{14}C release under 0.3M $KBrO_3$ solution from powder and solid samples of BEPO, presents 0.9% release of the total ^{14}C inventory for the solid sample and 4.9% for the powdered sample.
A steady state of ^{14}C release is achieved by day 60 for both solid and powdered material under 1.5M H_2O_2 conditions. Surface area has increased the mobility and availability of the ^{14}C. Given the aggressive environment of 1.5M H_2O_2 and the powdered structure of the material only 15% of the ^{14}C was leached out, providing interesting results regarding the structure and bonding of the ^{14}C which remains. A possible conclusion would be that to remove the remaining ^{14}C from the graphite the material it must be destroyed. Employing more aggressive environments for long periods of time will provide further data to support such a statement.

Summarizing phase one

The oxidizing environment of H_2O_2 yielded the highest release activities for both of ^{3}H and ^{14}C removal. The highest values of release where achieved under 2.5M H_2O_2. H_2O_2 reacted with the graphite promoting ^{3}H and ^{14}C releases.

Graphite taken from different channels behaved differently under all leaching conditions. The trend of release rate of ^{3}H and ^{14}C versus leaching environment were consistent with BEPO Channel 16 results. Levels of ^{3}H and ^{14}C removal under water conditions were at the LOD limits for the LSC.

H_2O_2 and $KBrO_3$ were considered from this experiment as an aggressive oxidizing environments leading to the promotion of significant isotopic release. Comparing 0.5M conditions of both solutions H_2O_2 is noted to give the greater release rates.

An average overall weight loss of 12% was recorded, with 4% attributed to transfer between containers and filtering the material at the end of the experiment. The mass loss, compared to

the fractional removal of C-14, reveals that there is no selectivity on the removal: a simple corrosion process took place.

4.2.1.3 Tritium Release at phase two

Phase two leaching test were carried out at room temperature, with a weekly testing frequency up to 190 days. Samples from BEPO reactor and Magnox Wylfa were used.

I-graphite from BEPO channel 1 was leached under water, pH1, pH13, 1M H_3PO_4, 0.5M H_2O_2 and 0.5M $KBrO_3$. Very limited quantities of BEPO Channel 1 graphite was available so these conditions where chosen to provide a comparison to leaching phase one data as well as to provide information on the mobility of the isotopes under an acidic environment. A solution of 1M H_3PO_4 was chosen as the acidic environment and was kept remain constant throughout leaching phase two program this was to provide a contrast to the pH1 buffer which contained 0.2M Hydrochloric acid (HCl).
In this test 4.4% of the total ^3H was released under water conditions, 7.8% under pH1, 4.3% under pH13, 9.6% was released under 1M H_3PO_4, 4.7% under 0.5M $KBrO_3$ and 23.2% of the total ^3H inventory was released under 0.5M H_2O_2 conditions.

The results for cumulative fractional release for BEPO Channels 1 and 16, including BEPO Channel 16 solid samples under pH1 and pH13 buffered solution. Tritium release for BEPO powdered samples under pH1, ranging within 7.8%-11.2%, of the total ^3H inventory being the ^3H release of solid sample in this conditions 3.2%. Under pH13 the same samples ranging from 4.3% to 3.4% respectively. Decontamination factor of 0.27% of the total ^3H inventory was released from BEPO channel 16 solid graphite.

From this data the conclusion can be drawn that, as seen previously for tests with solid graphite samples, which are that under these three conditions hydrogen ion isotopic exchange, can only occur if the ^3H is easily accessible. Limited release is consistently observed under pH13 as well as ^3H release under acidic conditions gives results in the same order of magnitude as previously achieved.

^3H release under all acidic conditions for BEPO powdered samples shows 10.5% decontamination factor under 1M H_3PO_4 and under 0.1M H_2SO_4, 11.8% under 1M HCl and 11.2% under pH1. These data support the previous results for isotopic exchange being the mechanism behind ^3H removal as long as there is hydrogen atoms present in the right environment isotopic exchange with ^3H will occur. The other species present such as Cl^-, SO_4^{2-} and PO_4^{3-}may promote the availability of ^3H through intercalation within the graphite structure but they do not appear to be directly responsible for the release rate.

The same conditions utilized in phase one for BEPO Channel 1 material was tested on Magnox Wylfa graphite. The results achieved for ^3H release tests was 0.13% under water conditions, 9.3% under pH1, 0.11% under pH13, 19.0% under 1M H_3PO_4., 0.09% under 0.5M KBrO3 conditions and 0.47% under 0.5M H_2O_2 conditions. Limited amounts of ^3H were released under water, H_2O_2 and $KBrO_3$. The Magnox material was supplied in a granulated form with a smaller surface area than the powdered BEPO graphite.

Figure 4.2.3 Shown de decontamination factors of H-3 for all conditions and all samples included in this summary

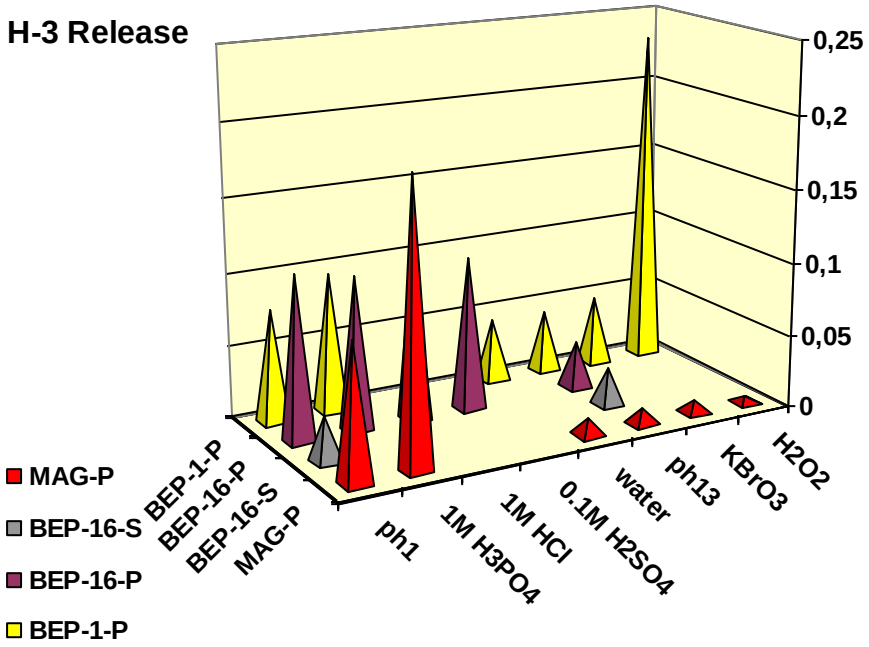

Figure 4.2.3: Tritium decontamination factors in Long Term Leaching tests phase one and two for all conditions. (P: powder; S: Solid //1, 16: Channel n#)

4.2.1.4 Radiocarbon Release at phase two

Decontamination factor of Carbon-14 for BEPO channel 1 graphite under water gave 2.9%, under pH1 20.8%, under pH13 conditions 4.6%, under 1M H_3PO_4 conditions 19.8%, under 0.5M $KBrO_3$ conditions 6.5% and under 0.5M H_2O_2 conditions 0.31%. Regarding phase one lower release of ^{14}C under H_2O_2 conditions were observed, however such an extremely low result should be considered inaccurate.

The data shows that limited amounts of ^{14}C have been released under pH13 and 0.5M $KBrO_3$ there in an increase in release compared to water which was observed under phase one. Interestingly the acidic environments have removed more ^{14}C from the graphite material than previously observed under any other conditions. The mechanism behind this acidic attack is thought to be intercalation of the surface material (penetration of interlayer spaces within the graphite structure), which is a significantly different process to the mechanism behind ^{3}H release. This ^{14}C release under acidic conditions is thought to be due to intercalation.

BEPO Channel 16 powder graphite releases 23.8% of ^{14}C inventory under 1M H_3PO_4, 24.8% 0.1M H_2SO_4, 26.5% under 1M HCl and 25.4% released under pH1. These data support the previous results for intercalation being the mechanism behind ^{14}C removal. The species present in the acids such as Cl^-,SO_4^{2-} and PO_4^{3-} are all capable of intercalation. Using stronger concentrations of these acidic would result in the complete breakdown of the graphite structure. Interesting experiment are also performed within CW-WP4 task where analyze how much ^{14}C is released under such conditions.

Decontamination factors of ^{14}C from Magnox Wylfa graphite showed 2.5% under water conditions, 18.4% under pH1, 1.1% under pH13, 26.8% under 1M H_3PO_4, 1.6% under 0.5M $KBrO_3$ and 3.5% under 0.5M H_2O_2 solution. No significant ^{14}C release under water, alkaline conditions, H_2O_2 and $KBrO_3$ are registered. The acid concentration seems the reason why pH1 solution gives a lower release than 1M H_3PO_4 media. The specific activity of Magnox Wylfa samples probably leads a higher isotopic release for ^{14}C regarding to BEPO. In addition the surface area reduction may have limited the pH1 intercalation effectiveness. From these results ^{14}C appears to be present within the graphite structure in two forms, leachable and non-leachable ^{14}C species. This could well be related to the two main production pathways of ^{14}C origin. Figure 4.2.4 summarized the C-14 decontamination factors in this study.

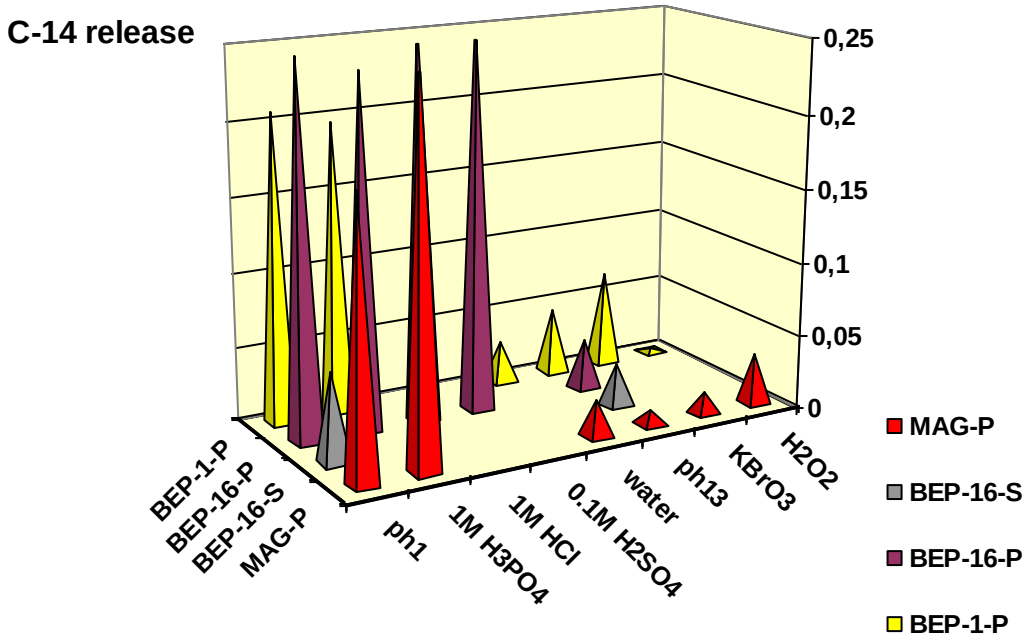

Figure 4.2.4: Radiocarbon decontamination factors in Long Term Leaching tests phase one and two for all conditions. P: powder; S: Solid//1, 16: Channel n#

4.2.1.5 Leach Rate Comparison of BEPO to Wylfa Graphite

The decontamination factors plotted in figures 4.2.3 and 4.2.4 allows the comparison of amount of ^{3}H and ^{14}C released under powder and solid samples to be compared as it takes into account surface area.

The Magnox material tested has significantly difference irradiation history to that of the BEPO material. Magnox graphite has been subject to radiolytic oxidation as well have received a higher fluence than BEPO graphite. This may have contributed to the lower leach rates observed here as surface bound activity of Wylfa graphite may have already been removed due to these two processes, particularly the former. BEPO material was irradiated in an air environment with a lower fluence at a temperature around 40˚C. The isotopic inventory present in BEPO material may therefore have had less processes promoting migration of interstitials and as a result more mobile surface bound species are present giving rise to increased leach rates.

4.2.2 Soxhlet Extraction (FzJ)

4.2.2.1 Experiments with Merlin Samples

Results of total activity of Merlin samples were measured by LSC. When comparing the measured values, the differences in the dissolving power of the solvents become clearly apparent. In contrast to the acids, all of the other solvents removed only very little or no activity at all.

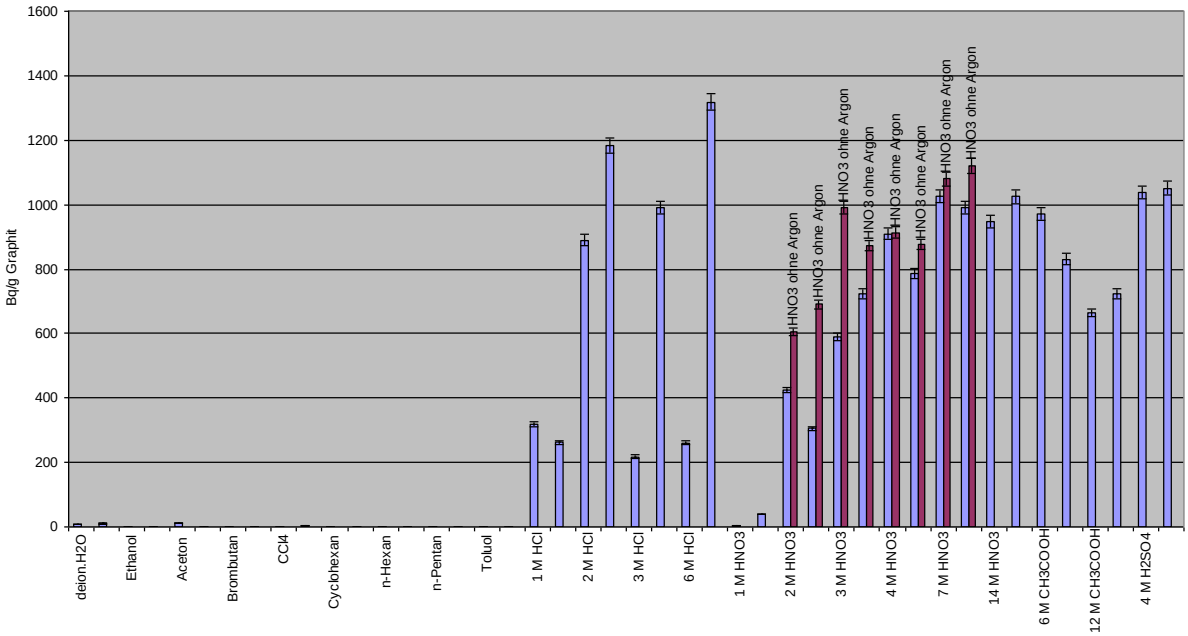

Figure 4.2.5: Overview of all of the measuring results from the Merlin leaching samples

Water, ethanol and acetone remove only very little activity (As ≤ 12 Bq/g) from the graphite samples. All other organic solvents only remove small quantities (As ≤ 1 Bq/g) of radionuclides from the reactor graphite. All neutral solvents are therefore not suitable for decontaminating reactor graphite and were not be given any consideration in the tests with AVR samples

HCl removes radioactivity from reactor graphite samples in all concentrations. In contrast to the other acids, the results for the sample duplicates fluctuated strongly. This could be the result of the graphite samples heterogeneity with respect to structure, grain size, reactor coordinates and the location of the nuclides in the graphite.

In HCl, it seems that any increase in concentration will generally result in greater activity removal. However, due to the strong fluctuations in the measured values, this cannot be positively verified with respect to the sample duplicates. As the 6 M HCl removes the highest level of activity, this is also the solvent that will be used for the decontamination tests on the AVR graphite.

The tests performed with the nitric acid in different concentrations show that the higher the concentration, the higher the activity remove in the samples and that the maximum level of activity is being removed at a concentration above 7 mol/L.. For this reason, this is the concentration that will be used for the series of tests performed on the AVR graphite.

When leaching Merlin graphite with HNO_3, a small amount (As< 3 Bq/g) of ^{14}C becomes gaseous. The measured values within the sample duplicates fluctuated very strongly. This can be explained by the very small measured values, which are subject to significantly larger measuring errors than high measured values.

The other acid solvents that were used were acetic acid and sulphuric acid. The comparison of the results shows that increasing the concentration of acetic acid from 6 M to 12 M does not result in an increase in the activity release.

In order to ascertain whether repeatedly extracting radionuclides from the same sample using new solvents respectively would remove more total activity than through a leaching test, the same sample duplicate respectively will undergo extraction with the following fresh solvents four or six times for 5 hours each. The acids' concentration is selected in accordance with their effect on the extraction thimbles. The number of extraction tests is chosen in accordance with the respective result obtained from measuring the samples after the extraction. The solvents and concentrations used were: 1 M HCl, 1 M HNO_3, 6 M CH_3COOH, 4 M H_2SO_4

The test results obtained with the H_2SO_4 can only be compared within limits with the other results as, due to no comparable results were possible to collected and their test conditions varied.

In part, the results of the HCl and HNO_3 extraction tests follow a similar course. The course of the curves of the duplicate HCl is rather non-conclusive, only a small amount of activity was removed from the samples after the 4th leaching process. The sum of the values of the 2nd and 3rd extraction is higher than the measuring result of the 1st extraction and the total sum of all extractions is at least twice as high as the value of the 1st extraction. This trend was even more pronounced with HNO_3. During the 1st extraction, only 1 % (8% in the second replicate) of the total sum achieved by all of the extractions taken together is being removed.

In general, the profile of extraction results in the proposed interactive extraction tests, can be concluded that they do not justify the efforts involved in performing multiple extractions. It is consequently more effective to immediately use acids with higher concentrations, which achieve the same results in only one single leaching test.

Since only the results of the extracting agents that are capable of removing high amounts of activity are of interest for the second series of tests, only the Merlin samples of the solvents with the highest values will be analysed by γ spectrometry.
These are 6 M HCl (A_{max} = 1319 Bq/g), 7 M HNO_3 (Amax = 1026 Bq/g), 6 M CH_3COOH (Amax = 970 Bq/g) and 4 M H_2SO_4 (Amax = 1051 Bq/g). The 2 M HCl samples were also analyzed in order to determine the reasons for the high activity of 1185 Bq/g in one of the two sample duplicates.

The solid material samples were not analysed by γ spectrometry before the extraction tests. For this reason, the sum of the residual γ activity in the solid material sample and the sum total of the γ activity of the liquid sample are used as a comparison value.
This value is comparatively imprecise as, because of the extremely small sample size of 0.5 mL and the count rate of less than 1, it will no longer be possible to measure even relatively large levels of activities like, for example, the ^{154}Eu value of the sample with the 6 M HCl.

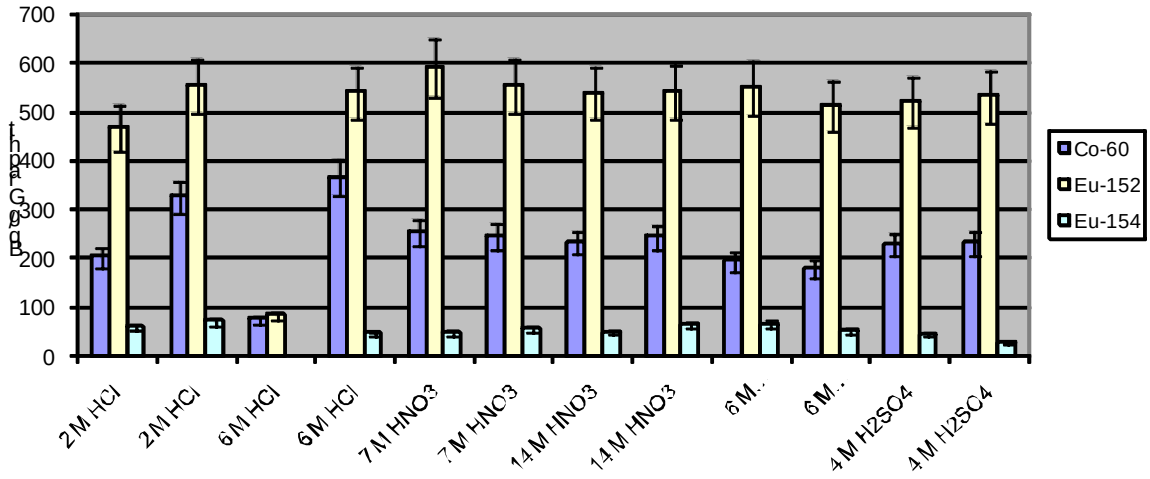

Figure 4.2.6: Comparison of the activity of the Merlin leaching samples

In the samples with high total activity, the residual activity of the solid material samples was established after the extraction tests. Just as with the liquid samples, the values of the HCl duplicates are also not conclusive when comparing the replicates.

The results of the liquid samples of the other solvents only fluctuate marginally within the sample duplicates. When taking into account a fluctuation margin that can be explained on the basis of the samples' heterogeneity and a 10 % uncertainty of measurement, they are roughly identical. The same can be also be anticipated to apply to the measured values obtained from the duplicate solid material samples.

However, there is no positive indication of a relationship between the removed amounts and remaining amounts of activity.

According to the data obtained at least 45% of the ^{60}Co content are removed, Acetic acid removes approx. 45%, nitric acid removes ~55%, sulphuric acid slightly more than 60% and hydrochloric acid up to 85% of the ^{60}Co content. These tests also showed that the measured values obtained with the hydrochloric acid sample duplicates fluctuated more significantly than those of the other samples

Decontamination factors of all solvents used, with the exception of 6 M HCl, remove at least 70% of ^{152}Eu. The removed activity ratio of ^{154}Eu ranges within 30% and 65%. 2 M HCl, nitric acid and acetic acid reached approx. 50%. All of the sulphuric acid and the 6 M HCl tests remain below this value.

Since, at max. 1.8 Bq/g of tritium, the measured activities are too low and the concentrated acids cannot be used with the selected method of sub-boiling. Due to the high fluctuations of the measured values it is not possible to determine whether there are any significant differences between the liquid samples and the evaporated samples. This indicates that the samples only contain a very small amount of free tritium.

Comparing the activity of the total measured γ-spectrometry values and the total LSC clearly shows that the LSC values are higher than the γ values. As the samples do not contain any ^{90}Sr, it can be assumed that the difference between the LSC and γ values are caused by bound tritium and ^{14}C in the leaching samples. The ratio between the measured γ and the LSC values in the liquid samples is predominantly approx. 80% (±20% errors). This indicates that the ratio between the content of pure β emitters (tritium and ^{14}C) and the γ emitters is roughly the same. The exact total bound ^{3}H and ^{14}C content can only be estimated, but not accurately determined. Since, because of its low energy, the measured count rate of tritium is only approx. 0.3 and that of ^{14}C only approx. 0.9, the actual total activity will be higher than the measured one.

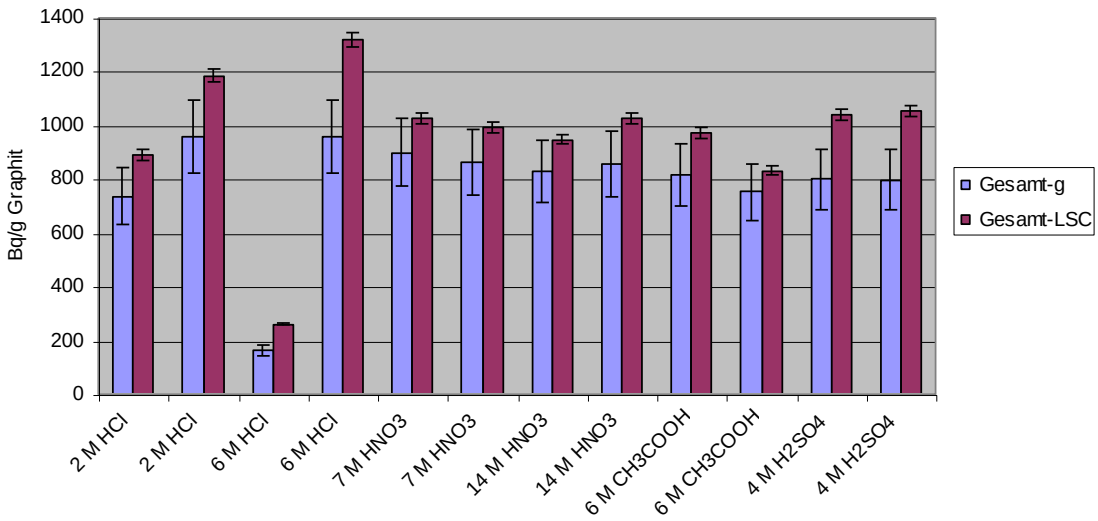

Figure 4.2.7: Comparison of the total activity measured by γ spectrometry and LSC .(Gesamt = Total)

Merlin graphite does not contain any organic ^{14}C. Although numerous pulses were measured in some of the samples, an analysis of the spectra shows that these measured values are the result of luminescence interference that is caused by organic substances such as, e.g. phenolphthalein. The spectra also show that the peaks of the luminescence interference do not overlap with any other peaks, as they are located on the far left of the spectrum.

4.2.2.2 Experiments with AVR Samples

The values of the total activities within the AVR sample duplicates fluctuated significantly with the exception of the acetic acid samples. The measured values are sum of the results obtained from the 1st and 2nd extraction of the same sample.

This clearly shows that the acids are also capable of removing more activity from the more heavily contaminated reactor graphite. This is not the result of the significantly higher amount of solvent used in relation to the quantity of reactor graphite (Merlin: 120 mL/g vs AVR: 1250 mL/g). This is made evident on the one hand by the results of the multiple extraction tests performed on the Merlin samples, and on the other, the fact that a significantly lower amount of activity respectively was removed during the 2nd extraction of the same reactor graphite sample than during the 1st extraction (see figure 26).

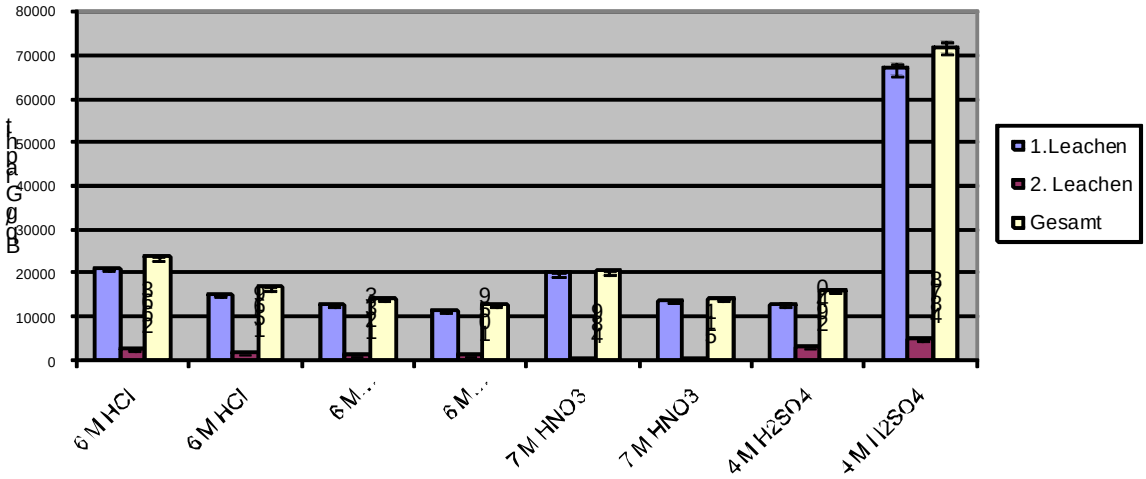

Figure 4.2.8: Total LSC result obtained from leaching the same sample twice (Leachen: Leaching; Gesamt = Total)

The lowest decontamination rates were achieved with the acetic acid, while the HCl tends to produce better values than the nitric acid. The results obtained with the sulphuric acid are difficult to estimate. On the one hand, the total activity measured for the 1st sample duplicate is the average of all of the values, while, the total activity measured for the 2nd sample duplicate is about three times as high as all of the other results. Comparing the spectra of the 1st extraction and the 2nd extraction of both of the duplicates clearly shows how much of the total activity is produced by H-3 and how much by C-14.

Comparing the initial activities with the residual activities of the solid material samples shows that the amount of individual nuclides that is removed does not depend on the amount of nuclides contained in the sample. This becomes evident in the case of ^{133}Ba. These values remain nearly unchanged in comparison to the values of the other nuclides

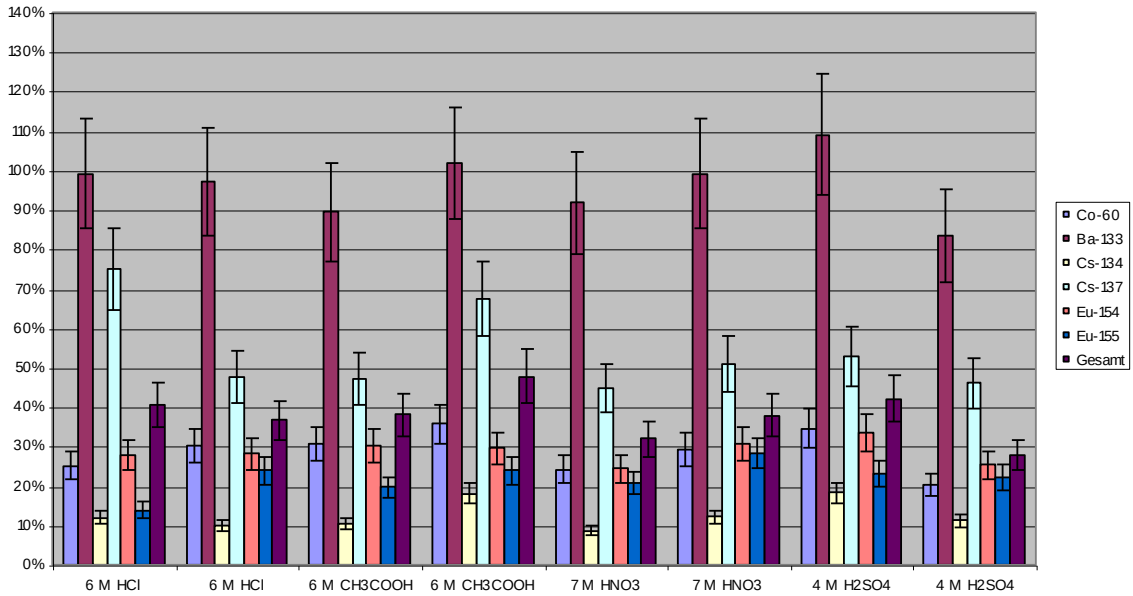

Figure 4.2.9: γ -activity ratios of the solid material samples before and after leaching

- ^{60}Co fractional removal ranging within 79% - 64%
- ^{133}Ba fractional removal ranging within 16% - 0%
- ^{134}Cs fractional removal ranging within 90% -80%
- ^{137}Cs fractional removal ranging within 55% -25%
- ^{154}Eu fractional removal ranging within 75% - 65%
- ^{155}Eu fractional removal ranging within 85% - 70%

The barium values, some of which are higher than 100%, are an indication of measuring errors. These are at 14% and are due to the measuring device.

Comparing the solid material samples' γ-activity before the tests with the total sum of all of the measuring results after the tests shows that the initial activity of the nuclides is generally higher in the solid material samples than the total sum of the activity of all samples.

Individual separations on Sr-90 were performed on AVR samples decontamination liquids. In the case of Sr-90 the low concentration and the background together with a short measuring time leads to a inaccurate measurement of this nuclide.

Detection of organic Carbon, as with the Merlin samples, some of the samples were found to contain numerous pulses that were higher than the background level. However, the samples' spectra show that these count rates are not the result of ^{14}C, but only of luminescence interference, which is probably caused by low-boiling organic substances (phenolphthalein), that were transferred into the washing bottles. These “ghost peaks” are so far on the left of the energy spectrum that it is clearly evident that they do not cover any other peaks

4.2.2.3 Comparison of the Merlin and AVR Results

The percentage of pure β emitters (^{3}H and ^{14}C) in the untreated Merlin graphite samples is more than 71% of the total radionuclide inventory. The percentage measured in the extraction solutions is only 20%.

If one were to assume that the ratio in the leaching solutions is the same as in the untreated leaching solutions it is possible to calculate the activity of the sample. The actual percentage of both nuclides in the total inventory would then not be approx. 20%, but approx. 44%. However, this value would still be lower than the 71% measured for the untreated samples.

The following charts show the calculated values and the ratios between the β emitters and the total inventory:

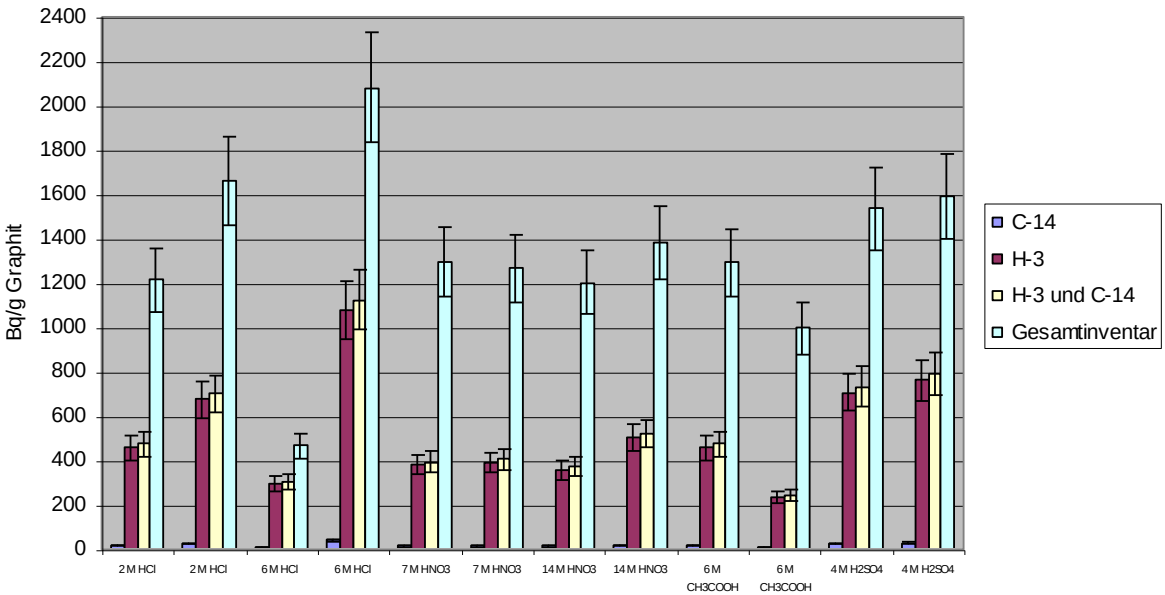

Figure 4.2.10: Comparison of the β activities and total activity (hypothesis) (Gesamtinventar: Total Inventory)

Regarding the AVR samples, it is furthermore problematic that the quantity of pure ß emitters (^{3}H, ^{14}C and ^{90}Sr) inside the untreated samples is an unknown. For this reason, the radionuclide ratios of known AVR samples were used for comparison.

Despite the high differences in activities, the ratio between pure ß emitters and the radionuclide inventory is approx. 95%. In the extraction solutions, the measured percentage of pure ß activity is between 20% and 55%, and in the sample with the highest activity, more than 75%. The measured percentage of pure ß emitters in the sample solutions of both series of tests is therefore smaller than their percentage in the untreated solid material samples. However, the actual percentage of pure ß emitters in both series of tests is higher than the measured percentage, as the low count rate of ≤ 1, which is due to the weak energies, also has to be taken into account. This is also evident from the spectra of the LSC measurements.

According to the hypothesis, the total inventory contains up to 92% of pure beta emitters. The sample with the highest activity reaches this value. This sample's total inventory is made up to 88% of tritium. At approx. 41%, the Merlin samples' total inventories contain the lowest percentage of pure ß emitters (mostly 40%).

The comparison shows that more pure ß emitters are usually removed from the AVR graphite than from the Merlin graphite. There may be several reasons for why this percentage is higher in the AVR graphite, such as:

- In contrast to the Merlin graphite, the AVR graphite or the leaching samples contain ^{90}Strontium.
- The presumably very high percentage (up to 95%) of pure ß emitters in the AVR graphite
- The higher neutron radiation in the AVR reactor increases the reaction probability and the
- AVR graphite therefore reacts more easily with the solvents.
- The higher neutron radiation has damaged the graphite lattice to such an extent as to make it easier for the solvents to remove the radionuclides from the graphite.

4.2.3 INR Inorganic Agents Leaching Test

In view of getting some information with regards the behavior of radionuclides in contact with water a certainly quantity of i-graphite was contacted for 3, 6 and respectively 100 days with demineralized water. The leached beta total activity and the leached radionuclides are presented in the Table 4.2.1.

Table 4.2.1: The leached activity during the water contact

No. sample	Contacting time (days)	% leached beta global activity*	% leached activities			
			^{60}Co	^{137}Cs	^{152}Eu	^{152}Eu
a-g	100	52.12	9.13	100.00	13.43	8.14
b-g	3	15,13	2.50	-	11.22	6.82
c-g	6	22,41	1.09	22.05	12.11	-

The samples prepared by INR, using the method described in 4.1.1, were measure and the results for gross beta determination are in the bar-diagram of figure 4.2.11 that shows the effectiveness of the treatment for Gross beta activity

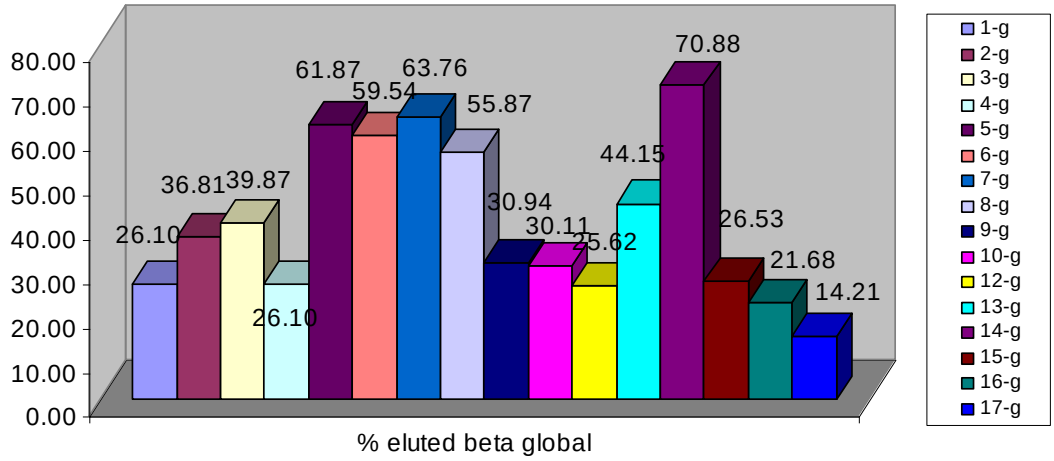

Figure 4.2.11: Beta total removal efficiency

It is shown within the set of experiments the decontamination efficiency with regards at the global beta activity is the highest (71%) in case of sample no. 14 (decontamination solution: 2.5 ml HCl 37%+ 2.5 ml H_2SO_4 98%+ 5 ml demineralized water), followed by the samples 5, 6, 7, 8 (efficiency = 59-63%) – the experiments where H_2SO_4 98% and H_3PO_4 85% were used (experiments no. 5 and 7) and in mixture with demineralized water, in volumetric ratio 1:1 in the experiments 6 and 8.

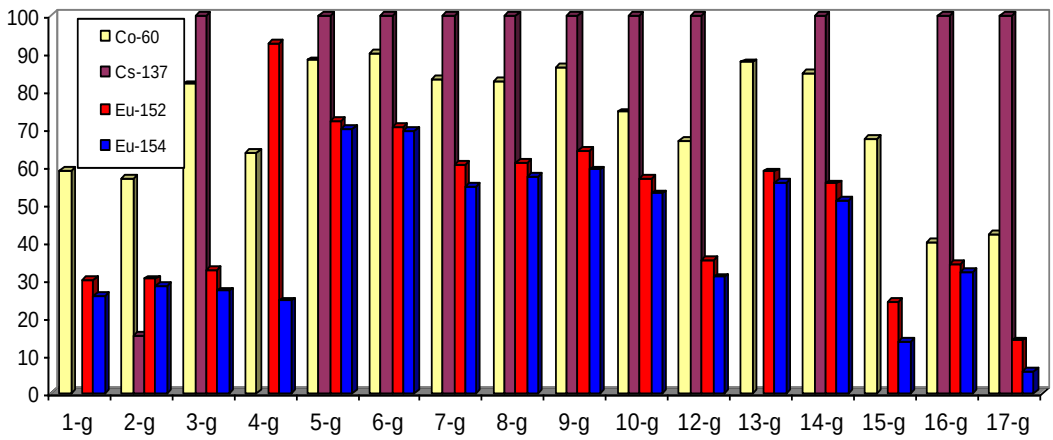

Figure 4.2.12: Gamma-emitters removal efficiency

4.2.4 CIEMAT Inorganic Agents Leaching Tests

4.2.4.1 Alpha and Gamma Emitters Decontamination Results

CIEMAT approach consists in putting in contact 0.15g of graphite powder from UNGG sleeves and a 5 mL decontamination agent solution into a vial and shaking 24 hours. Then, the mixture was centrifuged and the supernatant was removed and passed through a 0.20 µm filter. The filtrate was measured both by alpha and gamma spectrometry. The leaching procedure was carried at three different temperatures 20, 60 and 80ºC and using different solutions. The results are shown on figures 4.2.13 to 4.2.15 and expressed as % of the specific activity release.

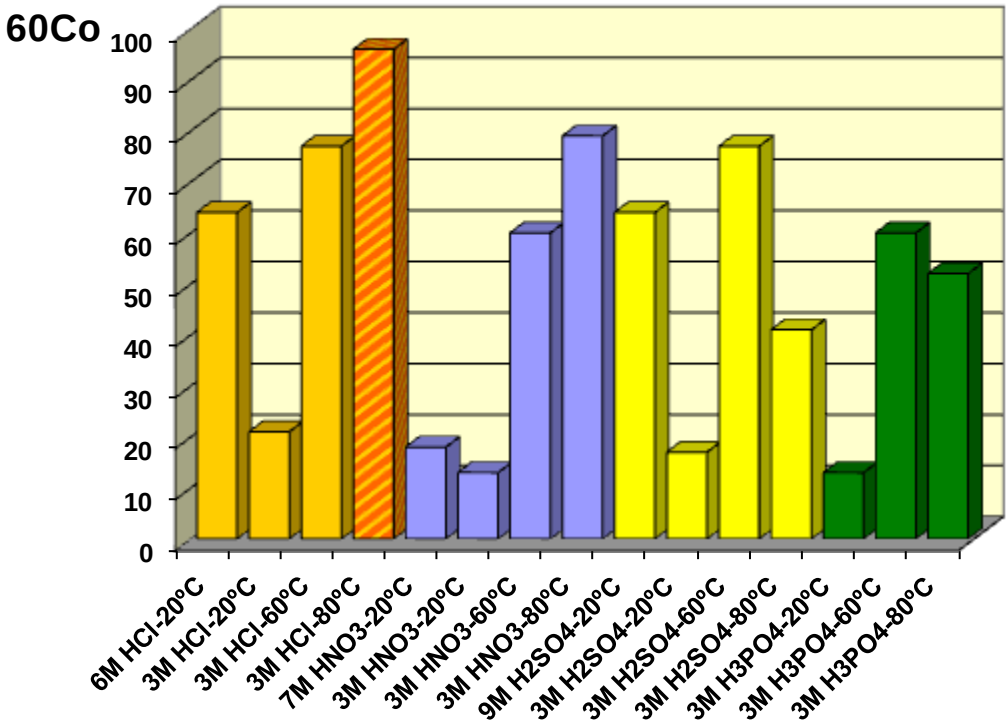

Figure 4.2.13: ^{60}Co decontamination factors for different acidic conditions

Cobalt-60 release shows a good behaviour in concentrate acidic media with UNGG powder graphite. In each leachants the tendency is improving decontamination factor as concentration increase (factor ≈3 for HCl and H_2SO_4) and temperature increase. The best results are found with 3M HCl at 80ºC. Decontamination factor at 80ºC varies between 96% for 3M HCl and 41% for 3M H_2SO_4 being the order 3M HCl > 3M HNO_3 > 3M H_3PO_4 ≈ 3M H_2SO_4. This behaviour is in accordance with the exfoliation of graphite in acidic media, the specific surface of the powder and the affinity of Cl^- for Co cation.

The other gamma emitters nuclides tested (^{137}Cs, ^{154}Eu and ^{94}Nb) only were measurable in high temperature leaching test (figure 4.2.14). The results for ^{137}Cs are in average 55% for every leachant. ^{154}Eu also is leached in a margin between 84% and 100%, and Nb leaching presents the higher resistance to leaching with a maximum of 77% in 3M HCl at 80ºC.

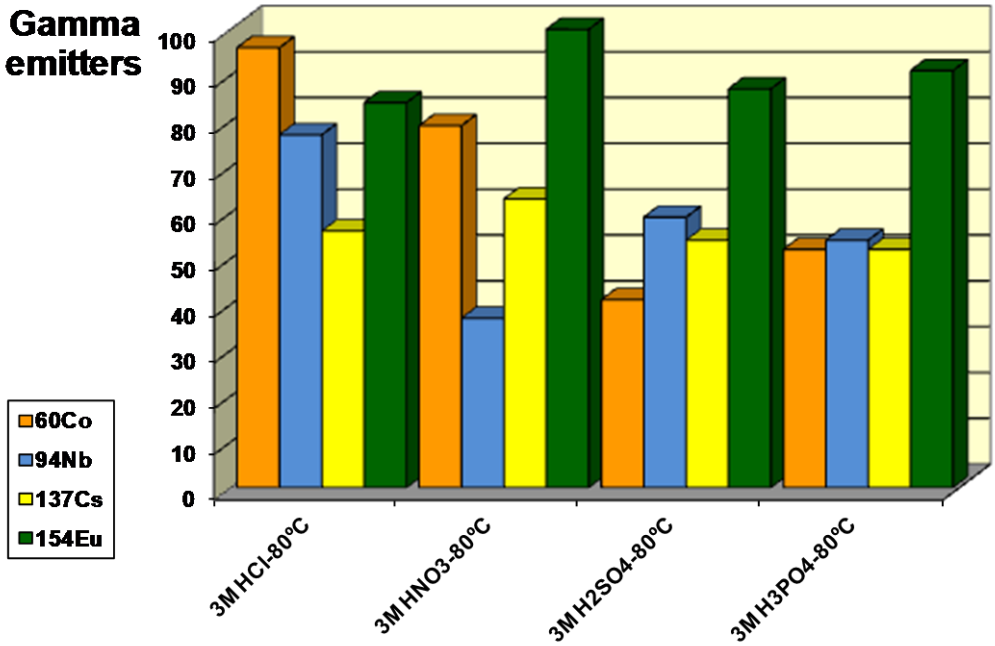

Figure 4.2.14: Gamma emitting decontamination factors for different acidic conditions at 80ºC

Alpha emitters were also analysed, by alpha spectrometry, after leaching of UNGG graphite in the conditions described. Results are in figure 4.2.15.

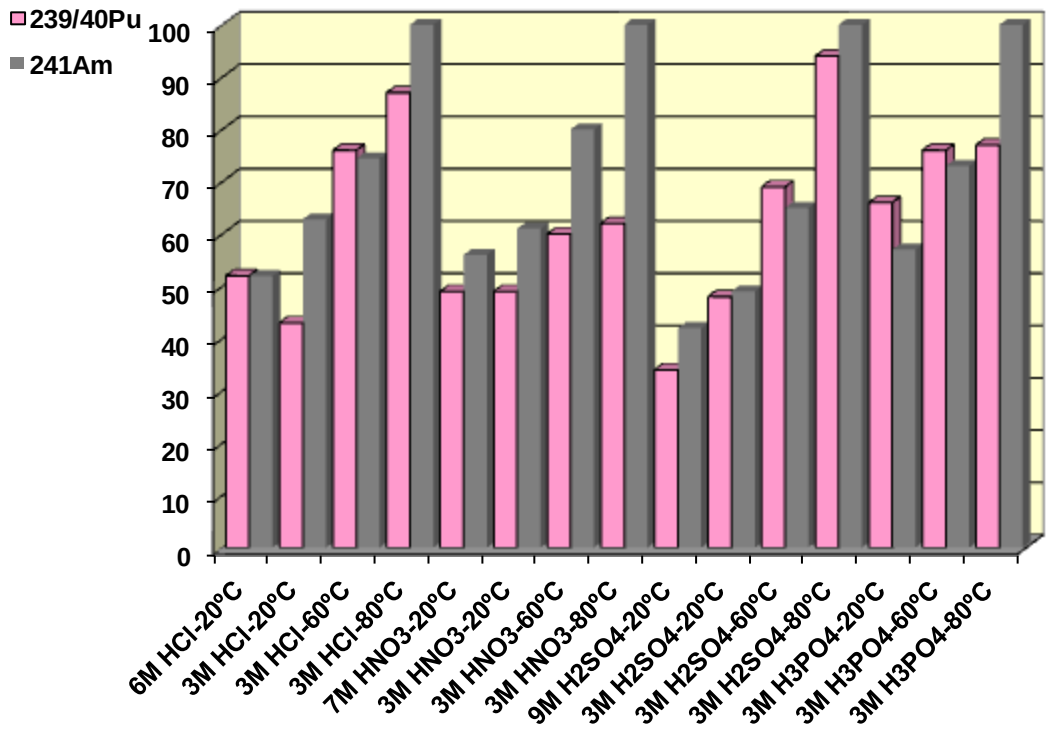

Figure 4.2.15: Alpha-emitting decontamination factors for different acidic conditions

The leaching of Am and Pu with any acid solution increases when the concentration decreases. On the other hand, the leaching of both increases when the temperature does within the range of temperatures and concentrations studied. The best conditions for the leaching of Am, 100%, are with any 3M acid solution at 80 ºC. The best result for the decontamination of Pu (94%) is when the leaching is carried out with 3M H_2SO_4 at 80 ºC.

In order to increase the capabilities of the conditions studied another set of leaching test have been carried out using either 0.5 M citric acid, 0.5 M oxalic acid or their mixtures with 3M nitric, hydrochloric, phosphoric and sulphuric acids. The idea behind is complexing the available cations together with exfoliation process with typical surface treatment agents. The results are shown on figures 4.2.16 expressed as % of the activity leached.

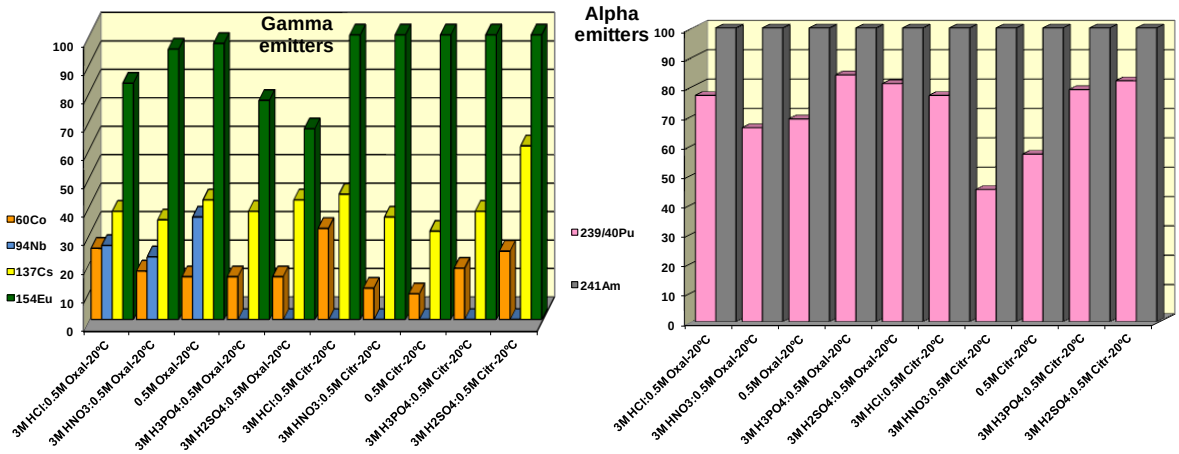

Figure 4.2.16: Gamma and Alpha emitting decontamination factors for different acidic conditions with addition of Citric and Oxalic acids

The leaching of Am is about 100% when the leachant is either 0.5M oxalic, citric acid or their mixture with any acid at 20 ºC. The highest percentage of leaching for Eu is using either a dissolution of 0.5M citric acid or its mixture with any acid at 20 ºC.

The decontamination of Pu increases when 0.5M oxalic acid is added to any 3M acid solution at 20ºC. The highest percentage of leaching for Pu, 84%, is when the leachant is a mixture of 0.5M oxalic and 3M phosphoric acid at 20 ºC

The decontamination of Co increases when either 0.5M oxalic acid or 0.5M citric acid is added to any 3M acid solution at 20ºC. The highest percentage of leaching for Co-60, 32%, is when the leachant is a mixture of 0.5M oxalic and 3M chlorhidric acid at 20 ºC.

For Nb the percentage of leaching decreases when the leachant is either oxalic, citric acid or their mixture with another acid. In the case of Cs the decontamination is less influenced by the presence of either oxalic or citric acid.

4.2.4.2 Tritium and Radiocarbon Decontamination Results

The method followed for the study of the decontamination of ^{3}H and ^{14}C in i-graphite powder from UNGG reactor graphite, has small differences from the one ol alpha and gamma emitters.

Tritium and radiocarbon are measure by difference in the dried graphite powder leached, separate by a catalytic furnace and measured in a LSC system with dual label calibration.

The leachants used were: 0.1M sodium hydroxide, 0.1M sodium hydroxide with hydrogen peroxide, 3M nitric acid, and mixtures of nitric, hydrochloric and sulfuric acids at 20ºC and 80ºC. The results are shown on figure 4.2.17 and expressed as % of the activity leached.

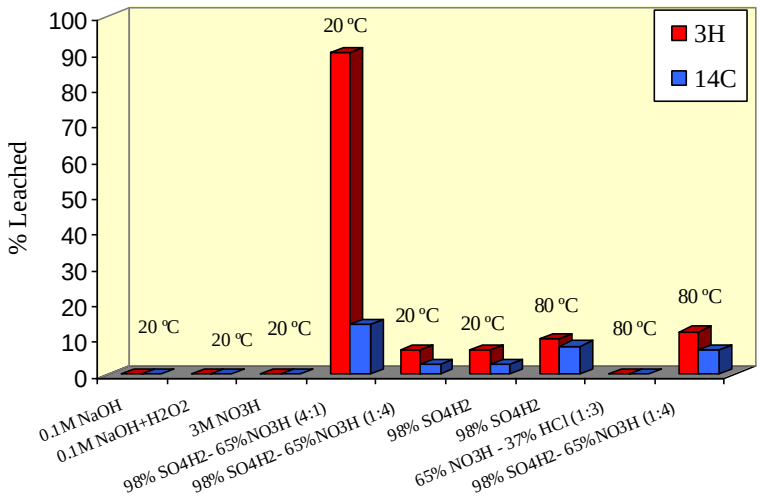

Figure 4.2.17: Decontamination factors for ^{3}H and ^{14}C

Neither ^{14}C nor ^{3}H are leaching at all with 0.1M sodium hydroxide or a mixture of 0.1M sodium hydroxide and hydrogen peroxide at 20ºC during 24 hours. The alkaline media with this ratios of solid and leachant do not promote the extraction of contaminants even with the addition of an oxidizer which was expected have reaction with the lattice through radicals.

The leaching of acidic conditions gives higher decontamination factors, H_2SO_4 98% ensure the exfoliation and is capable to produce the exfoliation in the fine powder sample and release 3% of the C-14 and 7% of the H-3 being a 10% of H-3 released if the temperature is 80ºC. leaching test with HNO_3 65% or mixtures of HNO_3 65% and HCl 37% at 80ºC are not enough reactive for H-3 and C-14 release from this samples.

Best results were obtained with the mixture H_2SO_4 98%-HNO_3 65% (4:1) at 20 ºC. This mixture leached both 90% of ^{3}H and 14 % of ^{14}C. This mixture is already used in the industry in the treatment of graphite to conduct intercalation processes, normally to dope the graphite structure to improve on the characteristics of the material, but in this process seems to be useful for the effectiveness decontamination of H-3, C-14 decontamination factor is not very high for scale-up the experiment but is an evidence of the ratio of C-14 achievable to the aggressive reagents. It is not necessary applied a correction factor of the $^{14}CO_2$ missing in the process due to the evaluation is performed by difference over the solid leached. On the other hand the concentrate acids mixture H_2SO_4 98%-HNO_3 65% (4:1) at 80ºC dissolved the powder of graphite.

It was studied the influence of the leaching time. This study was carried out in the same conditions as before but with two different leaching time: 4 or 8 days. The results are shown on figure 4.2.18.

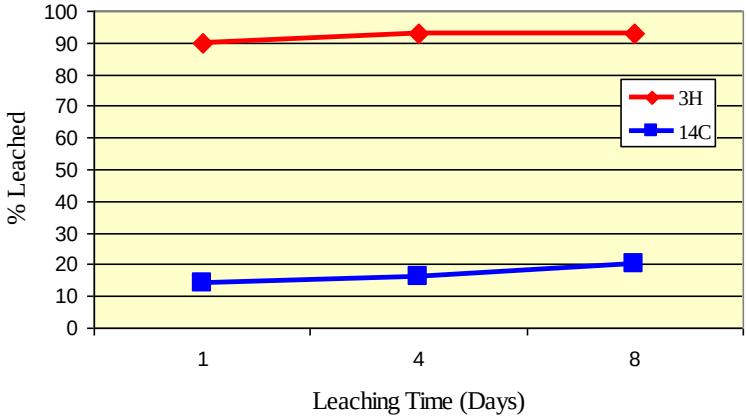

Figure 4.2.18: Results obtained for the decontamination ^{3}H and ^{14}C in i-graphite powder at different leaching time.

The results obtained for the decontamination of both ^{3}H and ^{14}C in i-graphite powder when the leaching time is either 4 or 8 days are similar the ones obtained when leaching time is one day.

When the same procedure of leaching with H_2SO_4 98%-HNO_3 65% (4:1) was applied six times repeatedly on the same graphite powder the decontamination for ^{14}C was 50% and 99% for ^{3}H but only 10 % of the graphite powder was recovered.

Finally, it has been study the stability of virgin graphite under the same conditions as the previous ones used for the leaching of i-graphite. The virgin graphite was dissolved with the mixture H_2SO_4 98%-HNO_3 65% (4:1) at 80 ºC while it was stable when it was treated with this leachant at 20 ºC. So the virgin graphite has the same behaviour as i-graphite.

4.2.4.3 Intercalation Process

An experiment was carried out to study the leaching of a virgin graphite block with a solution of H_2SO_4 98%-HNO_3 65% (4:1) at 20 ºC. When a 0.7 g virgin graphite block was put into a vial with 5 mL of a mixture of H_2SO_4 98%-HNO_3 65% (4:1) the block broke down into powder (Figure 4.1.19).

Figure 4.2.19: Virgin graphite block and graphite powder obtained after the treatment with the mixture H_2SO_4 98%-HNO_3 65% (4:1) at 20 ºC

The powder was washed several times with water until both sulphuric and nitric acids were removed. After several washings the water was analyzed by ion exchange chromatography in order to check the presence of sulphate or nitrate. The recovery of graphite powder was about 98 %. An examination of the structure for both the virgin graphite block and the virgin graphite powder was carried out by SEM. The images are shown on figure 4.2.20.

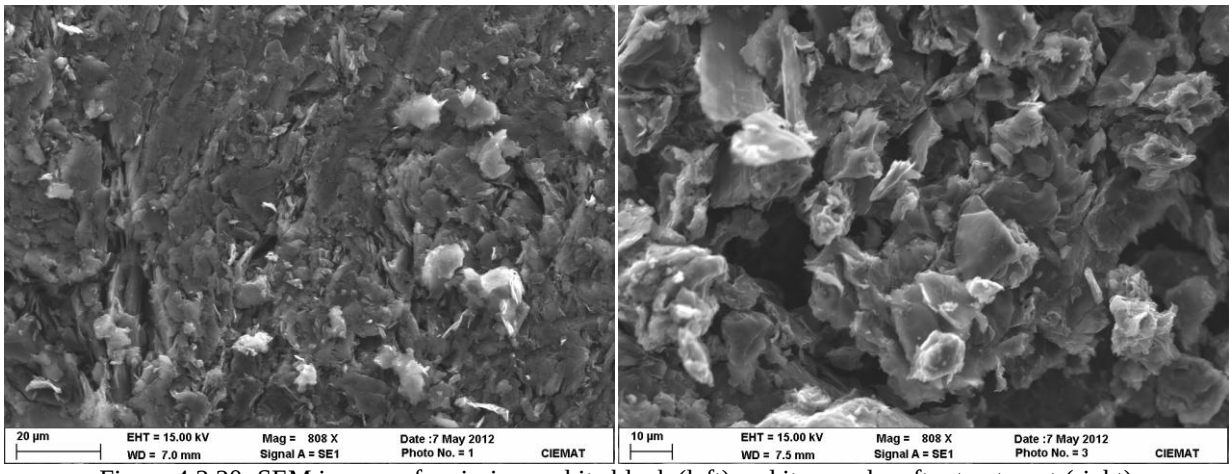

Figure 4.2.20: SEM images of a virgin graphite block (left) and its powder after treatment (right)

4.2.5 ENEA Organic Agents Leaching Test

4.2.5.1 Organic solvents and Sonication

It is started to test the process considering the three common and widely used dipolar solvents, as mentioned in the section 2.1.2 of this report, for their good solvency abilities:

N,N-Dimethylacetamide (DMA)
N,N-Dimethylformamide (DMF)
N-Methyl-2-pyrrolidone (NMP)

In this work, it is performed a sonication bath for 10 hour in a 35W power device on sample of about 0.1g of irradiated graphite samples with 10 ml of each solvents. The volume of the solvents used has been chosen for the aim described.

After sonication, the solution appear grey to dark in colour without a distinguishable sedimentation. They are left standing for a day with no changes in colour. After that, they are centrifuged for 1 hour at 12000 rpm. Only the NMP/dispersion still presents dark coloration, the others were clear. All the samples/solutions were filtered on RC (Regenerated Cellulose) Filter Disk 0.2µ and undergone LSC/γ-Spectrometry.

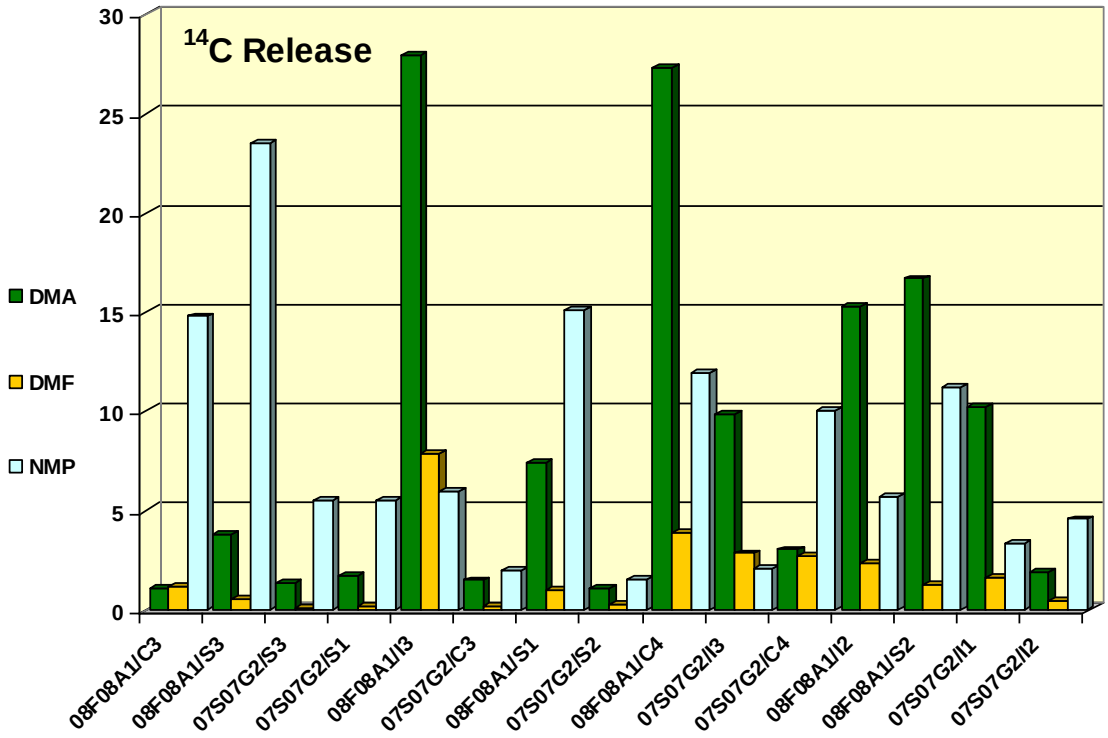

Figure 4.2.21: Overviews of Removal Efficiencies for Radiocarbon

^{60}Co			
	Removal Efficiencies (%)		
	in DMA	in DMF	in NMP
Variation range on all samples	0.1 – 8.9	0.1 – 7.0	0.4 - 2.4

Table 4.2.2: Overviews of Removal Efficiencies for Cobalt-60

Although the overall results seem to be relatively low, these are the first results obtained with this new kind of decontamination process aimed to preserve the graphite as it is and avoiding both oxidation of the same and completely dissolution as acidic leaching or extraction perform.

These first and earliest results show that the removal efficiencies in the experimental conditions we used are best for N,N-Dimethylacetamide (DMA) and N-Methyl-2-pyrrolidone

(NMP) for ^{14}C removal, and N,N-Dimethylformamide (DMF) in the case of ^{60}Co. The logical answer could lie in the different chemical behaviour and bonding of the two radionuclides in the graphite matrix. Anyway, further investigations would prove the possibilities to reach an overall process able to extract a wide range of radionuclides despite of the differences in chemical properties of the elements.

Another point worth to be assessed is the sonication time plus the sonication power. The energy distributed for mass unit and time in a ultrasound bath is an important point to be investigated in order to reach an exhaustive desegregation (exfoliation-like) of the graphene layers making the intercalated compounds free from the matrix and dissolved in the solvent.

Moreover, a complete ICP-MS/γ-Spectrometry characterisation of the i-graphite samples will be performed to validate the destructive and non-destructive measurements carried out. This should be the starting point for the subsequent definitions of the degree of decontamination, comparing these values to those coming from the decontaminations trial and works.

4.2.5.2 Acidic Agents and Sonication

The results obtained from the leaching tests with previously mentioned are shown in the Table 4.2.3.

		Removal Efficiency (%)	
Sample	T (ºC)	^{60}Co	^{137}Cs
04F04A1/I1 H_2SO_4/H_2O_2	200	78	72
10F10A1/I4 HNO_3/ H_2SO_4	200	94	78
11F13A1/C4 HNO_3/HCl	200	79	3
10F10A1/I4 HNO_3/ H_2SO_4	Room	6	10
11F13A1/C4 HNO_3/HCl	Room	8	19

Table 4.2.3: Results of the tests on S2 (200ºC) and S3 (room T) sections with acid mixtures

It can states that in the leaching test at 200°C the best results are reached with mixtures containing H_2SO_4. On the other count the mixture HNO_3/HCl seems to not act as best regarding to the ^{137}Cs. Meanwhile, the leaching at room temperature shows low removal efficiency values in all the cases. It would be interesting to perform, in this last case, a long term leaching test although the results obtained with the warm acid mixtures seem to be more preferable than at room temperature.

In a perspective glance on the next works, it would be interesting to combine the two main procedures illustrated in this work (organic solvents plus acid mixtures) in order to gain a synergic action for an exhaustive removal treatment on i-graphite.

4.3 Decontamination with Liquid Agents: Main Achievements

Decontamination studies collected in this document have been carried out on irradiated graphite samples form Magnox reactors (Latina and Wilfa), UNGG Reactors (Vandellos I), MTR's (Triga, BEPO and Merlin) and HTR's (AVR).

Several techniques have been applied, as Semi-dynamic long term leaching experiments, short term leaching experiments with stirring or ultrasonic help, and solid liquid extraction.

The chemical agents tested are organic for several proposes: soft acidic, extractans with soft donors, complexant agents, solvents …) and inorganic, (acidic, alkaline, neutral, solvents, oxidizers…) at different temperatures.

Decontamination of beta-gamma emitters

Decontamination factors of Co-60:

- Acidic treat with Soxhlet can remove ~80% of Co-60 inventory in 4M H_2SO_4
- Acidic Leaching treatment with H_2SO_4 98% can remove ~90% of Co-60
- Acidic Leaching treatment with 3M HCl at 80ºC can remove ~87% of Co-60
- Acidic Leaching treatment with HNO_3/ H_2SO_4 at 200ºC can remove ~90% of Co-60
- Organic Leaching treatment with soft donors extractantes (DMA) can remove ~9% of Co-60

Decontamination factors of Europium Isotopes

- Acidic treat with Soxhlet can remove ~70-80% of $^{154/55}$Eu inventory in 4M H_2SO_4
- Acidic Leaching treatment with H_2SO_4 98% can remove ~70% of $^{152/54}$Eu inventory
- Acidic Leaching treatment with any acid tested mixed with complexants agents at 20ºC can remove ~100% of ^{154}Eu inventory

Decontamination factors of Caesium Isotopes

- Acidic treat with Soxhlet can remove ~90% of ^{134}Cs and ~50% of ^{137}Cs inventory in 7M HNO_3
- Acidic Leaching treatment with H_2SO_4 98% and H_3PO_4 85% can remove ~100% of ^{137}Cs inventory

- Acidic Leaching treatment with any acid tested mixed with complexants agents at 20ºC can remove ~100% of 154Eu inventory

- Acidic Leaching treatment helped with sonication and using HNO_3/ H_2SO_4 at 200ºC can remove ~70% of ^{137}Cs

Decontamination of Other gamma emitters

- Acidic treat with Soxhlet remove in the better case ~16% of 133Ba inventory in 4M H_2SO_4

- Acidic Leaching treatment with 3M HCl at 80ºC can remove ~77% of 94Nb

Decontamination of Gross beta and Total activity

- Acidic treat with 6M HCl in Soxhlet experiments remove the maximum amount of Total activity inventory.

- Acidic decontamination solution with HCl 37%: H_2SO_4 98% (1:1:2) remove ~70% of Gross beta activity

Decontamination of alpha emitters

- ^{241}Am decontamination factors are ~100% with 3M H_2SO_4,3M H_3PO_4,3M HNO_3 or 3M HCl at 80ºC or with any of this acids and 0.5 Oxalic or Citric acid as complexant at 20ºC

- $^{239/40}Pu$ decontamination factors are ~94% with 3M H_2SO_4 at 80º C

Decontamination of tritium and radiocarbon

- Acidic Leaching treatment with H_2SO_4 98%-HNO_3 65% (4:1) at 20ºC during 24 hours removes 90% of 3H and 14% of 14C.

- Soxhlet extraction studies can not give a decontamination factor of tritium and radiocarbon.

- Organic extractant treatment gave a removal of radiocarbon ~10% in average with maximum of 27% in a few cases.

- Phase one long term behaviour of graphite under >2 M H_2O_2 conditions (88 days) has a C-14 release of 15.4% for powder samples and 13.4% for H-3.

- Phase two long term behaviour (99 days) under 1M H_3PO_4 presents the maximum release for Magnox granulate sample tested in both case H-3 and C-14.

Acidic conditions for removal contaminants from irradiated graphite present good results. In general the use of H_2SO_4 alone or in combination with complexants or other strong acids as H_3PO_4, HCl or HNO_3 leads to a removal of contaminants with high efficiency.

Neutral, alkaline and organic agents have no relevant efficiency in the treatment methods tested.

Temperature of the treatment and concentration has a positive effect in the decontamination factors.

The availability of surface and pore structure of the samples have high influence in the efficiency of the process in general is found that the effectiveness of the process is scale as:

Powder> granulate>massive

The suspected ionic bounds in the surface of the graphite lattices of actinides, alkaline and transition metals can explain the efficiency of removal. Cases of alkaline-earths or Nb have to be explained probably the tendency to complexing with halogens (preferably Fluride) is in the base of explanation of the Nb behaviour in leaching experiments.

The chemical process with H_2SO_4 98%-HNO_3 65% (4:1) at 20ºC removes 90% of H-3 in 24 hours. The behaviour of BEPO graphite in long term leaching test with H_2O_2 that removes ~15% of the H-3 inventory in 88 days and ~18% of Magnox graphite H-3 inventory with 1M H_3PO_4 in 99 days.

Radiocarbon release has no effective removal with any treatment, organic solvents tested give poor results, H_2SO_4 98%-HNO_3 65% (4:1) at 20ºC removes 14% and long term leaching test of BEPO with H_2O_2 remove ~13% of the C-14 inventory in 88 days and ~27% of Magnox graphite C-14 inventory with 1M H_3PO_4 in 99 days.

This behaviour induces to evaluate the effectiveness of the process in function of availability of C-14 in the surface treated. The speciation of radiocarbon in the graphite, due to the different pathways of C-14 generation during reactor operation, in addition to pore structure and neutron damage, determines the capability of the chemical process applied.

Evidences and studies of intercalation process are found with the use of acidic media that can be used in the graphite retrieval process.

5. Graphite Decontamination by Microbiological Treatment

Microbiological or biochemical treatment is based on the principle of emulating naturally occurring processes to treat waste. Over billions of years, microorganisms have evolved mechanisms to survive in hostile environments and to adapt to changes in the environment. Microorganisms are also known to develop mechanisms to alter their environments to facilitate survival and reproduction. Microorganisms have already been isolated that are capable of reducing the toxic forms of transuranic waste (TRU) to less mobile precipitable forms (Lloyd, 2003). Other cultures have demonstrated remarkable resistance to high radiation doses, although not doing much to treat the waste (Battista, 1997; White et al., 1999). More recently, cultures of melanising fungi from cold regions have been shown to utilise ionizing radiation for metabolism (Dadachova et al., 2007). These findings indicate that they may be used beneficially in cleaning a wide range of hazardous substances and waste due to their adaptability to grow in extreme environments. Certain bacterial cultures are radiation resistant and thus able to withstand high levels of radiation, while simultaneously remediating organic waste and toxic metallic waste. The objective of the two-phase PBMR Waste Minimization Project was to investigate the possibility of using microbes in the treatment of its nuclear waste, particularly graphite. The project focused on removing 14C from the bulk 12C graphite by developing a microbial consortium that processes the 14C in the irradiated graphite, such that the activity of the graphite allows for recycling or less restrictive disposal. The 14C is known to be on the surface and within the open pore structure of an i-graphite specimen, so it will be bioavailable for the microbes to metabolize.

The main objective of Phase 1 was to compare and evaluate individual bacterial species as well as a mixed culture, and nutrient media for use in forthcoming Phase 2 experimentation. Comparisons were done by growing the bacteria in 3 different media. The bacteria were also grown in the presence of graphite to investigate the possible inhibitory effect which graphite may have on the growth of the bacteria as well as commercially available salts containing 14C. During these experiments only pH was used as an indicator of bacterial growth, as the growth media contained in the test tubes were insufficient for spectrophotometric analysis. The bacteria used during these experiments produce metabolites, such as organic acids that lower the pH of the growth medium, resulting in the decrease of the pH which can be correlated to bacterial growth in the system. The presence of graphite did not inhibit the bacterial growth; however, the amount of graphite did affect the amount of bacterial growth that occurred.

A schematic representation of the bioreactor system used is illustrated below. The bioreactors used during the experiments were 1 liter Erlenmeyer flasks, which contained the growth medium, ^{14}C compounds and the microbial consortium. Regulated carbon-free air was used to carry the off-gas from the bioreactors through the tube furnace, where the off-gas is oxidised at 700°C to form CO_2, which is trapped in a basic solution of 1M sodium hydroxide.

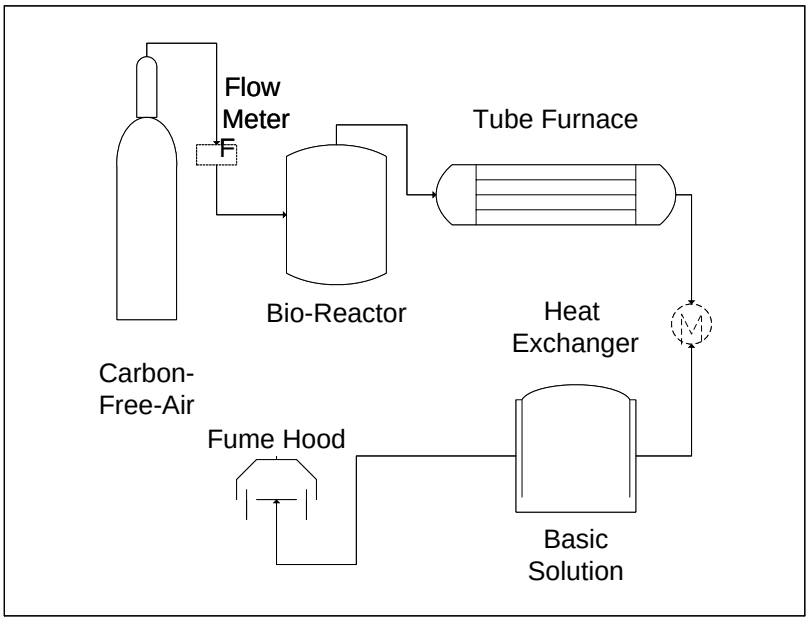

Figure 5.1.1: Schematic representation of the bioreactor system

Each bioreactor contained 250 ml of modified Štyriaková medium with the following composition: 0.42 g.l-1 sodium phosphate; 0.8 g.l-1 ammonium sulphate and 4 g.l-1 glucose. 1.7 g of a 14C-sodium acetate solution and a ^{14}C-sodium bicarbonate solution (GE Healthcare UK Limited, Buckinghamshire, UK) was added to separate bioreactors at a specific activity of 62.5 Bq.g-1. The bioreactors were inoculated with 1 ml of bacterial inoculum. The bioreactor system was operated at ambient temperature (25°C) for various incubation periods. Five separate bioreactors were used during the experiments using ^{14}C-sodium acetate and were incubated for 24 to 120 hours, while three separate bioreactors were used during the experiments using ^{14}C-sodium bicarbonate and were incubated for 24 to 72 hours. Negative control reactors were set up with the exception of using non-radioactive sodium acetate and sodium bicarbonate. In addition, reactors containing Štyriaková medium, and ^{14}C-sodium acetate and ^{14}C-sodium bicarbonate, respectively, were set up without the addition of the bacterial inoculum. These reactors acted as the biocatalyst negative control.
The calculated mass percentages of the ^{14}C in the different phases of the reactors containing ^{14}C-sodium acetate are illustrated in Figure 5.1.2.

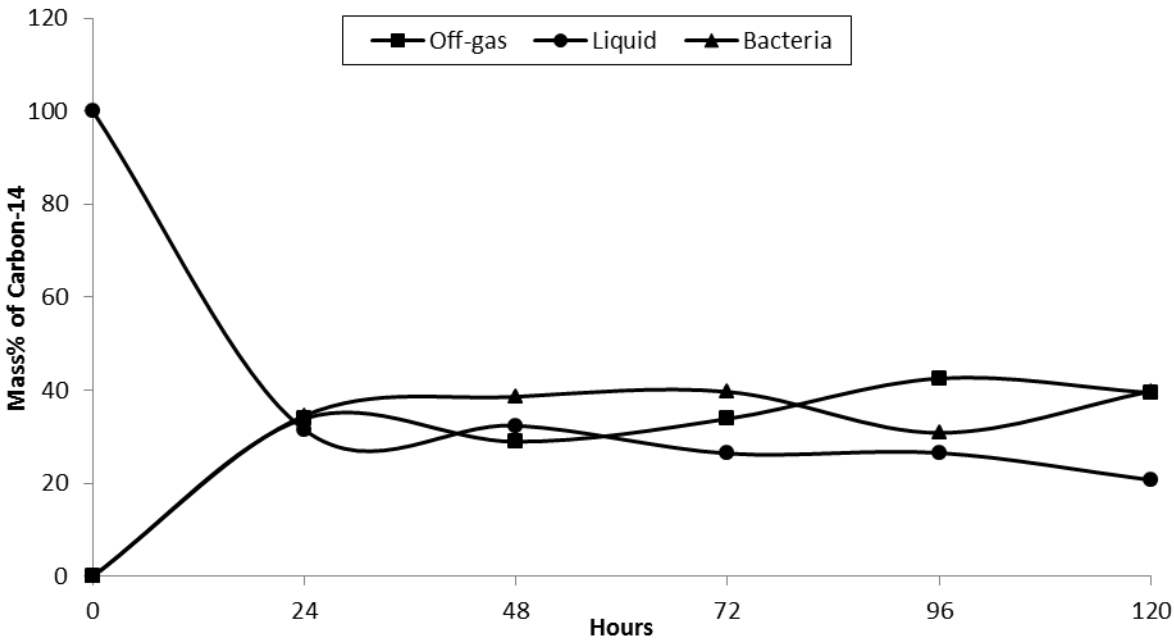

Figure 5.1.2: Carbon-14 distribution in the off-gas, liquid medium and bacterial biomass during the operation of the bioreactors containing sodium acetate

From the results obtained during the experiments using ^{14}C-sodium acetate, it was evident that the bacteria are able to metabolise the ^{14}C, thus acting as a biocatalyst reducing the 14C contained in the liquid waste by 79.29% over a period of 120 hours.

In contrast, during the experiments using the ^{14}C-sodium bicarbonate, the radioactivity in the liquid waste was reduced to 21.77% during the first 24 hours, while only 2.65% could be detected in the bacterial biomass. The biocatalyst negative control experiments, in which no bacteria were present, revealed that 74.96% of the ^{14}C in the liquid waste was detected in the off-gas after 24 hours, suggesting that the ^{14}C-sodium acetate undergoes chemical decay to ^{14}C-carbon dioxide in this period. This suggests that 0.62% of the 14C in the off-gas is as a result of bacterial respiration. No significant change in the 14C levels in the different phases of the system could be observed after operating the bioreactor system beyond 24 hours, and thus it is evident that when using sodium bicarbonate in the system, the bacteria do not play a significant role as a biocatalyst for the reduction of the ^{14}C contained in the liquid waste.

Therefore, the results indicate that the chemical form in which the ^{14}C would be present on the irradiated graphite waste would play a direct role in the ability of the bacterial consortium to remove it from the bulk graphite

Furthermore, a scoping study with the following objectives to determine has been undertaken:

- Bacterial species that will work best,
- Bacterial growth in the presence of graphite and
- Need for supplemental nutrients.

The bacterial growth on graphite chunks has been analysed via SEM. Best results were achieved with Styriakova media in glucose. Fig. 5.1.3 shows an example.

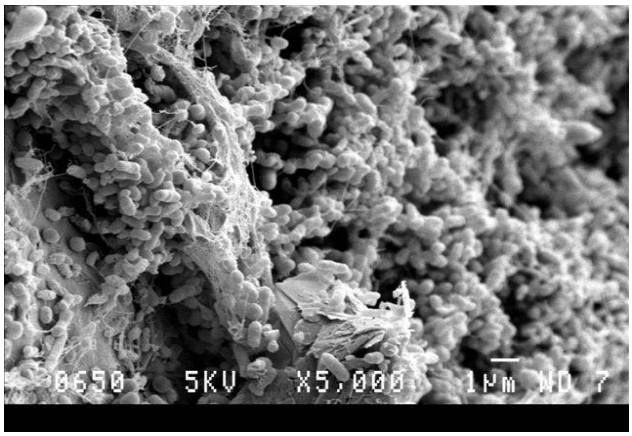

Figure 5.1.3: SEM micrograph of Styriakova media on a graphite surface

The laboratories were set up on the campus of the University of Pretoria. This included full refurbishment (civil) of the laboratories to ensure that they comply with the South African Department of Health's Class B License (Authority to possess and use radioactive nuclides) that is required for the initial work that would include work with bacteria, low-activity (commercial) Carbon-14 as well as purchasing of new equipment. Equipment included an Atomic Absorption Spectrometer, Gas Chromatograph Mass Spectrometer and a Liquid Scintillation Analyzer. In addition the necessary Carbon-14 material was acquired. The research group has done extensive work on the bacteria itself; this included an extensive literature study, running DNA analysis to aid identification of organisms, initial laboratory analysis to verify that the chosen organisms do in fact show a preference for graphite material (non-Carbon-14). Due to the closure of the PBMR project, the University of Pretoria decided not to continue the research on microbiological i-graphite treatment. The results are documented hereafter:

5.1 Bacterial growth with NaCl replaced by the carbon-containing sodium salts

Spectrophotometry was used to gauge bacterial growth in reactors used for the salt replacement experiments. Visible light (600 nm) absorbency measurements for bioreactor solutions were performed daily for 2 hours at 30-minute intervals. The sampling times were chosen according to the typical growth period of the bacteria. The objective was to carefully monitor the bacterial growth to determine how a change in the source of Na might affect the microbes.

Figure 4 presents absorbance data for the sodium chloride reactors on the basis of moles of sodium. In this form, the data can be meaningfully compared with results from the sodium acetate and sodium bicarbonate experiments, which contained different molar quantities of sodium. In the NaCl system absorbance per mole Na decreased with the increase of NaCl concentration, with the best bacterial growth (1.4 absorbency per mole sodium) recorded for the reactor containing 0.203 M NaCl medium. In the system with the lowest salt concentration (0.136 M), growth increased after the first day and stabilized after day 2. For the higher salt concentration systems, the bacterial population is stable until after day 2, when significant growth occurs. The delayed growth in these bioreactors is likely due to initial acclimatization of the bacteria to excess NaCl.

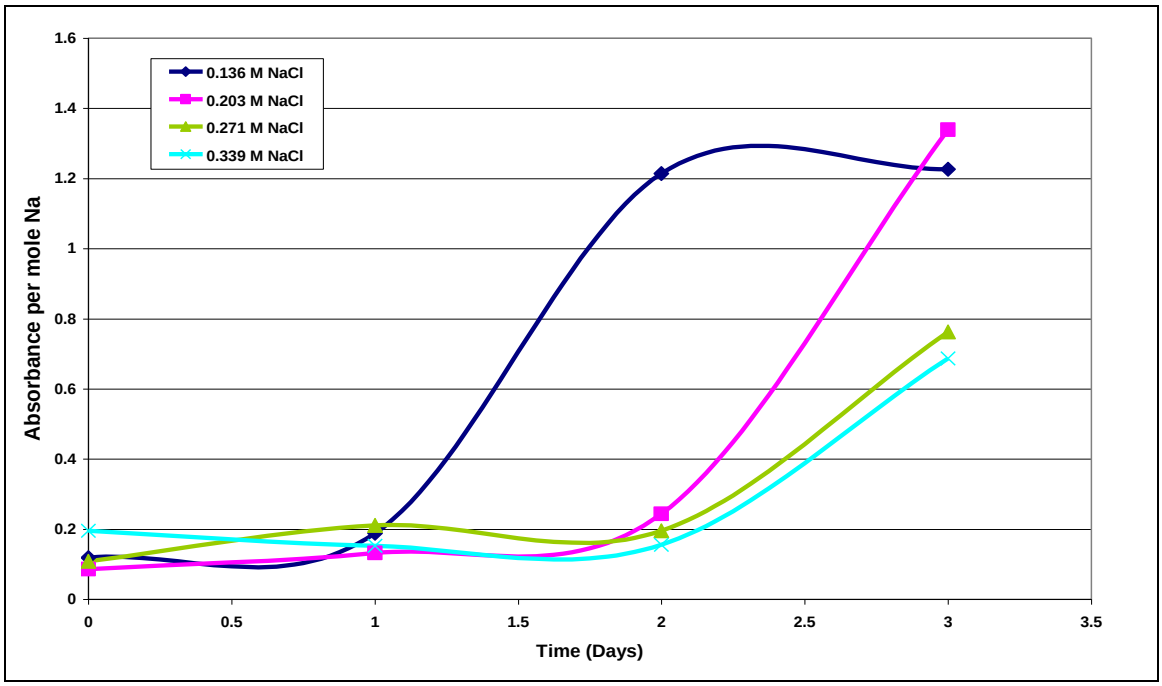

Figure 5.1.4: Absorbance per mole sodium for liquid media from bioreactors containing different concentrations of NaCl

In the bioreactors containing NaCl replacements, the most significant bacterial growth (Figures 5 and 6) was observed when using 0.097 M $NaCH_3CO_2$ and 0.094 M $NaHCO_3$ in the medium. The higher concentrations of $NaCH_3CO_2$ apparently had a negative effect on bacterial growth as indicated by the inverse relationship between absorbency and concentration. A similar correlation between growth and salt concentration is not indicated by absorbance data from the $NaHCO_3$ or NaCl bioreactors; however, the higher salt concentrations generally appear to have a negative effect on bacterial growth as indicated by the inverse relationship between absorbency and concentration in the graphs.

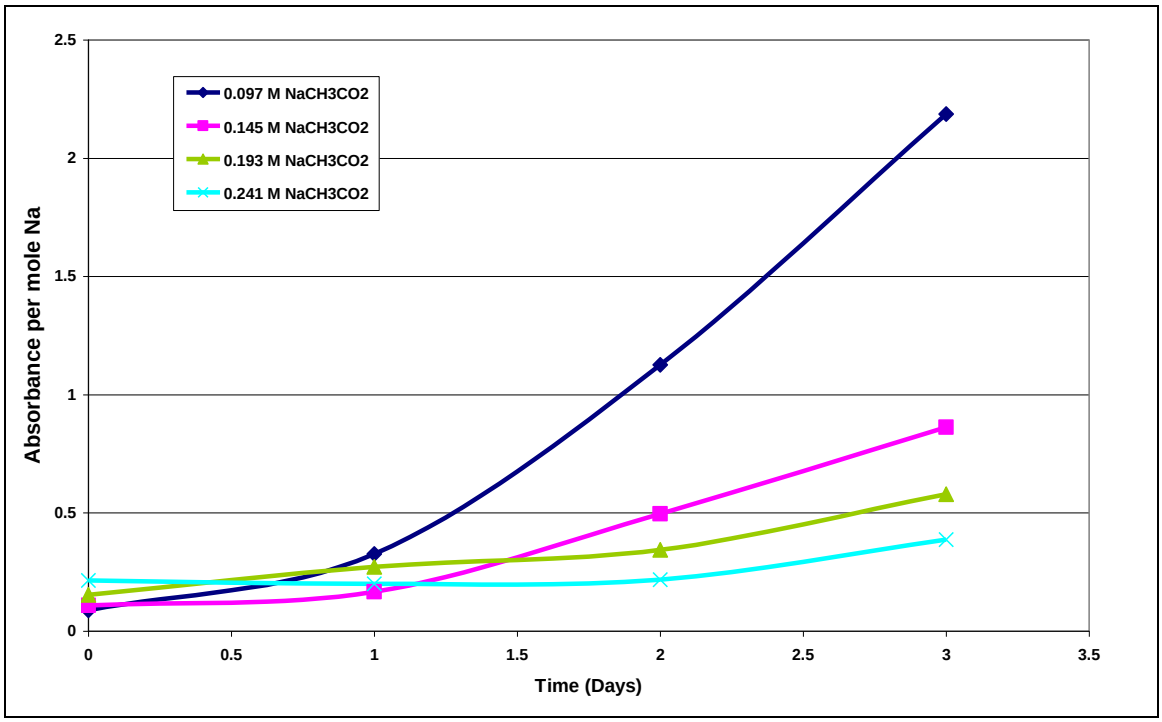

Figure 5.1.5: Absorbance per mole sodium for liquid media from bioreactors containing different concentrations of NaCH3CO2

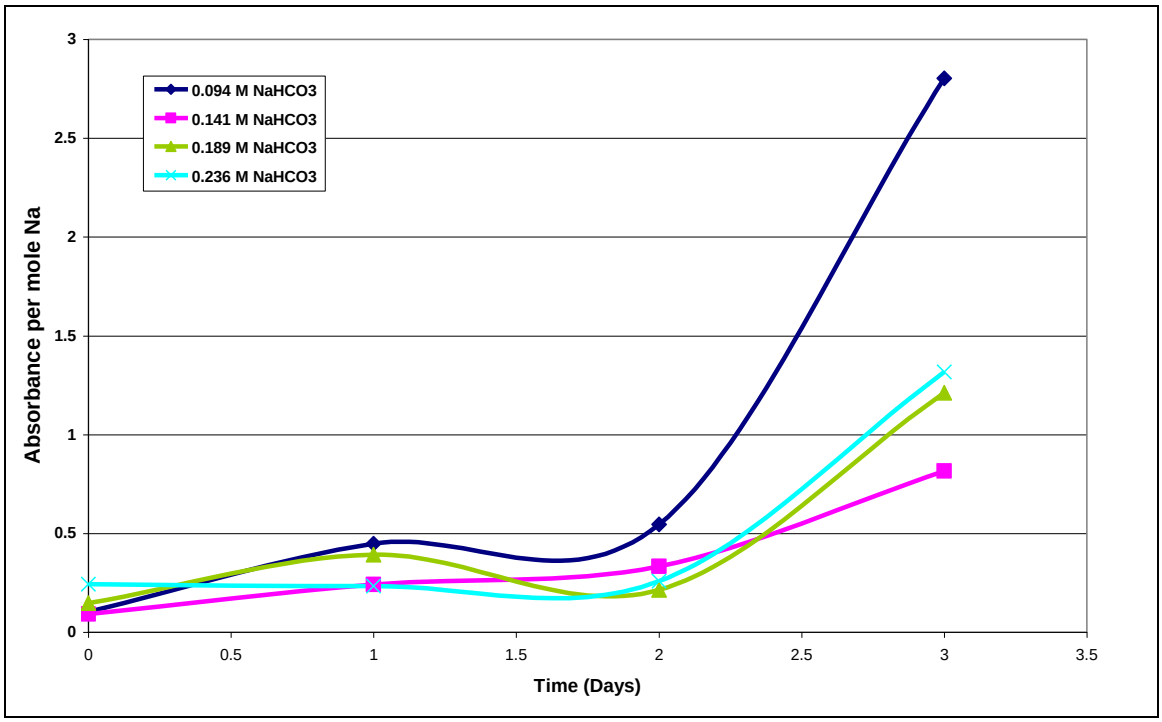

Figure 5.1.6: Absorbance per mole sodium for liquid media from bioreactors containing different concentrations of NaHCO3

5.2 Bacterial growth with glucose carbon replaced by carbon-containing sodium salts

In the experiments discussed here, glucose carbon was replaced by carbon in $NaCH_3CO_2$, $NaHCO_3$, or a mixture of the two salts. Reactors with 0% glucose and with 100% glucose (and no salt replacement) were operated to provide a basis for comparing results with those from the salt-replaced systems. The most significant growth, as expected, occurs in the system with 100% (0.6 M) glucose and the least growth with no glucose (See Figure 5.1.7). It is important to note, however, that although growth was less in the systems with salt and without glucose, growth was still observed. This fact seems to indicate metabolizing of the alternate C-source by bacteria.

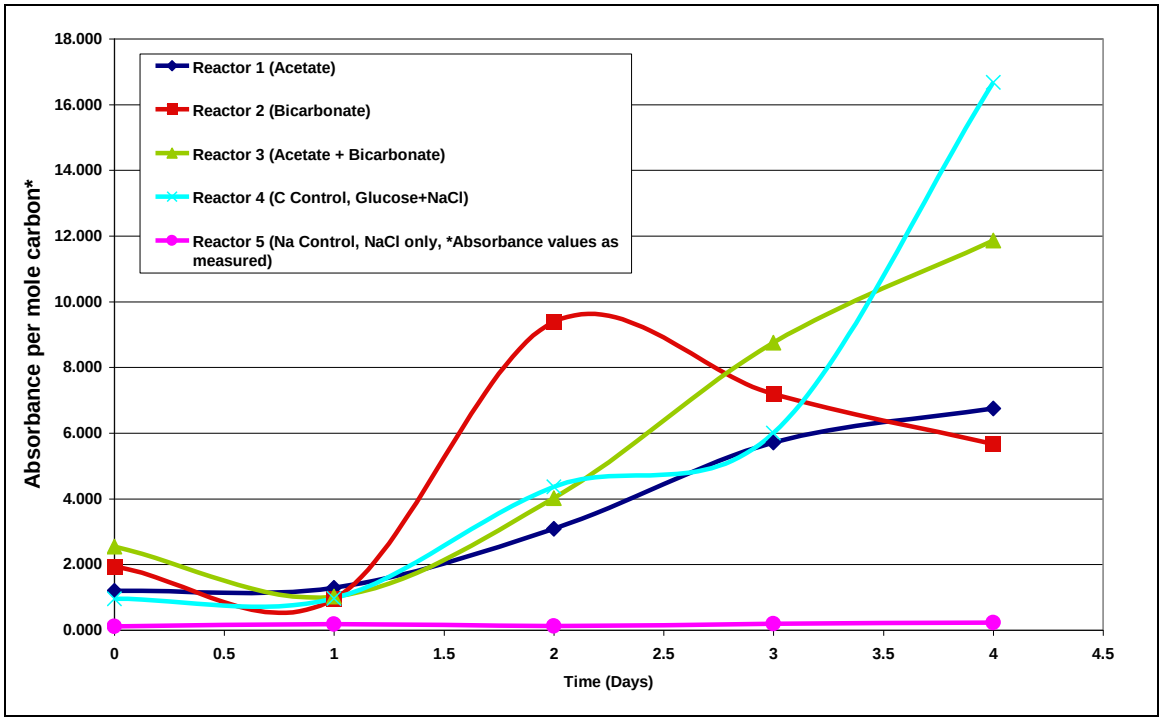

Figure 5.1.7: Absorbance curves for liquid media from bioreactors containing various NaCH3CO2 to NaHCO3 to (0% or 100%) glucose molar ratios

For the carbon-replaced systems, the most significant bacterial growth occurred in the reactor 3 system containing both acetate and bicarbonate salts at a molar ratio of approximately 2:1. At day 4 in this system, the absorbance per mole carbon was nearly 12. In contrast, in the bioreactors containing only one salt, the day 4 values for absorbance per mole carbon were 6.8 and 5.7 for acetate and bicarbonate salts, respectively.

5.3 Bacterial growth with glucose and NaCl replacement by carbon-containing sodium salts

The absorbency plots from experiments conducted to determine a narrow, operational range of values for the relative quantities of glucose and carbon-containing salts are illustrated in Figures 5.1.6 to 5.1.8. The objective was to find the smallest quantity of glucose that would promote bacterial growth and bacterial metabolizing of alternate carbon sources, acetate and bicarbonate sodium salts.

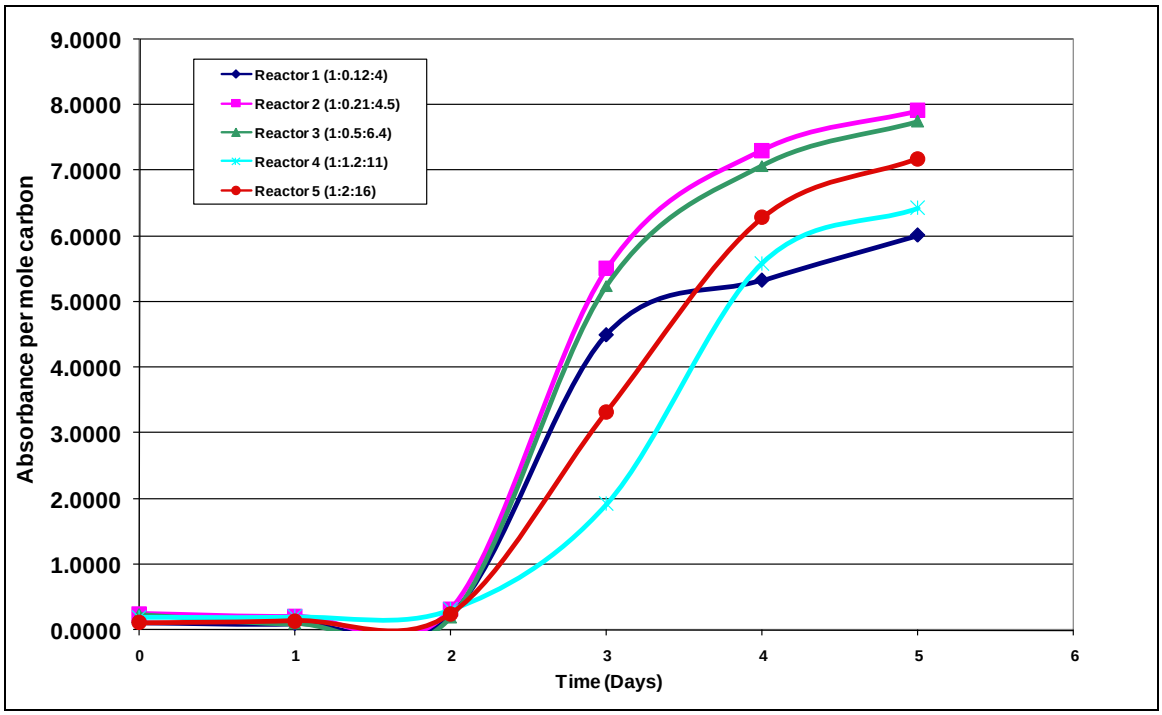

Figure 5.1.8: Absorbance per mole carbon in the system for liquid media from bioreactors containing various NaCH3CO2 to NaHCO3 to (100%) glucose molar ratios

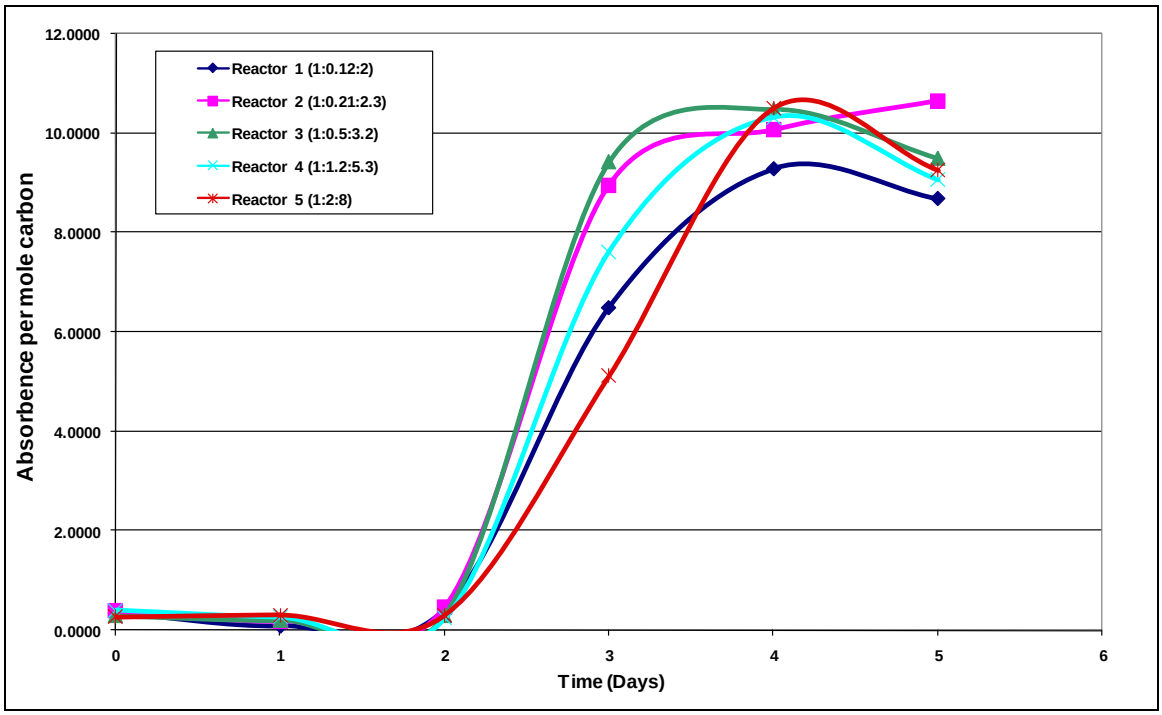

Figure 5.1.9: Absorbance per mole carbon in the system for liquid media from bioreactors containing various NaCH3CO2 to NaHCO3 to (50%) glucose molar ratios

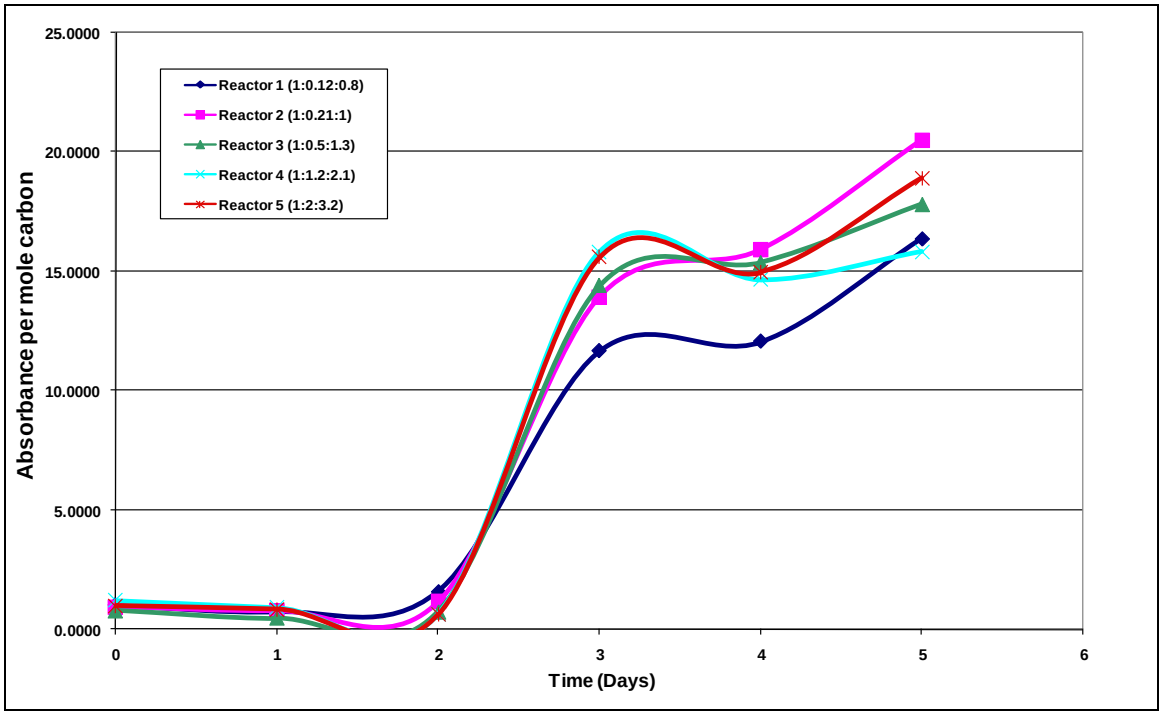

Figure 5.1.10: Absorbance per mole carbon in the system for liquid media from bioreactors containing various NaCH3CO2 to NaHCO3 to (20%) glucose molar ratios

As previously noted, bacterial growth (increased absorbance) in systems without glucose indicate that bacteria may metabolize the sodium salts. General trends in Figures 6 to 10 indicate less growth (lower absorbency per mole carbon) in experiments conducted with little

or no glucose in the system, which confirms that bacteria prefer glucose as (a carbon source) instead of the sodium salts. The most significant growth occurred in systems with more acetate carbon than bicarbonate carbon. This result is consistent with the previous experiments. As expected, bacterial growth occurred in a system with (100%) 0.6 M glucose. However, the system with (20%) 0.12 M glucose, had the most efficient bacterial growth (~20.5 absorbency per mole carbon), and was chosen for further experiments performed to gather evidence to reach the third objective.

5.4 Experiments with 14C-labelled sodium salts

The presence of growth in experiments performed with the non-active carbon-containing salts was not direct evidence that bacteria processed these alternative C-sources. It is possible, for example, that bacteria grew using some unknown impurity in the bioreactor systems. As such, the objective to create a bioreactor environment in which bacteria consume a source of surrogate graphite ^{14}C had yet to be achieved.
To gather the necessary evidence, experiments were performed with fractions of glucose replaced by radioactive ^{14}C-labelled ($NaC_2H_3O_2$ and $NaHCO_3$) sodium salts. Figure 5.1.11 and Figure 5.1.12 illustrates the phase (gas, liquid, bacterial solid) location of ^{14}C during bioreactor operation with ^{14}C-labelled sodium acetate and sodium bicarbonate salts. As previously discussed, the bioreactor phases were analysed via liquid scintillation counting.

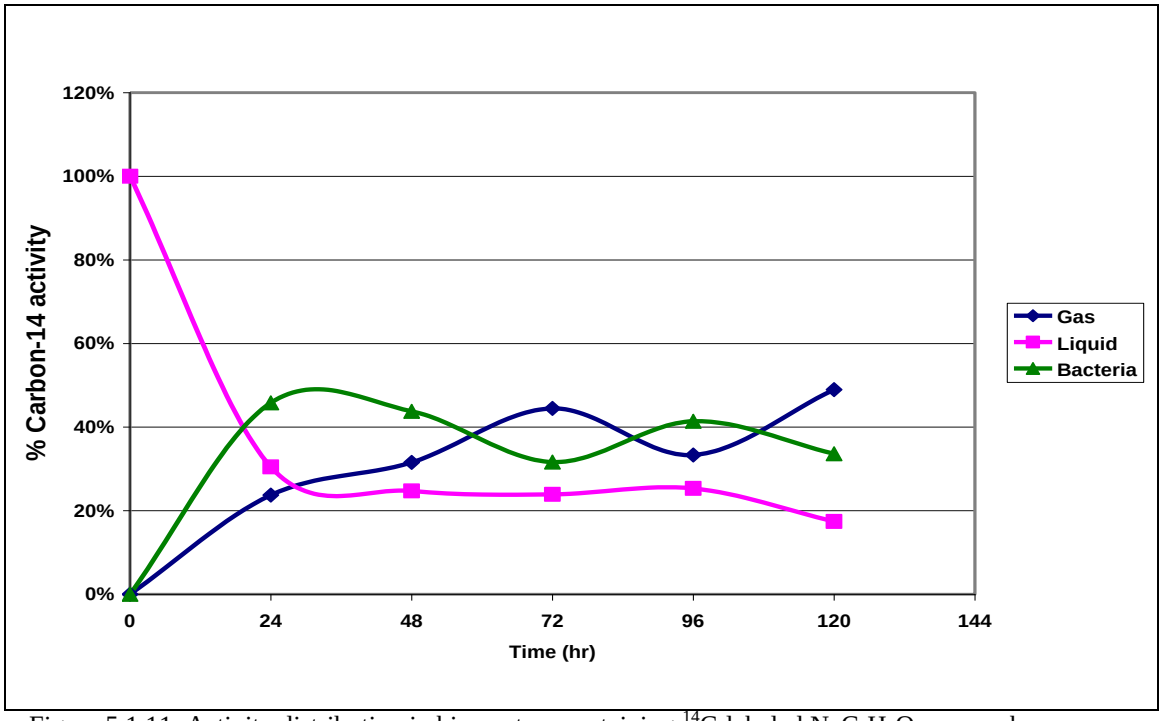

Figure 5.1.11: Activity distribution in bioreactors containing ^{14}C-labeled $NaC_2H_3O_2$ as a carbon source.

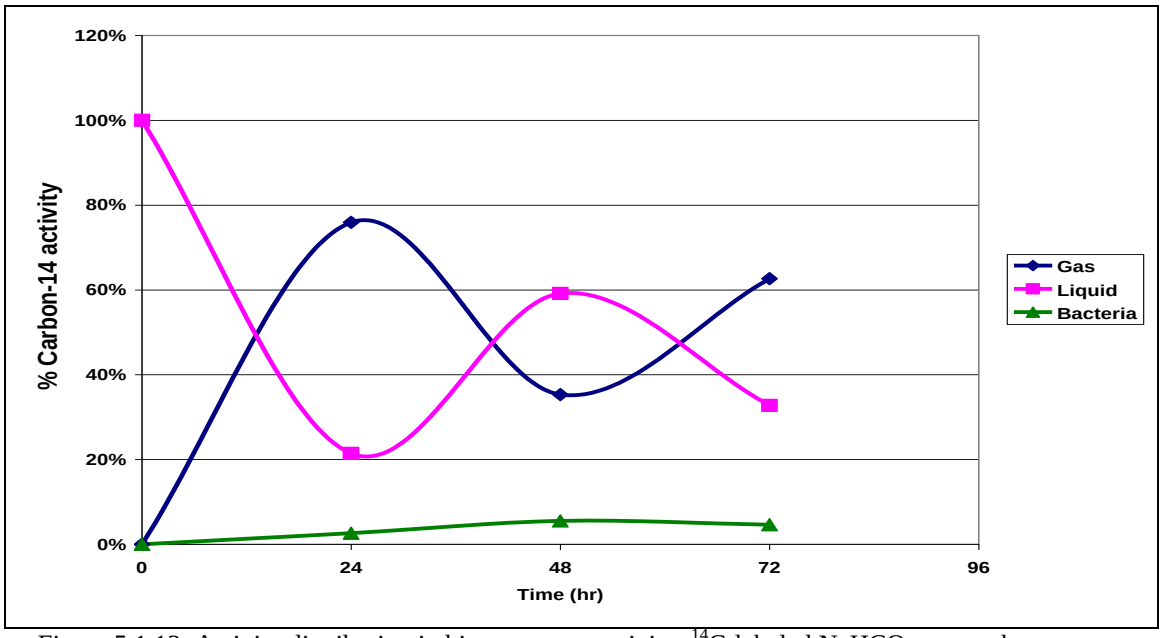

Figure 5.1.12: Activity distribution in bioreactors containing ^{14}C-labeled $NaHCO_3$ as a carbon source.

At time zero in the sodium acetate bioreactor system, all the activity was contained in the liquid phase because the ^{14}C-labelled $NaC_2H_3O_2$ salt was dissolved in the growth medium. The bacteria consumed the $NaC_2H_3O_2$ salt and proliferated as indicated by the increase in activity in the bacterial biomass (~46%) and the gas phase (~24%) during the first 24 hours. At the same time, activity decreased commensurately in the liquid phase to ~30%. The gradual decrease in activity between 24 and 72 hours in the bacterial biomass phase likely is due to depletion of sodium salt, which serves as a carbon source. Bacterial reproduction increases again as process metabolites become food sources. This phenomenon is marked by the increase in 14C activity in the bacterial biomass phase after 72 hours. The activity level in the liquid phase stays constant after the second day until the fourth.
The acetate ion in aqueous solution can chemically decompose to a carbonate ion, methane and carbon dioxide (Equation 5.1) when heated.

$$H_20 + 2NaC_2H_3O_2 \rightarrow Na_2CO_3 + 2CH_4 + CO_2 \qquad (5.1)$$

However, this reaction is not expected to occur under bioreactor system conditions. It is expected that sodium acetate is stable and remains in solution until affected by bacterial action. Sodium bicarbonate does not have the same stability as sodium acetate in aqueous solutions. At the start of experiments with ^{14}C-labelled $NaHCO_3$, all the activity was contained in the liquid phase, as was the case for NaC2H3O2. However, unlike the sodium acetate system, activity in the liquid phase decreased to ~21%, while only ~3% could be detected in the bacterial biomass phase. Activity in the gas phase increased to ~71% of the total system inventory. The high activity of the gas phase and low activity of the solid phase may be due to $NaHCO_3$ chemical decay to CO_2 (Equation 5.2).

$$2NaHCO_3 \rightarrow Na_2CO_3 + H_20 + CO_2 \qquad (5.2)$$

Results from experiments conducted with 14C-labelled sodium salts but no bacteria offer further evidence that bacteria consume the salts. With no bacteria present, ~69% of the activity

in the $NaC_2H_3O_2$ experiments stayed in liquid phase at 24 hours, with the balance going to the gas phase. In contrast, the liquid phase of the $NaC_2H_3O_2$ system charged with bacteria contained ~30% of the ^{14}C activity at 24 hours. In the ^{14}C-labelled $NaHCO_3$ system without bacteria, ~75% of the ^{14}C activity was detected in the gas phase with the remainder in the liquid. This result further supports the theory of $NaHCO_3$ decomposition due to chemical instability.

5.5 Decontamination by Microbiological Treatment: Summary

The CARBOWASTE project has demonstrated that an undisclosed microorganism consortium is capable of growth in radio-labelled C-14 sodium acetate solution with the subsequent accumulation of C-14 in the separated biomass. The studies did not demonstrate that the consortium was capable of discriminating between C-14 and C-12 materials. Equally there is insufficient evidence to suggest that the consortium could metabolise irradiated graphite, but it is likely that the consortium could metabolise carbonaceous deposits that are present on certain i-graphite. It is well documented that these carbonaceous deposits are far more reactive than the base graphite, possibly due to their high surface area/fine particulate form.
The potential to develop a microbial process for treatment of bulk i-graphite is extremely unlikely and therefore the emphasis should concentrate on identifying a selective process that will remove the carbonaceous material as this could account for the bulk of the C-14.
The issue with C-14 and i-graphite disposal is the release of the easily accessible fraction. Consequently any process that will mobilise/remove the easily accessible fraction will ultimately reduce the risks associated with graphite disposal. A biological treatment that removes and immobilises this fraction will improve graphite disposal. Fungi that generate organic acids to promote attachment and access to nutrients would be ideal for the treatment of graphite, in preference to bacteria. It is important that the fate of C-14 is known and how mobile it is in the biomass.
Microbes could have a number of adverse effects on the safety of a nuclear waste repository, including causing corrosion of metal waste containers that will promote adverse secondary effects. In concepts where the repository is to be kept open for a long period of time, to allow for monitoring and possible retrieval of wastes, there may be added difficulties with microbes due to the presence in the ventilated caverns of a humid, oxygen-filled environment. This could provide many potential niches for microbial growth, which could then affect the integrity of the storage canisters; in the infancy of the repository aerobic reactions will predominate and with the infusion of moisture/water the diffusivity of certain species from cement encapsulated waste i.e. graphite and/or the repository structure will be accelerated. Some of these leached species will stimulate the growth of certain organisms. There is limited knowledge on the diffusivity of species in/from cement under repository conditions (both aerobic and anaerobic) and how they will influence microbial growth.

In addition the post disposal fate of C-14 will also be of significant interest, if a microbial treatment results in the immobilisation of C-14 as carbonate or biomass will reduce the ultimate risks associated with this disposal. There is no real data on the fate of these compounds. Experimental studies in this area would be most helpful.

The generation of new data will greatly assist the impact assessment of these processes via biosphere modelling, which should be a crucial component of any future project.

The major challenge post CARBOWASTE is the demonstration of any treatment process and even disposal options at a realistic scale. Even with 80-year old i-graphite (80 years post removal of the fuel) it will still be sufficiently radioactive to limit the size of samples that can be handled and equipment without shielding. Developing a technique to produce non-radioactive graphite that replicates i-graphite and carbonaceous deposit will be of significance importance on moving from laboratory studies to demonstration scale.

6. Future Developments/needs

6.1 Identification of open issues

This section is listing several identified open issues related to i-graphite treatment.

- Systematic leach tests for different temperatures, leachants, graphite grades and position of origin in the reactor: a statistical approach considering several samples, together with a "mapping" of the graphite behaviour coming from different positions in the reactor, is advised in the next future in order to establish reliable predictions on the release behaviour of several radionuclides before/after thermal treatment, under disposal. Relying of few samples used in experiments by varying few parameters (as temperature of leaching or leachants) could lead to erroneous conclusions or even underestimation of the leach rates.

- Interaction of i-graphite with different atmospheres during storage / treatment: several options, including acidic/basic solutions and not neglecting humid air, have to be considered in the next future in order to obtain reliable predictions and more realistic medium/long-term leach rates. The behaviour of graphite under treatment must be better investigated considering all the parameters involved (temperature, pressure, oxidising species, history and origin of the sample, etc.).

- Modelling of release mechanisms and kinetics of i-graphite under treatment and disposal: Tritium release under thermal treatment fits well with the model proposed by Atsumi [15]. However, the fraction of the released HT and HTO are not clear, since it is believed that secondary reactions are taking place. Moreover, in the case of Radiocarbon only a preliminary simplified model has been proposed. Models for other radionuclides have still to be properly established. The definition/verification of such models will permit predictions also in a long-time scale.

- Organic radiocarbon: a fraction of the released radiocarbon revealed to be organic. Its origin and formation mechanism are still unknown: this knowledge, together with the identification of the species involved, will allow the establishment of a proper treatment/conditioning capable to remove/retain this environmentally mobile fraction.

- In general, the equipment used was not optimised for Cl-36 separation/detection. Future improvements, involving both devices upgrade/validation and sample size, are advised.

- Carbon brick, also known as "baked carbon", has been used extensively as thermal insulator surrounding the graphite reflector (AVR, THTR, etc.). The level of impurities of such material leads to generating contaminants, even in higher amounts than graphite. Characterization and leach behaviuor of such material is strongly adviced, since its radionuclide inventory cannot be neglected both in the decommissioning and disposal phase.

- Improved treatment / purification processes for different isotopes: up to now most of the scientific community has focused its attention on Tritium, Radiocarbon and partially Chlorine-36 removal, together with some actinides and activation products. A targeted separation of the different radionuclides in the next future could allow approaching the

case of a complete separation of all nuclides and recycling/declassification of the graphite waste.

- Structural changes of graphite structure need to be better investigated during irradiation/thermal treatment: radionuclide immobilization studies should be performed in that sense, in particular for what concerns Radiocarbon.

- Up-scaled treatment equipment: up to now only small samples have been investigated (in the order of grams). The question is whether those samples are representative of the entire amount of graphite present in the related reactor. In other cases, the specific activity (Chlorine-36) was lower than the detection limit of the instruments. In addition, the heterogeneous distribution of several nuclides did not allow establishing a clear understanding of some aspects, e.g. under thermal treatment. The usage of bigger samples/equipment will contribute to better evaluate the removal phenomena together with more accurate predictions linked to the overall reactor graphite.

- Different i-graphite grades coming from different reactor types should be more systematically tested, taking into account also the position in the reactor, the irradiation temperature, the estimated neutron fluence and keeping trace of the preparation process. This approach could lead to a clear separation of the multitude of variables affecting the behaviour of graphite under thermal treatment/disposal conditions.

- Pre- and post-characterization of untreated vs. treated i-graphite could provide evidence on the effectiveness of e.g. a thermal treatment from the point of view of the leaching behaviour/radionuclide stability.

- Analytical model for the treatment processes: the establishment of a model would permit the prediction of the graphite behaviour under treatment, allowing an optimization of a selective removal process.

- Analytical model for the long-term behaviour of i-graphite waste packages should be established, in order to predict the durability of the packages, considering also self-irradiation effects and leachability of radionuclides in a long time period.

- Leach tests of pre-treated/purified i-graphite should be performed in order to evaluate/quantify the effectiveness of the pre-treatment/purification process applied (thermal, chemical, microbiological, etc.)

- Accelerated leach processes (e.g. with temperature, ultrasound, microwave, induction heating, etc.) could be implied as fast verification of any treatment effectiveness on radionuclide leaching rates: values before/after treatment has to be compared. In addition, proper comparisons/calibration with normal leaching tests could lead to establishing a temporal parallelism and simulating then several years of “normal” leaching in short time (hours or even days).

6.2 Multi-Scale Modelling of Graphite

This section will introduce an innovative approach aimed to the development of a predictive model of radionuclide release from Nuclear Graphite under different atmospheres/environments.

Nuclear graphite is a complex technical material consisting of binder and filler material. Impurities, present in different amounts depending on the raw materials and manufacturing process used, lead to generating radionuclides after neutron activation. During operation inside the nuclear reactor several variables are affecting the amount, the bonds and the local concentrations of radionuclides: irradiation temperature, neutron fluence, atmosphere during irradiation, radiolytic corrosion, storage after irradiation, etc. The porous structure of graphite is the main pathway for radionuclides to be released to the environment. Release mechanisms are not well known, at the present state of the art, since a multitude of variables is affecting the characteristics of i-graphite at the end of its life. The creation of a dedicated model that considers the effects of different variables will allow predicting the long-term behavior under repository conditions as well as the behavior during treatment (e.g. thermal treatment), considering also the heterogeneous nature of graphite. The main target is to describe analytically the bonding, location and local concentration of radionuclides with respect to the short- and long-term release under storage and disposal. A targeted study on model substances, through a systematic simulation of different areas of the material, will be performed in particular on the following points, starting from the macroscopic point of view in descendent steps till the nanometric scale:
Adsorption and desorption investigations will lead to quantifying the amount of adsorbed gases under different conditions together with the identification of chemical bonds, activation energies and preferential locations.

- Filler: this fraction, by-product of oil refining or produced from cokes or natural graphite, is one of the main constituent of nuclear graphite.
    - The study of the location of adsorbed gases and chemical bonds on graphitized coke will be performed, together with investigations on the corrosion of the filler under treatment and storage/disposal. Different cokes will be considered.
    - A model substance for the idealistic graphite crystal, HOPG (highly oriented pyrolitic graphite) could be implied to investigate the bonding of implanted atoms, through several techniques (e.g. SIMS, XPS, DTA). A peculiarity of HOPG is the high purity together with a highly-ordered stacking of graphene layers. Such a substance is thought to be an idealistic model case for the ideal graphite crystal, due to its structural characteristics and the lack of porosity.
    - Radiolytic Corrosion: a gamma irradiation campaign under oxidizing atmosphere of the above mentioned simulants of the filler particles could support the evaluation of radiolytic corrosion on the radionuclides releases during reactor operation and storage/disposal.

- Binder: this fraction is known to be more porous and less graphitized than the filler one.
    - A dedicated creation of graphitized pristine binder, also in collaboration with the major graphite manufacturer, will allow investigating adsorbtion/desorbtion of gases, structural aspects and corrosion of the material. Different binders could be considered.
    - Another model material, representative of the behavior of the graphitized binder and the highly damaged structures, could be the activated coal: its high specific surface area (up to 250 times the one of graphite) has been deliberately designed to adsorb gases, so this material could be the extremization of the behavior of the micro porous areas, present due to radiation damage.
    - Radiolytic Corrosion: a gamma irradiation campaign under oxidizing atmosphere of the above mentioned simulants of the binder could lead to describe and evaluate the effects of radiolytic corrosion on the radionuclide release during reactor operation and storage/disposal.

- Pore System: special foams (e.g. POCO Foam) can be used to simulate adsorption and desorption processes, occurring in the pore system of nuclear graphite, enhanced in the proposed material by the highly accessible porosity (about 95%) and the relatively high surface area (more than 4 m^2/g).

- Hot Spots: heterogeneity of radionuclides in several i-graphites has been observed in many cases. The origin of such heterogeneities is still unclear.
    - "Chirurgical" removal of micrometric samples from nuclear graphite with FIB, together with the application of High Resolution TEM, could lead to a deeper understanding of the nature and origin of the heterogeneous radionuclide distribution.

- Doping of fillers/binders with targeted high impurities (such as Chlorine from chlorinated salts, cobalt, lithium, etc.) will allow an easier performance of several investigations by solving the detection limit problem of many techniques, well known in the case of Cl-36.

- Implantation experiments of model substances, like Cl-35 and Deuterium, together with several investigation techniques like (SIMS, XPS, Raman Spectroscopy, etc.), could allow the identification of the chemical bonds and location of such elements in nuclear graphite, representing the corresponding radioactive isotopes Chlorine-36 and Tritium. The aim is to simulate the bonding of the above mentioned radionuclides and their speciation in nuclear graphite, together with the investigation on annealing effects and release by thermal treatment, corrosion and leaching. These techniques allow investigations with high-resolution facilities outside radiochemical laboratories.

- Nanometric-scale stacked graphene layers allow the identification of preferential location(s) of adsorbed atoms/molecules (O_2, N_2, CO_2) in a perfect structure before and in a damaged one (by ion bombardment) after: the effect of recoil/damage on chemical bonds will be investigated. Parallelisms with Molecular Dynamic simulations will allow the improvement of a model on the nanometric scale.

The creation of a predictive model describing the radionuclide release behaviour of graphite has to be a multi-scale model where structure, physics and chemistry are interlinked. Through the investigation of model substances one could provide the necessary parameters for the model complementary to the systematic phenomenological and structural investigations on different i-graphite grades and origins. In addition, the validation of the model could be performed also by leaching tests on treated i-graphite, obtaining in such a way a quantification of the leach rates and the speciation of the released radionuclides.

7. Conclusions

Several methods for the decontamination of neutron-irradiated graphite have been accounted: thermal treatment, chemical treatment and microbiological treatment. The location and chemical speciation of the interested radionuclides is fundamental in order to develop an appropriate and efficient selective removal method. From this point of view, several studies have been reported in Work Package 3. However, some open issues are still remaining due to the difficulties created by the very low chemical concentrations and sometimes activities of some radionuclides (e.g. Cl-36).

Thermal treatments of i-graphite have been investigated, in particular implying inert gases (Argon or Nitrogen), oxygen and steam.
Inert gases thermal treatments, performed in virgin graphite as well as on irradiated one, underlined the presence of oxidising species in the graphite matrix, together with other impurities. The application of an inert atmosphere is favouring the desorption/pyrolysis/reaction of the above-mentioned species, resulting in a slight oxidation of the graphite, with typical mass losses typically lower than 0.5%. Excluding the cases on which small leakages occurred, the exhaustion of chemical reactions after a certain time took place, with saturation of the emissions.
In detail, Tritium release revealed to be well described by the model of Atsumi [15], with three different removal activation energies correlated with the irradiation history/conditions of graphite: 1.3, 2.6 and 4.6 eV. In particular, low activation energies are expected when trapping effect can be neglected, i.e. when the hydrogen is not significantly trapped e.g. at the edge surfaces of crystallites. Middle energies have been verified for low irradiation temperature and low irradiated graphite (e.g. Merlin); similarly, high temperature and high irradiated graphite (e.g. AVR) showed high activation energies. A special case is the medium temperature-irradiated and corroded graphite (UNGG and Magnox): significant mass losses occurred during reactor operation because of radiolytic corrosion, so high activation energies for Tritium removal are expected. It seems to be possible to remove completely the Tritium from i-graphite but further investigations, especially with massive samples and temperatures higher than 1300°C, are necessary to confirm the findings here reported.

Radiocarbon removal routes have been identified as following:
- Diffusion of C-14 atoms from interstitials or defects to the outer surface of the graphite matrix;
- Selective removal of C-14 from the enriched layers near the surfaces by slight oxidation;

Accordingly, an inert gas thermal treatment is not efficient for radiocarbon removal since, after the adsorbed/embedded oxidising species have reacted, no further decontamination can take place. Following the line of thought, the next step consists on applying oxidants, as oxygen or steam, in order to improve the removal of certain radionuclides by (radio-) chemical reactions.

Thermal treatments implying oxygen as reacting gas, in concentrations up to 1%, revealed to be inefficient from the point of view of radionuclide selectivity: graphite is a relatively stable material and it starts oxidising at relatively high temperatures. The application of oxygen revealed high reaction rates, but focused near the surface (regime II and III), resulting in a

nearly non-selective removal of radionuclide and approaching a simple corrosion of the sample.

Thermal treatments with water steam revealed to be promising from the point of view of both Tritium and Radiocarbon. Water vapour is a “mild” oxidising agent, which starts reacting at 800°C. The advantage of steam is the fact that all regimes establishing in the porous material are shifted upwards in temperature of about 300°C, compared to the case of oxygen. Accordingly, lower oxidation rates are possible in concomitance with a deeper penetration of the reactants in the sample. Three concatenated effects are causing the removal of Tritium: in descending order, isotopic exchange reactions, temperature and corrosion. The applicability of a thermal treatment with steam has to be evaluated since a dilution of Tritium could generate significant amounts of not-concentrated secondary waste. From the point of view of Radiocarbon, the removal is very effective, even though the loss of mass is still significant (in the range of some percents): for this reason, an optimization of the treatment parameters should be performed in order to limit the corrosion and maximise the selective removal.

Concerning the removable fraction of C-14, a total decontamination seems not to be achievable, unless an isotopic separation process is established. A first-approach model has been established. The removable fraction depends strongly on the graphite history. A particular recommendation for thermal treatments in inert atmosphere is the application of separate treatment steps: the MINOS (Multi INert Oxidising Step) process has been established. Following the possible identified removal mechanisms, the “temperature effect problem” must be considered: temperature is affecting in opposite ways the reaction rates and the established regime in the graphite sample. A separation of the steps, i.e. reactant loading and chemical reactions, could be an effective solution to remove C-14 more selectively without high corrosion of the graphite. MINOS process consists on separating the loading of reactants and occurring of chemical reactions, allowing in such a way a targeted removal of tritium as first and radiocarbon-enriched surfaces as second. Preliminary tests of the MINOS process have shown promising results.

An important radionuclide, volatile and extremely mobile in the environment, is Chlorine-36. It is present in nuclear graphite in very small quantities, typically 10-100 Bq/g. Consequently, its detection is rather difficult, especially when small samples are implied. Two methods have been evaluated in order to by-pass the “detection problem”: implantation of Chlorine-37 (IPNL) and direct SIMS analyses (FZJ) on Saint Laurent A2 virgin graphite. The obtained results revealed the presence of at least two Chlorine speciation, one of which is thermally stable (up to 450°C [37,38]).

A general recommendation is to consider any nuclear graphite with its own history as a unique case, since the effectiveness of a thermal treatment is significantly affected by several variables, as irradiation temperature, neutron flux, irradiation atmosphere, storage conditions, manufacture process and parameters, presence of impurities, etc. In addition, a systematic correlation with the above-mentioned parameters still needs to be done in order to have a better understanding of volatile radionuclides´ removal mechanisms and to develop a variable-dependent model for every single i-graphite (UNGG, HTTR, Magnox, MTR, etc.).

Several techniques as semi-dynamic long term leaching experiments, short term leaching experiments with stirring or ultrasonic help and Solid liquid extraction have been applied to several i-graphite: Magnox reactors (Latina and Wilfa), UNGG Reactors (Vandellos I), MTR's (Triga, BEPO and Merlin) and HTR's (AVR).

Neutral, alkaline and organic agents showed no relevant efficiency in the treatment methods tested. Acidic conditions for contaminants removal from irradiated graphite presented good results. In general the use of H2SO4 alone or in combination with complexants or other strong acids as H3PO4, HCl or HNO3 leads to a removal of contaminants with high efficiencies.
Temperature of the treatment and concentration showed to have positive effects in the decontamination factors.
The availability of surface and pore structure of the samples revealed high influence in the efficiency of the process. In general it is found that the effectiveness of the process is efficient, in descending order, for powder, granulate and massive.
Radiocarbon release showed no effective removal with any treatment, organic solvents tested gave poor results.
The chemical process with H2SO4 98%-HNO3 65% (4:1) at 20ºC removes 90% of H-3 in 24 hours.
The effectiveness of the process is a function of the availability of C-14 in the treated surface. The speciation of radiocarbon in the graphite, due to the different pathways of C-14 generation during reactor operation, in addition to pore structure and neutron damage, determines the capability of the chemical process applied.

A direct adoption of a chemical treatment is not advised for several reasons: dilution of Tritium is taking place by isotopic exchange with aqueous media, acids and H-containing molecules; dilution of Cl-36 is taking place by isotope exchange in the case HCl is chosen as decontaminating agent. Radiocarbon does not represent a problem from the point of view of its separation from the solution, but the selectivity on its removal must be high in order to avoid dilution with C-12. For the above-listed reasons it is recommended to use a thermal treatment (with optimized parameters) before adopting any chemical process.

An undisclosed microorganism consortium is capable of growth in radio-labelled C-14 sodium acetate solution with the subsequent accumulation of C-14 in the separated biomass. The studies did not demonstrate that the consortium was capable of discriminating between C-14 and C-12 materials.
The potential to develop a microbial process for treatment of bulk i-graphite is extremely unlikely and therefore the emphasis should concentrate on identifying a selective process that will remove the carbonaceous material as this could account for the bulk of the C-14.
The issue with C-14 and i-graphite disposal is the release of the easily accessible fraction. Consequently any process that will mobilise/remove the easily accessible fraction will ultimately reduce the risks associated with graphite disposal. A biological treatment that removes and immobilises this fraction will improve graphite disposal. Fungi that generate organic acids to promote attachment and access to nutrients would be ideal for the treatment of graphite, in preference to bacteria. It is important that the fate of C-14 is known and how mobile it is in the biomass.

Microbes could have a number of adverse effects on the safety of a nuclear waste repository, including causing corrosion of metal waste containers that will promote adverse secondary effects.

The presence in the ventilated caverns of a humid, oxygen-filled environment could represent a problem from the point of view of microbic presences: corrosion of metal waste containers and promoted secondary effects could take place, leading to accelerating the diffusivity of certain radionuclides into the environment. Up to now, there is limited knowledge on the diffusivity of species in/from cement under repository conditions (both aerobic and anaerobic) and how they will influence microbial growth.
A fundamental point is the post-disposal fate of C-14: if it will be immobilised through a microbial treatment as carbonate or biomass, the reduction of the disposal risks needs to be proven. Future studies should focus on the generation of new data that will greatly assist the impact assessment of these processes via biosphere modelling.

The post CARBOWASTE challenge is to demonstrate in a larger scale the feasibility of the proposed treatments, taking into account the obtained results, not neglecting the disposal options at a realistic scale. Future work should focus also on establishing predictive models for i-graphite behaviour under treatment/disposal: the validation could also go through leach tests on treated i-graphite, since it would provide radionuclides leach rates and speciation, to be compared with the untreated material, leading to long-term predictions and contributing on the improvement of the disposal strategies.

8. References

[1] R.E. Nightingale (Ed.), *Nuclear graphite*, Academic Press, New York, 1962.
[2] R. Dovesi, C. Pisani, F. Ricca, C. Roetti, *Chemisorption of periodic over-layers of atomic nitrogen on graphite*, Surface Sci. 77 (1978) 409–415.
[3] T. Fromherz, C. Mendoza, F. Ruette, *Chemisorption of atomic H, C, N and O on a cluster-model graphite surface*, Mon. Not. R. Astron. Soc. 263 (1993) 851–860.
[4] R.H. Telling, M.I. Heggie, *Radiation defects in graphite*, Phil. Mag. 87 (2007) 4797–4846.
[5] R. Nabbi, H. Probst, *Molecular dynamic simulation of the transport behavior of C-14 in irradiated nuclear graphite, Irradiation damage and ^{14}C formation in nuclear graphite*. Joint meeting in conjunction with the FP7 CARBOWASTE program, Manchester, 28th Nov 2012.
[6] P.G. Fischer, R. Hecker, H.D. Röhrig, D. Stöver, *Zum Verhalten von Tritium in Reaktorgraphiten*, J. Nucl. Mater. 64 (1977) 281–288.
[7] M. Florjan, *Dekontamination von Nukleargraphit durch thermische Behandlung, PhD thesis*, Rheinisch-Westfälische Technische Hochschule Aachen, 2009.
[8] W. Delle, K. Koizlik, H. Nickel, *Graphitische Werkstoffe für den Einsatz in Kernreaktoren*. Teil II: Polykristalliner Graphit und Brennelementmatrix, Karl Thiemig AG, München, 1983.
[9] R. Nieder, W. Sträter, *Langzeitverhalten von Verunreinigungen in einem HTR-Primärkreislauf*, VGB Kraftwerkstechnik 68 (1988) 755–760.
[10] N. Nakashio, M. Nishikawa, *Study on quantification of the system effects of tritium*, Fusion Technol. 33 (1998) 287–197.
[11] K. Katayama, M. Nishikawa, *Release behavior of tritium from graphite material*, Fusion Sci. Technol. 41 (2002) 53–62.
[12] R. Larciprete, S. Gardonio, L. Petaccia, S. Lizzit, *Atomic oxygen functionalization of double walled C nanotubes*, Carbon 47 (2009) 2579–2589.
[13] M.S. El-Genk, J.-M.P. Tournier, *Development and validation of a model for the chemical kinetics of graphite oxidation*, J. Nucl. Mater. 411 (2011) 193–207.
[14] C. MacKay, M. Pandow, P. Polak, R. Wolfgang, *The elementary chemistry of atomic carbon*, in: Chemical effects of nuclear transformations, Vol. 2, International Atomic Energy Agency, Vienna, 1961, pp. 17–26.
[15] H. Atsumi, *Hydrogen retention in graphite and carbon materials under a fusion reactor environment*, J. Nucl. Mater. 313–316 (2003) 543–547.
[16] P.C. Schmidt, *Alternativen zur Verminderung der C-14-Emission bei der Wiederaufarbeitung von HTR-Brennelementen*, Berichte der Kernforschungsanlage Jülich Nr. 1567, 1979.
[17] H. Marsh, A tribute to Philip L. Walker, Carbon 29 (1991) 703–704.
[18] K. Katayama, M. Nishikawa, *Release Behaviour of Tritium from Graphite Material*, Fusion and Science Technology Vol. 41 Jan. 2002
[19] R. Takahashi, M. Toyahara, S. Maruki, H.Hueda, T. Yamamoto, *Investigation of morphology and impurity of nuclear grade graphite, and leaching mechanism of carbon-14*
[20] H.Atsumi, *Hydrogen bulk retention in graphite and kinetics of diffusion*, Journal of Nuclear Materials 307–311 (2002) 1466–1470.
[21] P. G. Fischer, R. Hecker, H. D. Röhrig, D. Stöver, *Zum Verhalten von Tritium in Reaktorgraphiten*, J. Nucl. Mater. 64 (1977) 281–288.
[22] R. Moormann, "*A safety Re-Evaluation of the AVR*", ForschungszentrumJülich, Jül-4275

[23] G. Ramos, B.M.U. Scherzer, Radiation damage, trapping and release of deuterium in diamond and HOPG-graphite, Nuclear Instruments & Methods in Physics Research Section B-Beam Interactions with Materials and Atoms, 174 [3], 329, 2001.
[24] H. Yamagishi, N. Wakayama, H. Itoh, K. Sacasai, Measurement of neutron flux in the AVR, Berichte der KFA Jülich, JUEL-2467, 1991.
[25] Gmelin Handbuch der Annorganischen Chemie, Vol. 7, Verlag Chemie GmbH, Weinheimlbergstraße, 1966.
[26] T. Podruzhina, *Graphite as radioactive waste: corrosion behaviour under final repository conditions and thermal treatment*, Juel 4166, 2004.
[27] McGraw-Hill: Dictionary of Scientific and Technical Terms.
[28] Hutchinson encyclopaedia.
[29] C. Marnet, M. Wimmers, Decommissioning of the AVR reactor, concept for the total dismantling, Technical committee meeting on technologies for gas cooled reactor decommissioning, fuel storage and waste disposal, Vienna (Austria), 8-9-1997, 17, International Atomic Energy Agency, 1997.
[30] J. Fachinger, W. von Lensa, T. Prodruhzina: *Decontamination of nuclear graphite*, Nuclear Engineering and Design 238 (2008) 3086–3091.
[31] H.Atsumi, K. Tauchi, "Hydrogen absorption and transport in graphite materials", Journal of alloys and compounds", 356, 2003.
[32] H.Atsumi, T. Tanabe, T. Shikama, "*Hydrogen behaviour in carbon and graphite before and after neutron irradiation - Trapping, diffusion and the simulation of bulk retention*", J. Nucl. Mat. 417, 2011.
[33] H.Atsumi, S. Tokura, M. Miyake, J. Nucl. Mater. 155-157 (1988).
[34] H.Atsumi, J. Nucl. Mat. 313-316 (2003)
[35] M.I. Heggie, I. Suarez-Martinez, C. Davidson, G. Haffenden, "*Buckle, ruck and tuck: A proposed new model for the response of graphite to neutron irradiation*", J.Nucl. Mat. 413 (201) 150-155
[36] C.E. Vaudey, N. Toulhoat, N. Moncoffre, "*Thermal Behaviour of chlorine in nuclear graphite at a microscopic scale*", J. Nucl.mat. 395 (2009)
[37] C.E. Vaudey, N. Toulhoat, N. Moncoffre, "*Chlorine speciation in nuclear graphite: consequences on temperature release and on leaching*", Radiochim. Acta 98, 2010
[38] R. Takahashi, M. Toyahara, S. Maruki, H.Hueda, T. Yamamoto, "*Investigation of morphology and impurity of nuclear grade graphite, and leaching mechanism of carbon-14*"

List of Figures

Figure 2.1-a	Scanning electron micrograph of carbon brick, Large Field Detector
Figure 2.1-b	Scanning electron micrograph of carbon brick in back-scattering electron mode
Figure 2.2	Scanning electron micrograph of carbon brick in back-scattering electron mode [CW-T-3.2.3]
Figure 2.3	Depth profiles of 14N (detected as CN−) in irradiated and virgin AVR reflector graphite
Figure 2.4	Possible vacancy structures on graphite surfaces [4]
Figure 2.5	Possible places of carbon atoms between the graphite lattice planes [4]
Figure 2.6	Schematic view of a grapheme layer with perfect and imperfect zig-zag and arm-chair faces
Figure 2.7	Secondary ion mass spectra of irradiated AVR reflector graphite in comparison to virgin Saint-Laurent A2 graphite in the region of 14C
Figure 2.8	Repeat secondary ion mass spectra of irradiated AVR reflector graphite (same sample as in Fig. 2.7) in comparison to virgin AVR reflector graphite in the region of 14C
Figure 2.9	Secondary ion mass spectra of irradiated AVR reflector graphite in comparison to virgin Saint-Laurent A2 graphite in the region of 3H (same spectra as in Fig. 2.7)
Figure 2.10	Spatial distribution of negatively charged ions (sample: irradiated Saint-Laurent A2 graphite from the position 5120)
Figure 2.11	Displacement and energy loss of a 14C atom in a perfect graphite lattice structure [5]
Figure 2.12	Spatial distribution of positively charged ions (sample: irradiated Saint-Laurent A2 graphite from the position 5120)
Figure 2.13	Spatial distribution of beta-emitters determined by digital autoradiography (sample: irradiated Saint-Laurent A2 graphite from the position 5120; specimen diameter: 12 mm, thickness: 3 mm, mass: 0.2196 g) Left: Istant Imager (proportional Counter tube – FH Jülich); Right: Phosphor Imager (FZJ); Upper side of the sample.
Figure 2.14	Spatial distribution of beta-emitters determined by digital autoradiography (sample: irradiated Saint-Laurent A2 graphite from the position 5120; specimen diameter: 12 mm, thickness: 3 mm, mass: 0.2196 g) Left: Istant Imager (proportional Counter tube – FH Jülich); Right: Phosphor Imager (FZJ); Lower side of the sample
Figure 2.15	Optical image of the investigated sample
Figure 2.16	Autoradiograph showing increasing greyscale intensities with exposed Oldbury samples, B) graph showing the average intensity for Oldbury samples.
Figure 2.17a-b-c	Autoradiography of Saint-Laurent A2 graphite at different energy ranges
Figure 2.17 d-e-f	Autoradiography of Saint-Laurent A2 graphite at different energy ranges
Figure 2.18	2D tomography Radiographs of BEPO sample 16 graphite contained within a “Harwell can”.
Figure 2.19	3D volume reconstructions of BEPO Graphite using Amira© software

Figure 3.1.1 Model of Atsumi for Hydrogen trapping sites and transport in graphite [31,32]
Figure 3.1.2(a) Release of tritium in inert gases at different temperatures
Figure 3.1.2(b) Release of tritium in inert gases at different temperatures
Figure 3.1.3 Release of tritium in argon at 866 °C plotted as diffusion reaction.
Figure 3.1.4 Release of tritium in argon at 1063 °C plotted as diffusion reaction.
Figure 3.1.5 Release of HTO from Magnox Oldbury 2 graphite in nitrogen at 1100 °C plotted as diffusion reaction.
Figure 3.1.6 Release of HT from Magnox Oldbury 2 graphite in nitrogen at 1100 °C plotted as diffusion reaction
Figure 3.1.7 Decontamination factors of H-3 for Merlin graphite in function of the isothermal treatment temperature
Figure 3.1.8 Comparison among sample densities before and after irradiation in the reactor core at vertical position 1680 mm and 5120 mm, SLA2 sleeve graphite. Indicative values.
Figure 3.1.9 Decontamination factors of H-3 for SLA2 graphite in function of the isothermal treatment temperature
Figure 3.1.10 Decontamination factors of H-3 for Oldbury 2 graphite in function of the isothermal treatment temperature
Figure 3.1.11 Decontamination factors of H-3 for AVR graphite in function of the isothermal treatment temperature
Figure 3.1.12 Tritium release in argon atmosphere: a small ingress of oxygen occurred after 8-9 hours during the experiment “Merlin graphite powder 1050°C” [26]
Figure 3.1.13 ^{14}C release from AVR and Merlin graphite in argon: a small ingress of oxygen occurred after 8-9 hours during the experiment “Merlin graphite powder 1050°C” [26]
Figure 3.1.14 Comparison among two tritium release curves from similar experiments, with different oxygen amounts in the adduct gases
Figure 3.1.15 Mass loss of DIDO virgin graphite at different temperatures and humidity, 2 h isothermal
Figure 3.1.16 Release of Tritium from Merlin-1 sample (mass loss after 4 h of isothermal steam reforming: 1.45%)
Figure 3.1.17 Release of Tritium from Merlin-2 sample
Figure 3.1.18 Tritium release from Merlin graphite powder during oxidation at saturated water vapour pressure 7.4 kPa;
Figure 3.1.19 Tritium release from Merlin and AVR graphite at 1060°C and saturated water vapour pressure 2.3 kPa.[26]
Figure 3.1.20 Release of tritium in Ar/H20 1.6 kPa at 1000°C, SLA2 R1 sample
Figure 3.1.21 Release of tritium in Ar/H20 1.6 kPa at 1000°C, SLA2 R4 sample
Figure 3.1.22 Overview of Tritium removal against mass loss for different samples and temperatures in inert gases
Figure 3.1.23 Overview of Tritium removal against mass loss for different samples and temperatures

Figure 3.1.25 Schematic illustration of the model proposed by Atsumi on hydrogen trapping and transport in a graphite material [15]. The reported values are not the most recent ones (e.g. 4.4 eV instead of 4.6) and the percentages (90%,10%) are referred to unirradiated graphite.
Figure 3.2.1 Release of radiocarbon in inert gas at different temperatures
Figure 3.2.2 Release of radiocarbon in inert gas at different temperatures [26]
Figure 3.2.3 Release of radiocarbon in inert gas at different temperatures as diffusion reaction
Figure 3.2.4 Release of radiocarbon in nitrogen with 1% oxygen at different temperatures (the upper number gives the % 14C released and the lower number the % carbon consumed)
Figure 3.2.5 Release of total carbon in nitrogen with 1% oxygen at different temperatures
Figure 3.2.6 Release of total carbon in argon/nitrogen for Merlin graphite (MM=massive; MP=powder) at different temperatures
Figure 3.2.7 Release of 14CO2 from Magnox Oldbury 2 graphite in nitrogen at 1100 °C plotted as diffusion reaction
Figure 3.2.8 Release of 14CO from Magnox Oldbury 2 graphite in nitrogen at 1100 °C plotted as diffusion reaction
Figure 3.2.9 Model of a graphite surface with 3H and 14C as functional groups (surface complexes)
Figure 3.2.10 Release of 14CO2 from SLA2 graphite in Argon at 1000 °C, isothermal section plotted as diffusion
Figure 3.2.11 Release of 14CO from SLA2 graphite in Argon at 1000 °C, isothermal section plotted as diffusion reaction
Figure 3.2.12 Profile of Oxygen (water) in the three regimes taking place in graphite depending on the applied temperature.
Figure 3.2.13 Fractional release of radiocarbon vs. fractional release of total carbon in nitrogen with 1% oxygen at different temperatures
Fig. 3.2.14-a,b Fractional release of C-14 (a) and mass loss (b) during Merlin graphite oxidation with water steam (7.4 kPa) [26]
Fig. 3.2.14-c,d Fractional release of C-14 (c) and mass loss (d) during Merlin and AVR graphite oxidation with water steam (2.3 kPa) at 1060°C. [26]
Figure 3.2.15 Release of 14C from Merlin-1 sample, 1000°C, 1.6 kPa steam partial pressure.
Figure 3.2.16 Secondary release of 14C from the same Merlin-1 graphite sample and under the same experimental conditions as indicated in Fig. 3.2.15 (mass loss after 6 h of isothermal steam reforming: 2.19%)
Figure 3.2.17 Release of 14C from SLA2 R1 sample, 1000°C, 1.6 kPa steam partial pressure
Figure 3.2.18 Release of 14C from SLA2 R4 sample, 1000°C, 1.6 kPa steam partial pressure.
Figure 3.2.19-a Comparison among different treatments in inert gases at different temperatures (MM=merlin massive, MP=merlin powder)
Figure 3.2.19-b Comparison among different treatments with steam and argon, at different temperatures.

Figure 3.2.20 Schematic view of the controversial effect of temperature on reaction rates and regime in porous media.
Figure 3.2.21 Scheme of the MINOS process
Figure 3.2.22 Schematic view of a graphene layer with active sites, with ideal and imperfect edge structures.
Figure 3.2.23 Repeated thermal treatment of AVR reflector graphite at 900 °C under nitrogen atmosphere after intermediate exposure of the sample to air at room temperature for 20 hours (cumulated 14C release: 35.5%, cumulated release of total carbon: 2.7%, 14C enrichment in the gas phase: 13-20:1) [7]
Figure 3.2.24-a Comparison among different treatments with different gases and temperatures together with the first results of MINOS process, zoomed.
Figure 3.2.24-b Comparison among different treatments with different gases and Temperatures together with the first results of MINOS process.
Figure 3.2.25 First Approach model (FZJ) of C-14 location/removal, before thermal treatment (based on neutron damaged structure of [35])
Figure 3.2.26 First Approach model (FZJ) of C-14 location/removal, after thermal treatment (based on neutron damaged structure of [35])
Figure 3.4.1 Release of 14C from TA graphite in N2 with 0.1% O2 at 900 °C (mass loss after 5 h: 0.70%)
Figure 3.4.2-a,b Spatial distribution of beta-emitters on the surface of the TA (Test Assembly) graphite sample from Fig. 3.34 after thermal treatment determined by digital autoradiography (specimen diameter: 15 mm, thickness: 5 mm, mass: 0.7684 g)
Figure 3.4.3 ^{14}C profile of an HTR fuel pebble [16]
Figure 3.5.1 A model of changes from mesophase to graphite during heat treatment [17]
Figure 4.1.1 Method followed to study the decontamination of ^{60}Co, ^{241}Am, $^{239,40}Pu$, ^{137}Cs, ^{94}Nb and ^{154}Eu in i-graphite powder with several leachants.
Figure 4.1.2 Experimental set-up for leaching experiment for tritium and radiocarbon including separation procedures for determination.
Figure 4.1.3 Representation of the main steps for the graphite exfoliation process promoted by organic solvents and ultrasound assisted
Figure 4.2.1 Powder BEPO ^{3}H release under H_2O_2 conditions
Figure 4.2.2 Powder BEPO ^{14}C release under H_2O_2 conditions
Figure 4.2.3 Tritium decontamination factors in Long Term Leaching tests phase one and two for all conditions. (P: powder; S: Solid //1, 16: Channel n#)
Figure 4.2.4 Radiocarbon decontamination factors in Long Term Leaching tests phase one and two for all conditions. P: powder; S: Solid//1, 16: Channel n#
Figure 4.2.5 Overview of all of the measuring results from the Merlin leaching samples
Figure 4.2.6 Comparison of the activity of the Merlin leaching samples
Figure 4.2.7 Comparison of the total activity measured by γ spectrometry and LSC .(Gesamt = Total)
Figure 4.2.8 Total LSC result obtained from leaching the same sample twice (Leachen: Leaching; Gesamt = Total)

Figure 4.2.9 γ -activity ratios of the solid material samples before and after leaching
Figure 4.2.10 Comparison of the β activities and total activity (hypothesis) (Gesamtinventar: Total Inventory)
Figure 4.2.11 Beta total removal efficiency
Figure 4.2.12 Gamma-emitters removal efficiency
Figure 4.2.13 ^{60}Co decontamination factors for different acidic conditions
Figure 4.2.14 Gamma emitting decontamination factors for different acidic conditions at 80ºC
Figure 4.2.15 Alpha-emitting decontamination factors for different acidic conditions
Figure 4.2.16 Gamma and Alpha emitting decontamination factors for different acidic conditions with addition of Citric and Oxalic acids
Figure 4.2.17 Decontamination factors for ^{3}H and ^{14}C
Figure 4.2.18 Results obtained for the decontamination ^{3}H and ^{14}C in i-graphite powder at different leaching time.
Figure 4.2.19: Virgin graphite block and graphite powder obtained after the treatment with the mixture H_2SO_4 98%-HNO_3 65% (4:1) at 20 ºC
Figure 4.2.20 SEM images of a virgin graphite block (left) and its powder after treatment (right)
Figure 4.2.21 Overviews of Removal Efficiencies for Radiocarbon
Figure 5.1.1 Schematic representation of the bioreactor system
Figure 5.1.2 Carbon-14 distribution in the off-gas, liquid medium and bacterial biomass during the operation of the bioreactors containing sodium acetate
Figure 5.1.3 SEM micrograph of Styriakova media on a graphite surface
Figure 5.1.4 Absorbance per mole sodium for liquid media from bioreactors containing different concentrations of NaCl
Figure 5.1.5 Absorbance per mole sodium for liquid media from bioreactors containing different concentrations of $NaCH_3CO_2$
Figure 5.1.6 Absorbance per mole sodium for liquid media from bioreactors containing different concentrations of $NaHCO_3$
Figure 5.1.7 Absorbance curves for liquid media from bioreactors containing various $NaCH_3CO_2$ to $NaHCO_3$ to (0% or 100%) glucose molar ratios
Figure 5.1.8 Absorbance per mole carbon in the system for liquid media from Bioreactors containing various $NaCH_3CO_2$ to $NaHCO_3$ to (100%) glucose molar ratios
Figure 5.1.9 Absorbance per mole carbon in the system for liquid media from Bioreactors containing various $NaCH_3CO_2$ to $NaHCO_3$ to (50%) glucose molar ratios
Figure 5.1.10 Absorbance per mole carbon in the system for liquid media from Bioreactors containing various $NaCH_3CO_2$ to $NaHCO_3$ to (20%) glucose molar ratios
Figure 5.1.11 Activity distribution in bioreactors containing 14C-labeled $NaC_2H_3O_2$ as a carbon source.
Figure 5.1.12 Activity distribution in bioreactors containing 14C-labeled $NaHCO_3$ as a carbon source.

List of Tables

Table 3.1.1 Diffusion coefficients of H-3 at different temperatures for Merlin and AVR graphite [26]

Table 3.1.2: Comparison among sample densities before and after irradiation in the reactor core. Indicative values.

Table 3.5.1: Isotopic inventory of Merlin and Magnox Oldbury 2 graphite (date: 15th June 2012).

Table 4.2.1: The leached activity during the water contact

Table 4.2.2: Overviews of Removal Efficiencies for Cobalt-60

Table 4.2.3 Results of the tests on S2 (200ºC) and S3 (room T) sections with acid mixtures